**University of Novi Sad**
**FACULTY OF TECHNICAL SCIENCES**
**DEPARTMENT OF PRODUCTION ENGINEERING**
**21000 NOVI SAD, Trg Dositeja Obradovica 6, SERBIA**

UDK 621 ISSN 1821-4932

# JOURNAL OF

# PRODUCTION ENGINEERING

Volume 18 Number 2

Novi Sad, November 2015

*Journal of Production Engineering, Vol.18 (2015), Number 2*

*Publisher:* FACULTY OF TECHNICAL SCIENCES
DEPARTMENT OF PRODUCTION ENGINEERING
21000 NOVI SAD, Trg Dositeja Obradovica 6
SERBIA



*Manuscript submitted for publication:* November 30, 2015.
*Printing:* 1st
*Circulation:* 300 copies

*CIP classification:*

CIP – Катаголизација у публикацији
Библиотека Матице српске, Нови Сад

621

JOURNAL of Production Engineering / editor in chief Pavel Kovač. – Vol. 12, No. 1 (2009)- . – Novi Sad : Faculty of Technical Sciences, Department for Production Engineering, 2009-. – 30 cm

Dva puta godišnje (2012-). Je nastavak: Časopis proizvodno mašinstvo = ISSN
0354-6446
ISSN 1821-4932

*Printing by: FTN, Graphic Center* ***GRID,*** *Novi Sad*

**ISSN: 1821-4932**

**INTERNATIONAL EDITORIAL BOARD**

---

*Editorial*

*The* ***Journal of Production Engineering*** *dates back to 1984, when the first issue of the* ***Proceedings of the Institute of Production Engineering*** *was published in order to present its accomplishments. In 1994, after a decade of successful publication, the Proceedings changed the name into Production Engineering, with a basic idea of becoming a Yugoslav journal which publishes original scientific papers in this area.*

*In 2009 year, our Journal finally acquires its present title -* ***Journal of Production Engineering****. To meet the Ministry requirements for becoming an international journal, a new international editorial board was formed of renowned domestic and foreign scientists, refereeing is now international, while the papers are published exclusively in English. From the year 2011 Journal is in the data base COBISS and KoBSON presented.*

*The Journal is distributed to a large number of recipients home and abroad, and is also open to foreign authors. In this way we wanted to heighten the quality of papers and at the same time alleviate the lack of reputable international and domestic journals in this area.*

*In this journal are published, reviewed papers from International Conference "MMA 2015" and "ICPM 2015" which were held in Novi Sad, Serbia and certain number of new scientific papers as well.*

*Editor in Chief*

*Professor Pavel Kovač, PhD*,

Journal of Production Engineering
Vol.18 No.2

# Contents

## REVIEW PAPER



## ORIGINAL SCIENTIFIC PAPER

Journal of Production Engineering
Vol.18 No.2
JPE (2015) Vol.18 (2) Review Paper
Kohli, G.S., Singh,T.

# REVIEW OF FUNCTIONALLY GRADED MATERIALS

Received: 05 October 2015 / Accepted: 20 November 2015

***Abstract:*** *The present work reviewed about Functionally Graded Materials (FGMs) as the functionally graded materials (FGMs), an innovative material belongs to a class of advanced material with varying properties over changing dimension. The final properties of FGM are unique and different from any of the individual material that forms it. Typically, under harsh temperature conditions, the conventional materials (metals or ceramics) alone may not survive which led to development of a advance material i.e Functionally graded material which is capable of withstanding high temperature under harsh conditions. Functionally graded materials are widely used in aircrafts, space vehicles and other products working at elevated temperatures. The area of application of FGMs is expected to increase as the cost of material processing and fabrication processes are reduced by improving these processes.*
***Key words:*** *Functionally graded materials, advanced materials, applications of FGMs*

**Pregled funkcionalno gradijentnih materijala.** *Ovaj rad prikazuje pregled funkcionalno gradijentnih materijala (FGM), koji predstavljaju inovativne materijale i pripadaju modernim materijalima sa promenljivim osobinama usled promena dimenzija. Osobine FGM su jedinstvene i drugačije od osobina pojedinačnih materijala koji ih čine. Obično pod teškim temperaturnim uslovima, konvencionalni materijali (metali ili keramika) sami po sebi možda ne bi opstali i to je dovelo do razvoja modernih materijala, odnosno funkcionalno gradijentnih materijala koji su u stanju da izdrže visoke temperature u teškim uslovima. Funkcionalno gradijentni materijali imaju široku primenu u avio industriji, svemirskim letelicama i drugim proizvodima koji rade na povišenim temperaturama. Očekuje se da će se oblast primene FGM povećavati usled smanjenja troškova proizvodnje sa unapređenjem procesa.*
***Ključne reči:*** *Funkcionalno gradijentni materijali, moderni materijali, primena FGM*

## 1. INTRODUCTION

The term material refers to a substance out of which something can be fabricated. The term 'materials' broadly describes everything we use to manufacture everyday objects from toys to automobile parts. But under the effect of high temperature and/or thermal gradients, the conventional materials (metals or ceramics) alone may not survive; we need *advanced* materials that provide high specific performance in comparison with conventional materials. Advanced materials are used for products that have some better properties. [1]

Functionally graded material (FGM) is relatively a new concept and is used for components/parts subjected to high thermo-mechanical loading. The technology for fabrication of FGM was first proposed in Japan in 1984 during a space plane project. Where a combination of materials used would serve the purpose of a thermal barrier capable of withstanding a surface temperature of 2000 K and a thermal gradient of 1000 K across a 10 mm section. Functionally Graded Material (FGM), an innovative material, belongs to a class of advanced materials with varying properties over changing dimension [2]. As shown in figure1, traditional composites consist of two or more constituents that are combined at macroscopic level and are insoluble in each other in which the reinforcement material is uniformly distributed in the matrix material. Functionally graded materials are microscopically inhomogeneous composites usually made from a mixture of metal and a ceramic. One surface is generally a pure metal while the opposite surface is purely ceramic or a majority ceramic in which the metal surface provides the structural support while the ceramic surface provides thermal protection when subjected to high thermal gradient [3].

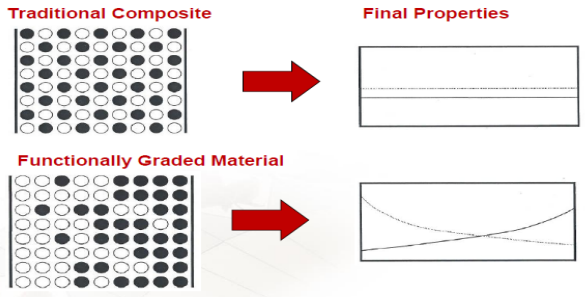


Figure 1. Traditional Composites versus FGMs

## 2. DISTRIBUTION OF REINFORCEMENTS

Several In order to study FGMs a model must be created that describes the function of composition throughout the material. The volume fraction, V, which describes the volume of reinforcement at any point, z, throughout the thickness, h, according to a parameter, n, which controls the shape of the function can be seen in Eqn. (1) below [4].

$$V = \left(\frac{z}{h} + \frac{1}{2}\right)^n \qquad (1)$$

It follows that the volume fraction of matrix material in the FGM is (1-V). A graphical representation of various values of the parameter n can be seen in Fig. 2 below,

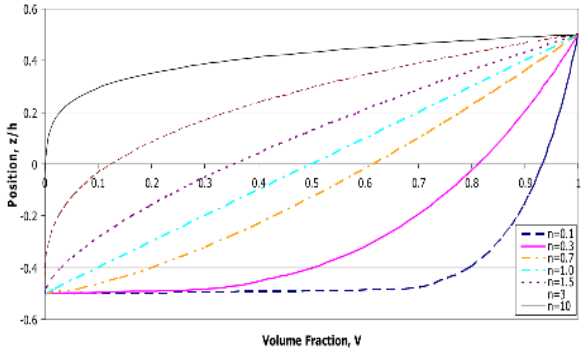

Figure 2. Variation in Parameter n.

The portion to the right of each line represents the amount of metal in the mixture and the portion to the left represents the ceramic component of the material. It should be noted that as n approaches zero the material approaches a homogeneous ceramic, while as n approaches infinity the material becomes entirely metal. At any point in between zero and infinity the material will contain both metal and ceramic. When n is set equal to one, the distribution is linear containing equal portions of ceramic and metal. The property of a material through thickness varies as a function of the volume fraction and can be seen in Eqn. 2.

$$P(z) = (P_t - P_b)V + P_b \qquad (2)$$

Where Pt and Pb represent the material property of the top and bottom respectively. Pt corresponds to Pc or the material property of the pure ceramic and Pb corresponds to Pm or the material property of the pure metal. This equation holds true for the many material properties like modulus of elasticity, density, thermal expansion, thermal conductivity and Poisson's ratio.

## 3. VARIOUS PROCESSING TECHNIQUES FOR FUNCTIONALLY GRADED MATERIALS

**3.1. Vapour Deposition Technique**: The various techniques of vapour deposition includes: (I) Chemical Vapour Deposition (CVD), (II) Sputter deposition and (III) Physical Vapour Deposition (PVD). These methods are energy intensive and a poisonous gas is produced as a byproduct. An excellent microstructure can be produced by using vapour deposition methods but only thin surface coating can be produced. [5]. The advantage includes that very thin layers can be produced and graded structure is easy to control by simply varying the composition of the gas phase. On the other hand attention must be paid on heat treatment process to avoid interdiffuion between the substrate and graded film.

**3.2. Powder metallurgy:** In order to produce functionally graded materials through Powder metallurgy the following three steps are involved. In first step, material A and material B are weighed, as shown in Fig. 3 (a). and then the two materials are mixed homogeneously by a V-shape mill, as shown in Fig.3(b). After that, stepwise staking of premixed powder can be obtained by predesigned spatial distribution of the composition Fig. 3(c). Finally spark plasma sintering (SPS) as shown in fig. 3(d) which is one of the most advanced method makes possible sintering high quality materials in small periods by charging the intervals between powder particles with electrical energy and high sintering pressure. The functionally graded material produced is a stepwise structure, and it is difficult to manufacture the functionally graded materials with continuous gradients. [6]

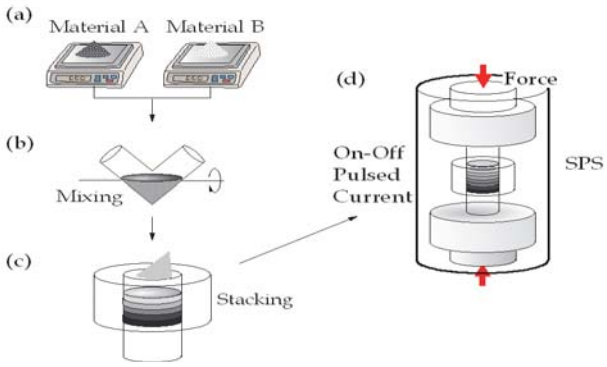

Figure 3. Fabrication process of the FGMs by powder metallurgy method. [6]

**3.3. Centrifugal casting :** Centrifugal casting is a pressure casting in which the gravitational force is increased by spinning the mould as shown in figure 4.

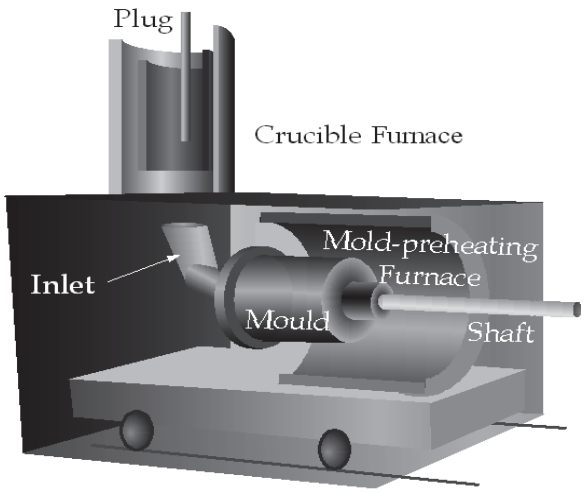

Figure 4. Apparatus for the centrifugal method. [6]

In centrifugal casting process the plug is pulled out to pour the molten metal from the inlet directly into the spinning mould. Before casting the spinning mould is preheated and the magnitude of the centrifugal force is expressed in G number, and G number is the ratio of the centrifugal force to the gravity, g, as given by the following equation:

$$G = 2DN2 \qquad (3)$$

where D is the diameter of the cast ring (m) and N is the rotation speed of the mould (s-1).Lastly the furnace

is removed and the mould is cooled until complete solidification of the mould takes place.[6]

**3.4. Centrifugal Slurry Method :** Although the powder metallurgy has many advantages to fabricate the FGMs, yet it is difficult to manufacture the FGMs with continuous gradients. By combination of the powder metallurgy and a centrifugal slurry method, this shortcoming can be overcome. In this method, two types of solid particles will be used in the slurry, one is high-velocity particle with larger density and/or larger particle size and the other one will be low-velocity particle with smaller density and/or smaller particle size. The particles gradients can be controlled by the difference of migration rate between the two kinds of particles. After complete sedimentation occurs, the left behind liquid part of the slurry wil be removed, and a green-body with continuous gradient can be obtained. The green-body is, then, sintered by SPS or other sintering methods, and finally an FGM with continuous gradient can be produced. [6]

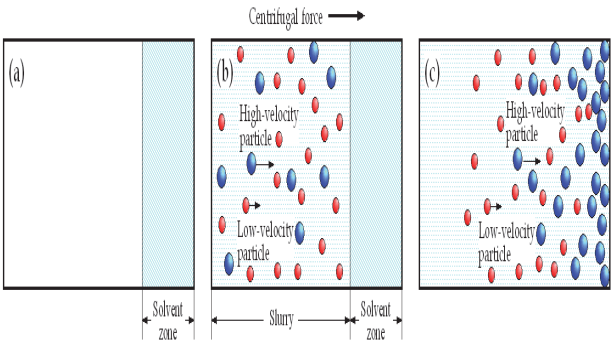


Figure 5. Schematic illustrations of the centrifugal slurry-pouring method.[6]

**3.5. Centrifugal mixed-powder method:** Figure given below shows centrifugal mixed-powder method for production of FGMs under the centrifugal force.

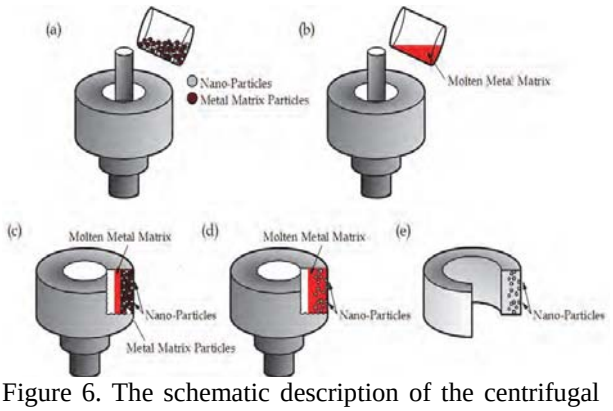


Figure 6. The schematic description of the centrifugal mixed-powder method [7]

To begin with, take a mixture of metal matrix particles A and dispersion particles B and insert them into a spinning mould, as shown in figure 6 (a). In the next step, molten metal matrix A is poured into the spinning mould with powder mixture A + B, as shown in Fig. 6 (b). Because of centrifugal force molten metal, A, penetrates into the space between the particles, as shown in Fig. 6 (c). At the same time, because of heat of molten metal matrix, the powder of matrix metal, A, is melted as shown in Fig. 6 (d). Finally, an FGM ring with dispersion-particles, B, spread on its surface, can be produced, as shown in Fig. 6 (e). [6]

## 4. APPLICATIONS OF FGMS

The concept of FGMs is applicable to many fields which are subjected to high thermo-mechanical loadings such as Aerospace, Chemical plants, Engineering, Electronics, Energy conversion, Biomaterial etc. There are several types of FGMs that exhibit exceptional multifunctional properties and multisectoral applications as shown below [8].

**4.1. Thermal protection in diesel engines:** Thermal Barrier Coatings (TBCs) are utilized in diesel engines for trucks, buses, locomotive, marine vehicles, tanks, military transport engines, and farm vehicles [9]. Their advantages in this application are increased power density, reduced heat loss, and reduced fuel consumption [10,11]. In addition, TBCs have been shown to reduce exhaust emissions [12]. Figure 7 shows the commercial application of TBCs at various locations on a diesel engine. Thick (2.5 mm) TBCs are used on piston crowns, and thinner (0.5mm) ones are used on valve faces and cylinder heads. Experimental TBCs have been tested on cylinder liners, exhaust valve systems and valve seats [13]. It has been shown that a 5% reduction in fuel consumption is obtained by insulating the combustion chamber with 2mm thick functionally graded TBC. This performance gain could be increased to an overall 54% thermal efficiency for certain advanced diesel engine concepts. It has been shown that graded TBC have a much longer life time [14, 15, 16]

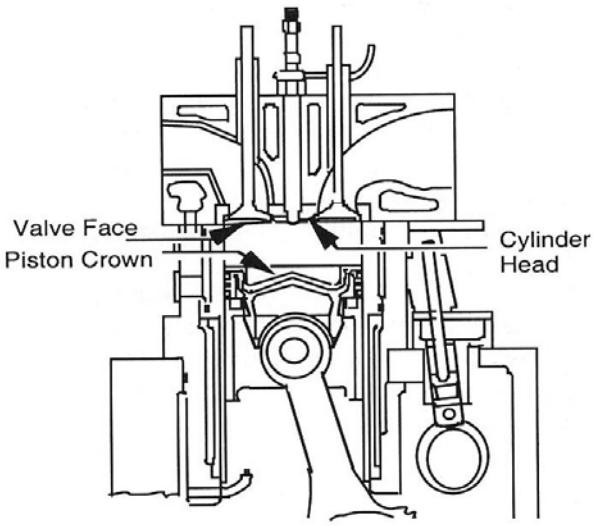


Figure 8. Location of TBCs on various components of Diesel Engine [17]

**4.2. Medicine:** Living tissues like teeth and bones are considered as functionally graded material from nature [18], and in order to replace these tissues, a suitable material is needed which will serve the purpose of the original bio-tissue. The ideal material for this

application is functionally graded material. FGM has find wide range of application in dental [19] and orthopedic applications for teeth and bone replacement.

**4.3. Aerospace:** Functionally graded materials has the ability of withstanding high temperature, which makes it suitable for use in aerospace industry but the processing cost of functionally graded material is high [20]. If processing technique is improved, FGM are promising and can be used in wider areas of aerospace.

**4.4. Defense:** One of the most important characteristics of functionally graded material is the ability to inhibit crack propagation. This property makes it useful in defense application, as a penetration resistant materials used for armour plates and bullet-proof vests [21].

## 5. CONCLUSION

Functionally graded material is an excellent advanced material that will revolutionize the manufacturing world in the 21st century. Functionally graded materials are very important in engineering and other applications but the cost of producing these materials makes it prohibitive in some applications. An overview is that this material can further be enhanced and also extended by bringing down the fabrication cost.

## 6. REFERENCES


[1] Lukkassen,D. and A. Meidell,A.: Advanced Materials and Structures and their Fabrication Processes, Book manuscript, Narvik University College, HiN, 2007.

[2] Mahamood,R.M., and Akinlabi,E.T.: Functionally Graded Material: An Overview, in Proceedings of the World Congress on Engineering, London, U.K.,( 2012).

[3] Chapman,B.D.: Characterization of Functionally Graded Materials, Air Force Institute of Technology, Wright-Patterson Air Force Base, ohio (2006).

[4] Reddy, J.N.: Mechanics of Laminated Composite Plates and Shells, (2nd edition) Boca Raton FL: CRC Press, LLC (2004).

[5] Groves, J.F., and Wadley, H.N.G.: Functionally graded materials synthesis via low vacuum directed vapor deposition, Composites Part B: Engineering, vol. 28.

[6] Watanabe, Y., and Sato, H.: Review Fabrication of Functionally Graded Materials under a Centrifugal Force, Nagoya Institute of Technology Japan.

[7] Watanabe, Y., Miura-Fujiwara, E. & Sato, H. : Fabrication of Functionally Graded Materials by Centrifugal Slurry-Pouring Method and Centrifugal Mixed-Powder Method, J. Jpn. Soc. Powder Powder Metallurgy, Vol. 57, No. 5, pp. 321- 326, ISSN 0532-8799 (2010).

[8] Moreno, A.V.: FGM in Technology: Needs and Applications.

[9] Winkler, M. F., Parker, D. W.: Greener, meaner diesels sport thermal barrier coatings, Adv. Mater. Process., 12, 18-23 (1992).

[10] Yonushonis, T.M.: Thick thermal barrier coatings for diesel components, Report CR-187111 NASA LeRC Contract DEN3-331(1991).

[11] Mendelson, M.I., Mckechnie, T.N.: Functionally gradient thermal barrier coating design, In: Ceramic Transactions, 34, Proc. Of the second Int. Symp. On FGM'92, J.B. Hoit, M. Koizumi, T. Hirai, Z.A. Munir (edit), Am. Ceram. Soc., Westerville, OH, 417-424 (1993).

[12] Assanis, D.: Investigation of the effects of thin ceramic coatings on diesel engine performance and exhaust emissions, In: Proc. Coatings for advanced heat engines workshop, Castine Maine (1990).

[13] Miller, R.A., et al.: Thermal barrier coatings for gas turbines and diesel engines, NASA technical Memorandum 102408 (1989).

[14] Beardsley M.B.: Functionally graded thermal barrier coatings for diesel engines, Presented at MRS meeting, Boston, MA (1997).

[15] Beardsley, M.B.: Thick thermal barrier coatings for diesel, In: Proc. Thermal barrier coating workshop, Cleveland, OH, NASA conference publication 3312, 203-216 (1995).

[16] Yonushonis, T.M.: Overview of thermal barrier coatings in diesel engines, In: Proc. Thermal barrier coating workshop, Cleveland, OH, NASA conference publication 3312, 113-126 (1995).

[17] Meledelson, M.I.: Thermal protection system for high heat flux environments (1995).

[18] Pompea, W., Worch, H., Epple, M., Friess, W., Gelinsky, M., Greil, P., Hempele, U., Scharnweber, D., and Schulte, K.: Functionally graded materials for biomedical applications, Materials Science and Engineering, vol. A362, pp. 40–60 (2003).

[19] Matsuo, S., Watari, F., and Ohata, N.: Fabrication of functionally graded dental composite resin post and core by laser lithography and finite element analysis of its stress relaxation effect on tooth root, Dental Mater J, vol.20 (4), pp. 257–274 (2001).

[20] Marin, L.: Numerical solution of the Cauchy problem for steady-state heat transfer in two dimensional functionally graded materials, Int J Solids Struct, vol. 42, pp. 4338-4351 (2005).

[21] Lu, L., Chekroun, M., Abraham, O., Maupin, V., and Villain, G.: Mechanical properties estimation of functionally graded materials using surface waves recorded with a laser interferometer, NDT & E International, Vol. 44(2), pp 169-177 (2011)



***Authors:*** **Gagandeep Singh Kohli, Assistant Professor,** Department of Mechanical Engineering, Baba Banda Singh Bahadur Engineering College, Fatehgarh Sahib, Punjab, India affiliated to Punjab Technical University, Kapurthala, Punjab, India.

[*]**Tejeet Singh, Associate Professor,** Department of Mechanical Engineering, Shaheed Bhagat Singh State Technical Campus, Feozepur, Punjab, India.

E-mail: engg_kohli@yahoo.co.in
tejeetsingh@rediffmail.com

[*]**(Corresponding Author)**

Journal of Production Engineering
Vol.18 No.2
JPE (2015) Vol.18 (2) Review Paper
Kraišnik, M., Vilotić, D., Šiđanin L., Stefanović, M.

# EXPERIMENTAL AND NUMERIC ANALYSIS OF STEEL C45E FORMABILITY IN THE UPSETTING PROCESSES OF TAPERED SPECIMEN

Received: 27 September 2015 / Accepted: 20 November 2015

***Abstract:*** *Commercial application of plastic forming technological methods has to be based on the principle of minimal material, time and energy consumption in creation of metal components with high performances. However, design of adequate technological procedure is not simple but, on the contrary, very complex demand to answer and I can not be achieved without prior research focused on the behavior of the material under various forming conditions from the standpoint of achieving maximum strain value. For that reason the forming limit diagram-FLD[1] became the most successful and most widely used tool which enables establishing of optimal and rational production concept.*

*In this paper is explored the possibility to apply steel C45E tapered specimen upsetting with the aim to more precisely define FLD in the ß-factor positive area. Results have shown that there is a need to include tapered specimen upsetting model in the existing methodology of FLD defining.*

***Key words:*** *Formability, Cold upsetting, Tapered specimen, Stress-strain state, Forming limit diagram*

**Eksperimentalne i numeričke analize sposobnosti deformisanja čelika C45E sabijanjem valjka konusnog uzorka.** *Praktična primena tehnoloških metoda plastičnog deformisanja treba da bude zasnovana na principima minimalnog utroška materijala, vremena i energije u cilju definisanja metalnih komponenti sa visokim performansama. Međutim, projektovanje adekvatne tehnologije u suštini nije tako jednostavno, već naprotiv, veoma složeno zbog veoma specifičnih zahteva koji ne mogu biti postignuti bez prethodnog istraživanja ponašanja određenog materijala pod različitim uslovima deformisanja sa stanovništva postizanja maksimalnih vrednosti napona. Zbog prethodnog navedenog, granični dijagram deformisanja postaje veoma uspešan i široko rasprostranjen alat koji se primenjuje i koji omogućava postizanje optimalnih i racionalnih koncepata proizvodnje. Ovaj rad prikazuje mogućnost deformisanja čelika C45E procesom sabijanje na konusnom uzorku sa ciljem da se preciznije definiše granični dijagram deformisanja u pozitivnom području ß faktora. Dobijeni rezultati prikazuju da postoji potreba da se uključi model sabijanja valjka konusnog oblika u postojeću metodologiju pri definisanju graničnog dijagrama deformisanja..*

***Ključne reči:*** *Sposobnost deformisanja, Hladno sabijanje, Konusni uzorak, Odnos napon-deformacija, Granični dijagram deformisanja*

## 1. INTRODUCTION

Material formability is the ability of permanent change of shape under specific forming conditions without formation of cracks, deformation localization or any other macroscopic contact or free surface damage and internal microstructure damage to the workpiece. Due to the complex impact of various factors which are generally divided into material factors and forming conditions factors, formability function can only be defined in the implicit form:

$$F_M \equiv \varphi_e^l = f\left(H_M, S_M, T_O, \dot{\varphi}, T_\sigma \ldots\right) \qquad (1)$$

where:

$F_M$ – is formability which is quantitatively expressed with the value of effective strain limit $\varphi_e$[1],

$H_M$ – is chemical composition of the material;

$S_M$ – is microstructure state of the material;

$T_O$ – is forming temperature; $\dot{\varphi}$ -is strain rate;

$T_\sigma$ – is stress state determined by stress tensor.

If the formability research deals with the material of certain chemical and microstructure state under conditions of cold conventional forming, then equation (1) can be reduced to the expression (2) which points out to the dominant impact of stress state to the size of strain limit:

$$F_M = f\left(T_\sigma\right) = f\left(\beta\right) \qquad (2)$$

where:

ß-is indicator of stress state in the critical zone of the specimen.

Graphic interpretation of equation (2) is FLD and there are three basic forming models to define it (uni-axial tension - ß=+1, pure torsion - ß=0 and uni-axial upsetting - ß= -1) [1], Fig. 1. Identical methodology was used in other papers, as in [1-3].

In order to define FLD a different kind of methodology can be used. It is based on establishment of functional dependence between main strains in the moment macroscopic damage to the material occurs [4].

[1] FLD – forming limit diagram

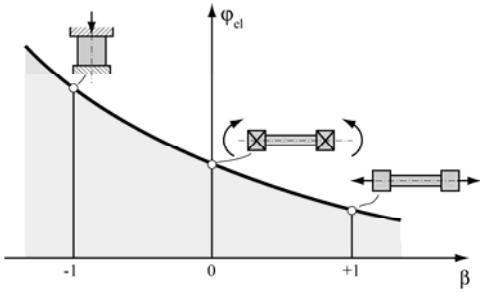

Fig. 1. Forming limit diagram - Basic models [1]

In this paper are presented the results for steel C45E formability in the basic forming models which enabled preliminary definition of FLD. After that, using experimental and numeric approach, the data was obtained and it relates to the process of tapered specimen upsetting with flat plates. Research was realized on specimens in normalized state.

Aim of the research is establishment of possibility to introduce the model of tapered specimen upsetting for the purposes of widening FLD definition in the positive area of stress state indicators. Similar efforts were presented in paper [5], but they are aimed at defining FLD for brass CW603N.

## 2. THEORETICAL ASPECTS OF DETERMINING STRESS- STRAIN STATE

In order to form functional dependence $\varphi_e$=f(ß) it is necessary to identify changes of stress-strain state in the zone of free surface of the specimen where first macroscopic damage occurs. In the following lines are presented mathematical formulations based on theoretical and experimental method which aid determination of all the parameters necessary to define FLD. Identical methodology was used in a number of other papers [2-3, 5, 8].

Starting with relation which connects stress-strain components in the area of plastic flow (3), pattern through which hydrostatic stress is defined (4) and using Von Misses yield criterion (5):

$$\frac{d\varphi_\theta}{\sigma_\theta-\sigma_m}=\frac{d\varphi_z}{\sigma_z-\sigma_m} \tag{3}$$

$$\sigma_m=\frac{\sigma_r+\sigma_\theta+\sigma_z}{3}=\frac{\sigma_\theta+\sigma_z}{3} \tag{4}$$

$$\sigma_\theta^2+\sigma_z^2-\sigma_\theta\cdot\sigma_z=\sigma_e^2 \tag{5}$$

Vujović and Shabaik [1] defined equations for defining stress components $\sigma_z$ and $\sigma_\theta$ in the place where crack occurred:

$$\sigma_z=\pm\sigma_e\cdot\left[1-\left(\frac{1+2\alpha}{2+\alpha}\right)+\left(\frac{1+2\alpha}{2+\alpha}\right)^2\right]^{-\frac{1}{2}} \tag{6}$$

$$\sigma_\theta=\sigma_z\cdot\left(\frac{1+2\alpha}{2+\alpha}\right) \tag{7}$$

Based on previous equations, indicator of state of stress $\beta$ can be defined as follows:

$$\beta=\frac{\sigma_r+\sigma_\theta+\sigma_z}{\sigma_e}=-\frac{1+\frac{1+2\alpha}{2+\alpha}}{\sqrt{1-\frac{1+2\alpha}{2+\alpha}+\left(\frac{1+2\alpha}{2+\alpha}\right)^2}} \tag{8}$$

Where:

$\sigma_r$, $\sigma_\theta$ and $\sigma_z$ – are components of main stresses in the direction of $r$, $\theta$ and $z$ axis,

$\sigma_m$ – is hydrostatic stress,

$\sigma_e$ – is effective stress.

Coefficient $\alpha$ represents deformation accrual rate and it is defined with the following pattern (9):

$$\alpha=\frac{d\varphi_\theta}{d\varphi_z} \tag{9}$$

In order to apply previous equation it is necessary to determine "strain path" $\varphi_\theta = f(\varphi_z)$. In this paper dependence in question is approximated with second degree polynomial:

$$\varphi_\theta=f(\varphi_z)=A\varphi_z+B\varphi_z^2 \tag{10}$$

Where:

A and B are coefficients of approximated function.

Principal strain components $\varphi_z$, $\varphi_\theta$ and $\varphi_r$ in the critical zone of the specimen are determined according to the height of the marked area Z (Fig. 2) and specimen size in equatorial plane, using incompressibility condition:

$$\varphi_z=ln\frac{Z_i}{Z_0},\quad \varphi_\theta=ln\frac{D_i}{D_0},\quad \varphi_r=-(\varphi_z+\varphi_\theta) \tag{11}$$

Where:

$Z_0$ and $D_0$ – are initial values of marked area height and specimen size,

$Z_i$ and $D_i$ – are values of marked area height and specimen radius after $i$ upsetting phases.

Effective strain at the lace cracks occurred is determined according to the following pattern (12):

$$\varphi_e=\frac{\sqrt{2}}{3}\sqrt{(\varphi_z-\varphi_\theta)^2+(\varphi_\theta-\varphi_r)^2+(\varphi_r-\varphi_z)^2} \tag{12}$$

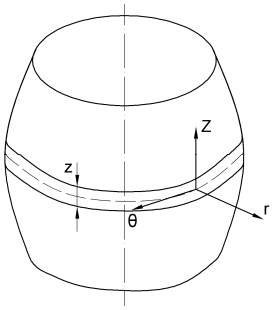

Fig. 2. Cylindrical specimen after deformation [3]

In formability tests which are based on non-monotonous plastic forming processes it is necessary to identify change in state of stress indicators $\beta$ during forming and during defining FLD it is necessary to use average value $\beta_{av}$, which is determined as follows [3, 6]:

$$\beta_{av} = \frac{1}{\varphi_e^l} \int_0^{\varphi_e^l} \beta(\varphi_e) d\varphi_e \qquad (13)$$

Here:

$\beta(\varphi_e)$ – is forming process history which is state of stress indicator of change serving as function of effective strain at the place the crack occurred.

In order to determine average value of state of stress indicator $\beta_{av}$ we observe that if the critical material damage occurs at the free surface of the specimen, we can also use methodology based on flow theory [6-7].

## 3. EXPERIMENTAL RESERACH

Normalized steel C45E specimens were used for the research purposes. Microstructure consisted of ferrite grains and lamellar pearlite colonies. Preliminary form of FLD was determined using basic forming models and afterwards the results obtained in the process of tapered specimen upsetting were integrated in the same diagram. In Fig. 3-5 are shown specimens used for defining of FLD.

Fig. 3. Specimens after deformation:
a) uni-axial tension, b) torsion

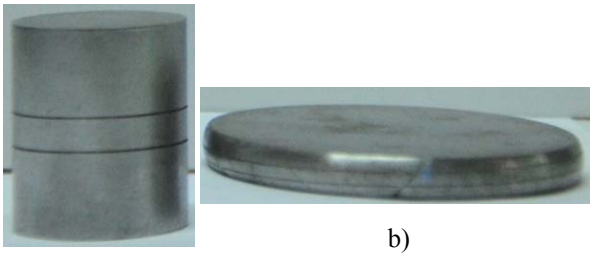

Fig. 4. Upsetting of cylinder by flat plates
a) initial specimen, b) specimen after forming

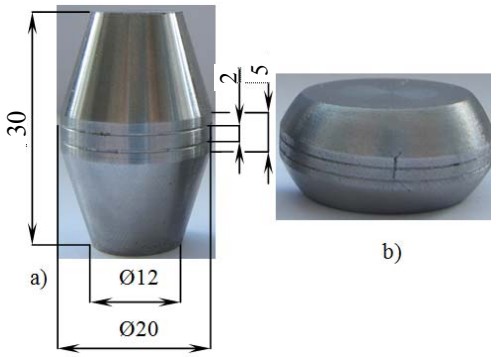


Fig. 5. Upsetting of tapered specimen: a) initial specimen, b) specimen after forming [2, 8]

All experimental research was conducted on Faculty of Technical Sciences in Novi Sad – Department for Production Engineering (Metal Forming Laboratory and Laboratory for Material Testing). Upsetting of the specimens was conducted using hydraulic press with triple action "Sack & Kieselbach", with nominal force of 6.3 MN.

## 4. NUMERIC SIMULATIONS

FEM simulations of tapered specimen upsetting with flat plates were conducted using program pack Simufact.Forming 10 in order to make a comprehensive analysis of steel C45E formability. Modeling of the tools' geometry and the workpiece was conducted using software Solid Edge v.18. Tapered workpiece 3D model and upsetting process is shown in Fig. 6.

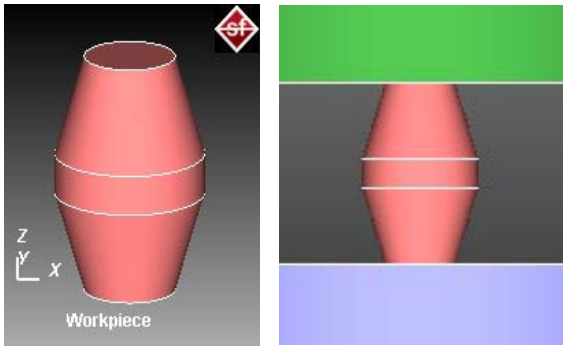


Fig. 6. 3D model – tapered workpiece and upsetting process [2]

Working elements of the tools were modeled as solid bodies and tapered specimens as formable bodies using experimentally determined flow curve in the form of Ludwik relation [2]:

$$K=462.84+451.9177\varphi^{0.3787} \qquad (14)$$

Data from the database of Simufact.Forming software database was used in the course of modeling specimen material, and it is as follows: Young's modulus of elasticity E = 210000 MPa, material density $\rho = 7800$ kg/m$^3$ and Poisson ratio $\mu = 0.3$. Modeling of contact friction was conducted according to the results from the previous research realized in the Metal Forming Laboratory and Laboratory for Virtual Projecting and Rapid Prototype Production (Department for Production Engineering – Faculty of Technical Sciences Novi Sad). Adopted value of friction coefficient is $\mu=0.12$.

Choice of machine model (hydraulic press with constant speed of tool movement 0.2 mm/min) was made according to the conditions of experimental research. Numeric simulations were realized in the cold forming conditions with defined temperature of tools and workpiece at 20 °C. Model disking was conducted using 6351 finite element of Quads type. Mesh was generated automatically using a mesher Advancing Front Quad – Fig. 7.

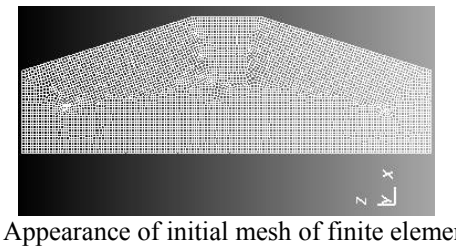

Fig. 7. Appearance of initial mesh of finite elements [2]

The above mentioned type of the finite element and mesher was adopted according to software recommendation but also for simple initial and final workpieces model form.

## 5. RESULTS

Uni-axial tension and torsion tests were realized in conditions of monotonous forming. After processing experimental data we obtained following information:

- uni-axial tension ß=+1 $\varphi_e^l = 0.0780$
- pure torsion ß=0 $\varphi_e^l = 0.6212$

Due to non-monotonous forming processes, upsetting of tapered and cylindrical specimens was incrementally realized. During the process, in each upsetting phase strain state on outer surface of equatorial area of the specimen was identified. Experimental results made it possible to determine stress state components, forming history, strain limit and ß - factor average value according to equations stated in Chapter 2.

Relations of main strains $\varphi_\theta = f(\varphi_z)$ at the place the cracks occurred in cylindrical specimens is shown in Fig. 8, and forming history in Fig. 9.

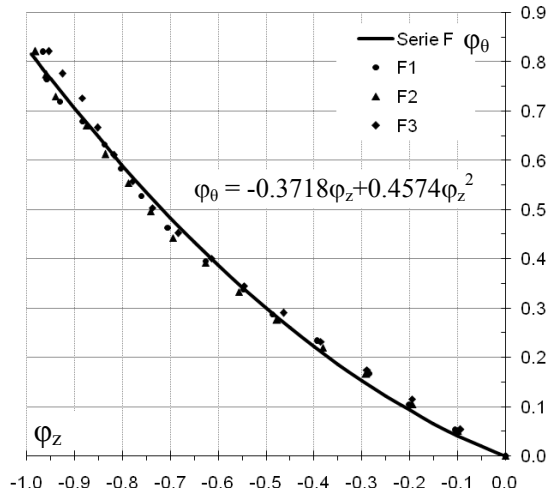


Fig. 8. "Strain path" - upsetting of cylinder by flat plates [2, 8]

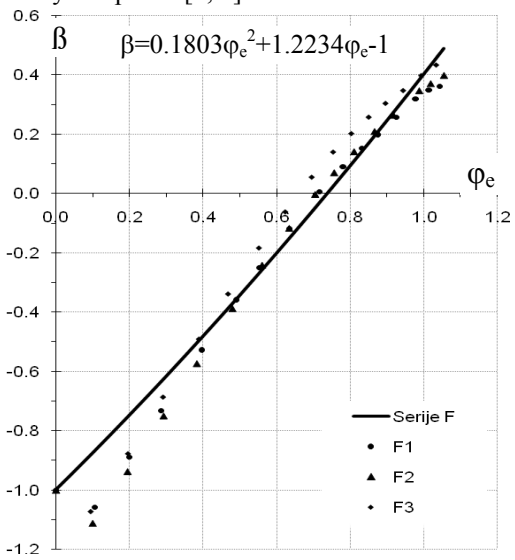


Fig. 9. "Forming history"- upsetting of cylinder by flat plates [2, 8]

Finally, according to equations 12 and 13 and according to test results for three specimens, characteristic values for process of free upsetting of cylinder by flat plates were determined: $\varphi_e^l = 1.0434$ and $ß_{av}$=-0.2963.

Processing of experimental results for the process of upsetting tapered specimens was conducted in the same manner as for the cylindrical specimens. Average values $ß_{av}$ and strains limit $\varphi_e^l$ for individual specimens $T_{1-3}$ are presented in Table 1. Representative results of experimental research for T series in comparison with FEM analysis results are presented in Table 2.

| Specimen mark | $\beta_{av}$ | $\varphi_e^l$ |
|---|---|---|
| T1 | 0.2041 | 0.3565 |
| T2 | 0.1445 | 0.3556 |
| T3 | 0.2073 | 0.3668 |

Table 1. $ß_{av}$ and $\varphi_e^l$ – Upsetting of tapered specimens by flat plates [2, 8]

Numeric simulation of upsetting of tapered specimen was realized in order to identify changes in stress-strain state and determination of mutual dependence of strains in the directions of z and Θ axis ($\varphi_\Theta = f(\varphi_z)$) in the critical area of free surface. The third strain component ($\varphi_r$) was calculated from the law of volume constancy. Criterion of plastic fracture which would enable determination of the exact moment the macroscopic damage on numeric models occurred was not used in simulations. Due to that fact, maximal movement of virtual tools was defined according to data matching strain limits under experimental conditions of the research.

Overall results of FEM analysis of stress-strain state at the place of intersection of equatorial plane and free surface of the model (critical forming zone) were presented in [2]. In Fig. 10 and Fig. 11 is presented a part of results relating to distribution of stress-strain components to limit forming level.

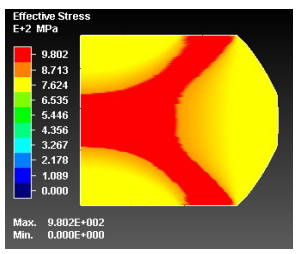


a) $\sigma_{ef}$ stress

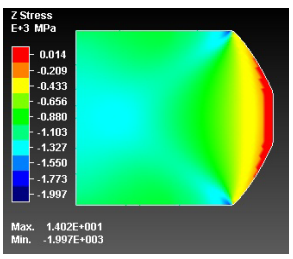


b) $\sigma_z$ stress

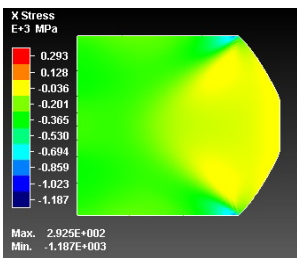


c) $\sigma_r$ stress

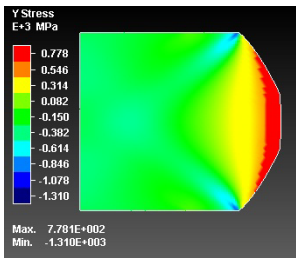


d) $\sigma_\Theta$ stress

Fig. 10. Distribution of stress components for limit forming level – tapered specimen

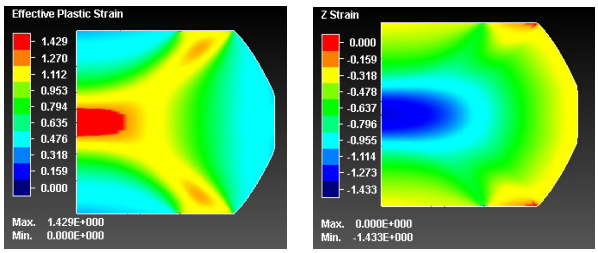


a) $\varphi_{ef}$ strain b) $\varphi_z$ strain

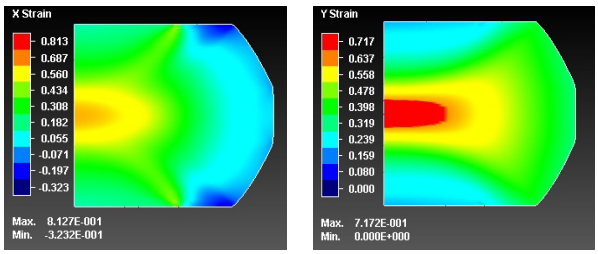


c) $\varphi_r$ strain d) $\varphi_\Theta$ strain

Fig. 11. Distribution of strain components for limit forming level – tapered specimen

Overall research results for the research of process of tapered specimen upsetting by flat plates made it possible to use regressive analysis for the purpose of defining dependence of logarithm strains $\varphi_\Theta=f(\varphi_z)$, or indicators of stress state of effective strain $\beta=f(\varphi_e)$, and then to determine effective strain limits ($\varphi_e^l$) and average values of stress state indicators ($\beta_{av}$). Theoretical approach based on forming theory was used for the purpose of determining $\beta_{av}$.

Sum overview of the results is presented in Table 2. In the following figures is presented graphic comparison of experimental and numeric results: dependence of logarithm strains $\varphi_\Theta=f(\varphi_z)$ in Fig. 12 and change of stress state indicators $\beta$ depending on effective strain, $\beta=f(\varphi_e)$ in Fig. 13.

Regardless of the approach used, it is evident that the position of tapered specimen upsetting by flat plates in FLD almost identical. Observing it numerically, strain limit obtained through FEM analysis is about 2% larger than experimental value. For that reason we can draw a conclusion that numeric simulation results support general flow of the forming limit curve whose process of defining is based on basic forming models.

| Series mark | Approximate function $\varphi_\theta = f(\varphi_z) = A\varphi_z + B\varphi_z^2$ $\beta=f(\varphi_e)=a\varphi_e^2+b\varphi_e-1$ | Correlation coefficient - $R^2$ | $\varphi_z^l$ | $\varphi_\theta^l$ | $\varphi_e^l$ | $\beta_{av}$ |
|---|---|---|---|---|---|---|
| Series $T_{exp}$ | $\varphi_\theta = -0.3360\varphi_z+2.5986\varphi_z^2$ | 0.9799 | -0.3006 | 0.3212 | 0.3595 | 0.1862 |
| | $\beta=-9.4133\varphi_e^2+8.8553\varphi_e-1$ | 0.9733 | | | | |
| Series $T_{sim}$ | $\varphi_\theta = -0.3267\varphi_z+2.7323\varphi_z^2$ | 0.9996 | -0.2945 | 0.3365 | 0.3667 | 0.1658 |
| | $\beta=-5.5052\varphi_e^2+7.7038\varphi_e-1$ | 0.9757 | | | | |

Table 2 . Analytical forms of functions "strain path" - $\varphi_\theta = f(\varphi_z)$, "forming history"- $\beta=f(\varphi_e)$, Strain limit - $\varphi_e^l$ and average values of ß-factor - $\beta_{av}$

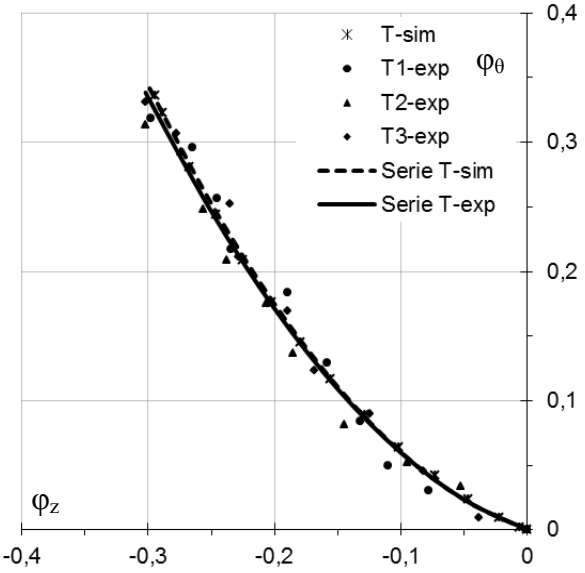


Fig. 12. "Strain path" - upsetting of tapered specimen by flat plates

In Fig. 14 is presented FLD with input of FEM analysis results ($\beta_{av}$, $\varphi_e^l$). Approximation of forming limit curve was performed according to experimental data and it is aimed to comparison with numeric simulation results.

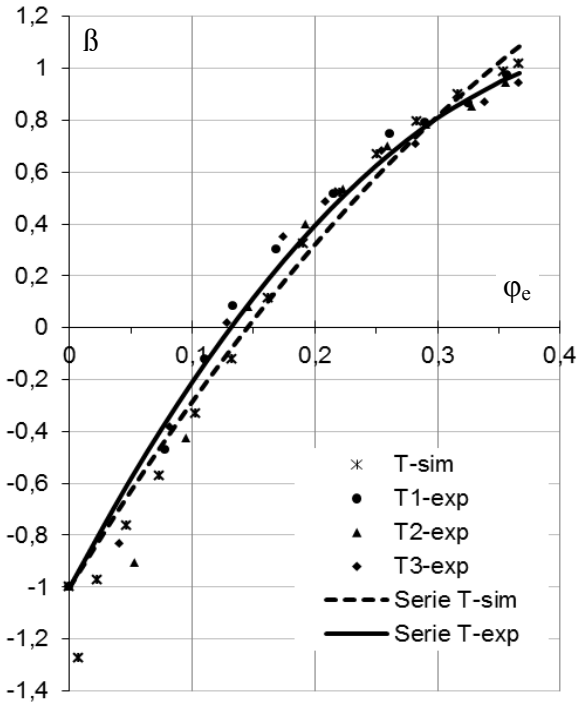


Fig. 13. "Forming history"- upsetting of tapered specimen by flat plates

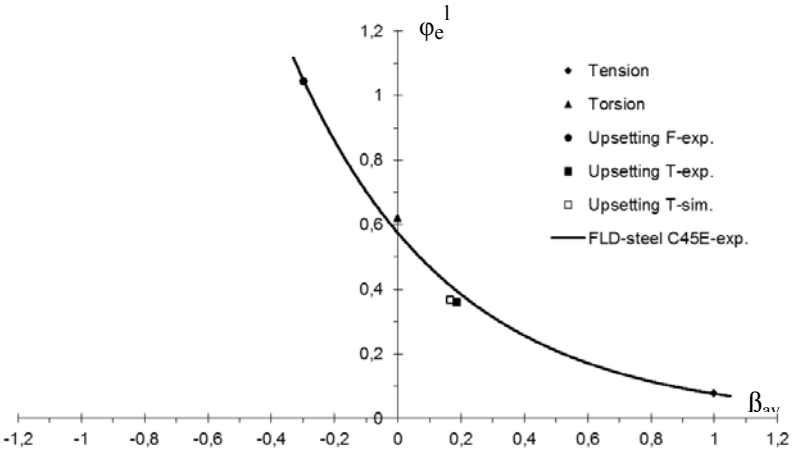

Fig. 14. FLD of steel C45E – comparative overview of experimental and numeric results

## 6. CONCLUSION

According to experimental research and FEM numeric simulations we can draw following conclusions:

- Stress state identification results on tapered specimen free surface have shown that shape and dimensions of workpieces have strong impact to the changes of stress components.
- Increase of forming limit degree leads to reduction of pressure component of normal stress $\sigma_z$, which is more strongly pronounced in the final upsetting phases. On the other hand, value of tangential component of normal stress $\sigma_\theta$ is continuously increasing.
- If the trend of changes of stress components on thee free surface of the specimen is analyzed in the context of their impact to material formability, it can be noted that in the course of upsetting the tapered specimen a continuous worsening of forming conditions occurs where the dominant impact comes from tangential component of normal stress $\sigma_\theta$ whose tension impact accelerates reaching the critical level of accumulated damage to microstructure.
- If we consider the dependence of tangential (tension) stress ($\sigma_\Theta$) on intensity of tangential stress on contact surfaces, i.e. friction coefficient, we can hypothetically state that tapered specimens show the same behavior as cylindrical specimens under the condition that the upsetting process of cylindrical specimens by flat plates is realized under the conditions of high coefficients of contact friction. Direct consequence is reduction in steel formability in the processes of tapered specimen upsetting in relation to the process of upsetting the cylinder.
- Average values of stress state indicators ($\beta_{av}$ =0,1862 – exp. and $\beta_{av}$ =0,1658 – FEM) which together with limit values of effective strain ($\varphi_e^l$=0,3595 – exp. and $\varphi_e^l$=0,3667 – FEM) determine the position of tapered specimen upsetting process in FLD enabled more precise determination of forming limit curve in the positive area of β-factor.
- Finally, model of tapered specimen upsetting by flat plates provides new information of steel C45E formability in relation with basic forming models with justified necessity for its incorporation to the existing FLD defining methodology.

## 7. REFERENCES

[1] Vujović, V., Shabaik A.: *Workability Criteria for Ductile Fracture*. Trans., ASME J. Engng. Mater. Technol., Vol. 108, p.p. 245-249., 1986.

[2] Kraišnik, M.: *Impact of stress-strain state to development of microstructure damage and material formability in the process of cold bulk forming*, Doctoral dissertation, Faculty of Mechanical Engineering, East Sarajevo, 2014.

[3] Vilotić, D., Alexandrov, S., Plančak, M., Movrin, D., Ivanišević A., Vilotić, M.: *Material Formability at Upsetting by V-Shape Dies*, Steel research international, p.p. 923-928, Special Edition 10th International Conference on Technology of Plasticity - ICTP, Aachen, Germany, 25th – 30th September 2011.

[4] Hartley P., Vilotic D., Plancak M.: *Formability maps in cold forging with conical dies*, Proceedings of the 8th ESAFORM Conference on Material Forming, Cluj-Napoca, Romania, pp. 527-530., 2005.

[5] Ivanišević A., Vilotić D., Kačmarčik I., Milutinović M.: *Upsetting of brass billets by flat dies,* Journal for Technology of Plasticity, Vol. 38, N$_0$ 2, pp. 191-199., 2013.

[6] Vilotić D., Plančak M., Čupković Đ., Alexandrov S., Alexandrova N.: *Free Surface Fracture in Three Upsetting Tests*, Experimental Mechanics Vol.46: p.p. 115–120, 2006.

[7] Alexandrov, S.: *Fracture prediction in steady ideal plastic flows*, Acta Mechanica Vol.163, p.p. 127–138, 2003.

[8] Kraišnik M, Vilotić D, Šiđanin L, Petrović Ž.: *Initial microstructure state impact to steel C 45E formability*,11th International Scientific Conference MMA 2012- Advanced Production Technologies, Novi Sad, p.p. 453-458., 2012.

***Authors:*** **Assistant Professor, Milija Kraišnik,** University of East Sarajevo, Faculty of Mechanical Engineering, Vuka Karadžića 30, 71123 East Sarajevo, Phone.:+387 57 340847, **Prof. dr Dragiša Vilotić**, **Prof. emeritus dr Leposava Šiđanin,** University of Novi Sad, Faculty of Technical Sciences, Department for Production Engineering, Trg Dositeja Obradovića 6, 21000 Novi Sad, Serbia, Phone.: +381 21 4852349, **Prof. dr Milentije Stefanović,** University of Kragujevac, Faculty of Engineering, Sestre Janjić 6, 34000 Kragujevac, Phone.: +381 34 336001

E-mail: milijakraisnik@yahoo.com, vilotic@uns.ac.rs lepas@uns.ac.rs, stefan@kg.ac.rs

Journal of Production Engineering
Vol.18 No.2
JPE (2015) Vol.18 (2) Review Paper
Milošević, M., Lukić, D., Đurđev, M., Antić A., Borojević, S.

# AN OVERVIEW OF GENETIC ALGORITHMS FOR JOB SHOP SCHEDULING PROBLEMS

Received: 22 August 2015 / Accepted: 18 October 2015

***Abstract**: This paper reviews modern genetic algorithm based approaches for solving job shop scheduling problems Genetic algorithms represent one of the most popular and mostly used metaheuristic methods applied for solving many optimization problems within last few decades. Job shop scheduling represents one of the hardest combinatorial optimization problems where number of possible schedules drastically increases with number of operations and machines. Here, different types of genetic components used for this particular problem are considered. Also, some modern genetic algorithm-based approaches from the literature are discussed as well as some approaches for integrated process planning and scheduling approach.*
***Key words:** genetic algorithm, job shop, scheduling, process planning, optimization*

**Pregled primene genetskih algoritama za rešavanje job shop problema terminiranja proizvodnje.** *U radu je dat pregled savremenih pristupa baziranih na genetskim algoritmima za rešavanje job shop problema terminiranja proizvodnje. Genetski algoritmi predstavljaju jednu od najpopularnijih i najviše primenjenih metaheurističkih metoda za veliki broj problema optimizacije u poslednjih nekoliko decenija. Job shop problem terminiranja je jedan od najtežih problema kombinatorne optimizacije za koji važi da se broj mogućih termin planova drastično uvećava sa povećanjem broja operacija/zahvata i mašina. Ovde su razmatrani različiti tipovi genetskih komponenata za rešavanje ovog konkretnog problema. Takođe, pomenuti su različiti savremeni pristupi bazirani na genetskim algoritmima razmatrani u literaturi kao i određeni pristupi za rešavanje problema integrisanog projektovanja tehnoloških procesa i terminiranja proizvodnje.*
***Ključne reči:** genetski algoritam, job shop, terminiranje, projektovanje tehnološkog procesa, optimizacija*

## 1. INTRODUCTION

Production scheduling represents the process of making the best possible utilization of resources by allocating them over some time period with the purpose of performing some tasks and satisfying certain criteria [1,2]. This type of problem belongs to the group of combinatorial optimization problems and goal is to find best solution within a discrete set of alternative solutions [1]. A significant number of published papers are related to the optimization of production scheduling problems like the ones that will be discussed later. In this paper we are focused on job shop scheduling problem which is the most popular problem of this group. Job shop environment consists of a set of different resources/machines (lathes, milling machines, drilling machines etc.) that are able to perform operations of some jobs where jobs represent parts to be produced [3]. One of the simplest definitions of job shop scheduling (JSS) problem is provided by authors [4]: Given n jobs which have to be processed on m machines, each job consists of a sequence of task operations. Each of these operations requires to be processed without interruption for a given period of time on a given machine (no pre-emption). All machines in the shops are capable of processing at most one job at a time. Tasks of the same job cannot be processed simultaneously & each of them needs to meet each machine only once and the aim is to generate a time schedule to perform the operations on machines. One of the most attractive and mostly considered objectives is to find a scheduling plan that minimizes the makespan, that is, the time needed to complete all the jobs [4]. These assumptions are usually considered in static and deterministic models of classical JSS problems which are widely considered in the literature.

During the years, metaheuristics became very popular approaches which are capable of solving instances of problems that are believed to be hard in general, by exploring the usually large solution search space of these instances [5]. Genetic algorithms (GA) are widely known metaheurstics which have been successfully applied to many different optimization problems in last few decades. They belong to the class of evolutionary algorithms which are based on the principles of natural evolution [6] and are very applicable to different combinatorial problems such as job shop scheduling.

This paper reviews genetic algorithms as implementation method for solving job shop scheduling problems. Many different types of GA components are mentioned and briefly discussed and some modern examples from the literature are analysed. Besides that, integrated process planning and scheduling approach is shortly mentioned and some examples are shown.

## 2. JOB SHOP SCHEDULING PROBLEM

JSS problem belongs to the class of strongly NP hard problems which means the number of feasible schedules increases exponentially with the increase in number of jobs and operations of each job [1]. Due to

high level of complexity, efficient methods for solving this type of problem are required.

Classical JSS problems consider allocation of "n" jobs to "m" different machines in shop environment. Each job represents part that need to be manufactured, and consists of sequence of operations in some pre-specified order. The order in which operations need to be performed depends on given technological and precedence constraints [1]. In the literature authors often consider basic assumptions while solving JSS problem [7]:

- Job cannot visit one machine more than once;
- Simultaneous performing of operations not possible;
- Machine can process only one job at current time;
- No specifications of release and due dates;
- No pre-emptions of operations.

During the years, research in the field of JSS problems has expanded towards flexible job shop scheduling problems (FJSS) in which more than one machine for performing each operation are considered. This problem exhibit additional complexity in comparing to the classical JSS.

Two different types of FJSS are considered in the literature: Total FJSS, where each operation can be processed on any machine on the shop floor, and partial FJSS, where each operation can be processed on some machine of subset of few existing machines on the shop floor. Table 1 shows example where operations of jobs 1 and 2 have different machines as alternatives with given processing times for each.

| Job | Operation | M1 | M2 | M3 | M4 | M5 |
|---|---|---|---|---|---|---|
| J1 | O11 | 2 | 6 | 5 | 3 | 4 |
| | O12 | - | 8 | - | 4 | - |
| J2 | O21 | 3 | - | 6 | - | 5 |
| | O22 | 4 | 6 | 5 | - | - |
| | O23 | - | 7 | 1 | 5 | 8 |

Table 1. Example of FJSS for two jobs and different machines [8]

## 3. GENETIC ALGORITHMS AND APPROACHES FOR IMPROVEMENT

Like the other algorithms in the class of evolutionary algorithms, genetic algorithm is based on population of individuals which assumes that population of possible solutions evolve through iteration process. As population based method, GA is exploration oriented, meaning that algorithm will ensure that all regions of search space are visited [5].

Genetic algorithm was firstly introduced by John Holland in 1975[9] and belongs to the group of evolutionary algorithms, like genetic programming among others. Since then, GA was applied on large number of various types of optimization problems including job shop scheduling. Davis [10] makes the point that although GAs work very well across a range of different problems, they can never be considered the best optimization method for any particular problem. Based on some disadvantages, like slow convergence and lack of exploitation ability (reduced possibility of finding best possible individual in visited regions, i.e. bad local search abilities) [11], there are three different hybridization approaches that improve efficiency of GA [2,10]:

1. Adaptation of genetic operators – This approach considers modification or invention of new reproduction operators (crossover and mutation) that will be suitable for given representation of individuals.
2. Heuristic-featured genetic operators – In this approach new genetic operators are created based on inspiration from some conventional (meta)heuristics.
3. Hybrid genetic algorithms – Here, useful features of some other (meta)heuristic are combined with GA wherever possible.

In [12] authors represented most used architectures of evolutionary algorithms (EAs) where hybridization can be realized between some EAs (GA and GP-genetic programming, for example), then, with assistance of neural networks, fuzzy logic, particle swarm optimization, ant colony optimization, bacterial foraging optimization and some other heuristics such as local search, tabu search, simulated annealing and so on.

## 4. BASIC COMPONENTS OF GENETIC ALGORITHM

In this chapter different types of GA components for successful implementation to job shop scheduling problems are briefly introduced. As already mentioned, GAs work with a population of individuals. These individuals are identified as chromosomes in combinatorial optimization and they are further split into number of genes. Simple GA procedure is given in [1]:

1. Choose initial population
2. Evaluate the fitness of each individual in the population
3. Repeat
    a. Select best-ranking individuals to reproduce
    b. Breed new generation through genetic operations (crossover and mutation)
    c. Evaluate the individual fitness of the children
4. Until termination criteria reached.

### 4.1 Representation (encoding) solutions

Many authors classify GA representations in two basic ones: direct and indirect. Main distinction is that for direct representations, schedules are directly encoded into chromosomes, while, on the other side, for indirect representations that is not the case. For job shop scheduling problems several GA representations are used. Two main categories are model-based and algorithm based GA representations according to the authors [6,13,14]. Different types of these representations are illustrated on Figure 1.

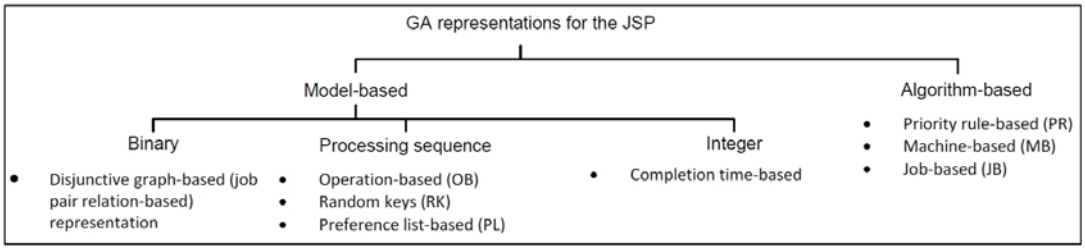

Figure 1. GA types of representations for JSS problem [13]

For model-based representations, the structure of the genotype (configuration of genes) is based on the decision variables of particular job shop mathematical model and the genotype can be directly interpreted to feasible or infeasible solution. If infeasible solution is obtained, it has to be transformed into a feasible one. On the other side, in algorithm based representations genotype used to store information which can be used by an algorithm to generate feasible solutions. Model-based representation are divided into three groups based on decision variables that are considered; those are binary, processing sequence and integer variables as shown on Figure 1 [6,13].

### 4.2 Selection procedures

After evaluating fitness values for each individual in population, standard procedures for selecting best individuals (schedules) are considered. According to author [6] fitness-proportional selection (popular as roulette wheel) and tournament selection are mostly used for job shop problems.

### 4.3 Crossover and mutation strategies

Usually, crossover and mutation operators adapted for popular travelling salesman problem (TSP) are also considered for JSS. Crossover (reproduction) operator, by first, represents the main operator in GA which task is to mix genes of two selected individuals and generate new (possibly better) solutions with probability $P_c$. There are many different crossover operators proposed in the literature. Based on the literature information, these operators are mostly applied: partially-mapped crossover (PMX), order crossover (OX), linear order crossover (LOX), cycle crossover (CX), order-based crossover (OBX), position-based crossover (PBX), job-based order crossover (JOX), subsequence-exchange operator, uniform crossover, partial schedule exchange crossover and so on [6,13,15]. Due to significant information about crossover, only three operators are shown in this paper. Figure 2 illustrates PMX and OX crossover operators that are used for JSS problems.

The PMX operator selects two random points and for generating offspring, it copies segment between these points from one parent, and replaces this segment of the second parent. Resulted offspring is called proto-offspring which has to be repaired by mappings from parent 1 to parent 2.

The OX operator determines two random points on parent 1 similarly like in the previous case. The segment between these points is automatically copied to the offspring and rest of the genes are filled in the relative order of second parent, excluding those already copied from parent 1[6].

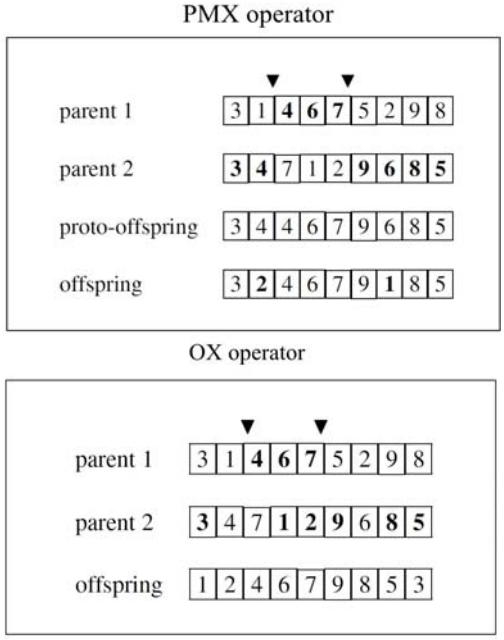

Figure 2. PMX and OX operators of GA [6]

Considering mutation operator in GAs, there are different mechanisms that are implemented with purpose of exchanging determined random genes in chromosome [13]. Mutation in GA is used as divergence operation and is intended to prevent search from falling to local optima. There are few distinct mutation operator widely used for JSS problems, such as swap, inversion, insertion (shift) and displacement mutation [6,13,15].

Swap mutation exchanges two randomly selected genes in chromosome. Inversion is based on inverting the order of the genes between two randomly selected points in the chromosome. Shift mutation chooses random gene and shifts it to some random position to the right or left from its current position. This operator is also very common for process planning problems. Similar to insertion mutation is displacement where, instead of one gene, subset of few genes is used [13]. Figure 3 shows the example of shift mutation. Number 3 is shifted to random location while creating a new individual.

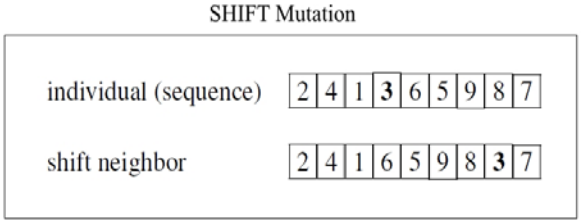

Figure 3. Shift mutation procedure [6]

### 4.4 Termination criteria of GA

Often a maximal number of generations or a maximal time limit are imposed as stopping criteria of GA. Alternatively, one can use a termination criterion such that the algorithm stops if for a specific number of generations no improvements in the best objective function value have been obtained, or if the relative deviation of the best objective function value from a given lower bound does not exceed a particular value [6].

## 5. MODERN GA APPROACHES FOR JSS PROBLEM

In today's literature enormous amount of data about job shop scheduling problems can be found. Authors applied different approaches and considered different, static as well as dynamic aspects of scheduling problem. In this chapter some modern examples of GA implementation on JSS problems are mentioned and briefly discussed.

In [16] GA for JSS problem is introduced and results are obtained in the case study. Authors considered problem with 15 jobs and 15 machines on shop floor. Individuals in population are represented using permutations after which the next GA operators are used for reproducing new chromosomes: roulette wheel tournament as selection strategy, order crossover, swap mutation and maximum number of generations is used as termination criterion. Makespan is used as optimization criterion. Algorithm is coded in Matlab software language and experimental results are compared with longest processing time (LPT), shortest processing time (SPT) and first come first served (FCFS) dispatching rules where GA outperformed all three of those.

One of the latest GA implementations is a new genetic algorithm (NGA) applied for FJSS problems [8]. This algorithm uses different solutions for searching the regions. New job permutation is applied as encoding strategy where array of integers is used and each integer value refers to the index of array of operation for each job. Next, roulette wheel is used as selection strategy, uniform crossover and special, values mutation operator as strategies for generating new individuals. Matlab is also used as a tool for implementation, and NGA is applied to many different problem instances as well as to a problem of a real world drug company Saidal Group. This study covered the production of Suipuren drug which required three shop floors with different machine alternatives for each operation. Those shops are weighing room (10 jobs and 10 machines), production shop (10 jobs and 8 machines) and conditionment shop (10 jobs and 13 machines). Table 2 shows machine alternatives with processing times (in milliseconds) for performing job operations in weighing room. The data shown are partial and do not cover the ones for other two shops for this particular problem. Obtained results are compared to the results from SAIDAL company where NGA provided optimal results with minimum computational time. Figure 4 represents convergence curve for weighing room which shows the decrease of makespan values over generations.

In addition to both scheduling as well as process planning optimization problems considered individually, popular integrated process planning and scheduling (IPPS) approach attracted the attention of many researchers. This approach characterizes simultaneous performing of process planning and scheduling functions which greatly improves the performance of modern manufacturing systems. Theory and different approaches of IPPS can be seen in brief review from authors [17].

| Job | Shop | Operations | Machines | Processing Time (ms) |
|---|---|---|---|---|
| Suipuren 180 ml (partially) | Weighing room | O11 | BP1 | 57600 |
| | | | BP2 | 0 |
| | | O12 | BA1 | 72000 |
| | | | BA2 | 600 |
| | | O13 | B1 | 43200 |
| | | | B2 | 50400 |
| | | | B3 | 0 |
| | | O14 | IM1 | 7200 |
| | | | IM2 | 0 |
| | | | IM3 | 9000 |

Table 2. Different machines for given FJSS problem (partial view) [8]

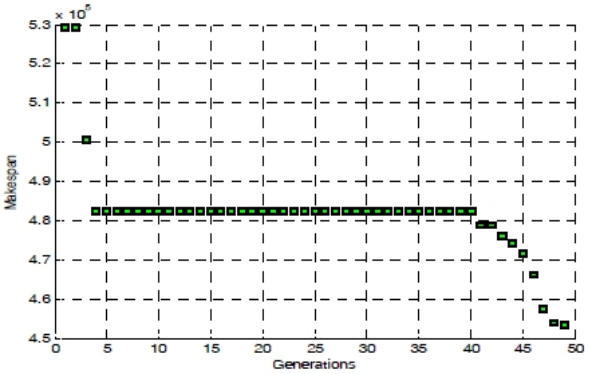


Figure 4. Convergence curve for weighing room [8]

IPPS has many advantages, including consideration of all alternatives of process plans, real dynamical situations on shop floor, multicriteria optimization, simultaneous performing of process planning and scheduling functions and so on. One example of implementation of GA for IPPS problem in job shop environment is given in [18]. Modified GA is used, with slight modifications in representation and genetic operators. This model is coded in C++ language and fine solutions are obtained. Authors in [19] introduced new object-coding GA with special representation and corresponding genetic operators as well. Objects represent machining operations that are directly used to represent genes. This specific model of GA is coded in JAVA language with MySQL database. Algorithm proved very efficient for some benchmark test problems in comparing to other methods.

## 6. CONCLUSION

In the paper the brief overview of genetic algorithms for job shop problems is introduced. Three basic approaches for improving GA efficiency are mentioned in the second chapter. Different types of representations, selection strategies, genetic operators (crossover and mutation) and termination criteria of GA for successful implementation in the search for optimal scheduling plans are given in the third chapter. Last chapter considers few GA implementations on some problem instances in the literature. Some modern approaches are shortly discussed with one example in the real world pharmaceutical production. At the end the importance of integrated process planning and scheduling approach is emphasised with some examples found in the literature.

## 7. REFERENCES


[1] Kumar, R., Sankha, D.: *A Genetic Algorithm-Based Approach for Optimization of Scheduling in Job Shop Environment*, Journal of Advanced Manufacturing Systems, Vol. 10, p.p. 223-240, 2011.

[2] Gen, M., Cheng, R.: *Genetic Algorithms and Engineering Optimization*, John Wiley & Sons, Inc., New York, 2000.

[3] Blazewicz, J., Ecker, K., Pesch, E., Schmidt, G., Węglarz, J.: *Handbook on Scheduling: From Theory to Applications*, Springer Berlin Heidelberg, p.p. 345-396, Berlin, 2007.

[4] Shafia, M. A., Pourseyed Aghaee, M., Jamili, A.: *A new mathematical model for the job shop scheduling problem with uncertain processing times*, International Journal of Industrial Engineering Computation, Vol. 2, p.p. 295-306 , 2011.

[5] El-Ghazali, T.: *Metaheuristics: From Design to Implementation*, John Wiley & Sons, Inc., New Yersey, 2009.

[6] Werner, F.: *Genetic Algorithms for Shop Scheduling Problems: A Survey*, chapter 8, in: Siarry, P.: *Heuristics: Theory and Applications*, Nova Science Publishers, Inc., New York, 2013.

[7] Bagchi, T.: *Multiobjective Scheduling By Genetic Algorithm*, Springer US, New York, 1999.

[8] Driss, I., Mouss, K.N., Laggoun, A.: *A new genetic algorithm for flexible job-shop scheduling problems*, Journal of Mechanical Science and Technology, Vol. 29, p.p. 1273-1281, March 2015.

[9] Holland, J.A.: *Adaptation in natural and artificial systems*, MIT Press, USA, 1975.

[10] Partridge, D.: *A review of "Handbook of Genetic Algorithms"* from Davis, L.D., Taylor & Francis Group, Vol. 3, p.p. 446-448, 1991.

[11] Beasley, D., Bull, D.R., Martin, R.R.: *An Overview of Genetic Algorithms: Part 1, Fundamentals*, University Computing, Vol.15, p.p. 58-69, 1993.

[12] Grosan, C., Abraham, A.: *Hybrid Evolutionary Algorithms: Methodologies, Architectures, and Reviews*, Studies in Computational Intelligence, Vol. 75, p.p. 1–17, 2007.

[13] Abdelmaguid, T. F.: *Representations in Genetic Algorithm for the Job Shop Scheduling Problem: A Computational Study*, J. Software Engineering & Applications, Vol. 3, p.p. 1155-1162, December 2010.

[14] Cheng, R., Gen, M., Tsujimura, Y.: *A Tutorial Survey of Job-Shop Scheduling Problems using Genetic Algorithms – I. Representation*, Computers & Industrial Engineering, Vol. 30, p.p. 983-997, September 1996.

[15] Cheng, R., Gen, M., Tsujimura, Y.: *A Tutorial Survey of Job-Shop Scheduling Problems using Genetic Algorithms – II. Hybrid genetic search strategies*, Computers & Industrial Engineering, Vol. 36, p.p. 343-364, April 1999.

[16] Maghfiroh, M.F.N., Darmawan, A., Yu, V.F.: *Genetic Algorithm for Job Shop Scheduling Problem: A Case Study*, International Journal of Innovation, Management and Technology, Vol. 4, February 2013.

[17] Đurđev, M., Milošević, M., Lukić, D., Jovičić, G., Vukman, J.: *A review on integrated process planning and production scheduling approach*, 12th International Scientfic Conference MMA 2015-Flexible Technologies, p.p. 117-120 , Novi Sad, 25-26 September, 2015.

[18] Shao, X., Li, X., Gao, L., Zhang, C.: *Integration of process planning and scheduling – A modified genetic algorithm-based approach*, Computers & Operations Research, Vol. 36, pp. 2082–2096, July 2008.

[19] Zhang, L., Wong, T.N.: *An object-coding genetic algorithm for integrated process planning and scheduling*, European Journal of Operational Research, Vol. 244, p.p. 434-444, January 2015.



***Authors*: Assistant prof. Mijodrag Milošević, Assistant prof. Dejan Lukić**, **MSc Mića Đurđev, Associate prof. Aco Antić,** University of Novi Sad, Faculty of Technical Sciences, Department of Production Engineering, Trg Dositeja Obradovica 6, 21000 Novi Sad, Serbia, Phone: +381 21 485-2346, Fax: +381 21 454-495.

**Assistant prof. Stevo Borojević,** University of Banja Luka, Faculty of Mechanical Engineering, Vojvode Stepe Stepanovica 71, 78000 Banja Luka, Republika Srpska, BiH, Phone: +387 51 433 068.

E-mail: mido@uns.ac.rs
lukicd@uns.ac.rs
mdjurdjev@live.com
antica@uns.ac.rs
stevoborojevic@hotmail.com



**Note**: This paper is part of a research on project "Modern approaches to the development of special bearings in mechanical engineering and medical prosthetics", TR 35025, supported by the Ministry of Education, Science and Technological Development, Republic of Serbia.

Journal of Production Engineering
Vol.18 No.2
JPE (2015) Vol.18 (2) Original Scientific Paper
Chinchanikar, S., Kulkarni, A.P., Choudhury, S.K.

# HARD TURNING UNDER DRY AND MINIMUM QUANTITY LUBRICATION (MQL): COMPARATIVE ASSESSMENT THROUGH MULTI-OBJECTIVE OPTIMIZATION

Received: 15 November 2015 / Accepted: 30 November 2015

**Abstract:** *In present work, cutting parameters under dry and minimum quantity lubrication (MQL) were optimized to address the widely debated topic of application of coolants in hard turning. Mathematical models were developed to predict and optimize the machining performance in terms of three components of cutting force, surface roughness and tool life. Study reveals optimum cutting speed of 121 and 136 m/min under dry and MQL conditions. Experimental results shown a significant improvement in tool life, almost by 30% under MQL. However, no significant difference in the values of cutting forces and surface roughness was observed under dry and MQL conditions.*
**Key words:** *Hard turning, MQL, machining performance, multi-objective optimization.*

**Tvrdo struganje pri suvoj obradi i obradi minimalnom količinom sredstva za hlađenje (MQL): poređenje pomoću višekriterijumske analize.** *U ovom radu su predstavljeni rezultati optimizacije parametara rezanja kod suve obrade i obrade minimalnom količinom sredstva za hlađenje (MQL), sa ciljem doprinosa debati korišćenja sredstva za hlađenje tokom tvrde obrade. Generisani su matematički modeli za optimizaciju i predviđanje sila rezanja, hrapavosti obrađene površine i postojanosti alata. Istraživanje je pokazalo da su optimalne vrednosti brzine rezanja 121 m/min za suvu obradu i 136 m/min za obradu korišćenjem minimalne količine sredstva za hlađenje i podmazivanje. Experimenti pokazuju povećanje postojanosti alata za skoro 30% kod metode minimalne količine tečnosti za hlađenje. Međutim nije primećena značajna razlika kod vrednosti sila rezanja i hrapavosti obrađene površine između suve i obrade minimalnom količinom sredstva za hlađenje i podmazivanje.*
***Key words:*** *Tvrdo struganje, MQL, performanse obrade, višekriterijumska optimizacija.*

## 1. INTRODUCTION

Today, manufacturing is changing rapidly due to environmental replenishing and emerging technologies [1]. Demands for dry or machining with minimum quantity of lubrication (MQL) are increasing as cutting fluids pose a serious problem to the preservation of the environment and to human health [2]. Most of researchers have made great effort to compare dry cutting, wet cutting and cutting with MQL. Shokrani et al. [3] in their review article identified different cooling techniques which complement to reduce or eliminate the use of conventional cutting fluids.

A group of researchers [4-6] observed better performance under MQL than that of dry and conventional wet turning during turning of AISI 4340 steel. However, Bruni et al. [7] observed that MQL technique did not significantly reduce the tool wear, whilst wet cutting produced the worst surface finish. Liao and Lin [8] claimed that MQL provides extra oxygen to promote the formation of a protective oxide layer in between the chip–tool interface which acts as a diffusion barrier helps in improving the tool life. Leppert [9] found that the effectiveness of the cooling and lubricating technique to a large extent depends on the cutting parameters, namely the cutting speed and feed rate.

Dhar et al. [10-11] observed significant reduction in tool wear rate and surface roughness under MQL mainly through reduction in the cutting zone temperature and favorable change in the chip–tool and work–tool interaction. Kilickap [12] observed better performance in terms of surface characteristics under MQL condition than that of compressed air and dry drilling. Chinchanikar et al., [13] observed that hard turning under dry condition produced lower values of surface roughness; however, at higher cutting speeds they observed lower values of surface roughness with coconut oil. Khan et al. [14] claimed that MQL assists in lowering the tool wear rate due to abrasion, adhesion and diffusion type wear. Attanasio et al. [15] pointed out that although, MQL gives some advantage, but it presents difficulty in exactly reaching the lubricant at the cutting zone. Chinchanikar and Choudhury [16] observed improvement in tool life under MQL due to better cooling and lubricating effects.

From the literature reviewed, it has been observed that there is a disagreement between researchers about the use of coolants in hard turning. With this view, in the present work, cutting parameters under dry and minimum quantity lubrication (MQL) were optimized to address the widely debated topic of application of coolants in hard turning. The correlations between the cutting parameters and the performance measures, namely, three components of cutting force, surface roughness and tool life were developed based on experimental observations.

## 2. EXPERIMENTAL DETAILS

Hard turning experiments were performed on AISI 4340 steel (55 HRC) using TiSiN-TiAlN coated

carbide tool. A right hand style tool holder designated by ISO as PCBNR 2020K12 was used for mounting the insert. Central composite rotatable design matrix was used for planning of experiments [17].

Experiments were performed using a mist formed by minimum quantity of water-based cutting oil (60 ml/hr) and compressed air with a pressure of 5 bars. A minimum quantity of fluid flow was obtained by mixing the pressurized air and oil just outside of the nozzle. Nozzle used has two inlets, one for the cutting fluid and the other for the air at 90$^o$ to each other. A needle of a syringe was fixed at the outlet of the nozzle to obtain a minimum flow of cutting fluid. Detailing of the MQL set-up can be referred from the author's earlier work [16].

## 3. RESULTS AND DISCUSSION

### 3.1 Cutting forces and surface roughness

Average values of the cutting force components were measured by using a three-component piezo-electric dynamometer. Surface roughness values were measured by a Qualitest surface roughness tester. Experimental matrix along with results of cutting force components and surface roughness under dry and MQL is shown in Table 1(a). Analysis of the experimental results was performed using standard response surface methodology technique, so as to investigate the effect of cutting parameters on performance measures and to identify the region of interest where performance measures reached its optimum or near optimum value. Regression equations for tangential force ($F_c$), feed force ($F_f$), radial force ($F_r$) and surface roughness ($R_a$) which were developed based on experimental data using Stat-Ease Design Expert® software are shown below.

Cutting force components and Surface roughness (suffix D: Dry and M: MQL conditions),

$$F_{C_D} = -251.1 - 0.328V + 6385.1f - 5.294Vf + 0.002V^2 - 23210.2f^2 \quad (1)$$

$$F_{f_D} = -276.7 + 1.44V + 4808.5f - 19.4Vf + 0.001V^2 - 9116.2f^2 \quad (2)$$

$$F_{r_D} = -24.66 - 0.2616V + 3455.7f - 1.74Vf + 0.0009V^2 - 11960.6f^2 \quad (3)$$

$$F_{C_M} = -304.1 + 0.94V + 6290.5f - 16.47Vf + 0.002V^2 - 14449.6f^2 \quad (4)$$

$$F_{f_M} = -96.74 + 0.28V + 2917f - 11.17Vf + 0.002V^2 - 5276.1f^2 \quad (5)$$

$$F_{r_M} = -94.75 - 1.33V + 2524.9f + 1.17Vf + 0.003V^2 - 9148.4f^2 \quad (6)$$

$$R_{a_D} = 1.41 - 0.024V + 23.48f - 0.08Vf + 0.0001V^2 - 25.26f^2 \quad (7)$$

$$R_{a_M} = 5.07 - 0.065V + 4.76f + 0.058Vf + 0.0002V^2 - 24.05f^2 \quad (8)$$

The adequacies of the developed equations were checked by Analysis of Variance (ANOVA) technique. Results of the statistical analysis showed the values of R-Squared close to 1. The model F-values obtained showed that the developed models could be used to predict the responses and hence to support the optimization studies within the domain of the cutting parameters.

Curves showing the three components of cutting force are plotted by varying one of the input parameters and keeping the other parameters constant. Fig. 1(a) depicts that all the three components of cutting forces are marginally higher when machining under MQL in comparison to dry cutting conditions. The radial component of cutting force is the largest in magnitude and decrease in tangential component can be seen with the increase in cutting speed. However, this effect can be seen as more prominent when machining under dry cutting conditions due to thermal softening effect.

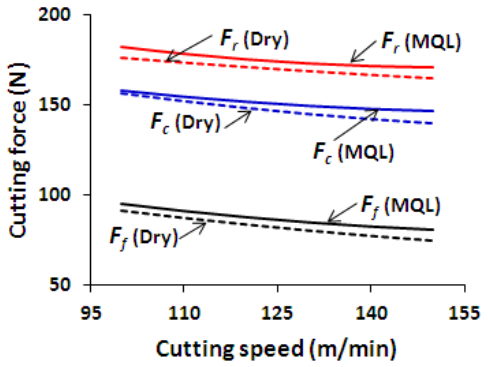

(a)

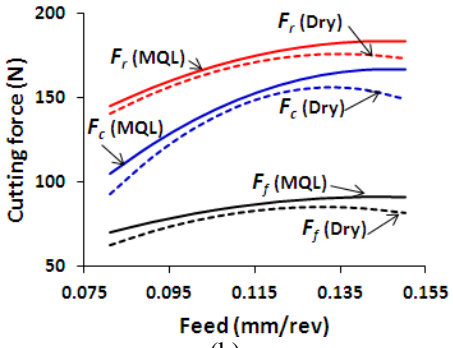

(b)

Fig. 1. Effect on cutting force when machining under dry and MQL conditions by (a) Cutting sped and (b) Feed

Fig. 1(b) depicts that cutting forces, especially the tangential force, initially vary almost linearly with feed, however remains practically unaltered at higher feed values when machining under MQL condition and decrease significantly when machining under dry cutting condition. ANOVA results revealed that cutting forces get affected mostly by feed (nearly 60 to 80 % contribution) and cutting speed has little influence. Cutting forces observed to be reduced significantly at higher cutting speed when coupled with higher values of feed which could be attributed to reduction in shear strength of the work material due to generation of higher temperature especially under dry cutting

condition [18].

Experiemtnal results showed lower values of surface roughness when machining under MQL conditions which could be attributed to better chip breaking and chip control under MQL in comparison to dry cutting. However, improvement in surface finish under MQL was not so significant as higher cutting forces employed in MQL resulted in more vibrations and hence, chatter marks remained on the machined surface. In summary, no significant benefit in terms of lowering the cutting forces and surface roughness could be obtained using MQL during hard turning.

| Expt. No. | $V$ (m/min) | $f$ (mm/rev) | Dry | | | | MQL | | | |
|---|---|---|---|---|---|---|---|---|---|---|
| | | | $F_c$ (N) | $F_f$ (N) | $F_r$ (N) | $R_a$ (μm) | $F_c$ (N) | $F_f$ (N) | $F_r$ (N) | $R_a$ (μm) |
| 1 | 150 | 0.113 | 78 | 162 | 144 | 1.4 | 79 | 172 | 152 | 1.38 |
| 2 | 108 | 0.138 | 102 | 176 | 163 | 1.68 | 99 | 190 | 174 | 1.63 |
| 3 | 108 | 0.088 | 68 | 149 | 111 | 1.29 | 76 | 161 | 115 | 1.31 |
| 4 | 100 | 0.113 | 89 | 181 | 157 | 1.58 | 97 | 179 | 159 | 1.57 |
| 5 | 142 | 0.088 | 69 | 148 | 102 | 1.29 | 78 | 149 | 118 | 1.09 |
| 6 | 125 | 0.113 | 85 | 168 | 144 | 1.42 | 89 | 173 | 148 | 1.36 |
| 7 | 142 | 0.138 | 70 | 172 | 145 | 1.53 | 82 | 180 | 149 | 1.51 |
| 8 | 125 | 0.113 | 82 | 174 | 141 | 1.41 | 88 | 178 | 146 | 1.34 |
| 9 | 125 | 0.113 | 86 | 167 | 147 | 1.47 | 85 | 172 | 158 | 1.29 |
| 10 | 125 | 0.15 | 81 | 175 | 151 | 1.64 | 83 | 183 | 172 | 1.53 |
| 11 | 125 | 0.081 | 64 | 141 | 97 | 1.15 | 68 | 144 | 106 | 1.13 |
| 12 | 125 | 0.113 | 78 | 171 | 147 | 1.42 | 83 | 170 | 150 | 1.34 |
| 13 | 125 | 0.113 | 81 | 169 | 154 | 1.38 | 87 | 176 | 152 | 1.35 |

Table 1(a). Experimental matrix showing results of force and surface roughness under dry and MQL

### 3.2 Tool life model

Dino-Lite, a compact digital microscope powered by USB was used to monitor flank wear and its growth at regular intervals of length of cut. Experimental results of tool life which was obtained at different cutting conditions using constant depth of cut of 0.3 mm is shown in Table 1(b).

| Condition index | $V$ (m/min) | $f$ (mm/rev) | Tool life ($T$) (min) | |
|---|---|---|---|---|
| | | | Dry | MQL |
| 1 | 150 | 0.113 | 16 | 22 |
| 2 | 108 | 0.138 | 63 | 79 |
| 3 | 108 | 0.088 | 85 | 99 |
| 4 | 100 | 0.113 | 71 | 95 |
| 5 | 142 | 0.088 | 32 | 43 |
| 6 | 125 | 0.113 | 44 | 56 |
| 7 | 142 | 0.138 | 23 | 33 |
| 8 | 125 | 0.15 | 38 | 49 |
| 9 | 125 | 0.081 | 60 | 72 |

Table 1(b). Experimental matrix and results for tool life test under dry and MQL conditions

A typical tool nose wear progression under dry and MQL is shown in Fig. 2. Plot reveal higher tool life under MQL in comparison to dry cutting as in case of MQL the cutting tool edge sustained for longer time. In almost all the cutting conditions, chipping at the nose of the tool was observed. Results of tool life ($T$) were analyzed using the least square error method. A modified Taylor tool life equation shown below was developed based on experimental observations. The exponent of speed, feed and values of constant were determined using Data-Fit software.

Tool life model (suffix D: Dry and M: MQL conditions),

$$T_D = 272.24 \times 10^6 V^{-3.593} f^{-0.748} \quad (9)$$

$$T_M = 134.4 \times 10^6 V^{-3.328} f^{-0.6069} \quad (10)$$

From the values of exponents and constant, it can be seen that cutting speed is the most influencing parameters on tool life. However, this effect can be seen as more prominent when machining under dry cutting condition. Table 1(b) depicts higher tool life under MQL; however, an increase in tool life can be seen as more significant at higher cutting speed and feed under MQL. Low tool life under dry condition, especially at higher cutting speeds was due to sudden fracture of the tool due to weakening of the cutting edge by an accelerated crater wear rate.

## 4. MULTI-OBJECTIVE OPTIMIZATION

In view of disagreement between the researchers about the use of coolants in hard turning, the optimum values of cutting parameters, which produce better tool life, minimum cutting forces and surface roughness under dry and MQL were obtained and compared. Optimization study was carried out in two different modules [19]. The first module generates a set of solutions which ensures minimum surface roughness and cutting forces. The second module selects a most optimum cutting condition among the solutions generated in module 1, which gives better tool life.

The Design Expert software was used to find the optimum cutting conditions, which ensures minimum cutting forces and surface roughness (module 1) as given in Table 2 (columns 1 to 4). The optimum cutting

conditions which ensures minimum cutting forces and surface roughness under dry and MQL are shown by their highest desirability level ($D_{PSR}$). Further, optimization study considering the tool life

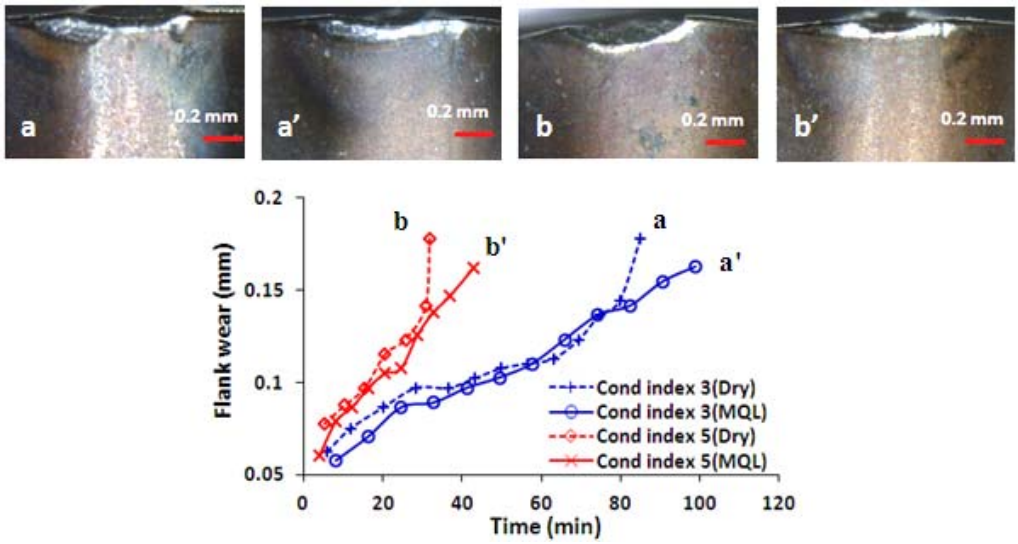


Fig. 2. Nose wear with time of cutting at $f$ = 0.088 mm/rev, and $V$ = 108 m/min (condition index 3) and $V$ = 142 m/min (condition index 5). Tool images indicate tool condition at the end of cutting shown by letters

| Sr. No. | $V$ (m/min) | $f$ (mm/rev) | 1 | 2 | 3 | 4 | 5 | 6 | 7 | 8 |
|---|---|---|---|---|---|---|---|---|---|---|
| | | | $F_c$ (N) | $F_f$ (N) | $F_r$ (N) | $R_a$ | $D_{PSR}$ | $T$ (min) | $D_T$ | $D_m$ |
| Dry cutting condition | | | | | | | | | | |
| 1 | 132.42 | 0.088 | 70 | 148 | 108 | 1.24 | 0.839 | 39.8 | 0.60 | 0.71 |
| 2 | 129.65 | 0.088 | 69 | 148 | 108 | 1.23 | 0.838 | 42.9 | 0.68 | 0.76 |
| 3 | 136.42 | 0.088 | 71 | 147 | 107 | 1.24 | 0.837 | 35.8 | 0.49 | 0.64 |
| 4 | 139.93 | 0.088 | 71 | 146 | 107 | 1.25 | 0.833 | 32.6 | 0.41 | 0.59 |
| **5*** | **121.07** | **0.088** | **68** | **150** | **110** | **1.24** | **0.827** | **54.9** | **1.00** | **0.91** |
| MQL cutting condition | | | | | | | | | | |
| **1*** | **135.93** | **0.088** | **75** | **151** | **120** | **1.12** | **0.842** | **46.5** | **1.00** | **0.92** |
| 2 | 137.01 | 0.088 | 75 | 150 | 120 | 1.12 | 0.842 | 45.3 | 0.95 | 0.89 |
| 3 | 138.41 | 0.088 | 75 | 150 | 120 | 1.12 | 0.841 | 43.8 | 0.88 | 0.86 |
| 4 | 139.54 | 0.088 | 75 | 150 | 121 | 1.12 | 0.840 | 42.6 | 0.83 | 0.83 |

*Optimized cutting parameters are shown in bold-case.

Table 2. Optimized cutting parameters under dry and MQL conditions

as one of the important aspects, was performed using the similar line of approach as discribed in ref. [19]. Tool life for each of the solutions generated in module 1, was calculated using Eqs. 9 and 10, namely, for dry and MQL conditions. Desirability for tool life ($D_T$) was calculated using one sided transformation as given in Eqs. 11 and 12,

$$D_T = \begin{cases} 0, \mathrm{T} \le 17.08 \\ \left[ \dfrac{\mathrm{T} - \mathrm{T}_{\min}}{\mathrm{T}_{\max} - T_{\min}} \right], 17.08 < \mathrm{T} < 54.97 \\ 1, \mathrm{T} \ge 54.97 \end{cases} \quad (11)$$

$$D_T = \begin{cases} 0, \mathrm{T} \le 24.25 \\ \left[ \dfrac{\mathrm{T} - \mathrm{T}_{\min}}{\mathrm{T}_{\max} - T_{\min}} \right], 24.25 < \mathrm{T} < 46.53 \\ 1, \mathrm{T} \ge 46.53 \end{cases} \quad (12)$$

Minimum limit of tool life ($T_{min}$) was calculated by substituting the higher values of cutting conditions in Eqs. 9 and 10 ($V$ = 150 m/min and $f$ = 0.15 mm/rev). Maximum limit of tool life ($T_{max}$) was selected from the set of solutions generated in module 1. In this way, $D_T$ was calculated as shown in column 7 of **Table 2**. Then, a single desirability function ($D_m$) was calculated, which is the geometric mean of the $D_{PSR}$ and $D_T$. The solution having the highest desirability is the optimum solution which ensures minimum cutting forces, surface roughness and better tool life as shown by bold face.

It can be seen that a cutting speed of 121 and 136 m/min and lower value of feed of 0.088 mm/rev when using constant depth of cut of 0.3 mm, are the optimum cutting conditions under dry and MQL cutting for better tool life, minimum cutting forces and surface roughness. A significant improvement in tool life, almost by 30% can be seen under MQL condition. Improvement in tool life under MQL can be attributed to lower cutting temperature resulting in reduced tool wear rate due to

chances of built-up edge formation and hence adhesion wear. Also, lower cutting temperature under MQL condition assisting in reducing abrasion by retaining tool hardness and temperature dependent diffusion types of wear.

## 5. CONCLUSIONS

In present work, the cutting parameters were optimized under dry and minimum quantity lubrication (MQL) to address the widely debated topic of application of coolants in hard turning. It has been observed that hard turning under MQL condition produced a significant improvement in tool life by almost 30% in comparison to dry cutting. However, no significant benefit in terms of lowering the cutting forces and surface roughness has been observed under MQL condition. It has been observed that a cutting speed of 136 m/min and lower values of feed and depth of cut of 0.088 mm/rev and 0.3 mm, respectively, is the optimum cutting condition under MQL hard turning. Nose wear, chipping off at the nose and clearance face were observed as dominant wear forms.

## 6. REFERENCES


[1] Grzesik, W.: *Advanced machining processes of metallic materials*, Elsevier, 2008.

[2] Diniz, A.E., Ferreira, J.R., Filho, F.T.: *Influence of refrigeration/lubrication condition on SAE 52100 hardened steel turning at several cutting speeds*, International Journal of Machine Tools and Manufacture, 43, p.p. 317–326, 2003.

[3] Shokrani, A., Dhokia, V., Newman, S.T.: *Environmentally conscious machining of difficult-to-machine materials with regard to cutting fluids*, International Journal of Machine Tools and Manufacture, 57, p.p. 83–101, 2012.

[4] Vikram Kumar, C.H.R., Ramamoorthy, B.: *Performance of coated tools during hard turning under minimum fluid application*, Journal of Materials Processing Technology, 185, p.p. 210–216, 2007.

[5] Kang, M.C., Kim, K.H., Shin, S.H., Jang, S.H., Park, J.H., Kim, C.: *Effect of the minimum quantity lubrication in high-speed end-milling of AISI D2 cold-worked die steel (62 HRC) by coated carbide tools*, Surface Coating Technology, 202(22-23), p.p. 5621–5624, 2008.

[6] Varadarajan, A.S., Philip, P.K., Ramamoorthy, B.: *Investigations on hard turning with minimal cutting fluid application (HTMF) and its comparison with dry and wet turning,* International Journal of Machine Tools and Manufacture, 42, p.p. 193–200, 2002.

[7] Bruni, C., Forcellese, A., Gabrielli, F., Simoncini, M.: *Effect of the lubrication-cooling technique, insert technology and machine bed material on the work part surface finish and tool wear in finish turning of AISI 420B*, International Journal of Machine Tools and Manufacture ,46, p.p. 1547–1554, 2006.

[8] Liao, Y.S., Lin, H.M.: *Mechanism of minimum quantity lubrication in high-speed milling of hardened steel,* International Journal of Machine Tools and Manufacture, 47, p.p. 1660–1666, 2007.

[9] Leppert, T.: *Effect of cooling and lubrication conditions on surface topography and turning process of C45 steel*, International Journal of Machine Tools and Manufacture, 51, p.p. 120–126, 2011.

[10] Dhar, N.R., Kamruzzaman, M., Ahmed, M.: *Effect of minimum quantity lubrication (MQL) on tool wear and surface roughness in turning AISI-4340 steel*, Journal of Materials Processing Technology, 172, p.p. 299–304, 2006.

[11] Dhar, N.R., Ahmed, M.T., Islam. S.: *An experimental investigation on effect of minimum quantity lubrication in machining AISI 1040 steel,* International Journal of Machine Tools and Manufacture, 47, 748–753, 2007.

[12] Kilickap, E.: *Empirical study regarding the effects of minimum quantity lubricant utilization on performance characteristics in the drilling of Al 7075*, Journal of Brazilian Society of Mechanical Science and Engineering, 33(1), p.p. 52-57, 2011.

[13] Chinchanikar, S., Salve, A.V., Netke, P., More, A., Kendre, S., Ramesh Kumar.: *Comparative evaluations of surface roughness during hard turning under dry and with water-based and vegetable oil-based cutting fluids*, Procedia Material Science, 5, p.p. 1966–1975, 2014.

[14] Khan, M.M.A., Mithu, M.A.H., Dhar, N.R.: *Effects of minimum quantity lubrication on turning AISI 9310 alloy steel using vegetable oil based cutting fluid*, Journal of Materials Processing Technology, 209, p.p. 5573–5583, 2009.

[15] Attanasio, A., Gelfi, M., Giardini, C., Remino, C.: *Minimal quantity lubrication in turning: Effect on tool wear*, Wear, 260, p.p. 333–338, 2006.

[16] Chinchanikar, S., Choudhury, S.K.: *Hard turning using HiPIMS-coated carbide tools: Wear behavior under dry and minimum quantity lubrication (MQL)*, Measurement, 55, p.p. 536- 548, 2014.

[17] Cochran, W.G., Cox, G.M.: *Experimental Designs*, John Wiley and Sons Inc., New York, 1957.

[18] Chinchanikar, S., Choudhury, S.K., Kulkarni, A.P.: *Investigation of chip-tool interface temperature during turning of hardened AISI 4340 alloy steel using multi-layer coated carbide inserts,* Advance Material Research, 701, p.p. 354-358, 2013.

[19] Chinchanikar, S., Choudhury, S.K.: *Effect of work material hardness and cutting parameters on performance of coated carbide tool when turning hardened steel: An optimization approach,* Measurement 46:1572-1584, 2013.



***Authors:*** **Dr. Satish Chinchanikar, Professor, Mr. A.P. Kulkarni**, **Associate Professor**, Department of Mechanical Engineering, Vishwakarma Institute of Information Technology, Pune, India and **Dr. S. K. Choudhury, Professor**, Department of Mechanical Engineering, Indian Institute of Technology Kanpur, India, Phone.: +91-020-26950200/400, Fax: +91-020-26950450.
E-mail: satish.chinchanikar@viit.ac.in, atul.kulkarni@viit.ac.in, choudhry@iitk.ac.in

Journal of Production Engineering
Vol.18 No.2
JPE (2015) Vol.18 (2) Original Scientific Paper
Gostimirović, M., Rodić, D., Kovač, P., Jesić, D., Kulundžic N.

# INVESTIGATION OF THE CUTTING FORCES IN CREEP-FEED SURFACE GRINDING PROCESS

Received: 27 September 2015 / Accepted: 29 October 2015

**Abstract:** *This paper examines the value and character of cutting forces in the creep-feed surface grinding. In order to identify the impact of cutting forces on the state of the process of deep grinding, according on the elements of the machining, experimental tests were determined dependence of the tangential and normal components of the grinding forces and ratio grinding force. In comparison with the traditional multi-pass grinding results show the occurrence of higher cutting forces in creep-deep surface grinding, especially normal components.*
***Key words:*** *creep-feed grinding, cutting forces, grinding force ratio, machining conditions*

**Istraživanje sila rezanja pri ravnom dubokom brušenju.** *U radu se istražuju vrednosti i karakter sila rezanja pri dubokom ravnom brušenju. U radu se istražuju vrednosti i karakter srednjih sila rezanja pri dubokom ravnom brušenju. Da bi se identifikovao uticaj sila rezanja na stanje procesa dubokog brušenja, u zavisnosti od elemenata režima obrade, eksperimentalnim ispitivanjima su određene zavisnosti specifične tangencijalne i normalne komponenti sile brušenja, kao i odnos tih sila. U odnosu na klasično višeprolazno brušenje, dobijeni rezultati ukazuju na pojavu viših sila rezanja pri dubokom ravnom brušenju, pogotovo normalne komponente.*
***Ključne reči:*** *duboko brušenje, sile rezanja, odnos sila brušenja, režimi obrade*

## 1. INTRODUCTION

Grinding is one of the most important methods of machining material. The basic advantages of grinding are high-accuracy machining and surface quality, the ability to process hard and machining difficult to cut materials or complex surfaces shapes [1].

In recent years, in addition to the classic multi-pass grinding, which is used for finishing operations, high productivity grinding processes are applied, which allow the use of grinding in the roughing and finishing operations [2, 3]. In these highly productive grinding procedures, increasing cutting speeds and/or depth of cut, significantly increasing productivity is relatively small, which has long been disadvantage of the classic grinding.

Deep grinding, as a representative of the highly productive grinding processes, increase productivity and reduce total processing time realizes one pass grinding with large depths of cut and low-speed auxiliary movement of the workpiece [4, 5]. On the other hand, due to the increase in the length and time of contact with the workpiece wheels, increases spending desktop grinding wheels, grinding temperature and cutting forces.

This paper analyzes the cutting forces in the creep-feed surface grinding and experimentally determined mean values of cutting force of abrasive grains that is currently in in the grip with the workpiece. Cutting forces are determined depending on the treatment regime for two types of corresponding wheels.

## 2. CUTTING FORCES IN GRINDING

The forces that occur in the processing of grinding as resistance to penetration into the workpiece by grinding grain, as a result of plastic deformation in the cutting zone and friction between the grinding surface and workpiece [6 , 7]:

$$F = F_{deformation} + F_{friction} \tag{1}$$

Cutting force one abrasive grain $F_{grain}$ and total force on grinding wheel were created at the same time by the number of active grains that are catched in the workpiece. In the research process dynamics processing grinding is used the total mean cutting force, because the cutting force of one abrasive grain is not significant [8]:

$$F = \sum_{1}^{N_a} F_{grain} \tag{2}$$

The size and character of the grinding force depends on machining conditions, characteristics of the grinding wheel, workpiece material, stiffness of machining system, cooling conditions, the process of dressing etc.

### 2.1. Mechanism of grinding process

The cutting process in grinding is achieved through simultaneously a large number of abrasive grains catch a very thin layer of material that is placed in the space between two abrasive grains and pores, Figure 1. When abrasive grains come out of catch with the material, chips leave the area under the influence of centrifugal force, or due to flushing agent for cooling and lubrication.

The process of cutting when grinding is defined by the kinematic and geometric parameters. Kinematic parameters are: cutting speed $v_s$ and workpiece speed $v_w$, respectively, feed $s$ if there is movement. The geometrical parameters are: wheels diameter $D_s$, workpiece diameter $D_w$, depth of cut $a$, the length of contact $l_c$ and average chip thickness $h_m$.

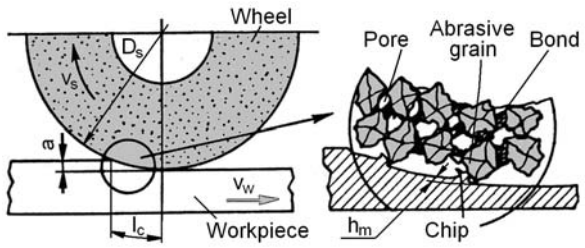


Fig. 1. Mechanism of grinding process

The length of contact of surface grinding is distance that actively grain exceeds from the moment of contact with the workpiece exit from a contact:

$$l_c = \sqrt{a \cdot D_s} \tag{3}$$

The average chip thickness is imaginary thickness that each time cutting abrasive grains, and is determined by:

$$h_m = \frac{a \cdot v_w}{v_s} = \frac{Q'}{v_s} \tag{4}$$

where is $Z'=a \cdot v_w$ - specific productivity grinding.

### 2.2. Components of the grinding force

Generally, in the processing of grinding occur resulting cutting forces. For practical reasons, the resulting force is split into components in several interesting directions. In the case of surface grinding, where there is no lateral movement of the table, usually resulting force has been divided: tangential (extensive) component Ft and normal (radial) component Fn.

Tangential component acts in the direction of the tangent to the surface of the grinding wheel and workpiece contact, i.e. in the direction of cutting speeds. The normal component acts normally to the surface of the wheels and workpiece. As the diameter of the wheels is far greater than the depth of cut, it can be assumed that the tangential and normal component supine in a horizontal or vertical plane, Figure 2.

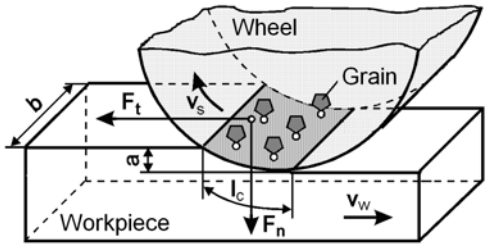


Fig. 2. Components of the grinding force

The relationship of normal and tangential components of the grinding forces is defined as the grinding force ratio:

$$\lambda = \frac{F_n}{F_t} = \frac{F'_n}{F'_t} \tag{5}$$

In the previous equation, the components of the grinding forces are reduced per unit width of grinding *b*, referred to as the specific grinding force:

$$F'_t = \frac{F_t}{b}$$
$$F'_n = \frac{F_n}{b} \tag{6}$$

Tangential grinding force is authoritative for determining the driving power machine tools, while the normal force significant from the point of processing accuracy and high surface quality. These components of the cutting forces during grinding are determined by measurement and calculation. To measure is applied dynamometers, to give the exact value of the force but, the defined conditions of processing. Calculation of forces grinding through analytical dependences obtained for certain processing conditions during experimental tests, limited test area, while the use of theoretically derived forms, because of its generality usually unreliable.

Generally known empirical equation for determining tangential (main) grinding forces, analogous expressions by Kronenberg in 1927, reads as follows [1]:

$$F'_t = h_m \cdot k_{mc} \tag{7}$$

where is $k_{mc}$ - main unit cutting force.

One of the most popular analytical models for assessing the normal components of the grinding forces was developed by Werner and is expressed by the following equation [9]:

$$F'_n = K \cdot \left( \frac{Q'}{v_s} \right)^{2\epsilon-1} \cdot a^{\epsilon} \cdot D_s^{1-\epsilon} \tag{8}$$

where is $K$ - proportionality factor and $\varepsilon$ - exponent whose value depends on the specific workpiece material.

## 3. EXPERIMENTAL SETUP

### 3.1. Conditions of the experimental setup

Workpiece material used in the experimental setup was the molybdenum high speed steel (HSS), which is widely used in the industry of cutting tools. Designation of the selected speed steel is DIN S 2-10-1-8. This steel belongs to a group of ledeburite steel with a microstructure consisting of martensite and fine mixtures of primary and secondary ledeburite cementite. The chemical composition of the test material was: 1,08 % C; 0,22 % Si; 0,23 % Mn; 0,014 % P; 0,019 % S; 4,1 % Cr; 1,5 % W; 9 % Mo; 1,1 % V and 8 % Co. Measured hardness on all samples ranged 66 ± 1 HRC. Experimental samples consisted of tiles measuring 40 × 20 × 16 mm.

Based on the recommendations, the chosen material of the workpiece and set the conditions of processing were selected two wheels similar characteristics: wheels »Norton« type 32A54 FV BEP and size 400×80×127 mm, respectively »Winterthur« type 53A80 F15V PMF and size 400×50×127 mm. The wheels are with high-quality abrasive grain, medium grain size, hardness soft, open structure with ceramic binder. All experiments were conducted with sharp wheels, and sharpening is done with a diamond planer alignment with a depth of 0,01 mm/speed and displacement of 0,1 mm/rev.

The machining conditions included variable depths of cut and workpiece speed. The depth of cut was $a$ = 0,05; 0,1; 0,25; 0,5; 1 mm and the workpiece speed was

$v_w$ = 2,5; 5; 10; 25; 50 mm/s. The adopted mean value of specific material removal rate is $Q'$ = 2,5 mm$^3$/mm·s. The wheel speed was held constant $v_s$ = 30 m/s.

### 3.2. Experimental procedures

Measuring the forces that occur during surface grinding was done using three component dynamometer »Kistler Instrumente AG«, type 9257. Used dynamometer works on the piezoelectric principle, which is reflected in the emergence of electricity on the surface of the crystal plate embedded in the dynamometer when the same force is exerted pressure. Electricity is amplified by means of amplifiers capacitive »Kistler«, type CA 5001 and then is converted into DC voltage in size from 0 to 10 V.

Measurement, analysis and control of the grinding force was performed using the information of the measuring system [10], where data acquisition is implemented by AD cards and cash integrated software package, Figure 3. The set information measurement data acquisition system is characterized by a high degree of accuracy, reliability, speed of response and the ability to reproduce measurement results. It allows real-time measurements, timely intervention if they appear illogical results, as well as comprehensive and rapid processing and analysis of results.

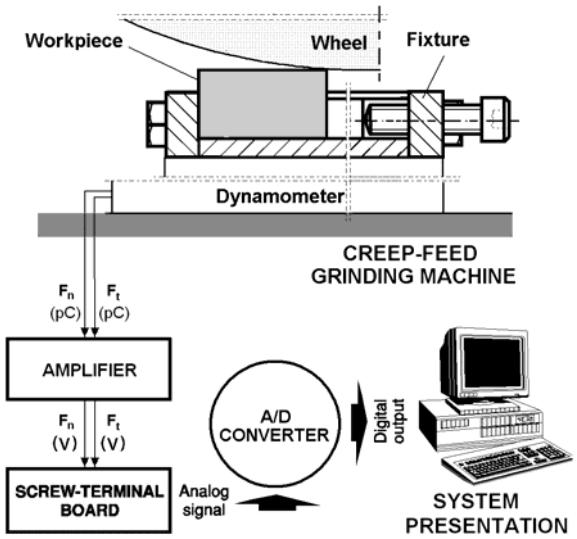


Fig. 3. Information system for measuring and processing of cutting forces during grinding

## 4. RESULTS

The measured values of the normal and tangential grinding force, depending on the mode of processing elements, point to a very reliable and safe measurement of the force components in the flat deep grinding. An example of measurement results of the cutting force during deep grinding, two wheels with similar characteristics but different manufacturers, is shown in Figure 4. It can be concluded that for the same processing conditions obtained different values of force components sanding, or about the same dynamic character.

Figure 5 and 6 are given depending on the specific components of cutting forces, as well as their relationship $F'_n/F'_t$, depending on the cutting depth and workpiece speed for two selected wheels. With diagrams shown it can be concluded that with increased cutting depth grinding forces are rising and decrease with increasing rotation of the workpiece.

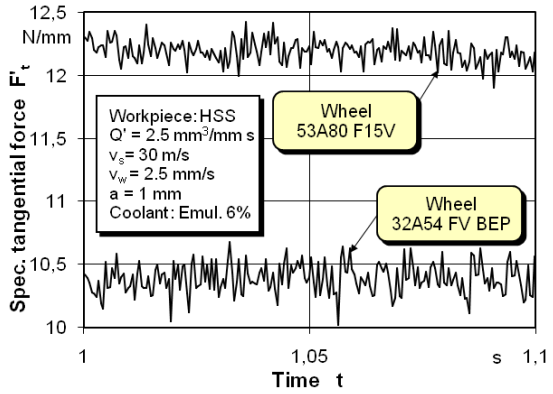


Fig. 4. Value and character of the measured tangential grinding force components

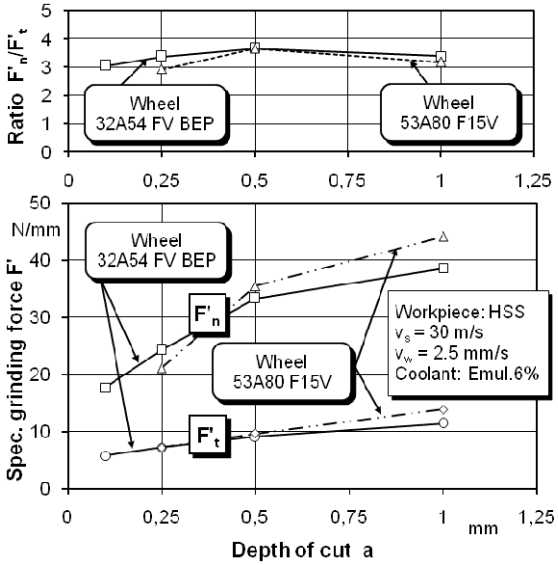


Fig. 5. The grinding forces, depending on the depth of cut

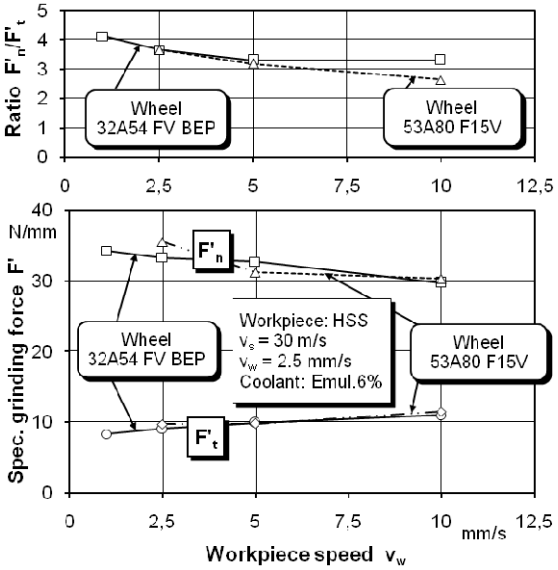


Fig. 6. The grinding forces, depending on the cutting speed

Changing of cutting force in grinding, depending on the elements of the treatment regime, and a constant specific productivity of grinding, is shown in Figure 7. The diagram shows that compared to conventional grinding, in creep-feed grinding appear higher cutting forces.

The ratio of normal and tangential grinding forces moved to within 2÷4, except that higher values related to creep-feed grinding.

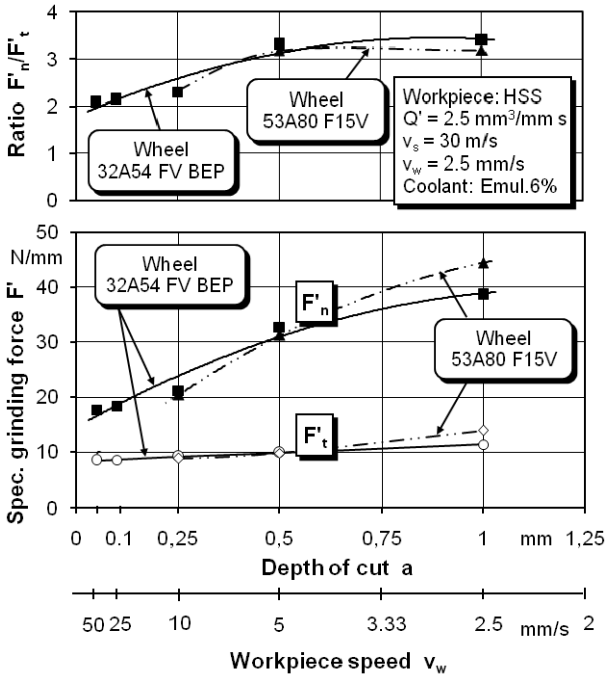


Fig. 7. Changing the cutting force depending on the elements of the treatment regime for creep-feed grinding

## 5. CONCLUSIONS

Based on the conducted experimental research and analysis can be performed the following conclusions:

- When creep-feed grinding reduces processing time, but also increase the cutting force;
- Cutting forces primarily depend on the type of workpiece material and elements of its processing;
- Cutting forces during creep-feed grinding, due to a greater number of active abrasive grains into engagement with the workpiece material, are significantly higher compared to conventional grinding;
- the grinding forces, the increasing length of contact of the grinding wheel and workpiece material, with increasing depth of cut growth;
- increase the speed of the workpiece grinding forces decrease because it reduces the cross-section of the affected layers of material by grinding grain;
- In creep-feed grinding can be observed greater grinding force ratio;
- Cutting forces during creep-feed grinding allow identification of the energy balance of machine tools and estimation of the level of accuracy in different processing conditions.

## 6. REFERENCES


[1] König, W.: *Fertigungsverfahren, Band 2 - Schleifen, Honen, Läppen*. VDI-Verlag GmbH, Düsseldorf, 1980.

[2] Kopac, J., Krajnik, P.: *High-performance grinding - A review*, Journal of Materials Processing Technology, Vol.175, No.1-3, pp. 278-284, 2006.

[3] Kovac, P., Gostimirovic, M., Sekulic, M., Savkovic, B.: *A review of research related to advancing manufacturing technology*, Journal of Production Engineering, Vol.12, No.1, pp. 9-16, 2009.

[4] Gostimirovic, M., Sekulic, M., Kopac, J., Kovac, P.: *Optimal control of workpiece thermal state in creep-feed grinding using inverse heat conduction analysis*, Strojniški vestnik - Journal of Mechanical Engineering, Vol.57, No.10, pp. 730-738, 2011.

[5] Gostimirovic, M., Kovac, P., Jesic, D., Skoric, B., Savkovic, B.: *Surface layer properties of the workpiece material in high performance grinding*, Metalurgija, Vol.51, No.1, pp. 105-108, 2012.

[6] Malkin, S., Guo, C.: *Grinding Technology - Theory and Applications of Machining with Abrasives*, Industrial Press, New York, 2008.

[7] Mishra, V.K., Salonitis, K.: *Empirical estimation of grinding specific forces and energy based on a modified Werner grinding model*, Procedia CIRP, Vol.8, pp. 287-292, 2013.

[8] Durgumahanti, U.S.P., Singh, V., Rao, P.V.: *A New Model for Grinding Force Prediction and Analysis*, International Journal of Machine Tools & Manufacture, Vol.50, pp. 231-240, 2010.

[9] Werner, G.: *Influence of work material on grinding forces*, Annals of CIRP, Vol.27, pp. 243-248, 1978.

[10] Gostimirovic, M., Kovac, P., Sekulic, M.: *An inverse heat transfer problem for optimization of the thermal process in machining*. Sadhana, Vol.36, No.4, pp. 489-504, 2011.


## ACKNOWLEDGEMENTS


The paper is the result of the research within the project TR 35015 (2011/15) financed by the Ministry of Education, Science and Technological Development of the Republic of Serbia and CEEPUS project..



***Authors:*** **Prof. dr Marin Gostimirović[1], M.Sc Dragan Rodić[1], Prof. dr Pavel Kovač[1], Dr Dusan Jesić[2], M.Sc Nenad Kulundžic[1].**

[1]University of Novi Sad, Faculty of Technical Sciences, Departman for Production Engineering, Trg Dositeja Obradovica 6, 21000 Novi Sad, Serbia, Phone: +381 21 450-366, Fax: +381 21 454-495.

[2]Tribotehnik, Titov trg 6/4, 51000 Rijeka, Croatia.

E-mail: maring@uns.ac.rs
rodicdr@uns.ac.rs
pkovac@uns.ac.rs
dusan.jesic@ri.hiner.hr
kulundzic@uns.ac.rs

Journal of Production Engineering
Vol.18 No.2
JPE (2015) Vol.18 (2) Original Scientific Paper
Kulundzic, N., Gostimirovic, M., Kovac, P., Sekulic, M., Savkovic, B.

# MICRO CUTTING SIMULATION OF ABRASIVE GRAINS IN THE GRINDING PROCESS

Received: 21 August 2015 / Accepted: 27 October 2015

***Abstract:*** *In the current work we present approach to study the mechanism of the cutting of abrasive grains in the grinding wheel using finite element analysis (FEA). The simulation process is done by separating two abrasive grains from the grinding wheels and the microprocess of material removal in the case of surface grinding is simulated. Modelling was done on the workpiece steel S-7 and material grain is SiC. Simulations of abrasive grains in the grinding process are performed by different conditions. Workpiece and abrasive grains are modelled using CREO Parametric software, and micro cutting simulation are done using ANSYS. Defining a finite element mesh, cutting regimes and material characteristic provided a temperature analysis with a lot of details and also an appearance of the grinding process.*
***Key words:*** *grinding modelling and simulation, finite element analysis, micro cutting temperature*

**Simulacija mikro rezanja abrazivnim zrnima pri procesu brušenja.** *U ovom radu prikazano je istraživanje o sečenju abrazivnim zrnima brusnog tocila, koristeći konačne elemente. Proces simulacije je izveden izdvajanjem dva abrazivna zrna iz brusnog tocila i simuliran je mikro proces skidanja materijala za slučaj ravnog brušenja. Materijal modela obratka je Steel S-7, a materijal zrna je SiC. Simulacija abrazivnih zrna pri procesu brušenja se obavlja u različitim uslovima. Obradak i abrazivna zrna modelirani su pomoću programa Creo Parametric, a simulaciju mikro rezanja je urađena uz pomoć programa ANSYS. Definisanje mreže konačnih elemenata, režima obrade i karakteristika materijala obezbeđuju analizu temperature sa mnogo detalja i takođe pojavu procesa brušenja.*
***Ključne reči:*** *modeliranje zrna i simulacija, metoda konačnih elemenata, temperatura pri mikro rezanju*

## 1. INTRODUCTION

Grinding is a highly precise manufacture process with the material removal applied in the various machine parts processing. Primarily it is applied to the finishing processing of the hard surfaces of the flat, cylindrical and complex shapes.

On the other side, the grinding process represents one of the most complex cutting processes. The complexity of the grinding process is caused by the simultaneous cutting of a large number of grinding grains uneven and undefined cutting geometry, which is constantly changing during the grinding process. In addition, unlike others processing methods with defined cutting geometry, there is no possibility to have a constant contact of the grinding grains with the workpiece during the grinding process. [1,2].

The cutting process of the grinding is achieved by a large number of grinding grains simultaneously process a very thin layer of a material. In that way, a large amount of micro chip is formed and it is placed between two adjacent grinding grains. When the grinding grains lose the contact with the material, the chip leaves the area by the influence of the centrifugal force or due to the cooling and lubricating liquid.

Even the grinding process is very difficult to analyse, the average shape of grinding grain can be isolated and through that grain the general mechanism of grinding process can be described, Figure 1. During the active cutting by the grinding grain the thickness of the cutting layer $h_{eff}$ is changing from zero to the maximum value. The process of the grinding grain acting to the workpiece material can be conditionally divided into 3 characteristic phases. In the first phase the grinding grain penetrates into the material and it comes to the elastic deformation of the material. In the second phase plastic deformation and the flow of material are realized. The second phase lasts until the grain penetrates to a certain depth in the workpiece, when the real chip formation begins. In the third phase simultaneously comes to material extrusion and chip forming. How many the material of workpiece will form the chip, and how many will be pressed, depends on the geometry of the grinding grain and the elements of the grinding mode. [3,4].

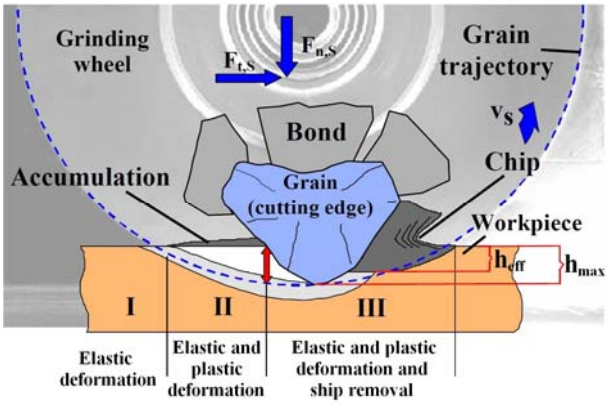


Fig. 1. Phases of chip formation in grinding [3]

Beside the elastic and plastic deformation, all 3 phases are accompanied by great friction between the surfaces of the grain and material. Therefore, it can be argued that the grinding process represents a mixture of the productive cutting (chip formation) and unproductive cutting (workpiece surface friction). If during the grinding process unproductive cutting prevails, a large amount of heat is developed, resulting in intense wearing of the working surface of the grinding wheel and it worsens the processing quality.

## 2. GRINDING TEMPERATURE

Intense heat generation and difficulty of its evacuation from the cutting zone leads to creation of high grinding temperature and can result in high thermal load of wheel and workpiece. This thermal load, mainly of workpiece, is a boundary condition for a further development of grinding process [5-8].

The study of thermal phenomena during the grinding process dates back to the mid-twentieth century. In the initial phase, this area of science about material removal primarily relied on experimental tests and theoretical analyses until the end of the ’70 when the mathematical process models are begun to be used which are solved by numerical methods.

Past years, the numerical methods, especially finite element method (FEM), becomes the main procedure in the simulation of metal cutting. Recently, programming systems are developed based on the finite elements method, which are only intended for the simulation of cutting process. Among scientists, that have examined this problematic couple of them have made quite interesting results [9-11].

## 3. FINITE ELEMENT ANALYSIS

Computer application has brought revolutionary changes in the field of different engineering and scientific disciplines, and one of the first was the mechanics of the solid bodies. In the number of computer calculation methods, created in the past four decades, the most widely accepted and developed is the finite element method (FEM), which, in its present form, dates from the late 1950's. Theoretical basis of the method are set by Hrenikoff (1941) and Courant (1943) and Levy is creditable for the first application of triangular finite element for the study of plane stress on one airplane construction [12].

The latest period of development is marked by the appearance of the FEM system working with discrete elements, thus enabling the simulation of gas flow with high speeds. For the reason of relative complexity of these kinds of problems, those systems are still the subject of interest for the small number of specialists.

Complex geometric shapes and complex loads of supporting and transmission elements of machines cause the complexity of their analysis and calculations. Numerical methods provide a general tool to analyze arbitrary geometries and loading conditions. Among the numerical methods, finite element analysis (FEA) has been extensively used with success; however, this kind of analysis requires the generation of a large set of data in order to obtain reasonably accurate results and consumes large investment in engineering time and computer resources.

FEA is one of the modern methods of numerical analysis. Theoretical basis of the finite elements method are made in 1950’s, but the practical application takes place with intensive computer application. It was created from the need for calculation of stress and deformations, and with development of the method the number of variables that can be calculated within the static, dynamic, thermal, electromagnetic and other analysis is increased.

The FEA simulations are increasingly used for investigating and optimizing the blanking processes. Many time-consuming experiments can be replaced by computer simulations. Therefore, highly accurate results of metal forming may be obtained by using the FEA simulation [9, 13].

## 4. GRINDING PROCESS MODELS

Grinding process models based on the complex relationship between process and machine parameters, and work results. The interaction is modelled by prediction of grinding forces, temperatures, energies, surface integrity etc., depending on the conditions of the grinding process. These include fundamental approaches as well as kinematic models, finite element method, molecular dynamics, physical and empirical approaches, artificial neural nets, and rule based models.

Due to the large number of abrasive grains with an unknown geometry which varies with time, grinding is a complex material removal operation. This chapter focuses on the prediction of micro cutting temperature occurring during grinding as an input value of process, in order to describe the interaction between the process and the machining conditions.

The large number of input variables complicates the development of a universal model. Due to different contact conditions, several models have been developed accounting for different grinding operations [14].

In this work, due to the impossibility of modelling an enormous number of active grinding grains of the grinding wheels, which are in simultaneous contact with the workpiece, it is modelled the micro cutting of the grinding grain. Figure 2 shows the characteristic grinding grain shapes, as well as the micro mechanisms for material removal. It can be seen that the speed and depth of the material cutting depend on the type of the grinding grain.[3,4].

Workpiece and wheel are modelled using CREO Parametric software, and micro cutting simulations are done using ANSYS. Necessary materials and thermal-physical characteristics are selected from material library of the FEA package. Material for grain is SiC, and for workpiece is Steel S-7. The cutting depth was $a$ = 0.05 mm, the workpiece speed was $v_w$ = 50 mm/s and the grinding wheel speed was $v_s$ = 30 m/s.

Figure 3 shows the grinding grains model and their meshes. The model defines real grain shape with defined cutting geometry.

Micro furrowing:
- *energetic very inconvenient*
- *removal mechanisms*

Micro ploughing:
- *energetic inconvenient*
- *removal mechanisms*

Micro flow cutting:
- *energetic convenient removal mechanisms*
- *big depth of cut*

Micro curled chipping energetic:
- *convenient removal mechanisms*
- *big depth of cut*

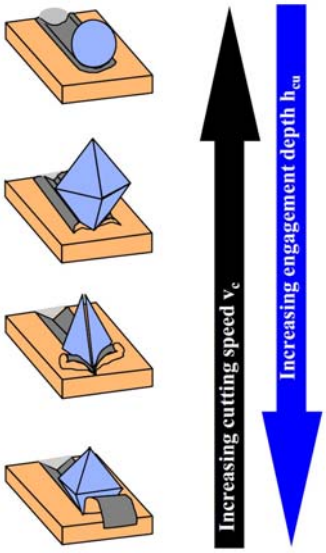


Fig. 2. Metal removal mechanisms of grinding [3]

Defining the parameters for the micro cutting simulation of abrasive grains in the grinding process includes the definition:

- Grinding model;
- Coordinate system;
- Connection;
- Meshing of the model;
- The wheels speed compared to the workpiece;
- Simulation of contact length in grinding;
- Results selection.

Meshing of the model will determine simulation of the contact length in grinding, but also the accuracy of the simulation. To form a mesh commands Refinement and Face Sizing are used. Using the command Refinement a more realistic and finer tool edge is got.

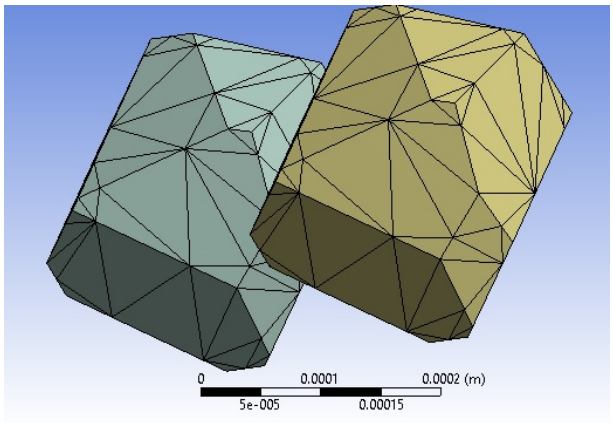


Fig. 3. Grinding grain model with mesh

In FEA mesh modelling, was used the tetrahedrons method of mesh forming. The top surface mesh is 3 times smaller structure as opposed to the lower surface, what can be seen in Figure 4. The total number of elements is 173.314, and the total number od nodes is 33.543 at the workpiece and grains This type of mesh has proven to be the most accurate for this type of simulation.

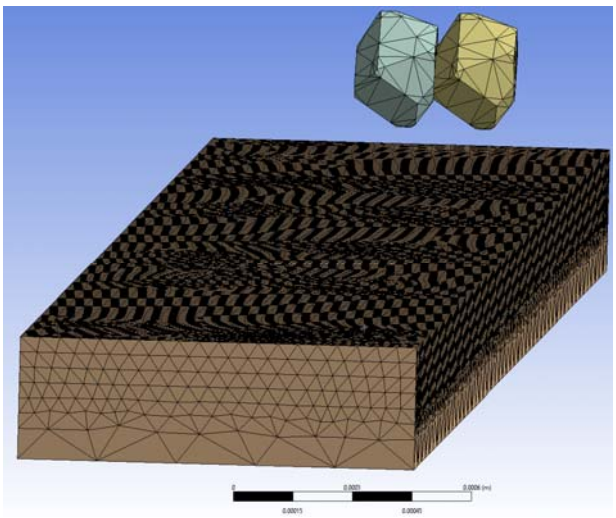

Fig. 4. Modelled mesh at the workpiece preview

## 5. THE SIMULATION RESULTS,

Fig. 5 shows the micro cutting simulation of two abrasive grains in the grinding process. It can be seen the material removal process after the travelled path of the grinding grains which is more than half of the length of contact with the workpiece. The shades of the blue to red colour graphically represent the temperature in the tested workpiece.

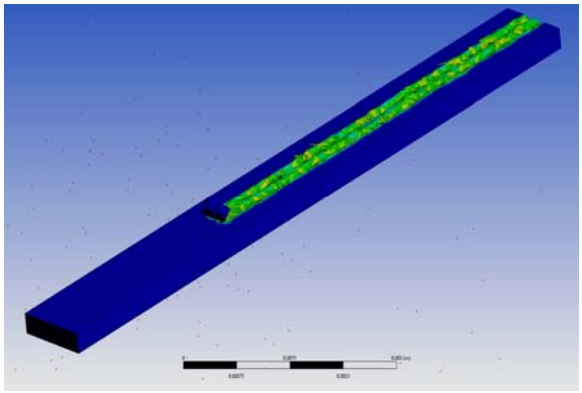

Fig. 5. Grinding simulation of two abrasive grains

Fig. 6 presents the grinding simulation at the beginning and in the course of the process, when maximum temperature in the workpiece is 930 °C and 940 °C, respectively. At the same time the maximal temperature in the removed material is 1.244 °C. It can be noticed that high temperatures occur immediately at the material removal process.

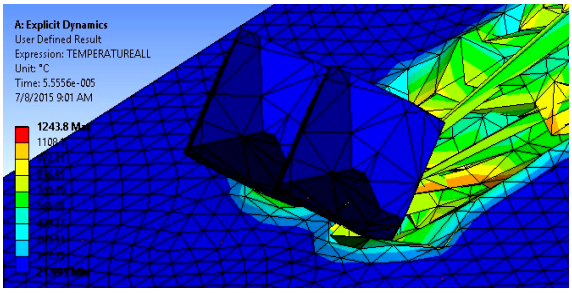


Fig. 6. Micro cutting simulation at the beginning and during the grinding process

Figure 7 shows only the workpiece with hidden grinding grains. At the same time the workpiece is cut lengthwise in order to better display the temperature field.

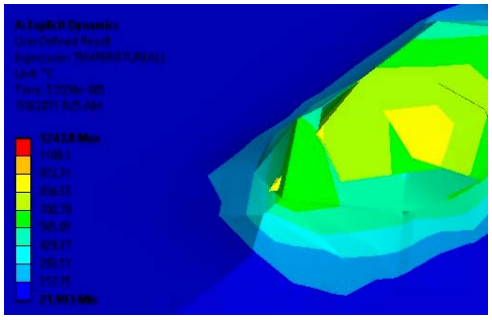

Fig. 7. Temperature field of the workpiece section

## 6. CONCLUSION

Simulation of grinding is still an academic-driven field of research accounting for many different simulation approaches which today mainly focus on grinding wheel-workpiece interaction inside the contact zone. Conducted simulations primarily help to increase the understanding of a grinding process with its millions of single grain engagements resulting.

From analysis made in this work, it was found that the grinding temperature can be easily tested in this way. Material defects could also be considered, which occur as a result of material production and as a result of machining.

This method of testing would be cost effective in complex assemblies, which are much more expensive to assemble in real world than virtual. Their testing in real conditions would be far more expensive than testing in simulation package.

The results obtained by testing needs to be taken with the material irregularities that are formed during the production of the material, as well as the vibration on all machines.

## 7. REFERENCES


[1] Malkin, S., Guo, C.: *Grinding Technology-Theory and Applications of Machining with Abrasives*, Industrial Press, New York, 2008.

[2] Kovac, P., Gostimirovic, M., Sekulic, M., Savkovic, B.: *A review of research related to advancing manufacturing technology*, Journal of Production Engineering, Vol.12, No.1, pp. 9-16, 2009.

[3] Klocke, F.: *Modeling and simulation of grinding processes*, 1st European Conference on Grinding, Aachen, Germany, pp 8.1-8.27, 2003.

[4] Rasim, M., Mattfeld, P., Klocke, F.: *Analysis of the grain shape influence on the chip formation in grinding*, Journal of Materials Processing Technology, Vol. 226, pp. 60-68, 2015.

[5] Guo, C. Malkin, S.: *Thermal analysis of grinding*, Annals of the CIRP, Vol. 56, pp. 760-782, 2007.

[6] Gostimirovic, M., Sekulic, M., Kopac, J., Kovac, P.: *Optimal control of workpiece thermal state in creep-feed grinding using inverse heat conduction analysis*, Strojniški vestnik - Journal of Mechanical Engineering, Vol.57, No.10, pp. 730-738, 2011.

[7] Gostimirovic, M., Kovac, P., Sekulic, M.: *An inverse heat transfer problem for optimization of the thermal process in machining*. Sadhana, Vol.36, No.4, pp. 489-504, 2011.

[8] Gostimirovic, M., Kovac, P., Jesic, D., Skoric, B., Savkovic, B.: *Surface layer properties of the workpiece material in high performance grinding*, Metalurgija, Vol.51, No.1, pp. 105-108, 2012.

[9] Mackerle, J.: *Finite element analysis and simulation of machining: an addendum. A Bibliography (1996–2002)*, Int J Mach Tools Manuf, Vol. 43, pp. 103-114, 2003.

[10] Kovac, P., Savkovic, B., Kulundzic, N., Gostimirovic, M., Holesovky, F. Sekulic, M., Savkovic, B.: *Simulation of temperature distribution on the 3D moving cutting tool*, Development in Machining Technology, Vol. 5, pp. 20-26, 2015.

[11] Kulundzic N., Kovac, P., Savkovic B., Soos L., Rokosz K.: *FEM Simulation of Cutting Processes*, 2013, Scientific Proceedings, Faculty of Mechanical Engineering, STU Bratislava, ISSN 1338-1954, pp121-130, 2013.

[12] Brenner, S. Scott, R.L.: *The Mathematical Theory of Finite Element Methods*, Springer, New York, 1994.

[13] M., Samuel,: *FEM simulations and experimental analysis of parameters of influence in the blanking process*, Journal of Materials Processing Technology, Vol. 84, pp 97-106, 1998.

[14] Brinksmeier, E., Aurich, J.C., Govekar, E., Heinzel, C., Hoffmeister, H.W., Peters, J., Rentsch, R., Stephenson, D.J., Uhlmann, E., Weinert, K., Wittmann, M.: *Advances in modeling and simulation of grinding processes*. Annals of the CIRP, Vol. 55, No.10, pp. 667-696, 2006.


## ACKNOWLEDGEMENTS


The paper is the result of the research within the project TR 35015 (2011/15) financed by the Ministry of Education, Science and Technological Development of the Republic of Serbia and CEEPUS project.



***Authors:*** **M.Sc Nenad Kulundzic, Prof. Dr Marin Gostimirovic, Prof. Dr Pavel Kovac, Prof. Dr Milenko Sekulic, M.Sc Borislav Savkovic**.
University of Novi Sad, Faculty of Technical Sciences, Departman for Production Engineering, Trg Dositeja Obradovica 6, 21000 Novi Sad, Serbia, Phone: +381 21 450-366, Fax: +381 21 454-495.
E-mail: kulundzic@uns.ac.rs, maring@uns.ac.rs
pkovac@uns.ac.rs, milenkos@uns.ac.rs
savkovic@uns.ac.rs

Journal of Production Engineering
Vol.18 No.2
JPE (2015) Vol.18 (2) Original Scientific Paper
Sahu, S.N., Nayak, N.C.

# MULTI-OBJECTIVE OPTIMIZATION OF EDM PROCESS: RSM MODELING AND GENETIC ALGORITHM APPROACH

Received: 15 September 2015 / Accepted: 22 October 2015

***Abstract:*** *Electric Discharge Machining (EDM) is one of the machining process, which is used to produce critical shape on any type of hard or brittle conductive material and it can also be well applied for materials that are impossible to machine with traditional machining processes. The present work mainly demonstrates the optimisation process of multiple responses i. e. MRR, TWR and OC of EDM by using genetic algorithm (GA). The primary experiments were conducted on Electronica Electraplus PS 50ZNC die sinking machine. GA has been conventionally applied to single-objective optimisation problems. The optimal process parameter setting form the composite function optimisation of GA is found to be Ip= 5A, Ton= 150µs, $T_w$= 1 and $T_{up}$= 0s. The experimental values of MRR, TWR and OC is found to be 11.0658 $mm^3$/min, 0.055988 $mm^3$/min and 0.1934 mm respectively from this optimal input parameter combination.*
***Key words:*** *EDM, GA, RSM, MRR, TWR, Multi objective optimization .*

**Višekriterijumska optimizacija procesa elektro erozivne obrade: modeliranje preko RSM i genetskih algoritama.** *Elektro erozivna obrada (EDM) je jedan od proizvodnih procesa koji se koristi za obradu složenih oblika na svim tipovima tvrdih i krtih provodnih materijala a takođe se može koristiti i na materijalima koji se ne mogu obraditi konvencialnim metodama. U ovom radu je sprovedena višekriterijumska optimizacija procesa kao što je MRR, TWR i OC kod EDM korišćenjem genetskih algoritma (GA). Osnovni eksperimenti su sprovedeni na elektro erozivnoj mašini sa punom elektodom Electronica Electraplus PS 50ZNC. GA su primenjeni na optimizaciju problema sa jednim kriterijumom optimizacije. Parametri procesa koji su dobijeni kao optimalni sa GA su Ip= 5A, Ton= 150µs, $T_w$= 1 and $T_{up}$= 0s. Utvrđene eksperimentalne vrednosti za MRR, TWR i OC su: 11.0658 $mm^3$/min, 0.055988 $mm^3$/min i 0.1934 mm, za gore navedenu optimalnu kombinaciju ulaznih parametara.*
***Ključne reči:*** *EDM, GA, RSM, MRR, TWR, Višekriterijumska optimizacija.*

## 1. INTRODUCTION

Electric Discharge Machining is one of the machining process, which is used to produce critical shape on any type of hard or brittle conductive material and it can also be well applied for materials that are impossible to machine with traditional machining processes [1]. In EDM process a series of rapidly recurring spark is generated between the tool and workpiece within a constant spark gap. These sparks cause the ionization of dielectric medium at a critical voltage and create an ionized channel called the plasma channel, which acts as the heat foundation causing melting and vaporization of the workpiece [2- 3].

Since its introduction, EDM has always been a major area of research for improving the quality of machining. A number of researchers have performed theoretical as well as experimental investigations in order to analyse and improve the different quality characteristics such as Material Removal Rate (MRR), Tool Wear Rate (TWR), Surface Roughness (SR), Over Cut (OC), surface hardness, white layer thickness etc. [4]. The Design of Experiment (DOE) techniques based studies applied so far mainly focused on the optimization of single quality characteristics. Multi-attribute optimization has become a highly challenged research area in EDM process and for other machining processes as well. Kuruvila and Ravindra [5] have investigated the multi objective optimization using single genetic algorithm in which the objective function is defined as composite function of the responses DR, SR and MRR i.e. objective = DE+SR-MRR. The objective function was minimized by executing the GA.

## 2. EXPERIMENTAL SET UP, MATERIAL AND METHOD

The primary experiments were conducted on Electronica Electraplus PS 50ZNC die sinking machine. In this experiment the tool and workpiece was set as anode and cathode respectively. An electrolytic pure copper with a diameter of 12 mm was used as tool electrode. The selected workpiece material for this experiment is AISI P20 tool steel has been shown in Fig.1 with electrode. The composition of the material is shown in Table 1.

Table 1: Composition of material

| Elements | C | Mn | Si | Cr | Mo | Cu | P | S |
|---|---|---|---|---|---|---|---|---|
| Weight % | 0.40 | 1.00 | 0.40 | 1.20 | 0.35 | 0.25 | 0.03 | 0.03 |

Commercial grade EDM oil (specific gravity = 0.763

freezing point = $94^0$C) was used as dielectric fluid. Lateral flushing with a pressure of 0.25kgf/cm$^2$ was used. The setup of experiment is shown in Fig.2.

Fig. 1. Tool and workpiece


Fig. 2. Experimental Setup

Experiments were conducted considering the effects of various machining parameters on EDM process. These studies were undertaken to investigate the effects of Ip, $T_{on}$, $T_{up}$ and $T_w$ on MRR, OC and TWR. The selected control parameters and their values at different levels are listed in Table 2 and other parameters are kept at their fixed level.

Table 2. Factor and their levels

| Control Parameter | | | | | |
|---|---|---|---|---|---|
| Parameter | Symbol | Level | | | Unit |
| | | 1 | 2 | 3 | |
| Discharge current | Ip | 1 | 3 | 5 | A |
| Pulse on Time | $T_{on}$ | 10 | 80 | 150 | µs |
| Work time | $T_w$ | 0.2 | 0.6 | 1.0 | S |
| Lift Time | $T_{up}$ | 0.0 | 0.75 | 1.5 | S |
| Fixed Parameter | | | | | |
| Duty Cycle | (ζ) | | 70 | | % |
| Voltage | V | | 45 | | V |
| Flashing Pressure | Fp | | 0.3 | | Kgf/cm$^2$ |
| Sensitivity | SEN | | 6 | | |
| Anti-arc sensitivity | ASEN | | 3 | | |

## 3. MULTI OBJECTIVE OPTIMISATION USING GENETIC ALGORITHM

Genetic Algorithms has been conventionally applied to single-objective optimisation problems. However many real world problems deal with multiple objective Functions generally contradicting in nature [6]. In order to make a best trade-off between these objectives Functions by a single-objective genetic algorithm these objective functions should be combined into a scalar fitness function that means to combine the individual functions into a single composite function. To combine the entire objective into single one any arithmetical operation like addition, multiplication or any other combination of arithmetical operation can be used [7]. One modest approach to combine multiple objective functions into a single composite function is the following weighted sum approach i.e., Equation 8 (assumption made here is all the objectives are to be maximized):

$f(x)= w_1.f_1(x)+\ldots+w_i.f_i(x)+...+w_n.f_n(x)$ …(1)

Where x is an individual or current approximation, f(x) is a composite function, $f_i(x)$ is the $i^{th}$ objective function, $w_i$ is a constant weight for $f_i(x)$, and n is the number of objective functions.

A random real number has been assign to each weight as follows,

$$w_i = \frac{rnd_i}{\sum_{j=1}^{n} rnd_j}, \text{ i=1, 2, 3… n …(2)}$$

Where $rnd_i$ and $rnd_j$ are non-negative random real numbers, n corresponds to number of random real number generated [8]. From equation (2), it can be observed that $w_i$ is real number in the closed interval [0,1].

Here there are 3 objective functions MRR, TWR and OC. The task is to optimize the 3 objectives simultaneously using single objective genetic algorithm, i.e., MRR is to be maximised at the same time we have minimised the TWR and OC. For that individual function is combined into a single composite function defined as objective=TWR+OC-MRR. This composite objective function will be minimized using genetic algorithm.

A random population of type double was initialised. Rank scaling function was used to convert the raw fitness scores that are return by the fitness function. The members called parents are selected by using stochastic uniform function. Reproduction options specify the elite count and crossover fraction that required creating children for next generation. The children of next generation can be created by preserving elite, performing crossover and performing mutation. Elite children can be defined as the individual in the current generation with best fitness values. Performing Migration means to introduce the movement of individuals between subpopulations, which the algorithm creates if the Population size has been set to a vector of length greater than 1. Migration operation can be controlled by three parameters that are migration direction, migration interval and migration

fraction. In migration operation the best individuals from one subpopulation replace the worst individuals in another subpopulation. After all these operations, the current population is replaced with the children to form the next generation. If any one of the stopping criteria is met, the algorithm stops. Otherwise the steps from performing selection operation to testing stopping criteria continue till the stopping criteria are met. The more details about the algorithm can be referred from Global Optimization Toolbox [9].

## 4. RESULTS

The composite objective function objective = TWR+OC-MRR was minimised using single objective genetic algorithm subjected to boundary condition:

$1 \leq Ip \leq 5$
$10 \leq T_{on} \leq 150$
$0.2 \leq T_w \leq 1$
$0 \leq T_{up} \leq 1.5$

| Category | Weightage | Optimum process parameter | | | | RSM predicted value | | |
|---|---|---|---|---|---|---|---|---|
| | | Ip | $T_{on}$ | $T_w$ | $T_{up}$ | TWR | OC | MRR |
| Case-1 | Neglecting weightage | 5 | 149.997 | 1 | 0 | 0.0585 | 0.182 | 10.5683 |
| Case-2 | Weightage on TWR= 0.0207<br>Weightage on OC = 0.6215<br>Weightage on MRR= 0.3577 | 4.998 | 149.999 | 1 | 0.001 | 0.0584 | 0.183 | 10.5804 |
| Case-3 | Weightage on TWR= 0.0668<br>Weightage on OC= 0.5626<br>Weightage on MRR= 0.3706 | 4.998 | 150 | 0.997 | 0.001 | 0.0579 | 0.180 | 10.2201 |
| Case-4 | Weightage on TWR=0.4671<br>Weightage on OC=0.4039<br>Weightage on MRR=0.1291 | 5 | 149.997 | 1 | 0.001 | 0.0611 | 0.1887 | 10.5770 |
| Case-5 | Weightage on TWR=0.4780<br>Weightage on OC=0.0777<br>Weightage on MRR=0.4443 | 5 | 150 | 0.999 | 0 | 0.0550 | 0.1865 | 10.3864 |
| Case-6 | Weightage on TWR=0.5110<br>Weightage on OC=0.4726<br>Weightage on MRR=0.0164 | 5 | 149.993 | 1 | 0.001 | 0.0586 | 0.1832 | 10.5867 |

Table 3. Tabulated result from genetic optimisation

Broadly the optimisation process was perform on two basis first one neglecting the weightage and the second one was considering the weightage on individual objective function. The weights of individual functions are shown in second column of Table 3. The optimal process parameters and respective RSM predicted responses for different cases obtained from the result of genetic algorithm also have been shown in the same table. The optimisation was continuously monitored throughout the generations. The best fitness and mean fitness from generation to generation was recorded in the form of fitness plot (fitness value vs. generation plot) in Fig. 3.

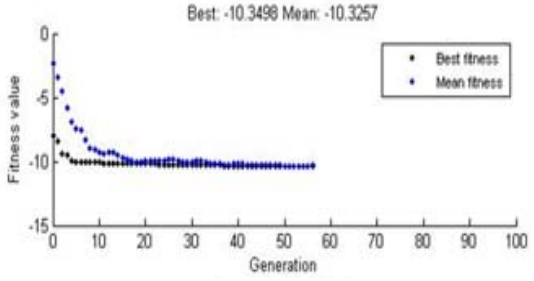


Fig. 3. Fitness vs. Generation

From the fitness plot it can be easily observed that the fitness value is converging towards the optimal from one generation to other generation. Vector entries of individual with the best fitness function value were observed in best individual plot (current best individual vs. number of variables) as shown in Fig. 4.

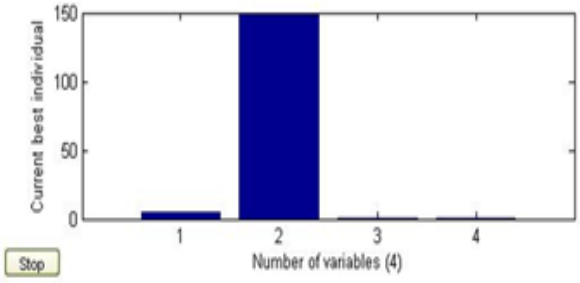


Fig. 4. Best individual vs. No. of variables

## 5. CONCLUSIONS

The present work mainly demonstrates the optimisation process of multiple responses i. e. MRR, TWR and OC of EDM by using genetic algorithm.

Similarly the optimal process parameter setting form the composite function optimisation of genetic algorithm is found to be Ip= 5A, $T_{on}$= 150µs, $T_w$= 1 and $T_{up}$= 0s. The experimental values of MRR, TWR and OC is found to be 11.0658 $mm^3$/min, 0.055988 $mm^3$/min and 0.1934 mm respectively from this optimal input parameter combination.

## 6. REFERENCES


[1] Chakravorty R., Gauri S.K., and Chakraborty S. Optimization of Correlated Responses of EDM Process. *Materials and Manufacturing Processes*, 27, pp. 337–347, 2011.

[2] Panda D.K. and Bhoi R.K.. Electro-Discharge Machining–A Qualitative Approach. *Materials and Manufacturing Processes*, 21, pp. 853–862, 2007.

[3] Panda D.K. and Bhoi R.K.. Analysis of spark eroded crater Formed under growing plasma Channel in electro-discharge Machining. *Materials and Manufacturing Processes*, 9, pp. 239–261, 2005.

[4] Ekmekci B., Elkoca O., Tekkaya A.E. and Erden A. Residual stress state and hardness depth in Electric Discharge Machining: de-ionized water as dielectric Liquid, *Machine Science and Technology*, 9, pp. 39–61, 2005.

[5] Nixon K. and Ravindra H. V. Parametric influence and optimization of wire EDM of hot die steel. *Machining Science and Technology*, 15, pp. 47–75, 2011.

[6] Tadahikorjlurata and Hisaoishibuchi. MOGA: Multi-Objective Genetic Algorithms Evolutionary Computation, *IEEE International Conference*, Vol-2, 1995.

[7] Carlos A. Coello Coello,. Lamont G. B, David A. Van Veldhuizen. Evaluation algorithm by solving multi-objective problem. *Springer science, Business media*, LLC, 2007.

[8] Murata T., Ishibuchi H. and Tanaka H. Multi-Objective Genetic Algorithm And Its Applications To Flowshop Scheduling. *Computers& Industrial Engg,* Vol. 30, No. 4, pp. 957-968, 1996.

[9] Matlab R2011b, Global Optimization Toolbox User's Guide, *MathWorks*, Inc. Natick, 2011.



***Author:*** **Shiba Narayan Sahu,** Ph D Scholar, Mechanical Engg Dept, Utkal University, India. Mail ID: shibacvrce@gmail.com and **Ph D Narayan C. Nayak,** Associate Professor, Mechanical Engineering Department, Indira Gandhi Institute of Technology, Sarang, Odisha, India. Mail ID: nayak.iem@gmail.com

Journal of Production Engineering
Vol.18 No.2
JPE (2015) Vol.18 (2) Original Scientific Paper
Saloyková, Š.

# DIAGNOSTICS OF VIBRATIONS BASED ON EXPERIMENTAL INVESTIGATION WHEN DIVIDING ROCKS WITH ABRASIVE WATER JET TECHNOLOGY

Received: 15 September 2015 / Accepted: 22 October 2015

***Abstract:*** *This article presents the investigation results of vibrations acceleration frequency spectrum courses by the influence of changes in technological head feed speed. Is among one of the technological factors that affecting the creation of vibrations on technological head. The experiments were carried out on selected rocks. Includes 1-parametric graphical dependences of vibrations acceleration amplitude on frequency, based on which are new knowledge created.*
***Key words:*** *material cutting, experiment, water jet, vibrations, frequency*

**Dijagnostika vibracija na osnovu eksperimentalnih istraživanja pri procesu obrade vodenim abrazivnim mlazom.** *Ovaj rad prikazuje rezultate istraživanja frekvencijskog spektra ubrzanja vibracija usled promena brzina pomeranja tehnološke glave. To je jedan of tehnoloških faktora koji utiče na nastajanje vibracija u tehnološkoj glavi. Eksperimenti su sprovedeni na određenim kamenovima. Takođe je prikazana i jednoparametarska grafička zavisnost amplitude ubrzanja vibracija i frekvencije, na osnovu čega su otkrivene nova saznanja.*
***Ključne reči:*** *materijal za sečenje, eksperiment, vodeni mlaz, vibracije, frekvencija*

## 1. INTRODUCTION

Abrasive water jet is often the only „tool“ for cutting certain types of materials. In conventional production plants, where are divided different types of materials, different sizes, sometimes it does not matter on the machined surface quality as on the fact, that it is at all possible in this way to divide the material. However is an effort to optimize the technological parameters so, that the quality requirements are a natural part of this progressive production technology. An accompanying sign in the operation of production systems with abrasive water jet technology are vibrations. The emergence and spread of vibrations is still popular and theoretically challenging issue. Based on the experimental investigation of selected technological parameters impact on technological head vibrations creation has been in the previously period on KPVP new knowledge obtained listed in dissertations [1], [2], [3] and publications [4], [5], [6]. The knowledge referred to in Article constitute the partial knowledge of the total KPVP knowledge and also complement significant knowledge focused on modeling and process diagnostics in the water jet technology solved on the water jet workplace of IF TU in Ostrava [7], [8].

## 2. MANUFACTURING SYSTEM FOR CARRYING OUT EXPERIMENTS

The experiments were carried out on a workbench X-Y CNC WJ1020-1Z-EKO for planar abrasive water jet dividing applications. The water pressure was created by PTV 19/60 HSQ 5x multiplier with a flow rate to 1,9 $l.min^{-1}$. For dividing the investigated material was a diamond head type PASER IIITM used with a water nozzle diameter of 0,25 mm and guidance tube diameter of 1,12 mm [1].

## 3. CONDITIONS OF THE EXPERIMENT

All measurements were performed from the same starting position X = 320 mm a Y = 370 mm with constant and changing settings of technological and material factors listed in Table 1 [1].

| | Parameter name | Value |
|---|---|---|
| Constant factors | Material thickness | 30 mm |
| | Working medium pressure | 380 MPa |
| | Type of abrasive | Austrálsky garnet |
| | Abrasive grain size | MESH 80 |
| | Abrasive mass flow | 225 g/min |
| Changing factors | Divided material | rock Azul Noche<br>rock Rosabeto Italie<br>rock Shiwakashi Indie<br>rock Juparaná Gold |
| | Feed speed | 100 mm/min<br>150 mm/min |

Table 1. Overview of technological and material factors used in the experiment

## 4. TECHNICAL SYSTEM FOR THE MEASUREMENT AND EVALUATION OF VIBRATIONS

### 4.1 Hardware

Piezoelectric accelerometer manufactured by Brüel & Kjær (type: 4507-B-004, parameters: IEPE, TEDS, 1-axis, 100mV/g) was mounted to the head (Fig. 2) so, that its axis is identical with the vibrations axis in the abrasive water jet direction. The accelerometer was

connected to the AD converter (AI ± 5V IEPE, sampling 25kSps) through which is the created data record stored into PC (LENOVO) as a time record of vibrations acceleration signal.

### 4.2 Software

For the time-based signal evaluation the SignalExpress was used which is a part of LabVIEW programming and development environment from the National Instruments Company. From the time record was a steady part of 10 seconds selected and from her by Fourier Transform a frequency spectrum in the range from 0 – to 10 kHz generated. The frequency spectrum envelope was obtained by using the filter algorithm and processed in environment of Microsoft Office Excel spreadsheet editor.

## 5. MEASURED VALUES AND THEIR EVALUATION

The measured values for the studied rock types and two technological head feed speeds are shown in the vibrations acceleration amplitude time courses form. An example of the vibrations acceleration amplitude time course for divided material rock Rosabeto Italy at feed speed of 100 mm/min is shown on Figure 1 and divided at feed speed of 150 mm/min is shown on Figure 2. Similarly have been shown time courses of vibrations acceleration amplitude for rocks Shiwakashi India, Azul Noche a Juparaná Gold and two technological head feed speeds.

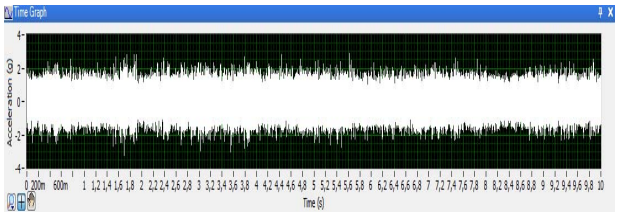


Fig. 1. The vibrations acceleration amplitude time course at dividing rock Rosabeto Italy and feed speed of 100 mm/min

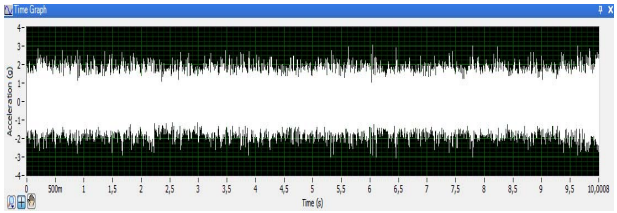


Fig. 2. The vibrations acceleration amplitude time course at dividing rock Rosabeto Italy and feed speed of 150 mm/min

## 6. THE OVERVIEW AND STRUCTURE OF EXPERIMENTS EVALUATION

The overview and structure of experiments evaluation is shown in the structure [9], [10], [11]:

- the vibrations acceleration amplitude graphical dependence of divided material Rosabeto Italy at technological head feed speed 100 mm/min
- the frequency spectrum envelope of divided material Rosabeto Italy at technological head feed speed 100 mm/min
- the comparative graph of vibrations acceleration amplitude envelope and frequency spectrums for selected set of divided materials at feed speed 100 mm/min and 150 mm/min
- the graph with maximum technological head vibrations acceleration amplitude values at feed speed of 100 mm/min in frequency range from 2,7 kHz to 7,7 kHz
- the graph with maximum technological head vibrations acceleration amplitude values at feed speed of 150 mm/min in frequency range from 3,0 kHz to 6,6 kHz

## 7. EVALUATION OF THE MEASURED VALUES

The evaluation involves the creation of technological head vibrations acceleration amplitude frequency spectrums in the range from 0 to 10 kHz. As an example is shown the course of change in vibrations acceleration amplitude on frequency for the dividing material Rosabeto Italie at feed speed of 100 mm/min (Figure 3) and frequency spectrum envelope on Figure 4. Analogously have been shown the graphical dependences of acceleration amplitude, vibrations frequency and frequency spectrum envelope for other examined types of materials and both technological head feed speeds.

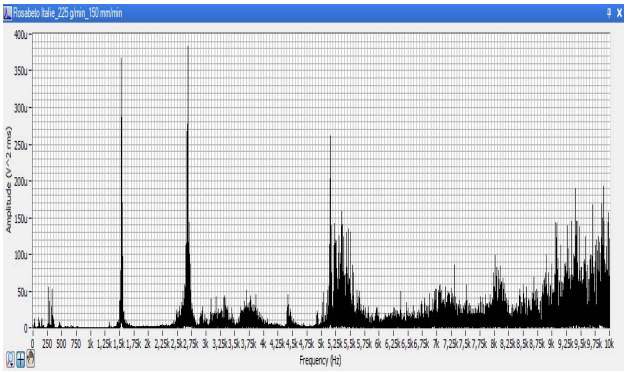


Fig. 3. Graphical dependence of acceleration amplitude and vibrations frequency for divided material Rosabeto Italie at feed speed of 100 mm/min

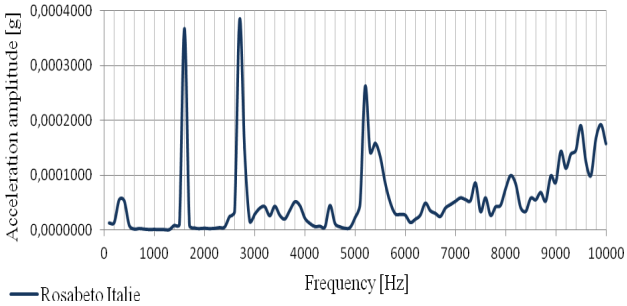


Fig. 4. Technological head vibration frequency spectrum envelope for divided material Rosabeto Italie at feed speed of 100 mm/min

The comparative graph of vibrations acceleration amplitude envelopes and frequency spectrums for selected set of divided materials at the feed speed of 100 mm/min is shown in Figure 5 and at the feed speed 150 mm/min in Figure 6.

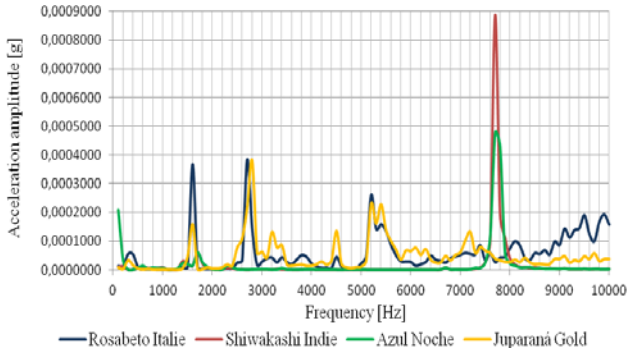


Fig. 5. Comparison of the technological head vibrations frequency spectrum envelopes for selected set of divided materials at the feed speed of 100 mm/min

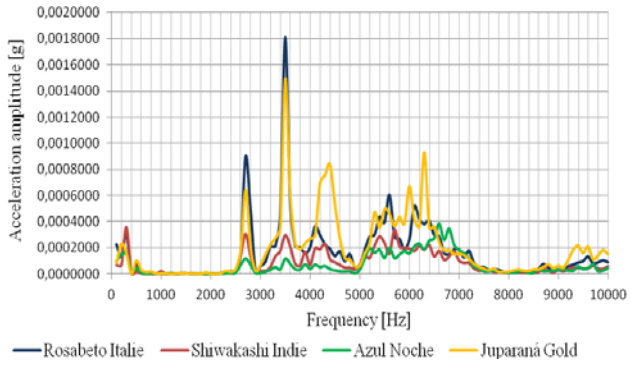


Fig. 6. Comparison of the technological head vibrations frequency spectrum envelopes for selected set of divided materials at the feed speed of 150 mm/min

The maximum technological head vibrations acceleration amplitude values in the frequency spectrum from 2,7 kHz to 7,7 kHz for examined set of materials at feed speed 100 mm/min are shown in Figure 7 depending on vibrations acceleration amplitude on material type.

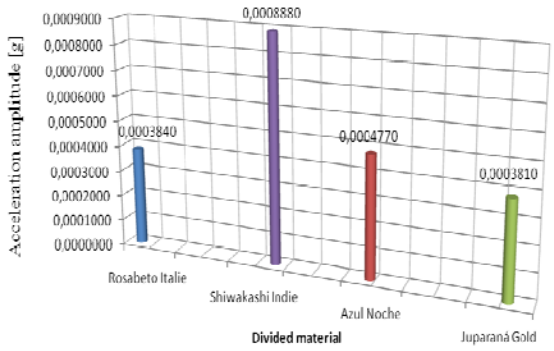


Fig. 7. Graphical representation of maximum vibrations acceleration amplitude values for selected set of divided materials at the feed speed of 100 mm/min

The maximum technological head vibrations acceleration amplitude values in the frequency spectrum from 3,0 kHz to 6,6 kHz for examined set of materials at feed speed 150 mm/min are shown in Figure 8 depending on vibrations acceleration amplitude on material type.

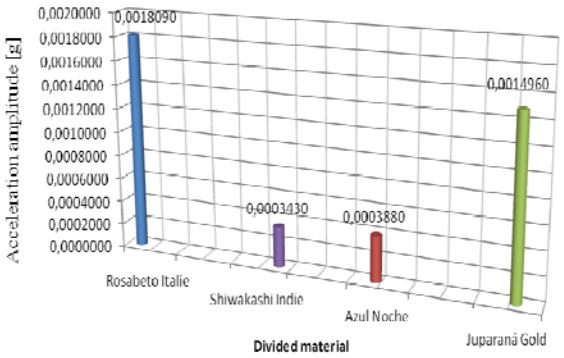


Fig. 8. Comparison of the technological head vibrations frequency spectrum envelopes for selected set of divided materials at the feed speed of 150 mm/min

## 8. DISCUSSION TO THE ACHIEVED RESULTS

From the comparison of graphical dependences and technological head vibrations acceleration amplitude frequency spectrums and their envelopes is a set of new knowledge formulated valid in accordance with the experiment conditions shown in Table 1:

- at dividing four selected types of materials and use technological head feed speed of 100 mm/min were the highest vibrations values from the monitored range 0 to 10,0 kHz found in the frequency range from 1,5 to 3,0 kHz and from 7,5 to 8,0 kHz
- at dividing four selected types of materials and use technological head feed speed of 150 mm/min were the highest vibrations values from the monitored range 0 to 10,0 kHz found in the frequency range from 2,5 to 7,3 kHz
- the maximum values of vibrations acceleration amplitude from four studied types of materials with the use of speed 100 mm/min occur in the frequency range from 7,5 to 8,0 kHz when dividing Shiwakashi Indie rock with the maximum reached value of 0,888 mg at a frequency of 7,7 kHz
- the maximum values of vibrations acceleration amplitude from four studied types of materials with the use of speed 150 mm/min occur in the frequency range from 3,3 to 4,0 kHz when dividing Rosabeto Italie rock with the maximum reached value of 1,809 mg at a frequency of 3,5 kHz
- in comparison two investigated feed speeds is the largest reduction of vibrations acceleration

amplitude achieved when machining Rosabeto Italie rock up to 78,77 %

- the largest reduction of vibrations acceleration amplitude (57,09 %) at feed speed of 100 mm/min will be achieved when comparing two selected rocks and that are Shiwakashi Indie and Juparaná Gold
- the largest reduction of vibrations acceleration amplitude (81,03 %) at feed speed of 150 mm/min will be achieved when comparing two selected rocks and that are Rosabeto Italie and Shiwakashi Indie

## 9. CONCLUSION

In the abrasive water jet technology is necessary for oscillation evaluation through the vibrations parameter taking into account except technological factors impact also type of divided material. From the experiments evaluation and knowledge about this technology it is possible to say, that also material factor has an impact on the size of vibrations. In the article are listed from the overall 28 evaluated original graphical dependences 6 graphical dependences, 2 from them are comparative graphs of frequency spectrum envelopes. In addition, it also contains graphical representation of maximum vibrations acceleration amplitude values for the examined types of materials, which occur in the frequency range from 2,7 kHz to 7,7 kHz at feed speed of 100 mm/min and from 3,0 kHz to 6,6 kHz at feed speed of 150 mm/min. Based on the analysis were found that the largest vibrations acceleration amplitude values at technological head feed speed of 100 mm/min were achieved by machining Shiwakashi Indie rock and at feed speed 150 mm/min by Rosabeto Italie rock. With proper feed speed selection is the assumption, that the vibrations emerging on technological head satisfy the requirements placed on technical system with water jet technology.

## 10. ACKNOWLEDGEMENT

The research work was supported by the Project of the SF of the EU, Operational Programme Research and Development, Measure 2.2 Transfer of knowledge and technology from research and development into practice, project: Research and development of intelligent nonconventional actuators based on artificial muscles. ITMS code: 26220220103, projects VEGA 1/0409/13 and KEGA 027 TUKE - 4/2014.

## 11. REFERENCES

[1] Salokyová, Š.: *Analysis, modelling and simulation of vibrations in manufacturing systems with water jet technology*, Dissertation. Prešov, 2012. 303 p.

[2] Bičejová, Ľ.: *Modelling and simulation of operational conditions influencing the formation and extent of vibrations in manufacturing systems*, Dissertation. Prešov, 2010. 184 p.

[3] Jacko, Patrik: *Modelling and simulation of technological parameters related to usage of non-traditional abrasives in AWJ technology*, Dissertation. Prešov, 2011. 163 p.

[4] Fabian, S., Salokyová, Š., Jacko, P.: Experimental verification of the freqeuncy spectrum of unwear and wears guidance tube on the technological head vibrations creation in the production system with AWJ technology. In: *Manufacturing Technology*. 12 (2012) 13, 105 – 108

[5] J. Kmec, Ľ. Bičejová, T. Krenický: AWJ production technology system technology head vibrations formation due to water press changes 2011. In: *Annals of Faculty of Engineering Hunedoara*. 9 (2011) 3, 343-344

[6] Fabian, S., Salokyová, Š., Olejár, T.: Analysis and experimental study of the technological head feed rate impact on vibrations and their frequency spectra during material cutting using AWJ technology. In: *Nonconventional Technologies Review*. (2011) 4, 27-32

[7] Kaličinský, J.: *Control of technological parameters of liquid jet in violation of materials*. Dissertation. Ostrava, 2009

[8] Gembalová, L.: *Determine the physical - mechanical properties of the material breach of its liquid jet*. Dissertation. Ostrava, 2010, 120 p.

[9] Jurko, J., Panda, A., Behún, M.: Analysis of cutting zone machinability during the drilling of XCr18Ni8 stainless steel. In: *Applied Mechanics and Materials, Trans Tech Publications*, Zurich, Switzerland, 224 (2012)142, 142-145

[10] Ťavodová, M.: The surface quality of materials after cutting by abrasive water jet evaluated by selected methods. In: *Manufacturing Technology*, Volume 13, Issue 2, 2013, Pages 236-241

[11] Vojtko, I., Kočiško, M., Šmeringaiová, A., Adamčík, P.: Vibration of worm gear boxes, In: *Applied Mechanics and Materials*, Volume 308, 2013, Pages 45-49

***Authors:*** **Ing. Štefánia Salokyová, Phd.,** Technical University of Košice, Faculty of Manufacturing Technologies, Department of Manufacturing Processes Operation, Bayerova 1, 080 01 Prešov, Slovakia
E-mail: stefania.salokyova@tuke.sk

Journal of Production Engineering
Vol.18 No.2
JPE (2015) Vol.18 (2) Original Scientific Paper
Ahmed, I. I., Jeleel Adekunle Adebisi, Taiwo Yahaya, Sulaiman Abdulkareem

# EFFECTS OF SOAKING TIME AND COLD WORK ON SENSITISATION OF AUSTENITIC STAINLESS STEELS

Received: 25 August 2015 / Accepted: 20 October 2015

**Abstract:** *The effects of soaking and coldworks on sensitisation of austenitic stainless steels were studied. Annealed and samples coldworked to 20% and 40% were subjected to sensitisation heat treatment at 650℃ for 24 and 72 hours. Metallographic analysis carried out showed that sensitisation occurred in both annealed and coldworked samples which manifested as ditches. Soaking for 72 hours showed more ditches than 24 hours. Intergranular ditches were more prevalent in annealed and lower coldworked samples. In contrast, heavily coldworked samples were more susceptible to transgranular carbide precipitation evident by ditches on slip bands and recrystallised grains*
***Key words:*** *sensitisation; soaking time; cold work; carbide; interganular*

**Uticaj vremena natapanja i hladne deformacije na senzitizaciju austenitnog nerđajućeg čelika.** *Uticaj vremena natapanja i hladne deformacije na senzitizaciju austenitnog nerđajućeg čelika. Pripremci koji su normalizovani i hladno deformisani na 20% i 40% su bili izloženi procesu senzitizacije na 650℃ za 24 i 72 sata. Metalografska analiza je pokazala da se senitizacija javila i kod normalizovanih i hladno deformisanih pripremaka u vidu kanala. Natapanje od 72 sata je pokazalo više kanala nego natapanje od 24 sata. Intergranularni kanali su bili više izraženi kod normalizovanih i slabije deformisanih pripremaka. Sa druge strane više deformisani pripremci su bili podložniji transgranularnom izlučivanju karbida sa vidljivim kanalima na ravnima klizanja i rekristalizovanim zrnima.*
***Ključne reči:*** *senzitizacija, vreme natapanja, hladna deformacija, karbid, intergranularno*

## 1. INTRODUCTION

Austenitic stainless steels (ASS) remain preferred candidate materials for engineering structural application owning to their good strength and excellent corrosion resistance [1-5]. Austenitic stainless steels may be graded as high carbon (e.g. ASS 304H) and low carbon grade (e.g. ASS 304L) depending on their carbon content if is higher than and less than 0.03wt% respectively [2]. The application requirements of theses steels often determine the choice of the grade that may be considered. High carbon grade ASS type 304 (ASS 304H) remained a preferred choice for reactor cap design on account of their excellent creep resistance despite their probable risk of sensitisation [6]. The propensity of high carbon grade to sensitisation constitutes a marked difference in their applications compare to the less susceptible low carbon grade. Sensitisation is a phenomenon used to describe the localised precipitation of chromium carbide usually at the grain boundary area being a region of higher energy [1], when the material is soaked in the temperature range 500$^{o}$C-850$^{o}$C, thereby leading to chromium depletion adjacent to the grain boundaries and eventual loss of passivity [6, 7] (see Figure 1).

The linking of the Cr-depleted zones (Figure 1) provides a continuous path of lower corrosion resistance along the grain boundaries. It is along this path that the propagation of intergranular corrosion or SCC occurs [8]. Sensitized microstructures may also develop during slow cooling from high temperatures, heat treatment, high temperature service and welding. The higher affinity of chromium for the carbon makes this precipitation reaction readily feasible and occurred in form of $M_{23}C_6$), though reactions with other elements like nitrogen may also occur to form chromium nitride of the form MxNy. Where M denotes elements including: Fe; Cr; Mo etc [2, 3].

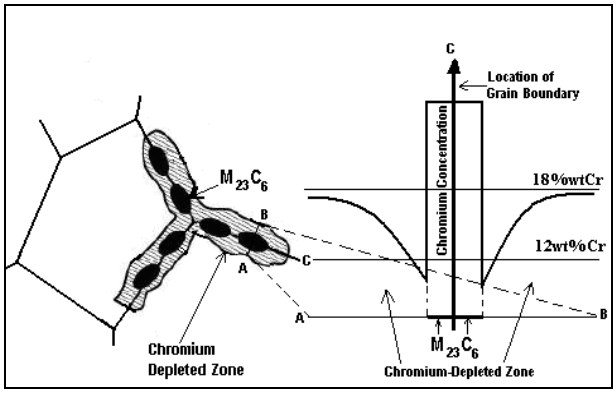

Figure 1. Schematic Illustration of Sensitization Mechanism [8]

On the other hands, cases of intragranular precipitation of carbides is not uncommon where precipitation of carbides occur within the grain matrix, usually on the dislocations structure of cold worked materials [3]. In addition, Kain et al.[9] also observed that susceptibility of ASS to sensitisation increases with cold reduction up till about 15-20% but later decreases beyond 20% cold work when carbides nucleation occurred within the grain rather than on the grain

boundary. This was attributed to rising internal energy with dislocation density [1, 9]. The above is consistent with the observation of Ahmed et al.[10] where it was found that material cold worked to 20% represented the the peak of intergranular stress development, with probable IGSCC failure mode. This is not unconnected with intergranular stress build up caused by strain mismatch, and beyond 20% cold work, the deformation becomes increasingly more uniform with less strain heterogeneity. At higher cold work levels, the slip band and dislocation line becomes probable carbide nucleation sites and Transgranular Stress Corrosion Cracking (TGSCC) mode becomes more dominant [11].

The danger of sensitization in ASS cannot be underestimated as it may lead to intragranular corrosion failure or intergranular stress corrosion cracking expecially in the pressurised areas of application including Pressurised Water Reactor (PWR) environment [1, 6, 8, 9]. Hence, the objective of this work was to highlight the capability of optical microscopy for the assessement of effects of cold work levels and soaking time on the sensitisation of austenitic stainless steels.

## 2. EXPERIMENTATION

### 2.1 Materials

The material used for this study was low carbon grade ASS, Type 304L, with the chemical composition shown in Table 1. The ASS plate (300×100×30mm) as-received was initially solution annealed at 1050°C for 30 minutes and quenched in water. Fast cooling was done to prevent probable intergranular precipitation of the chromium carbide by sensitisation process [11]. The material was subsequently heat treated at 400°C and furnace cooled to partially relieve internal stresses and remove any martensite which might have formed due to fast cooling. The material was subsequently cold worked by uniaxial rolling.

| C | Cr | Mn | N |
|---|---|---|---|
| 0.030 | 18.387 | 1.804 | 0.086 |
| **Ni** | **P** | **S** | **Si** |
| 8.133 | 0.034 | 0.005 | 0.411 |

Table 1. Chemical composition of as-received ASS Type 304L (wt %)

### 2.2 Experimental Procedures

#### 2.2.1 Cold Rolling

Cold working could be achieved through a number of methods. However, cold rolling was used because of the ease of achieving different degrees of cold work through reduction in the sample thickness and it equally allows test samples to be manufactured from different orientations of the rolled plates. Some of the annealed materials were cold worked by multipass uniaxial rolling to 20% and 40% reductions in thickness. Each rolling pass corresponds to thickness reduction of 0.5mm and the final thickness of rolled plates reduced from 30mm to 27mm and 18mm respectively. The degree of cold work was determined using Equation 1 [12]. Schematic illustration of the rolling process is shown in Figure 2.

$$\text{Cold Work}(\%) = \frac{h_o - h_f}{h_o} \quad (1)$$

Where $h_o$ and $h_f$ are the initial and final through thickness dimensions respectively.

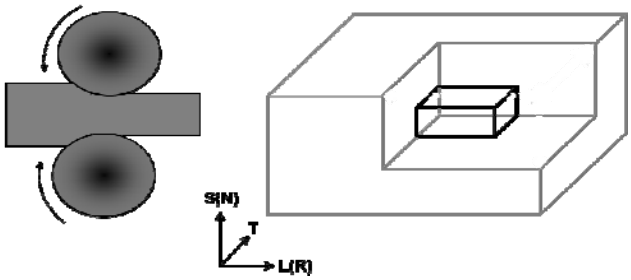


Figure 2. Schematic Diagram of Cold Rolling

#### 2.2.2 Sensitisation Heat Treatment

Annealed and cold rolled samples with the dimensions 1cm × 1cm were sensitized. The sensitisation heat treatment was carried out in an electric heating tube furnace. Argon gas was used to achieve oxygen-free inert envnironment. The sample was initially heated to 700°C in 30 minutes under steady flow of argon gas to prevent high temperature oxidation. The temperature was later stabilised at 650°C with the aid of thermocouple in contact with the sample. The sample was then soaked for 24 hours and 72 hours accordingly at 650°C and then air cooled to ambient temperature.

#### 2.2.3 Optical Metallography

The Rolling (R), Transverse (T) and Normal (N) directions of cold rolled plate correspond to the Longitudinal (L), Transverse (T) and Short-transverse (S) directions of the annealed material. The samples used for optical metallography were sectioned from the middle of the cold rolled plate. The samples Normal plane (R-T), perpendicular to the Normal direction were considered for metallography (see Fig 1.). The plane of the sample are defined by two orthogonal directions in the parenthesis.

The sample preparation was carried out following the metallographic wet grinding with silicon carbide paper in order of 320, 400, 600, 800, 1200 and 4000. The specimen was subsequently electropolished in a solution containing 8% Perchloric acid and 92% Acetic acid at 42V for 90s following the procedures of the ASTM standard E 1558-99 [13]. The electropolished sample was then electrolytically etched in a solution containing 10% Oxalic acid and 90% distilled water at current density of 1A/cm$^2$ for 60s in line with the ASTM standard A 262-01 [14]. Electrolytic etching with oxalic acid has the potential to reveal the austenite grain boundaries, the residual delta ferrite and the slip bands. The sample was then rinsed with deionised water and then in ethanol before it was dried with warm air. The etched samples were examined under the Optical microscope.

## 3. RESULTS AND DISCUSSION

### 3.1 Optical Metallography

The results of the optical metallography for the annealed samples are contained in Figure 3. The common microstructural features revealed in all the micrographs in Figure 3 are the austenite grain boundaries, the residual delta ferrite and twins within the austenite grains. The grains are fairly equiaxed. Figures 3A showed the un-sensitised optical micrograph while Figures 3B & C showed the micrographs of the annealed samples sensitised at 650°C for 24 hours and 72 hours respectively. Figure 3D was the optical micrograph of the sample sensitised for 72 hours but larger magnification for clarity. The obvious difference between annealed un-sensitised (Figure 3A) and sensitised samples (Figures 3B & C) could be seen on the austenite grain boundaries. The colour contrast also showed that sensitised samples are more darker than the un-sensitised sample and the degree of sensitisation was observed to more after the sample was sensitised for 72 hours than 24 hours samples. Higher magnification sample (Figure 3D) showed that the grain boundaries of the sensitised samples contained ditches compared with unsentised samples. The ditches were not found on the twin boundaries or the coincident site lattices nor was any observed within the austenite grain matrix and consistent with the Moura et al.[6]. The ditches on the sensitised austenite grain boundaries was attributed to the network of chromium carbide precipitate along grain boundaries during the sensitisation heat treatment at 650°C for prolonged time. The precipitation of noble chromium carbide along the grain boundaries resulted in the depletion of the much needed chromium adjacent to the grain boundaries [15] leaving behinde a network of nobler chromium carbide precipitate and neighbouring less noble region, with chromium level below minimium required for the stainless steel to maintain its passivity. The contact between the nobler chromium carbide precipitate and the less noble neighbouring region would make the material susteptible to galvanic corrosion attack in addition to electrolytic etching in oxalic acid

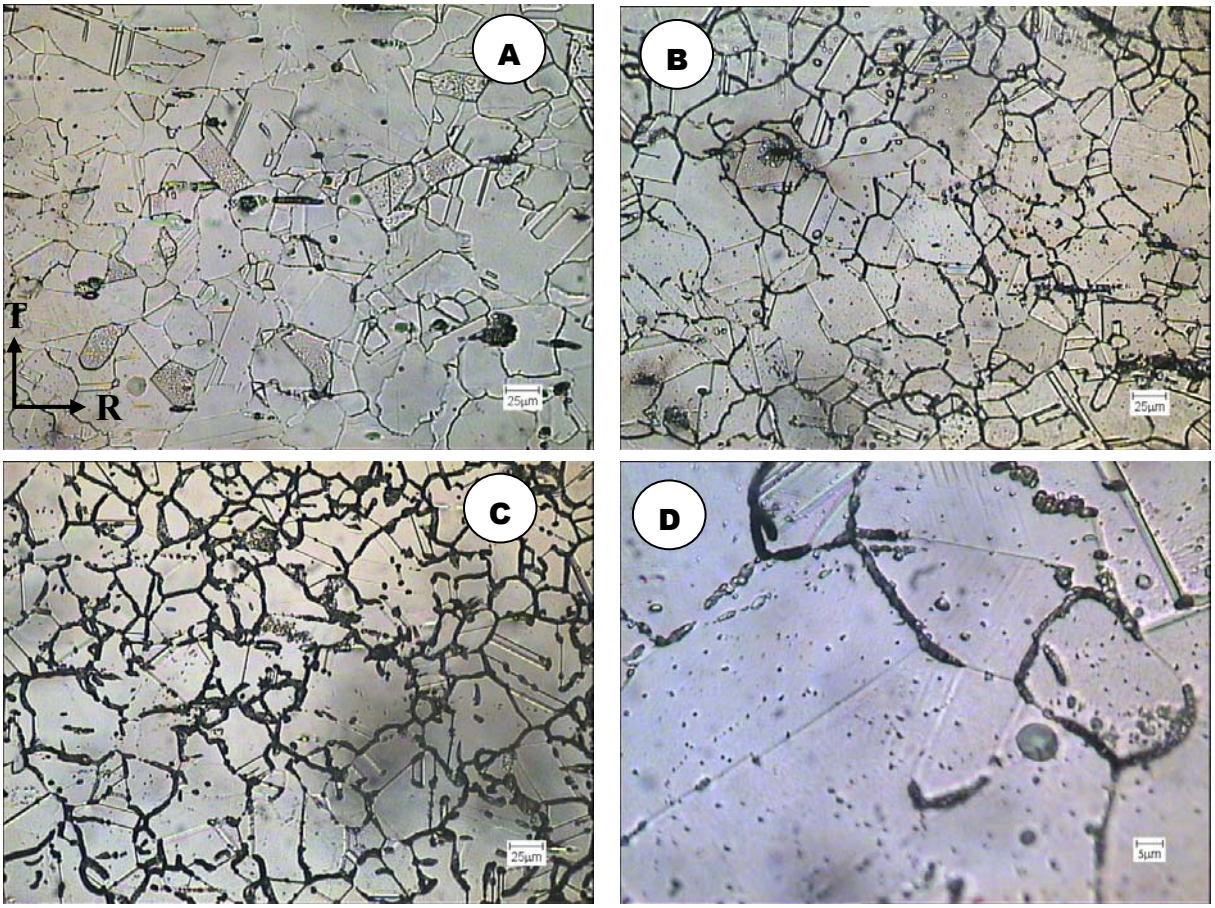


Figure 3. Normal Plane of ASS Annealed: un-sensitised (A), sensitised for 24Hr (x20) (B), sensitised for 72Hr (x20) (C), sensitised for 72Hr (x80) (D)

The result of optical microscopy of the 20% cold worked sample are contained in Figure 4. Figure 4A showed the macrograph of the un-sensitised sample, while Figures 4B & C were the optical micrographs of the cold rolled samples and sensitised at 650°C for 24 hours and 72 hours respectively. Figure 4D was the higher magnification micrograph of the sample sensitised for 72 hours. The difference between the un-sensitised and sensitised 20% cold worked samples is consistent with those observations in annealed sample. In addition to the ditches on sensitised austenite grain boundaries, there was evidence of recrystallisation in the 20% cold worked samples sensitised for 72 hours (Figure 4C & D) compare to sample sensitised for 24 hours (Figure 4B). The newly recrystallised grain boundaries also evidence of limited ditches which suggested that the boundaries

became carbide nucleation sites but the extent of these was not very pronounced. Similar observation was reported in the work of Alvarez et al.[16] on ASS cold rolled to 50% reduction and elsewhere [1].

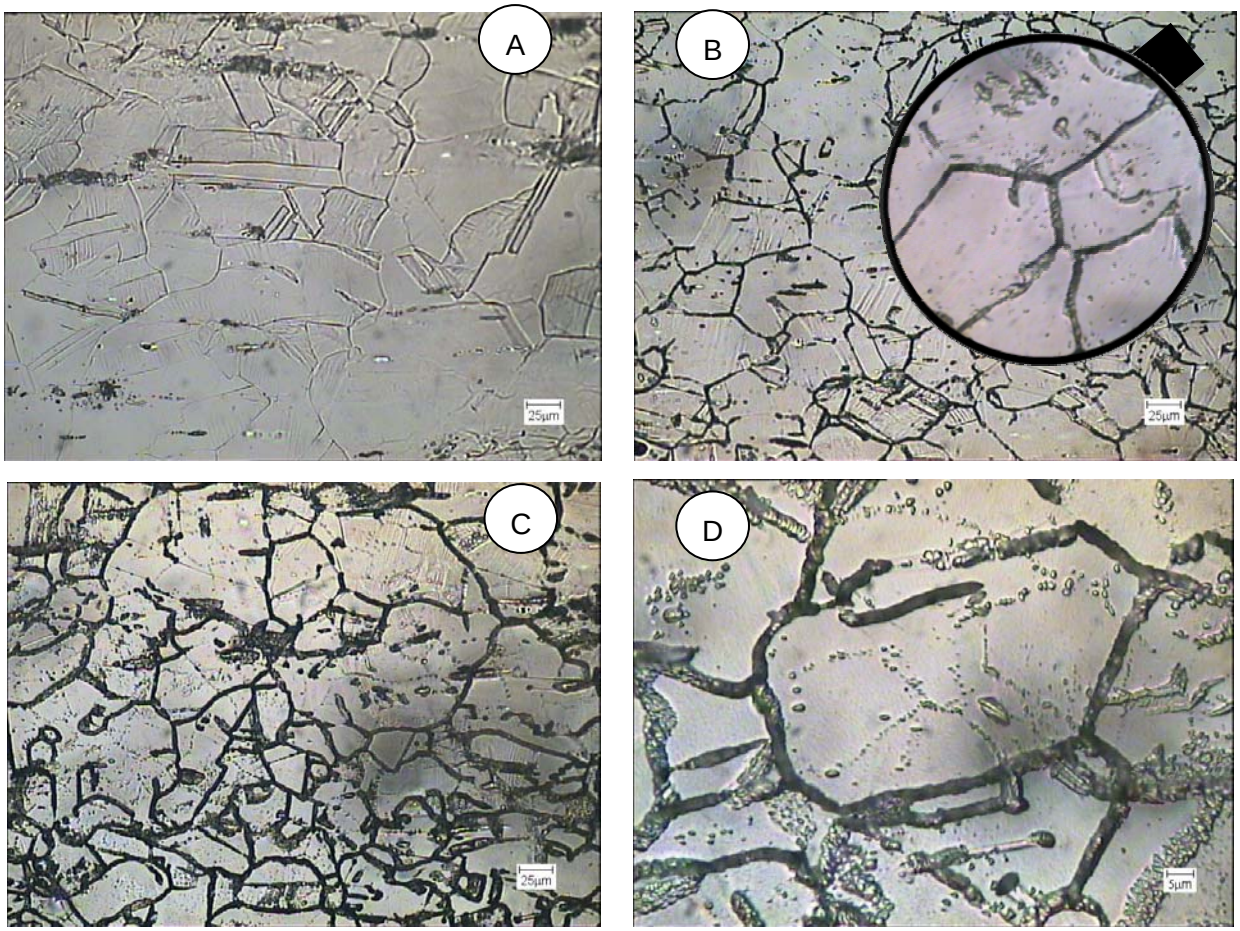


Figure 4. Normal Plane of ASS 20% Cold Rolled: un-sensitised (x20) (A), sensitised for 24Hr (x20) (B), sensitised for 72Hr (x20) (C), sensitised for 72Hr (x80) (D)

The result of optical microscopy of the 40% cold worked sample are contained in Figure 5. Figure 5A showed the macrograph of the un-sensitised sample, while Figures 5B & C were the optical micrographs of the cold rolled samples, sensitised at 650°C for 24 hours and 72 hours respectively. Figure 5D was the higher magnification micrograph of the sample sensitised for 72 hours. The difference between the un-sensitised and sensitised 40% cold worked samples is consistent with those observations in annealed and 20% cold worked samples. In addition to ditches on sensitised austenite grain boundaries, there was evidence of intragranular precipitation of chromium carbide within the austenite grains probably on deformation substructures including the slip bands. The slip bands within the 40% cold worked samples sensitised for 24 hours and 72 hours (Figure 5B & C) also appeared darker like the austenite grain boundaries due to galvanic corrosion ditches between the network of grain boundary carbides and adjacent neighourhood.

Alot of works have been carried out on cold worked ASS which showed that cold working is accompanied with dislocation and deformation bands within the austenite grain boundaries [10, 17, 18]. It has equally been shown that heavily cold worked ASS materials subjected to sensitisation heat treatment exhibit intragranular precipitation of chromium carbides rather than on the grain boundaries [1, 5]. The implication of grain boundaries carbide precipitation has been duely studied and has been linked to the intergranular stress corrosion cracking of the ASS in range of environments [5, 7, 19]. However, others have argued that grain boundary carbide precipitation was not that all bad. It has been shown that [20] grain boundaries carbides can help improve creep resistance of the material by under pinning and preventing the grain boundary slidding. On other hands, heavily cold worked material with high dislocation density and slip bands enhances intragranular precipitation of carbides [11], which is consistent with the results in Figure 5. This helps in two ways: prevention of intergranular failure and help with desensitisation by facilitating diffusivity of chromium back to the matrix through the deformation substructrures including dislocation and slip bands within close propinquity [5].

The effects of soaking time was obvious from the above results in two ways: Long soaking time allowed enough time for extensive precipitation of chromium carbides on the austenite grain boundaries in the annealed and lower cold worked level samples. While long soaking time in heavily cold worked sample allowed sufficient time for intragranular precipitation of chromium carbides on the recrystallised grains within the prior austenite grains.

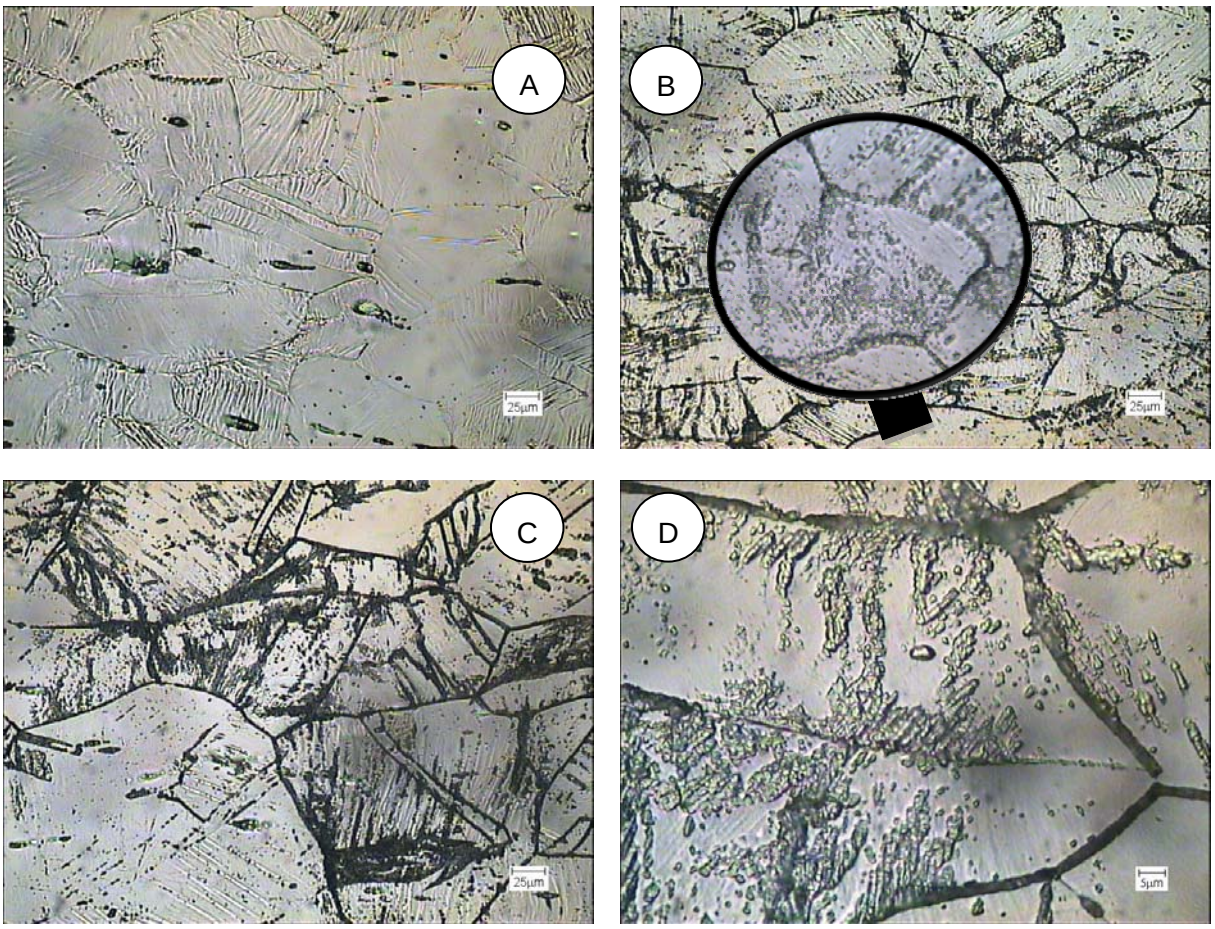

Figure 5. Normal Plane of ASS 40% Cold Rolled: unsensitised (A), sensitised for 24Hr (x20) (B), sensitised for 72Hr (x20) (C), sensitised for 72Hr (x80) (D)

The need requirement of the materials will have to determine how the grain boundaries may be engineered to meet the requirement. It has been highlighted in this work that sensitisation in annealed and lower cold worked austenitic stainless steels for shorter soaking time enhances intergranular precipitation of chromium carbide which makes the materials susceptible to intergranular stress corrosion cracking. On the other hands, intergranular carbide precipitation may equally be considered good for the materials as it increases the resistance of the materials to creep damage by preventing grain boundary slidding. It has also been shown in the work, that sensitisation of the heavily cold worked sample for a prolonged time enhances intragranular carbide precipitation on the recrystallised grains within the prior austenite grains. Though the material may be less susceptible to intergranular failure, however, it thus becomes vulnerable to transgranular stress corrosion cracking.

## 4. CONCLUSION

The following are the conclusions of study investigating effects of soaking time and cold worked levels on the sensitisation of austenitic stainless steels type 304L:

1. Sensitisation occured in austenitic stainless steels both in annealed and cold rolled conditions.
2. Sensitised microstructure showed evidence of galvanic corrosion ditches on the austenite grain boundaries.
3. The severity of the galvanic corrosion ditches increases with soaking time.
4. The corrosion ditches on the grain boundaries were attributed to galvanic interaction between nobler carbide precipitates and the chromium depleted within the close propinquity.
5. Intergranular precipitation of chromium carbide were more copius on the annealed and lower level of cold reduction (20% cold work), while heavily cold rolled samples (40% cold work) exhibited evidence of transgranular carbide precipitation.

## 5. REFERENCES

[1] Lo, K., Shek, C., and Lai, J., *Recent developments in stainless steels.* Materials Science and Engineering: R: Reports. 65(4): p. 39-104, 2009.

[2] Sedriks, A. J., *Corrosion of stainless steel*. John Wiley and Sons, Inc., New York, NY (United States), 1996.

[3] Marshall, P., *Austenitic stainless steels: microstructure and mechanical properties*. Springer, 1984.

[4] Couvant, T., Legras, L., Vaillant, F., Boursier, J., and Rouillon, Y. *Effect of strainhardening on stress corrosion cracking of AISI 304L stainless steel in PWR primary environment at 360 C*. in *Proceedings of the*

*12th international conference on environmental degradation of materials in nuclear power system water reactors, TMS (The minerals, metals & materials society)*.2005.
[5] Garcia, C., Martin, F., De Tiedra, P., Heredero, J. A., and Aparicio, M. L., *Effect of Prior Cold Work on Intergranular and Transgranular Corrosion in Type 304 Stainless Steels: Quantitative Discrimination by Image Analysis.* Corrosion. 56(3): p. 243-255, 2000.
[6] Moura, V., Kina, Y., Tavares, S., de Faria, M., and Mainier, F., *Investigation of cracks and sensitization in an AISI 304L stainless steel exposed to 500–600° C.* Engineering Failure Analysis. 16(1): p. 545-551, 2009.
[7] Singh, R., Chowdhury, S. G., and Chattoraj, I., *Modification of Sensitization Resistance of AISI 304L Stainless Steel through Changes in Grain Size and Grain Boundary Character Distributions.* Metallurgical and Materials Transactions A. 39(10): p. 2504-2512, 2008.
[8] Sourmail, T. and Bhadeshia, H. K. D. H. *Stainless Steels*. 2005.
[9] Kain, V., Chandra, K., Adhe, K., and De, P., *Effect of cold work on low-temperature sensitization behaviour of austenitic stainless steels.* Journal of nuclear materials. 334(2): p. 115-132, 2004.
[10] Ahmed, I. I., Grant, B., Sherry, A. H., and Quinta da Fonseca, J., *Deformation path effects on the internal stress development in cold worked austenitic steel deformed in tension.* Materials Science and Engineering: A. 614(0): p. 326-337, 2014.
[11] Garcia, C., Martin, F., De Tiedra, P., Alonso, S., and Aparicio, M., *Stress corrosion cracking behavior of cold-worked and sensitized type 304 stainless steel using the slow strain rate test.* Corrosion. 58(10): p. 849-857, 2002.
[12] Dieter, G. E. and Bacon, D., *Mechanical metallurgy*. Vol. 119. McGraw-Hill New York, 1986.
[13] ASTM, *Standard Guide for Electrolytic polishing of Metallographic Specimens, Designation: E 1558-99*. West Conshohocken, USA: ASTM International, 1999.
[14] ASTM, *Standard Practices for Detecting Susceptibility to Intergranular Attack in Austenitic Stainless Steels, Designation: A 262-01*. West Conshohocken, USA: ASTM International, 2001.
[15] Kim, S., Moon, H., Kang, T., and Lee, C., *Dissolution kinetics of delta ferrite in AISI 304 stainless steel produced by strip casting process.* Materials Science and Engineering: A. 356(1): p. 390-398, 2003.
[16] Alvarez, C., Almanza, E., and Murr, L., *Evaluation of the sensitization process in 304 stainless steel strained 50% by cold-rolling.* Journal of materials science. 40(11): p. 2965-2969, 2005.
[17] Fu, Y., Wu, X., Han, E.-H., Ke, W., Yang, K., and Jiang, Z., *Effects of cold work and sensitization treatment on the corrosion resistance of high nitrogen stainless steel in chloride solutions.* Electrochimica Acta. 54(5): p. 1618-1629, 2009.
[18] Lee, T.-H., Oh, C.-S., Kim, S.-J., and Takaki, S., *Deformation twinning in high-nitrogen austenitic stainless steel.* Acta materialia. 55(11): p. 3649-3662, 2007.
[19] Singh, R., Chattoraj, I., Kumar, A., Ravikumar, B., and Dey, P., *The effects of cold working on sensitization and intergranular corrosion behavior of AISI 304 stainless steel.* Metallurgical and Materials Transactions A. 34(11): p. 2441-2447, 2003.
[20] Morris, D. and Harries, D., *Creep and rupture in Type 316 stainless steel at temperatures between 525 and 900° C Part II: Rupture and ductility.* Metal science. 12(11): p. 532-541, 1978.

## ACKNOWLEDGEMENTS

The authors wish to thank Professor Pete S. Bate and Mr David Strong for their Technical supports during cold rolling.

***Authors:*** **Lecturer. Dr Ismaila Idowu Ahmed,** Material Performance Centre, University of Manchester, Oxford Road, Manchester, M13 9PL, UK **Lecturer. Mr Jeleel Adekunle Adebisi, Lecturer. Taiwo Yahaya,** Department of Materials and Metallurgical Engineering, University of Ilorin, P.M.B. 1515, Nigeria. +2347018271354
**Lecturer. Sulaiman Abdulkareem,** Department of Mechanical Engineering, University of Ilorin, P.M.B. 1515, Nigeria.
E-mail:
Ahmed.ii@unilorin.edu.ng
adebisi.ja@unilorin.edu.ng
yahaya.t@unilorin.edu.ng
abdulkareem.s@unilorin.edu.ng

Journal of Production Engineering
Vol.18 No.2
JPE (2015) Vol.18 (2) Original Scientific Paper

Babič, M.

# NEW METHOD OF HARDENING AND COMPARISON WITH ANOTHER METHOD

Received: 20 October 2015 / Accepted: 15 November 2015

**Abstract:** *In this article we present new method of robot laser hardening. We present different methods of hardening. The principles of laser heating are similar to those of conventional through heating. The time scales involved in the former are, however, typically an order of magnitude shorter. Where as heating is conventionally induced by a furnace, flame, arc or induction coil, the laser beam is focused or shaped into a suitable pattern and scanned over the component. The high energy density laser beam heats the surface much more rapidly, reducing the time for conduction into the bulk of the component. Laser heat treatment and surfacing techniques must compete directly with a wide range of comparatively low cost conventional processes and must therefore offer significant advantages. In the end we present results of hardness materials with different method of hardening and new method of laser hardening.*

***Key words:*** *hardening, laser, inductive, classical*

**Nova metoda kaljenja i poređenje sa drugim metodama.** *U ovom radu je predstavljena nova metoda kaljenja pomoć robotom vođenog lasera. Predstavljene su različite metode kaljenja. Princip zagrevanja pomoću lasera je sličan konvencionalnom zagrevanju. Vremenski period potreban za kompletno odvijanje procesa je kod lasera kraći nego kod konvencionalnih metaoda. Kod konvencionalng postupka se zagrevanje izvodi u peći, plamenom, lukom ili indukcionim kalemom, dok je kod laserskog postupka zrak usmeren na deo koji se termički obrađuje. Snop laserskog zraka visoke energije brže zagreva površinu i time skraćuje vreme širenja toplote u unutrašnjost komada. Termička obrada laserom i površinska obrada laserom mora da se takmiči sa nizom niskozahtevnih konvencionalnih procesa i stoga mora pružiti pozamašne prednosti. Na kraju su predstavljeni rezultati tvrdoće materijala kaljeni različitim konvencionalnim metodama i kaljeni novom metoda pomoću lasera.*

**Ključne reči:** *kaljenje, laser, induktivno, klasično*

## 1. INTRODUCTION

Power lasers offer rapid, high-quality and reproducible heat treatment methods. Laser surface hardening [1-4] consists of the rapid heating of a material's surface by laser beam, a short hold at the target temperature, and intensive cooling due to the high thermal conductivity of the material. Its ability to perform local hardening restricted to a prescribed location is a significant advantage of laser hardening. Hardening depth and the resulting hardness can be controlled as well. On-line control of temperature is available thanks to a pyrometer built intothe optical system. We use robot laser cell RV60-40 from Company Reis Robotics. Reis Robotics is a leading technology company for robotics and system integration. The articulated-arm robot series is the most important robot kinematics for industrial use. As 6-axes universal robots with high path speeds and large work envelopes the RV-robots are especially suited for the high demands of path-related tasks. The design based on FEM and CAD stands out due to its excellent static and dynamic behavior. Their robotic automation solutions are used by all major application fields such as solar energy, foundry, welding and hardening. The Reis Robotics group comprises three German subsidiaries and eight international subsidiaries as well as representative agencies in many countries.The advantages of laser hardening are less refinishing work and the ability to process irregular, three-dimensional workpieces. Costs related to refinishing work are reduced or eliminated entirely. To harden the workpiece, the laser beam typically warms the outer layer to just under the melting temperature (about 900 to 1400 degrees Celsius). Once the desired temperature is reached, the laser beam starts moving. As the laser beam moves, it continuously warms the surface in the processing direction. The high temperature causes the iron atoms to change their position within the metal lattice (austenization). As soon as the laser beam moves away, the hot layer is cooled very rapidly by the surrounding material in a process known as self-quenching. Rapid cooling prevents the metal lattice from returning to its original structure, producing martensite. Martensite is a very hard metal structure. The transformation into martensite yields greater hardness. The laser beam hardens the outer layer, or case, of the workpiece. The hardening depth of the outer layer is typically from 0.1 to 1.5 millimeters. On some materials, it may be 2.5 millimeters or more. Greater hardening depth requires a larger volume of surrounding material to ensure that the heat dissipates quickly and the hardening zone cools fast enough.Induction hardening [5] is a form of heat treatment in which a metal part is heated by induction heating and then quenched. The quenched metal undergoes a martensitic transformation, increasing the hardness and brittleness of the part. Induction

hardening is used to selectively harden areas of a part or assembly without affecting the properties of the part as a whole. These hardening and tempering furnaces are highly valued for durability and reliable with good tensile strength. Flame hardening [6] is often used to harden only a portion of an object, by quickly heating it with a very hot flame in a localized area, and then quenching the steel. This turns the heated portion into very hard martensite, but leaves the rest unchanged. Flame hardening is a very common surface hardening technique, which is often used to provide a very wear-resistant surface. A common use is for hardening the surface of gears, making the teeth more resistant to erosion. The gear will usually be quenched and tempered to a specific hardness first, making a majority of the gear tough, and then the teeth are quickly heated and immediately quenched, hardening only the surface. Afterward, it may or may not be tempered again to achieve the final differential hardness.The aim of the research is present different techniques of hardening.

## 2. MATERIAL PREPARATION AND METHOD

The study was undertaken using tool steel standard label EN100083 − 1.In Fig. (1-10) are presented different method of hardening. Fig. 1 presentrobot laser hardeningwith different speed and Temperature of hardening.In this positionwe can change two parameters of robot laser cell. In our case we change parameter of speed v $\in$[2, 5] mm/s instepsof 1 mm/s,and temperatureT$\in$ [0, 2000] °C.

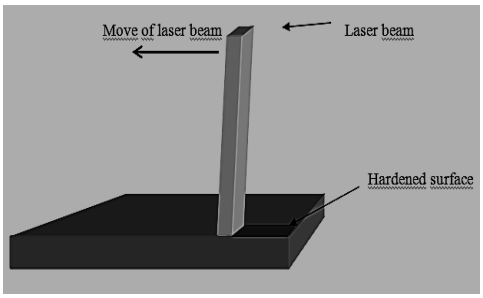

Fig. 1. Robot laser hardening with different speed and Temperature

Fig. 2 present point robot laser hardening. This case is similar like hardening in Fig. 1. In this position, we change only parameter of Temperature.

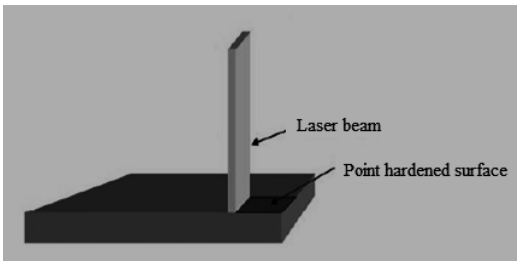

Fig. 2. Point robot laser hardening

Fig. 3 present robot laser hardening next to hardened cone of materials. Firstly, we hardened materials with differentspeed and Temperature of hardening. Second, we repeat equal process next to hardened cone of materials.

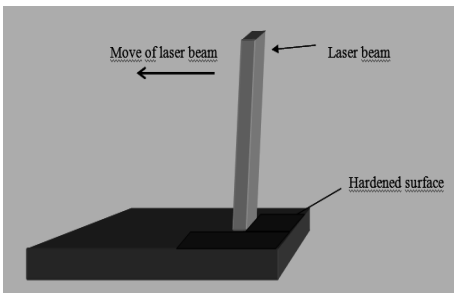

Fig 3. Hardening material next to hardened zone

Fig. 4 present robot laser hardening with overlapping of laser beam [7]. Process is similar like in Fig. 3, but in this case, we move laser beam over hardened cone of materials. In this position, we can move laser beam over hardened cone a few millimeters.

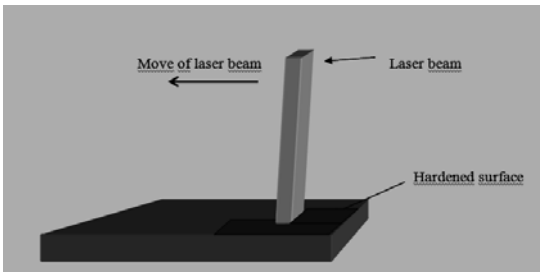

Fig 4. Hardening material with overlapping

Fig. 5 present robot laser hardening with different angles of laser beam [8].It this situation we have donetestsfor angles of$\varphi\in\{15°,30°,45°,60°,75°,90°\}$ between the right site of laser beam and the material surface.

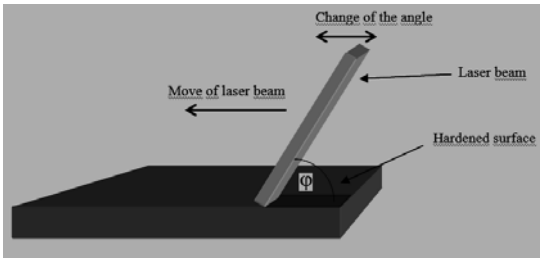

Fig. 5. Robot laser hardening: the variation of the incidence angle $\varphi\in(0, 90)°$ between the right site of laser beam and the material surface

Fig. 6 present robot laser hardening with different angles of laser beam. It this situation we have donetests for angles of$\varphi\in\{15°,30°,45°,60°,75°,90°\}$between the leftsite of laser beam and the material surface.

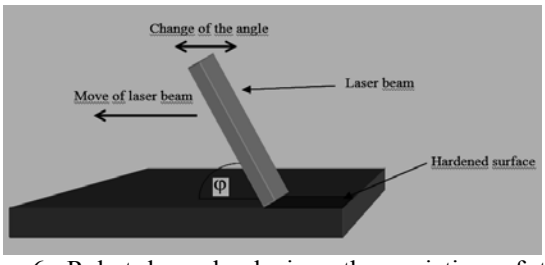

Fig. 6. Robot laser hardening: the variation of the incidence angle $\varphi\in(0, 90)°$ between the left site of laser beam and the material surface

Fig. 7 present robot laser hardening with different angles of laser beam. It this situation we change the angle in the regard to the perpendicular direction of the laser beam. Also, we have donetestsfor angles of$\varphi \in \{15°,30°,45°,60°,75°,90°\}$.

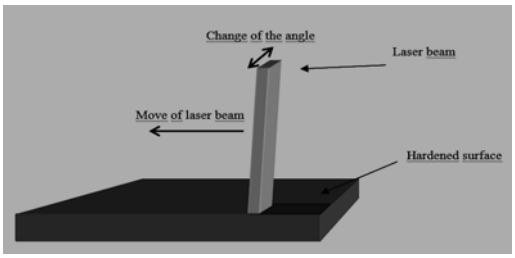


Fig. 7. Robot laser hardening: the lateral incidence angle of the laser beam on the material surface and the beam movement direction

Fig. 8 present inductive hardening.

Fig. 8. Inductive hardening

Fig. 9 present classical hardening.


Fig. 9. Classical hardening

Fig. 10 present flame hardening.

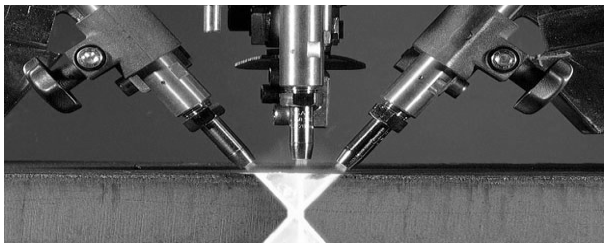

Fig. 10. Flame hardening

## 4. RESULTS AND DISCUSSION

In Table 1, the parameters and hardnessof hardened specimens. We mark specimens from P1 to P40. Parameter X1 presents the parameter of temperature [°C], X2 presents the speed of hardening [mm/s], X3 presents angle [°] of hardening and X4 presents hardness [HRc] of hardened specimens.P1-P8 present hardened specimens with process present in Fig. 1. P9-P16 present hardened specimens with process present in Fig. 3. P17-P19 present hardened specimens with process present in Fig. 2. P20 present hardened specimens with process present in Fig. 8. P21present hardened specimens with process present in Fig. 9. P22-P27 present hardened specimens with process present in Fig. 5. P28-P33 present hardened specimens with process present in Fig. 6. P34-P39 present hardened specimens with process present in Fig. 7. P40 present hardened specimens with process present in Fig. 10.

| S | X1 | X2 | X3 | X4 |
|---|---|---|---|---|
| P0 | 0 | 0 | 90 | 34,0 |
| P1 | 1000 | 2 | 90 | 60,0 |
| P2 | 1000 | 3 | 90 | 58,7 |
| P3 | 1000 | 4 | 90 | 56,0 |
| P4 | 1000 | 5 | 90 | 56,5 |
| P5 | 1400 | 2 | 90 | 58,0 |
| P6 | 1400 | 3 | 90 | 57,8 |
| P7 | 1400 | 4 | 90 | 58,1 |
| P8 | 1400 | 5 | 90 | 58,2 |
| P9 | 1000 | 2 | 90 | 57,4 |
| P10 | 1000 | 3 | 90 | 56,1 |
| P11 | 1000 | 4 | 90 | 53,8 |
| P12 | 1000 | 5 | 90 | 56,0 |
| P13 | 1400 | 2 | 90 | 55,3 |
| P14 | 1400 | 3 | 90 | 57,2 |
| P15 | 1400 | 4 | 90 | 57,8 |
| P16 | 1400 | 5 | 90 | 58,0 |
| P17 | 800 | 0 | 90 | 52,0 |
| P18 | 1400 | 0 | 90 | 57,0 |
| P19 | 2000 | 0 | 90 | 56,0 |
| P20 | 950 | 0 | 90 | 58,0 |
| P21 | 850 | 0 | 90 | 57,0 |
| P22 | 0 | 0 | 15 | 61,5 |
| P23 | 0 | 0 | 30 | 60,4 |
| P24 | 0 | 0 | 45 | 60,8 |
| P25 | 0 | 0 | 60 | 58,0 |
| P26 | 0 | 0 | 75 | 59,0 |
| P27 | 0 | 0 | 90 | 58,6 |
| P28 | 0 | 0 | 15 | 55,0 |
| P29 | 0 | 0 | 30 | 56,2 |
| P30 | 0 | 0 | 45 | 53,2 |
| P31 | 0 | 0 | 60 | 54,2 |
| P32 | 0 | 0 | 75 | 45,4 |
| P33 | 0 | 0 | 90 | 58,6 |
| P34 | 0 | 0 | 15 | 53,4 |
| P35 | 0 | 0 | 30 | 59,2 |
| P36 | 0 | 0 | 45 | 58,0 |
| P37 | 0 | 0 | 60 | 59,4 |
| P38 | 0 | 0 | 75 | 59,8 |
| P39 | 0 | 0 | 90 | 58,6 |
| P40 | 0 | 0 | 90 | 55,0 |

Tab 1.Parameters and hardness of hardened specimens

Specimens P0 present hardness before hardening. Specimen P22 has most hardness, 61,5HRc. Very interesting is problem presented in Fig. 7. In this situation, we harden materials at an incidence angle of

φ ≠ 90°.Fig. 7 show the situation, where we change angles in different direction.We see that the up perpart of the beam has a longer travel time than the lower part of the beam.This means that thelower part of thehardenedpiece is betterthan the upper. The work piecewill not be evenly hardened and the final result of laser hardening will not begood.By using angular functions we can calculate the width of hardening at a certain angle. Here, the following information is already known: the width of optics(d) and the angle (φ) under which the hardening is conducted. The hardening widthis calculated. The width of the beamoptics presents oneside of a right triangle, the angle (φ) of hardeningis the right triangle's opposite side, which was marked with the width ofoptics (d). Beam hardening of the work pieceis the hypotenuse of the right triangle, denoted by x. After delivery the sinusis

$\sin\varphi = d/x$ , $d \in \{5, 8, 13, 16, 23, 28\}$, $\varphi \in (0°, 180°)$ .

The purpose of this work has been to study how different techniques impact on the hardness of hardened specimens. We present how angles of robot laser cell impact the hardness of specimens. The presented problem could be solvedin order to modify the laser beam intensity a cross the width. This means that the first laser beam isdivided intoseveral parts.Then each part of the laser beam is divided intothe specified strength. The part ofthe laser beam, which made the longest jour neygave most of the power to that part ofthe beam, and the part which had the shortest path to the device, but was giventhe smallest amount of laser beam intensity.

## 5. CONCLUSSION

In this article we present different method of hardening. The robot laser hardening process has several advantages over conventional induction hardening. Thus, in the future we still have enough unsolved problems in robot laser hardening. Robot laser cells have several parameters that affect the final result of hardening. These laser parameters are power, energy density, focal distance, energy densityin the focus, focal position, temperature and speed of hardening. In the future we want to explore how different angles of a laser beam in the hardening process affect thehardenedpatterns in:

- Two laser-beam of robot laser hardening (laser beam is divided into two parts).

Also, here we present new method of robot laser hardening; two laser-beam of robot laser hardening. Situation is presented in Fig. 11.

In the future we want to present new techniques of robot laser hardening:

- twolaser-beam of robot laser hardening
- twolaser-beam of point robot laser hardening
- twolaser-beam of robot laser hardening with different speed and Temperature
- twolaser-beam of robot laser hardening with different angles
- point robot laser hardeningwith different angles

point robot laser hardenig with overlapping of laser beam.

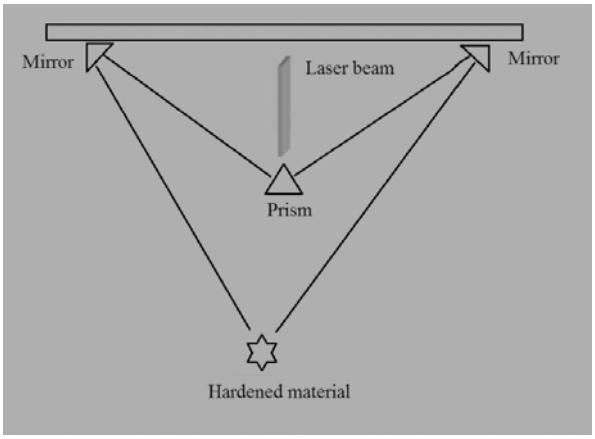

Fig. 11. Idea of two laser beam of robot laser hardening

## 6. REFERENCING

[1] J. Grum, P. Žerovnik, R. Šturm: Measurement and Analysis of Residual Stresses after Laser Hardening and Laser Surface Melt Hardening on Flat Specimens; *Proceedings of the Conference "Quenching '96"*, Ohio, Cleveland, 1996.

[2] Daley, W.W. Laser processing and analysis of material. Chapter 1: Laser and Laser radiation Plenum Press: New Yourk, 1983, 158-162.

[3] Gregson, V.G. Chapter 4: Laser and heat treatment. In Laser Materials Procesing. Bass, M., Ed.; Materials Procesing Theory and Practices; North-Holland Publishing Company: Amsterdam, 1983, Vol. 3, 201-234.

[4] J. Grum, R. Šturm. Calculation of Temperature Cycles Heatinh and Quenching Rates During Laser Melt – Hardening of Cast Iron. In: LAJL Sarton, HB Zeedijk eds., Proc. Of the 5th European Conf. On Advanced Materials and Processes and Applications, Materials, Functionality&Desing, vol. 3. Surface Engineering and Functional materials. Maastricht, NL 1997, 3/155 – 3/159.

[5] Rapoport, Edgar; Pleshivtseva, Yulia (2006), *Optimal Control of Induction Heating Processes*, CRC Press, ISBN 0-8493-3754-2

[6] A.K. Rakhit, Nitriding Gears, Chap. 6, Heat Treatment of Gears: A Practical Guide for Engineers, ASM International, p 133–158.

[7] BABIČ, Matej, BALIČ, Jože, MILFELNER, Matjaž, BELIČ, Igor, KOKOL, Peter, ZORMAN, Milan, PANJAN, Peter. Robot laser hardening and the problem of overlapping laser beam. *Advances in production engineering & management*, ISSN 1854-6250, 2013, vol. 8, no. 1, str. 25-32, ilustr.

[8] BABIČ, Matej, MILFELNER, Matjaž, BELIČ, Igor, KOKOL, Peter. Problems associated with a robot laser cell used for hardening = Problematika robotskega laserskega kaljenja. *Materiali in tehnologije*, ISSN 1580-2949. [Tiskana izd.], jan.-feb. 2013, letn. 47, št. 1, str. 37-41.

***Author:*** **Dr. Matej Babič, Bs.M.** Researcher, Slovenia
E-mail: babicster@gmail.com

Journal of Production Engineering
Vol.18 No.2
JPE (2015) Vol.18 (2) Original Scientific Paper
M. Plavšić, S. Mirjanić, Z. Božičković, P. Kovač, D. Ješić, D. Rodić

# DAMAGE MECHANISMS OF AUSTENITIC CHROMIUM-NICKEL PIPES IN EXPLOITATION

Received: 19 May 2015 / Accepted: 23 August 2015

**Abstract:** *In the exploitation of austenitic chromium-nickel pipes are different possible mechanisms of damage. In this study, a catalytic steam reformer pipes was used where presented different reactions and various problems. Materials of pipes were represented a special problems that form the mechanisms of damage due to the effects of high operating temperatures, corrosion and corrosive gases. The aim of the research is to determine the causes and extent of the mechanical and microstructural properties changes and cracking of the material ASTM A 297 exploited catalytic pipes. According to the plan of experimental research, were conducted the detailed mechanical testing of new materials and exploited pipes. The microstructural changes in materials exploited pipe were analyzed by light microscopy. The results of mechanical tests and metallographic new catalytic pipes of the same material was used as a basis for comparison of the results.*
***Key words:*** *catalytic pipes, inter-crystalline stress corrosion, carbides*

**Mehanizmi oštećenja austenitnih hrom-nikl cevi u eksploataciji.** *U eksploataciji austenitnih hrom-nikl cevi mogući su različiti mehanizmi oštećenja. U ovom radu, za primer su uzete katalitičke cevi parnog reformera kod kojih su prisutne različite reakcije i brojni problemi. Posebne probleme predstavljaju materijali cevi u kojima nastaju mehanizmi oštećenja usled dejstva visokih radnih temperatura i koroziono agresivnih gasova. Cilj istraživanja, bio je utvrditi uzroke i opseg mehaničkih i mikrostrukturnih promena osobina i pojave prslina u materijalu ASTM A 297 eksploatisane katalitičke cevi. Prema planu eksperimentalnih istraživanja, urađena su detaljna mehanička ispitivanja materijala nove i eksploatisane cevi. Uz pomoć svetlosne mikroskopije analizirane su mikrostrukturne promene u materijalu eksploatisane cijevi. Kao baza za poređenje rezultata, poslužili su rezultati mehaničkih i metalografskih ispitivanja nove kataltičke cevi od istog materijala.*
***Ključne reči:*** *katalitičke cevi, inter-kristalna, naponska korozija, karbidi*

## 1. INTRODUCTION

In the process industry, there are numerous problems, during the operation of catalytic pipes of a steam-reforming furnace. Due to the high operating temperatures and corrosive "aggression" working fluid, on the system components are different possible mechanisms of damage [1].

Working fluid at the entrance of the catalytic pipes is a mixture of gases, hydrogen and various carbon-hydrogen from oil processing plants and water vapor with temperature ~ 380 ° C and pressure of 1.4 MPa [2].

At the pipes exit, the working temperature is 760-780 ° C and pressure of 1.4 MPa, after the catalytic reaction, the produced is hydrogen - the main product, carbon dioxide, carbon monoxide and small amounts of methane (CH4 ≤ 1). Hydrogen, along with other products leads to further cooling and to the plant Hydrocracking. The capacity of the reformer, the quantity of hydrogen produced in $m^3/h$, or $m^3/day$, forms and construction are different [3]. Catalytic pipe that was studied (Figure 1), has worked to the emergence of sensitization and cracks around six months. The average life of the exploitation of these pipes is ~ 100 000 h [1]. It is well known that cracks are the most dangerous form of damages. Mechanisms of damage of catalytic pipes appear in the form of: corrosion, creep, thermal fatigue, distortion pipes etc. [4]. With stainless austenitic chromium - nickel steels, it is particularly important to point out to intergranular corrosion, spotted or pitting corrosion, galvanic and voltage corrosion [5].

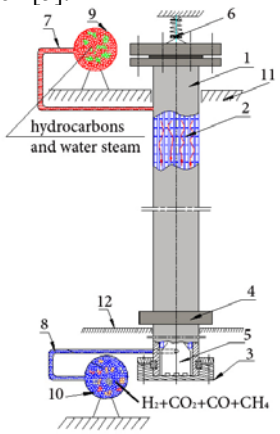


Fig. 1. Scheme of the catalytic pipes

Herein is: A catalytic pipe 1; 2 catalyst (charge pipes); 3 Flange; 4 Steel ring backbone; 5 Output of chamber (capsule form); 6 Elastic adjustable connection; 7 fluid inlet pipe 8 Outlet pipe of working fluid; 9 Upper - inlet collector; 10 Lower - output collector; 11 The upper ceiling - roof reformer; 12 The base of the reformer. Catalytic pipes are made by a

horizontal centrifugal casting. Castings are seam welded connecting to the intended length. Widely used are catalytic pipes of austenitic-carbide alloy HK-40 [6, 7].

The aim of the research is to determine the causes and extent of the mechanical and microstructural properties changes and cracking of the material ASTM A 297 exploited catalytic pipes. According to the plan of experimental research, were conducted the detailed mechanical testing of new materials and exploited pipes. The microstructural changes in materials exploited pipe were analyzed by light microscopy. The results of mechanical tests and metallographic new catalytic pipes of the same material was used as a basis for comparison of the results.

## 2. EXPERIMANTAL PROCEDURE

Metallographic examination of the structure of a catalytic material, (the label "N") and exploited pipe (label "S"), for comparison purposes are performed on three samples. Sample segment of exploited pipes, was catted from the zone of highest temperature around the crack. The tests were performed in a polished and etched condition at light microscope. For all mechanical tests were used in three standard pipes. Mechanical testing of fracture toughness for both pipes were made at temperatures of 20 ° C, 500 ° C and 900 ° C. The pipe material was centrifugally cast, fire-resistant, austenitic alloy carbide HK-40. Chemical composition of alloy HK-40 is defined by the standard of ASTM A 297. The chemical composition of the exploited and new pipes is shown in Table 1.

| **Exploited pipe** | | **New pipe** | |
|---|---|---|---|
| C | 0.521 | C | 0.436 |
| Si | 1.788 | Si | 1.813 |
| Mn | 0.420 | Mn | 0.322 |
| P | 0.018 | P | 0.019 |
| S | 0.020 | S | 0.021 |
| Cu | 0.197 | Cu | 0.209 |
| Al | 0.003 | Al | 0.007 |
| Cr | 24.71 | Cr | 24.68 |
| Mo | 0.166 | Mo | 0.148 |
| Ni | 19.61 | Ni | 19.76 |
| V | 0.036 | V | 0.041 |
| Nb | 0.063 | Nb | 0.251 |
| Co | 0.078 | Co | 0.123 |
| W | 0.221 | W | 0.186 |
| Fe | 52.14 | Fe | 51.9 |

Table 1. Chemical composition of exploited and new pipes

Experimental equipment: The chemical composition test of the new pipes material (marked "N") and exploited pipes (marked "S") was used alloy analyzer, "NITON XL3T"; for measuring the hardness Rockwell - KARL FRANK model Mannheim U2; for tensile testing - electro-mechanical testing machine "SCHENCK TREBEL RM-100"; for impact testing pipes - instrumented Charpy pendulum SCHENCK TREBEL 150J, Charpy specimens 10x10 mm; for recording energy generation and energy spread - instrumental pendulum; to create a fatigue crack - a high-frequency pulsar "AMSLER". Bending specimens was done on the testing machine SCHENCK TREBEL RM 100.

## 3. RESULTS

The hardness was measured at eight different locations across the thickness of pipes, symmetrically across section. Based on the measured hardness of Rockwell on a sample exploited the catalytic pipes, had a higher difference the hardness of the pipes over the cross section, where on the surface of cross section measured slightly lower hardness with the inner edge of the pipe wall. This decrease in hardness with the inner edge of the pipe wall, it is likely the result of decarburization and further increase the hardness of the inner the edge of the pipe wall, the result of carbonization. Measured hardness on the sample pipe is exploited in a catalytic is much greater than the standard values for this material, which points to the brittleness of the material. Hardness new pipes is within acceptable limits, oko170 HB. The hardness of exploited and new pipes as shone in Table 2.

| **Exploited pipe** | | **New pipe** | |
|---|---|---|---|
| I | 27,5 | I | 18,6 |
| II | 23,1 | II | 25,2 |
| III | 33,4 | III | 26,7 |
| IV | 24,4 | IV | 24,5 |
| V | 25,6 | V | 16,3 |
| VI | 28,1 | VI | 19,3 |
| VII | 34,7 | VII | 19,4 |
| VIII | 29,5 | VIII | 22,4 |

Table 2. The Rockwell hardness of exploited and new pipes

The resulting stress-elongation curve or diagram gives a direct indication of the material properties. Figures 2 and 3 shows the strain-stress curves for an exploited and new pipe.

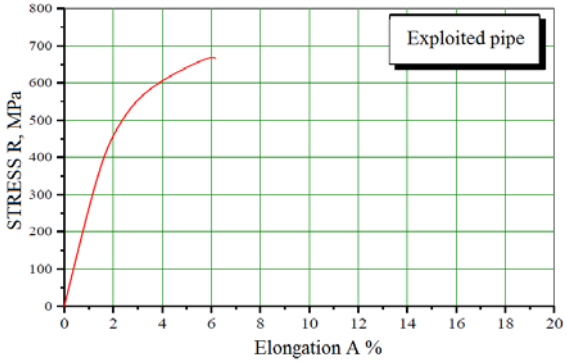


Fig. 2. Stress-strain curve for exploited pipe

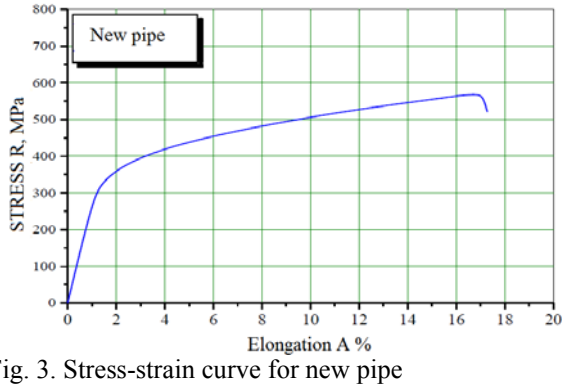


Fig. 3. Stress-strain curve for new pipe

The results from the tensile test, Table 3, predict how a material will react under other types of forces. Properties that are directly measured via a tensile test are ultimate yield strength, tensile strength and maximum elongation.

| Specimens | Yield strength $R_{p0,2}$ [MPa] | Tensile strength $R_m$ [Mpa] | Elongation A [%] |
|---|---|---|---|
| $S_{senz.}$ | 457 | 670 | 4,6 |
| $S_{st}$ | 441 | 638 | 6,3 |
| N | 369 | 586 | 14,9 |

Table 3. Values of tensile tests for exploited and new pipes

Toughness is the ability of a material to absorb energy and plastically deform without fracturing. Values of toughness tests for exploited and new pipes shown in Table 4.

| Test pipe | Test Temp. t [C°] | Total Impact energy $A_{uk}$ [J] | Crack initiation energy $A_I$ [J] | Crack propagation energy $A_p$ [J] |
|---|---|---|---|---|
| S | 20 | 2,2 | 0,5 | 1,7 |
| N | 20 | 7,5 | 2,3 | 5,2 |
| S | 500 | 4,3 | 1,6 | 2,5 |
| N | 500 | 24,5 | 10 | 14,5 |
| S | 900 | 7,9 | 3,6 | 4,3 |
| N | 900 | 22 | 6,3 | 15,7 |

Table 4. Values of toughness tests for exploited and pipes

Fatigue crack is the weakening of a material caused by repeatedly applied loads. The progressive and localized structural damage occurs when a material is subjected to cyclic loading. Fatigue crack of exploited and new material shown in Table 5.

| | Fatigue crack | | | | | Aver. $a_{sr}$ [mm] | Total value a[mm] |
|---|---|---|---|---|---|---|---|
| | $a_{z1}$ | $a_{z2}$ | $a_{z3}$ | $a_{z4}$ | $a_{z5}$ | | |
| N | 2,26 | 3,12 | 4,09 | 3,15 | 2,28 | 3,14 | 4,93 |
| S | 2,58 | 3,31 | 4,03 | 3,20 | 2,46 | 3,12 | 4,77 |

Table 5. Fatigue crack of exploited and new material

The stress intensity factor, K, is used in fracture mechanics to predict the stress state ("stress intensity") near the tip of a crack caused by a remote load or residual stresses. Values of stress intensity factor and critical length of fatigue of exploited and new material sown in Table 6.

| Test pipe | Temperature tests ° C | Stress intensity factor K,MPa·m$^{1/2}$ | Critical length of Fatigue $a_c$ [mm] |
|---|---|---|---|
| $S_{st}$ | 20 | 31 | 1,4 |
| N | 20 | 58 | 6,1 |

Table 6. Values of stress intensity factor and critical length of fatigue of exploited and new material

The amount of energy that the specimen absorbed during the entire impact test – from start to end. This value may be the same as energy to maximum load when the specimen abruptly fails at the maximum load point. The value is calculated from the time the load begins to rise until the first occurrence of zero load after the maximum point [8]. This value can be used as an indicator to a materials ductility or toughness, the higher the value the stronger the material. The dependence of the total energy of the impact, Auk, versus the tests temperature, for exploited and new pipes is given in Figure 4. The ratio of cracks creation energy AI, and crack propagation Ap in total energy Auk for the new pipe, shown in Figure 5. The ratio of cracks creation energy AI, and crack propagation Ap in total energy Auk for the exploited pipe shown in Figure 6.

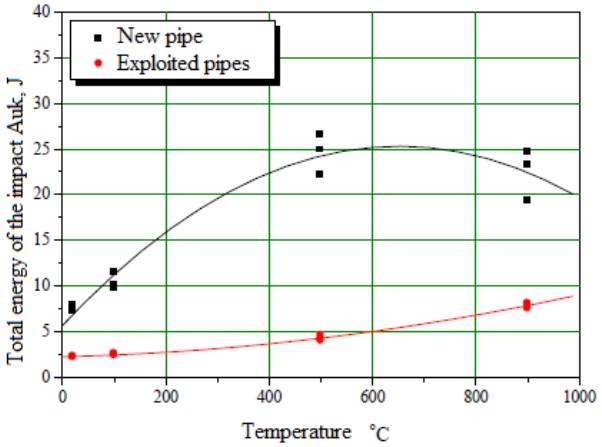


Fig. 4. Dependence of $A_{uk}$ versus temperature for exploited and new pipes

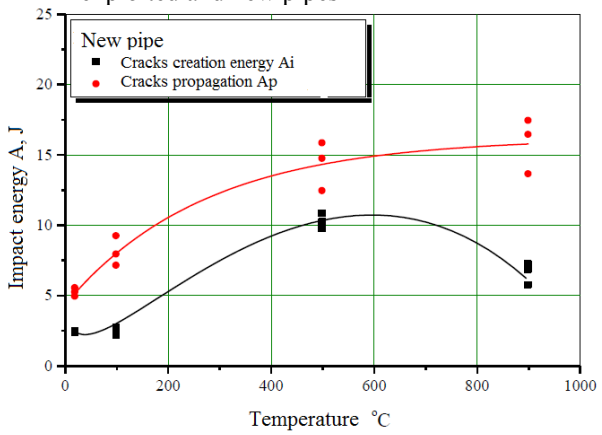


Fig. 5. The ratio of cracks creation energy $A_I$, and crack propagation $A_p$ in total energy $A_{uk}$ for the new pipe

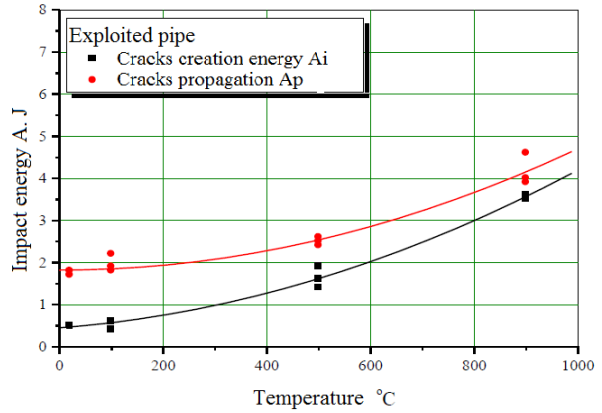


Fig. 6. The ratio of cracks creation energy $A_I$, and crack propagation $A_p$ in total energy $A_{uk}$ for the exploited pipe

Figures 7, is shown metallographic capture new pipe ($MN_1$, $MN_2$). The microstructural state of the material is austenitic, with the presence of primary carbides distributed along grain boundaries and is eutectoid nature. Eutectic carbide is mainly in the shape of a continuous form (carbide bands).

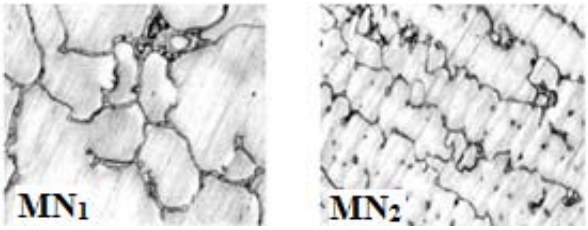


Fig. 7. Metallographic images ($MN_1$ 400x, $MN_2$ 200x)

Figures 8, is shown metallographic capture exploited pipe (MN3, MN4). The presence of carbide is highly expressed on the austenite grain boundaries it is sensitization. Deep intercrystal microcracks on the outside of pipe are detected. The presence carbide is intense, which is interpreted highpercentage C, and it is very expressed within austenite grains.

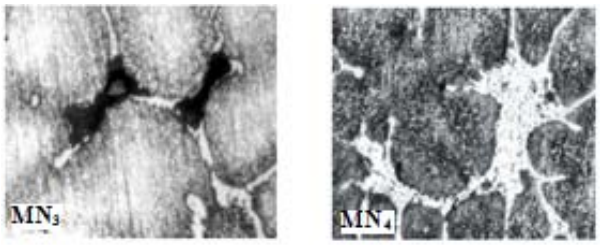


Fig. 8. Metallographic images ($MN_3$ 1000x, $MN_4$ 1000x)

Figure 9. shows sensitization cracks from the outside and view from the inside of the HK'40 material exploited chromium nickel pipes.

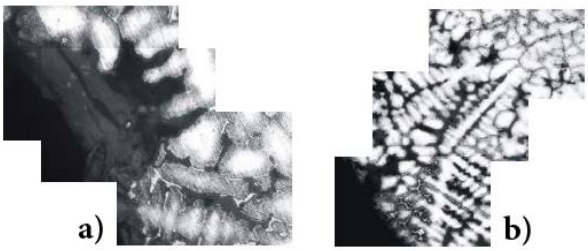


Fig. 9. Structure of materials exploited pipes: a) a view from the outside, b) the view from the inside

## 4. CONCLUSION

Due to the high carbon content (above 0.45%, the maximum value according to ASTM A 351 94a, for this material) and a low content of Mn and stabilizing elements such as Nb, which forming special carbide NbC in austenitic material of pipe. After that comes up spills very hard carbide $Cr_{23}C_6$ and and another short phase ("σ" phase) at the border of austenitic grain sensitization, depletion of chromium along the grain boundaries and appearance of intergranular corrosion.

The action of very aggressive corrosion agents (H2, CH4, CO2, CO, steam atmospheres) further accelerates the corrosion processes. Large microstructural changes in the pipe, Figure 5, caused microstructural corrosion. Due to the effects of microstructural corrosion and stress leads to a pipe fracture. Results of mechanical tests show that the impact stress corrosion on the mechanical properties very unfavorable and it is a very brittle material.

## 5. REFERENCES

[1] Padilha, A. F., Plaut, R. L., & Rios, P. R. (2003). Annealing of Cold-worked Austenitic Stainless Steels. *ISIJ international*, *43*(2), 135-143.

[2] da Silveira, T. L., & Le May, I. (2006). Reformer Furnaces: Materials, Damage Mechanisms, and Assessment. Arabian Journal for Science and Engineering, 31(2), 99.

[3] Sidorov, B. A., Ershova, O. B., & Shchayuk, E. P. (1994). Corrosion cracking of austenitic chrome-nickel steel in the environment of primary fatty alcohol manufacture—a subject for discussion. Chemical and Petroleum Engineering, 30(8), 398-400.

[4] Tawancy, H. M. (2012). Damage Analysis of Catalyst Pipe of a Reformer Furnace Used in Hydrogen Production. Metallography, Microstructure, and Analysis, 1(5), 199-207.

[5] Cuevas-Arteaga, C. (2008). Corrosion study of HK-40m alloy exposed to molten sulfate/vanadate mixtures using the electrochemical noise technique. Corrosion Science, 50(3), 650-663.

[6] Navaei, A., Eslami-Farsani, R., & Abbasi, M. (2013). Evaluation and modification of inclusion characteristics in HK40 heatresistant cast steel. International Journal of Minerals, Metallurgy, and Materials, 20(4), 354-359

[7] Kim, Y. J., Lee, D. G., Jeong, H. K., Lee, Y. T., & Jang, H. (2010). High temperature mechanical properties of HK40-type heat-resistant cast austenitic stainless steels. Journal of Materials Engineering and Performance, 19(5), 700-704.

[8] Yamamoto, Y., Brady, M. P., Lu, Z. P., Liu, C. T., Takeyama, M., Maziasz, P. J., & Pint, B. A. (2007). Alumina-forming austenitic stainless steels strengthened by laves phase and MC carbide precipitates. Metallurgical and Materials Transactions A, 38 (11), 2737-2746

## ACKNOWLEDGEMENTS

The paper is the result of the research within the project TR 35015 (2011/15) financed by the Ministry of Education, Science and Technological Development of the Republic of Serbia and CEEPUS project.

***Authors:*** **Prof. dr. Milan Plavšić[1], prof. dr. Slađana Mirjanić[2], prof. dr. Zdravko Božičković[3], prof. dr. Pavel Kovac[4], dr. Dušan Ješić[5], MS.c Dragan Rodić[4]**. [1]College of Applied and Legal Sciences "Prometej", Banja Luka, Bosnia and Herzegovina. [2]University of Banja Luka, Faculty of Sciences Mladena Stojanovića 2, Banja Luka, Bosnia and Herzegovina. [3]University of East Sarajevo, Faculty of Mechanical Engineering, Vuka Karadžića 30, 71126 Lukavica, Istočno Sarajevo, Bosna i Hercegovina. [4]University of Novi Sad, Faculty of Technical Sciences, Institute for Production Engineering, Trg Dositeja Obradovica 6, 21000 Novi Sad, Serbia. [5]Međunarodna Tehnološko-Menadžerska Akademija-MTMA, Trg D.Obradovića 7, 21000 Novi Sad, Serbia. E-mail: m.plavsic2013@gmail.com; sladjanamirjanic@yahoo.com; pkovac@uns.ac.rs; dusanjesic@hotmail.com; rodicdr@uns.ac.rs

Journal of Production Engineering
Vol.18 No.2
JPE (2015) Vol.18 (2) Original Scientific Paper
Yahaya, T., Adedayo, S.M.

# POST WET-WELDING ANNEALING TEMPERATURE EFFECTS ON WELDMENT MECHANICAL PROPERTIES OF MEDIUM CARBON STEEL

Received: 18 September 2015 / Accepted: 28 October 2015

**Abstract:** *Wet-welding alters the mechanical properties of welded metal and consequently a post weld ameliorative treatment may be required. This work examines the effect of different annealing temperatures applied after wet and dry welding on mechanical properties of AISI 1018 steel plate. Test specimens were extracted at 15 and 30 mm from weld line and machined to BS specification. Welded specimens were heat treated at temperature range of 200 to 600°C at 100°C interval. Toughness reduced with annealing temperature. Hardness reduced as soaking temperature is increased with wet welds having higher values while tensile strength decreases in both welding conditions.*
***Key words:*** *Post weld heat treatment, annealing, toughness, hardness, tensile strength*

**Uticaj temperature normalizacije na mehanička svojstva zavara pri mokrom podvodnom zavarivanju srednje ugljeničnih čelika.** *Mokro podvodno zavarivanje menja mehaničke osobine zavarenih metala i stoga se može desiti da je potrebno žarenje. Ovaj rad ispituje uticaj različitih temperatura normalizacije koje se primenjuju posle mokrog i suvog podvodnog zavarivanja na mehanička svojstva AISI 1018 čeličnog lima. Uzorci su uzeti sa udaljenosti od 15 i 30 mm od linije šava i obrađeni po BS specifikaciji. Uzorci zavara su termički tretirani u temperaturnom opsegu od 200 do 600 °C u intervalima od 100 °C. Žilavost se smanjuje sa temperaturom normalizacije. Tvrdoća se smanjuje sa povećanjem temperature natapanja, tako da mokri zavari imaju veće vrednosti dok se zatezna čvrstoća smanjuje kod oba postupka zavarivanja.*
***Key words:*** *Naknadna obrada posle zavarivanja, žarenja, žilavost, tvrdoća, zatezna čvrstoća*

## 1. INTRODUCTION

Underwater welding is classified as either wet or dry [1]. Wet welding are situations where the welder and work have direct contact with the underwater environment. Dry welding processes are when the arc is protected from the water. Dry and wet welding is an effective in – situ method for submerged pipeline, watercraft, seashore components repairs and other harbor devices [2]. Welding processes gives high joint efficiency, flexibility and low fabrication costs however very steep temperature gradients and cooling rates occur around the heat affected zone (HAZ) consequently altering the microstructure, mechanical properties and development of residual stresses. Cracks and planar discontinuities are possible consequences of rapid cooling which therefore informed the need for post weld heat treatment. The annealing process relieves internal stresses, enhances ductility of metal and refinement of grain structure [3]. Reheating a weldment to below the lower transformation temperature at a controlled rate, allowing for soaking followed by control cooling is referred to as Post weld heat treatment (PWHT) [4]. It is an effective procedure through which HAZ properties and hydrogen induced cracking (HIC) are curtailed [5]. Adedayo, *et al.* [6] observed that hardness values are higher close to weld centerline with this effect more pronounced with saline water cooling. Szelagowski, *et al.* [7] applied "in situ" post weld heat treatment in wet welding and observed hydrogen entrapment reduced and a better microstructure was examined. An investigation of the correlation between process variables in welding and post weld heat treated mechanical properties [8], the results show that increase in welding current results in hardness increase while in post weld heat treatment (PWHT), increasing normalizing temperature causes a reduction in hardness. Post weld heat treatment substantially reduces the residual stresses and improves the mechanical properties [9]. Olabi, *et al.* [10], post weld heat treatment soaking temperature of 750°C virtually relieved all residual stresses in a welded martensite stainless – steel welded component. In another work by Olabi, et al. [11], they found that longer soaking time and slower cooling rate during PWHT improves mechanical properties of low carbon steel. Water temperature affects crack formation and weld quality in underwater welding [12]. Brown [13] examined effects of water environment on metallurgical structures of welds. Water medium produces rapid solidification and cooling of the weld bead. This work examines PWHT soaking temperature effect on mechanical properties and microstructures of medium carbon steel welded in an aqueous environment.

## 2.0 EXPERIMENTAL METHODS

### 2.1. Weld material

The material on which welding was carried out was AISI 1018 with a carbon equivalent of 0.27. The chemical analysis as obtained by spectrometric analysis is as shown in Table 1 and the filler metal used was AWS E6013.

| C | Mo | Mn | Ni | Cr | Cu | Fe |
|---|---|---|---|---|---|---|
| 0.152 | 0.001 | 0.676 | 0.015 | 0.025 | 0.028 | 98.81 |

Table 1. Chemical composition of AISI 1018

## 2.2 Welding procedure

A 12 mm AISI 1018 thick plate was machined to rectangular dimension 90 mm x 70 mm and beveled along the 90 mm length to a semi–vee weld groove of 15$^{o}$ with root height of 5 mm. To create the water welding environment, a water jacket cuboid of dimension 200 x 150 x 200 mm fabricated from a 2 mm thick steel plate with a rectangular slit opening of 12 x 90 mm on one side for entrance of the weld plate. Fig.1. shows the weld plate positioning in the coolant jacket.

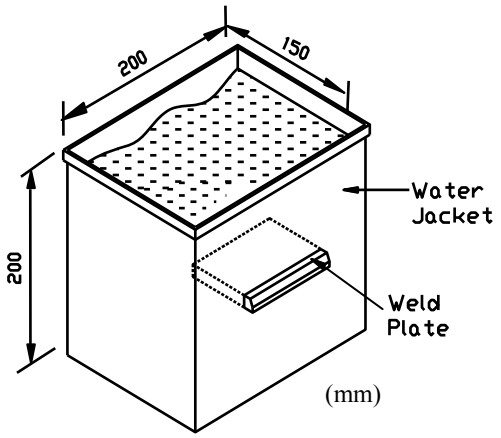


Fig.1.Water welding coolant jacket

The weld plate incorporated a thermocouple hole of 2 mm diameter by 6 mm depth. Welding process entailed both dry and wet boundaries with weld arc protected from water contact through use of sealants along contact line of water jacket and weld plate. Welding process parameters applied are current 320 A, voltage 176 V, speed 1.29 mm/sec corresponding to a weld heat input of 43.65 kJ/mm. Electrode specification is AWS E6013 ( Gauge 10 ). The welding temperature profile was recorded using a type K thermocouple at a distance 5 mm from weld centerline and recorded with MTM – 380SD thermometer monitor. After the completion of welding, the weldment from the two batches were cut into 8 pieces of 90 x 12 x 12 mm dimension at distances of 15, 30, 45 and 60 mm from weld centerline.

## 2.3 Post weld heat treatment (PWHT)

Post weld heat treatment was carried out on samples in a Uniscope SM9080 Muffle furnace at soaking temperatures of 200, 300, 400, 500 and 600$^{o}$C for 90 minutes and normalized in still air.

## 2.4 Mechanical tests and microstructural examination

Tensile strength samples of gauge diameter 5 mm were machined to British standards BS EN 10002-1. Three test samples were prepared for each of the five post-weld heat treatments and as–weld condition. They were tested on a Monsanto Tensometer and mean values of three readings reported.

Micro-hardness tests were carried out on machined sample surfaces at transverse sections parallel to the weld-line at perpendicular distances 15 and 45 mm. Three repetitive samples were used for each of the five post-weld heat treatment tests consisting of dry and water weld environment. The Vickers hardness tester with a 60 Kg indenter was used for the hardness evaluation.

Square cuboid shaped Izod test samples of dimensions 90 x 10 x 10 mm, 2 mm/45$^{o}$ V – notch were cut and machined at perpendicular distances 15, 30, 45 and 60 mm from weld line in accordance with BS 131. The tests were carried out using Avory – Denison machine (KD-A 3 FC), 150 J maximum range and 1 J resolution. Three repeated tests were carried out on each of the five post weld soaking temperatures examined and mean values reported.

Weldment microstructures were examined on transverse section at a perpendicular distance of 15 mm from weld centerline. The as-weld, 200 and 400$^{o}$C post weld heat treatment temperatures microstructures were examined. Samples were prepared by wet grinding on struers knuth – Rotor grinder with 120, 320 and 600 microns silicon carbide waterproof abrasive paper followed by fine polishing on Metaserv 2000 polisher using 6 micron Buchler Metadi diamond paste and 0.05 µm Buchler micro-polish gamma alumina. The samples were subsequently etched in a solution of 5% natal for 10 seconds for optical microscopic photographs. Photographs were taken at 200X magnification under a Epi-fluo attachment microscope.

## 3. RESULTS AND DISCUSSION

Fig. 2 shows the temperature history profile at a typical perpendicular distance 5 mm from the weld line for both dry and wet welds.

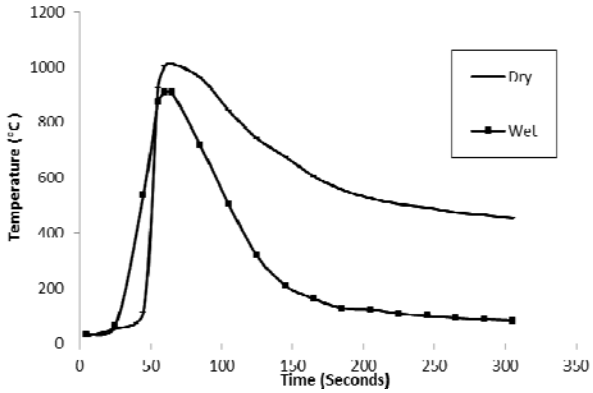


Fig. 2. Temperature variation profile with wet and dry and welding

Peak temperature values of 1011$^{o}$C and 908$^{o}$C were attained under dry and wet welding respectively. Table 2 shows cooling rate values at temperatures within and above the austenitic temperature range. Maximum cooling rates of 10.70 and 5.95°C/sec at interval temperatures 610 and 902$^{\circ}$C respectively. The pronounced cooling rate of 10.70°C/sec. was as a result of induced cooling of the heat affected zone. Non–equilibrium transformation microstructures of bainite and martensite are likely at indicated cooling rates.

| Time | Dry Welding | | Wet Welding | |
|---|---|---|---|---|
| Interval time (Sec.) | Interval temperature ($^oC$) | Cooling rate ($^oC$/sec.) | Interval temperature ($^oC$) | Cooling rate ($^oC$/sec.) |
| 75 | 986 | 2.45 | 813 | 9.55 |
| 95 | 902 | 5.95 | 610 | 10.70 |
| 115 | 792 | 5.10 | - | - |
| 135 | 708 | 3.30 | - | - |

Table 2. Cooling rates within and above the austenitic temperature range

Fig. 3 shows the variation of impact toughness with post weld soaking temperature at 15 and 30 mm distance from weld line. The averaged repetitive test results as presented in Fig.3 had a maximum standard deviation of 8.7 J. Toughness values around the HAZ reduced under wet weld due to higher martensite presence in wet weld. Maximum toughness of 130 and 120 J occurred at soaking temperature of 300$^o$C for dry and wet weld conditions respectively at distance 15 mm. This can be explained in terms of tempering of the martensite structure that started formation during the cooling range at temperature 423.9$^o$C. Tempering at this optimum temperature modified the grain structure such as to enhance toughness. At higher soaking temperatures of 400, 500 and 600$^o$C all above the $M_s$ temperature tends to obliterate the martensite phase causing martensite reversion.

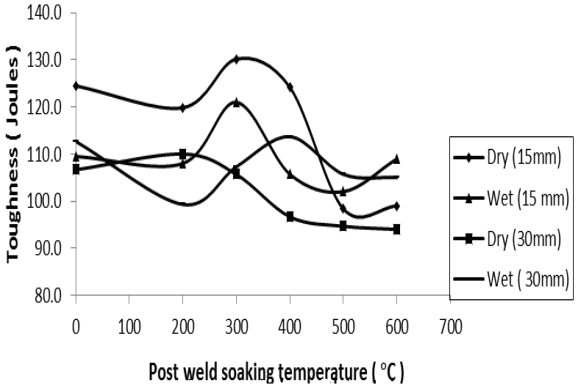


Fig.3. Metal toughness variation with PWHT soaking temperature

Fig. 4 shows the effect of post weld soaking temperature on hardness values. The averaged readings used has a maximum standard deviation of 4.5 HV. Weldment hardness reduced as soaking temperature is increased with wet weld having higher values. At a distance 15 mm from weld line, hardness values of 45.3 and 38.2 HV were observed for wet and dry welds with 500$^o$C soaking temperature causing 8.6 and 16.5% reduction in their hardness respectively. Rapid cooling associated with wet welding is likely to have caused martensite formation resulting into enhanced hardness. Post weld heating tempered the martensite in proportion to the soaking temperature.

Fig. 5. shows variation of tensile strength with soaking temperature at distance 15 mm from weld center line. Slightly high variability of test samples observed with a maximum standard deviation of 60.2 N/mm$^2$. A consistent decrease of tensile strength with soaking temperature was observed in both dry and wet welding conditions. Post weld soaking temperature of 500$^o$C caused a reduction of 13.06 and 20.49% respectively in tensile strength of dry and wet welds respectively. Post weld heat treatment tempered the martensite resulting into softening of the matrix and reduction in its resistance to plastic deformation.

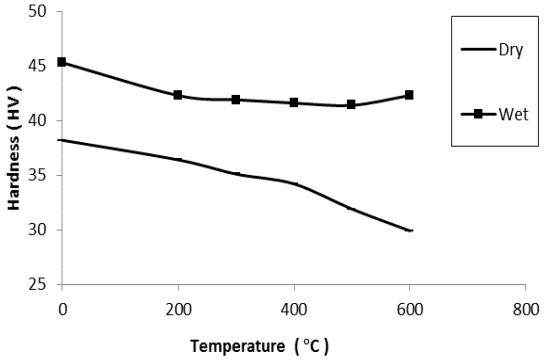


Fig. 5. Variation of Hardness with PWHT temperature

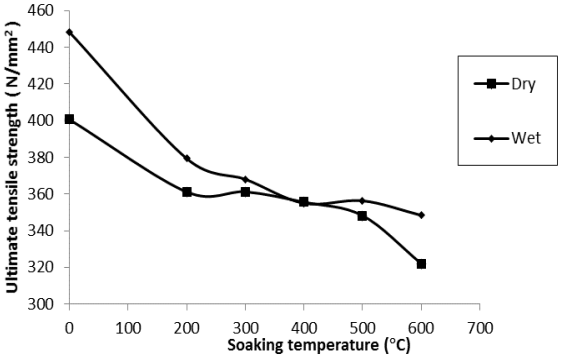


Fig. 6. Variation of UTS with PWHT temperature at 15 mm

Fig. 6 ( a – f ) shows microstructures of wet and dry weld without post weld heat treatment, wet and dry weld at 200 and 400$^o$C post weld heat treatment respectively. Ferrite in martensitic structure is identified which resulted from high cooling rate associated with wet weld. Fine martensite grains are seen and explainable in terms of the welding temperature being close to the $AC_3$ temperature. The dry weld shown in Fig.6 (b) has ferrite microstructure from austenitic range. It is stable with hardness values lower than wet weld. The microstructure of the wet and dry weld with 200$^\circ$C PWHT is shown in Fig.6(c) and 6(d) respectively. Presence of cementite is observed in wet weld. Fig 6(e) and 6(f) shows the micrographs of wet and dry weld with 400$^\circ$C PWHT. Fig. 6(f) shows a more pronounced ferrite structure and few dispersed cementite layer. Grain structures in dry weld are more coarse compared with wet weld.

Fig. 6(a) Wet weld (as-weld) X200

Fig. 6(b) Dry weld (as-weld) X200

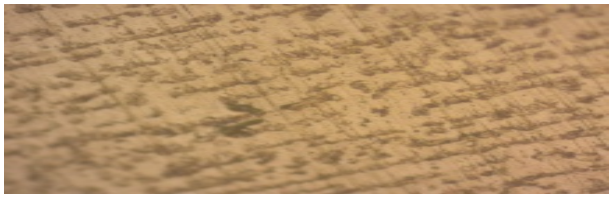

Fig. 6(c) Wet weld (200°C PWHT) X200

Fig. 6(d) Dry weld (200°C PWHT) X200

Fig. 6(e) Wet weld (400°C PWHT) X200

Fig. 6(f) Dry weld (400°C PWHT) X200

## 4. CONCLUSION

An investigation into post weld heat treatment of wet welds had been carried out and the following conclusions can be deduced;

- Higher levels of hardness are induced under wet welds.
- Tensile strength and hardness of weld metal deteriorates with increasing PWHT temperature.
- Weldment toughness is generally higher under dry welds with 300°C PWHT temperature uniquely enhancing toughness values.

Cooling rate is significantly higher with wet weld than dry weld.

## 5. REFERENCE


[1] AWS Committee on Welding in Marine Construction, Specification for Underwater Welding, American Welding Society, U.S.A, 1992.

[2] H. C. Cotton, "Welding under water and in the splash zone – a review," in *Proceedings of the International Conference*, Underwater Welding. Trondheim, Norway, 1983.

[3] Steelworker, Available from: http://www.hnsa.org/doc/pdf/steelworker1.pdf. Cited on 21st April, 2014, 1996.

[4] Welding Technology Institute of Australia, "*Post Weld Heat Treatment of Welded Structures*", Available from: http://www.wtia.com.au, cited on 18th June, 2014, 2012.

[5] R.S. Funderburk, "*Postweld Heat Treatment*," in *Key Concepts in Welding Engineering*, 1998.

[6] S.M. Adedayo, and V.O. Oyatokun, "*Effect of Saline Water Cooling on Service Quality of a Welded AISI 1013 Carbon Steel Plate,"* Annals of Faculty Engineering Hunedoara - International Journal of Engineering, Tome XI (Fascicule 2), 2013.

[7] Adedayo, S. M. and S. O. Momoh "*Effect of Initial Preheat on Mechanical Properties and Microstructures of Arc-welded Steel Plate"* Indian Journal of Science and Technology, Vol. 3 (12), pp. 1224-1228, 2010.

[8] Olawale, J. O., Ibitoye S. A., Oluwasegun K. M., Shittu M. D. and Ofezie, R. C., "*Correlation between Process Variables in Shielded Metal-Arc Welding (SMAW) Process and Post Weld Heat Treatment (PWHT) on some Mechanical Properties of Low Carbon Steel Welds*", Journal of Minerals and Materials Characterization and Engineering, Vol. 11, pp. 891-895, 2012.

[9] Al-Olabi, A. G. "*Residual Stresses and Heat treatment for Metallic Welded Components",* School of Mechanical and Manufacturing Engineering, Ph. D. Thesis, Dublin City University, Dublin, 1994.

[10] A.G. Olabi and M.S.J. Hashmi, "*Effects of Post-Weld Heat-Treatment Soaking Temperature on the Mechanical Properties and Residual Stresses of a Martensite Stainless-Steel Welded Component,"* Journal of Materials Processing Technology, ELSEVIER, Vol. 38, 1993.

[11] Olabi, A. G. and M. S. J. Hashmi, "*The Microstructure and Mechanical Properties of Low Carbon Steel Welded Components after the Application of PWHTs"* ELSEVIER: Journal of Materials Processing Technology, Vol. 38(10), pp. 88-97, 1996.

[12] R.D. Manning, "*Analysis of Underbead Cracking in Underwater Wet Weldments on A516 grade 70 Steel*," in Mechanical Engineering, Naval Postgraduate School: United State Coast Guard Academy, 1998.

[13] Brown, R.T. and K. Masubuchi, "*Effect of Water Environment on Metallurgical Structures of Welds*," in Welding Research Supplement, p. 178s - 188s, 1975.



***Authors:*** **Yahaya Taiwo*, Dr. Adedayo S. M** University of Ilorin, Faculty of Engineering and Technology, Department of Materials & Metallurgical Engineering*, Department of Mechanical Engineering, Ilorin, Nigeria.
Phone.: +2348168545566, +2348095345002
E-mail: yahaya.t@unilorin.edu.ng
amsegun@unilorin.edu.ng

Journal of Production Engineering
Vol.18 No.2
JPE (2015) Vol.18 (2) Original Scientific Paper
Košarac, A., Zeljković M., Mlađenović, C., Živković, A.

# CREATE SISO STATE SPACE MODEL OF MAIN SPINDLE FROM ANSYS MODEL

Received: 27 September 2015 / Accepted: 20 November 2015

***Abstract:*** *This paper shows identification of dynamic characteristics of working unit module main spindle, based on application of APDL ANSYS and MATLAB software. Single Input Single Output (SISO) state space MATLAB model will be developed from an APDL ANSYS main spindle model. The first step in defining the state space model is to define the eigenvector elements for all modes for only the input and output degrees of freedom. The next step is analysing the each mode contribution and sort them from the largest to smallest. One of the modal reduction technique is then applied, and modes with smallest contribution are simply truncated.*
***Key words:*** *Main spindle, modal parameters, model size reduction, state space*

**Redukcija reda modela sklopa glavnog vretena metodom skraćivanja i analiza dinamičkog ponašanja u prostoru stanja.** *U radu je prikazana identifikacija dinamičkih karakteristika glavnog vretena modula radne jedinice pinolebazirana na primjeni APDL ANSYS i Matlab softvera. Primjenom metoda konačnih elementa utvrđeni su modalni parametri glavnog vretena, na osnovu kojih semodel konačnih elemenata transformiše u manje zahtjevan model, model prostora stanja, koji sa dovoljnom tačnosti opisuje dinamičko ponašanje modela. Na primjeru glavnog vretena prikazna je jedna od metoda redukcije reda, metoda skraćivanja, čijom primjenom se smanjuje računarska složenost modela i vrijeme simulacije.*
***Ključne riječi****: Glavno vreteno modula pinole, modalni parametri, redukcija reda modela, prostor stanja*

## 1. INTRODUCTION

One of the biggest obstacle in work with finite element models is system size. During a sequence of FEM analysis of complex mechatronic system like machine tool is, nodal displacement are computed for mesh which can have up to $10^5$, even $10^6$ degree of freedom (DOF). Considering that design process is very interactive, so FEM analysis needs to be repeated frequently, it is obvious that perform finite element analysis repeatedly can be very time consuming. Although modern computers are becoming more and more powerful, dealing with such huge models is still a problem. Model order reduction (MOR) techniques reduces the size of the FEM model while input/output relationship remains preserved.

Using modal analysis eigenvalues (resonant frequencies) and eigenvectors (mode shape) are determined. Since the number of eigenvalues and eigenvectors is equal to number of DOF, it is obvious that this is too large to be inserted into state space in MATLAB model. Therefore, the goal to be achieved is not only obtaining a reliable dynamic model, since such a model exist and that is a FEM model. The objectives to be achieved are:

- Convert a large finite element model (by "large model" it is assume model with thousands of hundreds DOF) to a smaller MATLAB model which still provide correct response for the forcing input, i.e. still maintaining the input / output relationship, Fig. 1.,
- Obtained MATLAB model can be inserted into complex control system models and be used do define system dynamic.

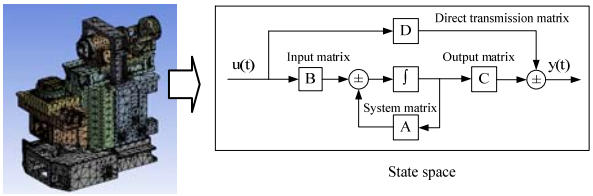

Fig. 1. Model size reduction

The mathematical model obtained by finite element method is linear time-invariant model. The entire structure is described by the mass, damping and stiffness matrices and can be represented by linear ordinary differential equations with constant coefficients. This model can be transformed into state space representation where a system an $n^{th}$ order differential equation is replaced with a single first order matrix differential equation.

When carrying out certain analysis, such as for example modal analysis, considered system has a highly complex mathematical model which solving can take a long time. In order to reduce the time required for the execution of the simulation, still maintaining the input / output relationship, different model reduction technique are applied. Maglie [3] used the FEM model to determine the relative movement of the tool tip to the workpiece under the influence of the cutting force. Maglie [3] presented a platform for the exchange of data between ANSYS WORKBNCH and simulation model developed in MATLAB / Simulink in which further static and dynamic analysis are performed. The platform integrates modules that contain characteristics of joints, while set of macros is exporting models from ANSYS WORKBNCH into MATLAB / Simulink, including the properties of the joints, stiffness and

damping. Maglie [3] used MOR for ANSYS, commercial model order reduction software tool for reading ANSYS files and performing Krylov-based model reduction.

Vesely [5] analysed the impact of natural frequencies of the machine tool mechanical structure on the dynamic behaviour of the feed drive. Machine tool structure is being observed in two ways: as lumped mass in one, and as a finite element model in the second case. Machine tool is modelled as a system of elastic bodies, and model order reduction of FEM model is performed by applying Craig – Bamton reduction techniques. This technique allows the selection of a certain number of natural frequencies the reduced model will keep comparing to the original model, and the selection of so-called "interface" nodes that are used for coupling with other bodies. Also, Vesely [5] analysed two methods for determining the influence of the machine tool structure on the dynamic behaviour, the first way - modal decomposition technique in which the transformation is performed on mass, damping and stiffness matrix obtained from the FEM system, and otherwise - by solving the equation of motion in modal coordinates.

## 2. MAIN SPINDLE MODAL ANALYSIS

In this paper, on the main spindle example, Fig. 2., is shown how the model can be transformed from finite elements into state space representation, how to do modal reduction sorting modes by dc gain and peak gain, preform sorted modes modal truncation and finally find solution in physical coordinates through the next steps, [4]:

1. Perform modal analysis, and determination of natural frequencies and mode shapes in ANSYS (eigenvalues / eigenvectors),
2. Transformation of the FEM model so that the modal matrix include only those degrees of freedom where the force is applied and/or outputs desired,
3. Analysing the modal contribution of each mode and sort them in descending order, as well as reducing the number of modes by modal truncation including only modes which have significant contribution to desired response,
4. Create modal state space form equations of motion,
5. Find solution in physical coordinates in frequency or time domain.

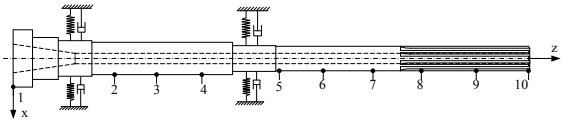


Fig. 2. Equivalent dynamic model of spindle with measurement points

Main spindle, shown in Fig 2., is supported by the two sets of angular contact ceramic ball bearings in front, SKF S7011 CD/HCP4A and two sets of angular contact ceramic ball bearings in rear SKF 7008 CD/HCP4A, installed back to back, Fig 2. Values of bearing stiffness depending on the preload are provided in the table 1 [6], [2].

| | Preload | | | | | |
|---|---|---|---|---|---|---|
| | Small | | Middle | | Big | |
| | Front brg set | Front brg set | Front brg set. | Front brg set | Front brg set | Front Brg set |
| Radial stiffness N/μm | 400 | 280 | 560 | 387 | 690 | 475 |
| Axial stiffness N/μm | 69 | 48 | 115 | 82 | 170 | 120 |

Table 1. Stiffness of bearing [6], [2]

Considering that quill unit moves horizontally (feed movement), the main spindle assembly has a specific construction, with free end of the main spindle relatively large length, [6], [7]. Therefore, it is especially interesting to consider the dynamic behaviour of the main spindle free end. Fig. 3. shows main spindle modelled in APDL ANSYS with two elastic support on the bearing places. The material is linear isotropic structure steel. Young's modulus is E= 2*10MPa, Poisson's ratio is ν=0.3, material density ρ = 7850 N/m$^3$. SOLID186 a higher order 3-D 20-node solid element is used to simulate main spindle. Total numbers of nodes and elements are 85032 and 17167 respectively. When assigned material to model in ANSYS, the spindle mass is 9.2 kg. Spring damper element COMBIN 14 is applied to simulate the elastic support of the two set of bearings. Eighteen elements was set along the circumferential direction of the spindle on each set of bearing, simulating rolling elements. Since the inertial force and the thermal expansion of bearing elements affect the balls, an uneven distribution of contact forces and an uneven contact angle change occurs. The consequence of the aforementioned is the uneven distribution in bearing stiffness, depending on the position of the ball [7].

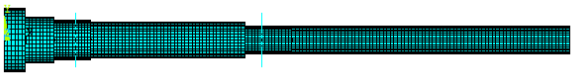

Fig. 3. Main spindle finite element model

The first ten eigenvalues (Tab. 2) and eigenvectors for bending motion of main spindle were extracted using Block-Lanczos method. Each of 10 column of modal matrix represent the eigenvector for that mode, normalized with respect to mass. Each row of the modal matrix show relative motion of points to which forces are applied and/or for which displacement are desired (measurement points from Fig. 2).

| $f_1$ (Hz) | $f_2$ (Hz) | $f_3$ (Hz) | $f_4$ (Hz) | $f_5$ (Hz) |
|---|---|---|---|---|
| 154,37 | 926,92 | 1641,06 | 2351,83 | 2538,17 |
| $f_6$ (Hz) | $f_7$ (Hz) | $f_8$ (Hz) | $f_9$ (Hz) | $f_{10}$ (Hz) |
| 4533,14 | 5687,47 | 6972,75 | 8228,99 | 9637,48 |

Table 2. Eigenvalues for bending motion of main spindle, Hz

## 3. MAIN SPINDLE STATE SPACE REPRESENTATION

In the state space formulation, n second order differential equations are converted to 2n first order differential equations. The most general state-space representation of a linear system is

$$\begin{aligned} \dot{x} &= Ax + Bu \\ y &= Cx + Du \end{aligned} \tag{1}$$

where first equation is state equation, and second output equation, and
x is the state vector,
u is the input (or control) vector,
y is the output vector,
A is the state (or system) matrix,
B is the input matrix,
C is the output matrix,
D is the "feedthrough (or feedforward) matrix" (in cases where the system model does not have a direct feedthrough, D is the zero matrix.
Rewriting the equation 3.1 in matrix form as:

$$\begin{bmatrix} \dot{x}_1 \\ \dot{x}_2 \\ \dot{x}_3 \\ \dot{x}_4 \end{bmatrix} = \begin{bmatrix} 0 & 1 & 0 & 0 \\ 0 & 0 & 0 & 0 \\ 0 & 0 & 0 & 1 \\ 0 & 0 & -\omega_2 & -2\varsigma_2\omega_2^2 \end{bmatrix} \begin{bmatrix} x_1 \\ x_2 \\ x_3 \\ x_4 \end{bmatrix} + \begin{bmatrix} 0 \\ F_{p1} \\ 0 \\ F_{p2} \end{bmatrix} \tag{2}$$
$$\dot{x} = \quad A \quad x + \quad Bu$$

It may be noted that along the diagonal two sets of uncoupled first order equations appear in block of 2x2 coefficients, where the first block 2x2 represent response of the first mode and second block represent response second mode.

$$\begin{aligned} &\text{Response of the first mode:} && \begin{bmatrix} 0 & 1 \\ 0 & 0 \end{bmatrix} \\ &\text{Response of the second mode:} && \begin{bmatrix} 0 & 1 \\ -\omega_2 & -2\varsigma_2\omega_2^2 \end{bmatrix} \end{aligned} \tag{3}$$

Damping ratio is known, either to be adopted as a single value for all modes, or column vector whose members are individual damping ratio for each mode. The natural frequencies (eigenvalues) are also known. This means that the process of determining the submatrix A can easily be expressed algorithmically, and thus the programmed. Uncoupled equation of motion of two first modes are

$$\begin{aligned} &\text{First mode} && \begin{bmatrix} \dot{x}_1 \\ \dot{x}_2 \end{bmatrix} = \begin{bmatrix} 0 & 1 \\ 0 & 0 \end{bmatrix} \begin{bmatrix} x_1 \\ x_2 \end{bmatrix} + \begin{bmatrix} 0 \\ F_{p1} \end{bmatrix} u \\ &\text{Second mode} && \begin{bmatrix} \dot{x}_3 \\ \dot{x}_4 \end{bmatrix} = \begin{bmatrix} 0 & 1 \\ -\omega_2 & -2\varsigma_2\omega_2^2 \end{bmatrix} \begin{bmatrix} x_3 \\ x_4 \end{bmatrix} + \begin{bmatrix} 0 \\ F_{p2} \end{bmatrix} u \end{aligned} \tag{4}$$

The transformation of the dynamic behaviour of finite elements in the state space involves performing two types of reduction: reducing the number of DOF of the FEM model and the modal reduction.

Reducing the number of DOF of the FEM model means that new model analysed in MATLAB include only the degree of freedom to which forces are applied and/or for which displacement are desired.

If the new model still comprises a number of degrees of freedom bigger than needed, then modal reduction based on the set of criteria is carried out. Analysis of the modal contributions of each individual modes and sort them according to the relative importance is the criterion for performing modal reduction.

The procedure is the following: modes are first ranked on the basis of their relative importance, and then performs the elimination of modes with a lower value modal contributions, i.e. **modal truncation**. Parameters on which determines the sorting mode is the **damping ratio** ζ. The criteria to be applied for sorting modes depends on whether the value of the damping ratio ζ considered unique or different for each mode.

In the first case the criterion for ranking modes is "**dc gain**", (3.5), while in the second case, the criterion used for ranking modes is "**pick gain**" (3.6) [1].

$$\frac{z_j}{F_k} = \sum_{i=1}^{m} \frac{z_{nji} z_{nki}}{\omega_i^2} \tag{5}$$

$$\frac{z_{ji}}{F_{ki}} = = \frac{-j}{2\varsigma_i} \left( \frac{z_{nji} z_{nki}}{\omega_i^2} \right) \tag{6}$$

Comparing (3.2) and (3.3) can be seen that peak gain is -90° phase shift at resonance, but to have greater amplitude for then dc gain. If relative damping has unique value for all modes, peak gain has larger amplitude but relative amplitude are the same. That means with unique relative damping ζ both methods give the same order of modes regardless which of the ranking criterion is applied. If relative damping has different values for all modes, then peak gain ranking criterion needs to be applied.

Usually the value of damping ratio is between 0,005 (0.5% of the critical damping) to 0.02 (2% of the critical damping). If the experimental results are available, i.e. real and imaginary part of the transfer function, damping ratio ζ can be determined for each mode, and in that case the obtained values of damping ratio are placed in a separate text file.

Fig. 4. shows dc gain value for all modes versus mode number for direct frequency response function (FRF) measurement location (X1/F1), and Fig. 5. for cross FRF (X10/F1). If the response is measured at the same location where force is applied then such FRF is called a direct, but if is measured at different location, this is cross FRF.

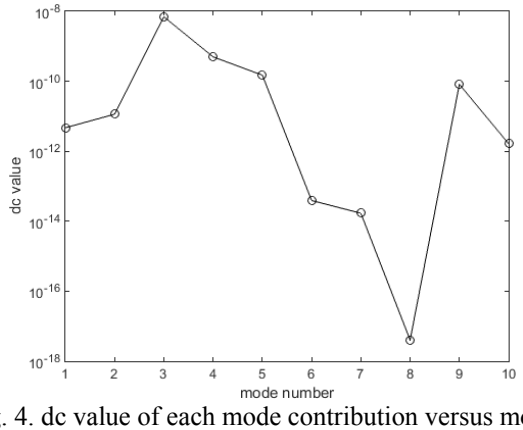


Fig. 4. dc value of each mode contribution versus mode number, direct FRF (X1/F1)

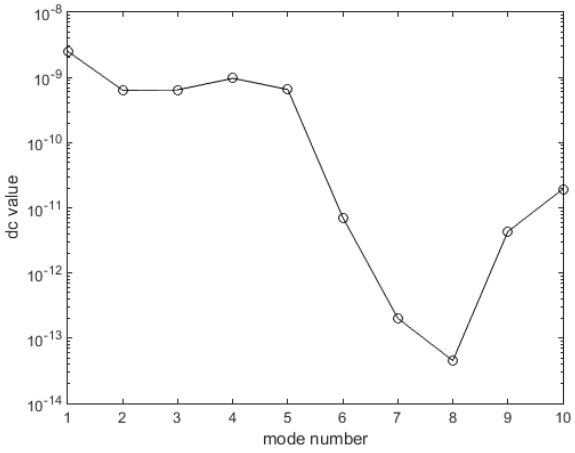

Fig. 5. dc value of each mode contribution versus mode number, cross FRF (X10/F1)

In this case constant damping ratio $\zeta = 0.001$ was considered as unique for all modes, so dc gain was used as a criterion for mode ranking. It can be seen that the mode 1 and 2 (frequencies 154.37 Hz and 926.92 Hz) have smaller modal contributions of modes 3,4 and 5. Accordingly, Fig. 6. and Fig. 7**.** show that the first two frequencies have such low gain that their resonant peaks are barely visible on the overall response.

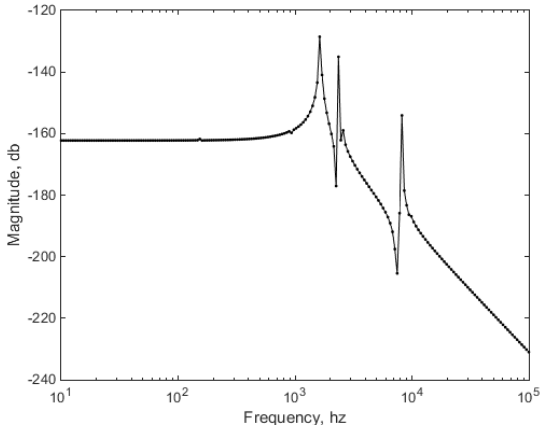

Fig. 6. Direct FRF, all 10 modes included

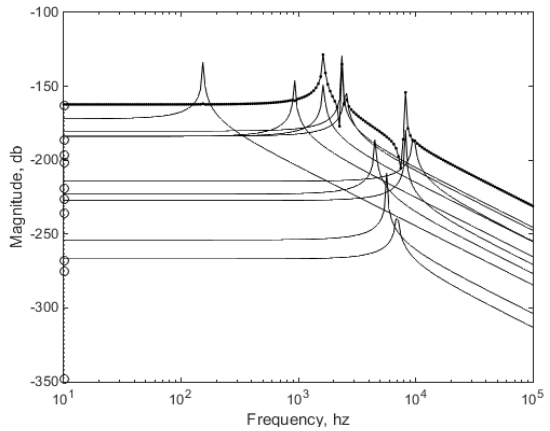

Fig. 7. Direct FRF, overlay of each individual mode contributions

Fig.**7** show the overall frequency response with overlaid SDOF (Single Degree of Freedom) response of all the individual modes. Fig. 8. shows overall mode contributions for four selected modes. It can be seen that modes 3,4,5 and 9 have the most significant modal contribution.

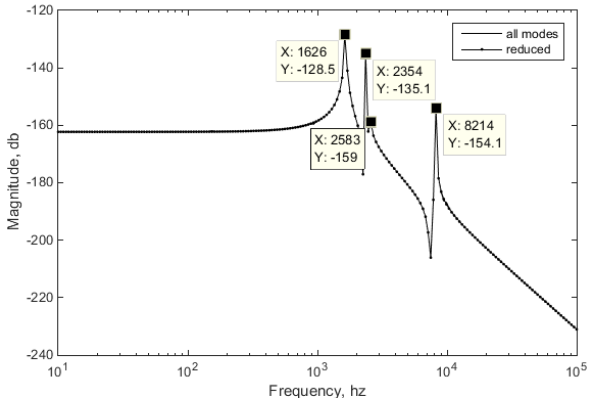

Fig. 8. Direct FRF – reduced sorted modal truncation frequency response –four modes included

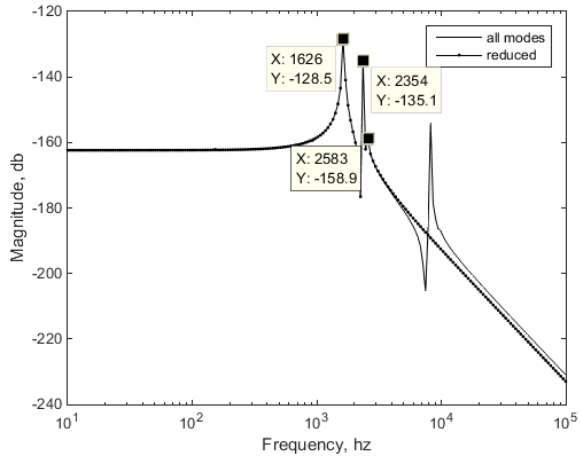

Fig. 9. Direct FRF – reduced sorted modal truncation frequency response –three modes included

If transfer function is plotted for three selected modes, it can be seen that the most significant modes are modes 3,4 and 5, Fig. 9. However, in the case of cross FRF, modal contribution of the first four modes is significantly higher than in other modes, Fig.10. Fig.11. shows overall mode contribution for all ten modes and four sorted modes for cross FRF (X10/F1). It can be noted that it is necessary to create at least two different state space models, the first includes all modes extracted from ANSYS, and second only desired number of modes, i.e. reduced number of modes.

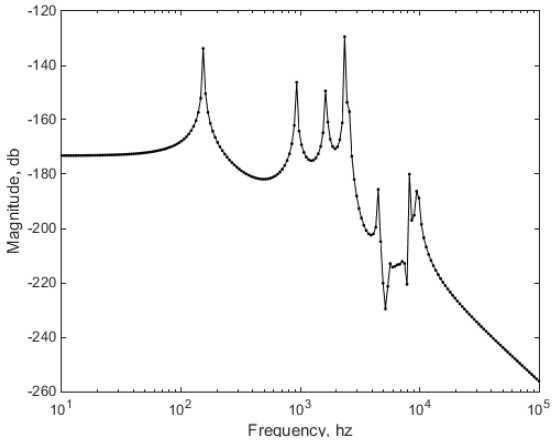

Fig. 10. Cross FRF (X10/F1)– all ten modes included

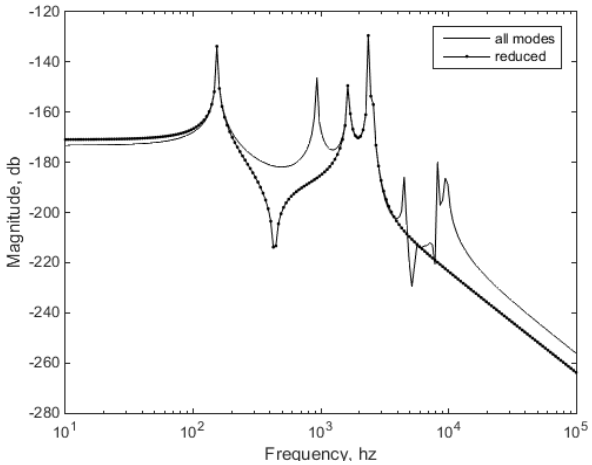

Fig. 11. Cross FRF (X10/F1), reduced sorted modal truncation, 4 modes included

From Fig. 11. can be seen that there is an error in the low frequency portion of the frequencies response. This is because the influence of truncated modes on dc gain did not take into account. This influence can be replaced using other techniques of modal reduction, which will be the subject of further research.

## 4. FINAL REMARKS

This paper shows how to take the results of finite element main spindle model created in ANSYS and reduce the model size extracting lower order state space model in MATLAB (model reduction). Then number of modes can be reduced (modal reduction) by ranking relative importance of each mode to overall response. It was shown modal truncation, as one of techniques for modal reduction. A reduced solution provides very reliable dynamic of the model with a significant reduction in number of states.

Reduced mode can be further inserted into a more complex control system model and used to find system dynamics.

## 5. REFERENCES

[1] [1] Hatch, M. R.: *MATLAB and ANSYS*, Chapman & Hall/CRC, 2001.

[2] Košarac, A., Zeljković, M., Mlađenović, C., Živković, A.: *Numerical-experimental identification of a working unit module dynamic characteristics*, VIII International Conference "Heavy Machinery-HM 2014", Zlatibor, 25-28 June 2014

[3] Maglie, P.: Parallelization of Design and Simulation: *Virtual Machine Tools in Real Product Development*, A dissertation submitted to the ETH ZURICH, 2012.

[4] Schmitz, T. L., Smith, K.S.: *Mechanical Vibrations Modeling and Measurement,* Springer, 2012.

[5] Vesely, J., Sulitka, M.: *Machine Tool Virtual Model*, MM Science Journal, December 2009, 146-151.

[6] Zeljković, M.: *Sistem za automatizovano projektovanje i predikciju ponašanja sklopa glavnog vretena mašina alatki*, Doktorska disertacija, Fakultet tehničkih nauka, Novi Sad, 1996.

[7] Živković, A., Zeljković, M., Tabaković, S., Milojević, Z.: *Mathematical modeling and experimental testing of high – speed spindle behaviour*, The International Journal of Advanced Manufacturing Technology, (2015) 77: 1071-1086.

***Authors:*** **Mr Aleksandar Košarac**, University of East Sarajevo, Faculty of Mechanical Engineering, **Prof. dr Milan Zeljkovic, Assistant Professor, Aleksandar Zivkovic. M.Sc. Cvijetin Mlađenovic**, University of Novi Sad, Faculty of Technical Sciences, Institute for Production Engineering, Trg Dositeja Obradovica 6, 21000 Novi Sad, Serbia, Phone.: +381 21 450-366, Fax: +381 21 454-495.
E-mail: akosarac@gmail.com; milanz@uns.ac.rs; acoz@uns.ac.rs; mladja@uns.ac.rs

Journal of Production Engineering
Vol.18 No.2
JPE (2015) Vol.18 (2) Original Scientific Paper
Vulić, M., Tomović, A., Pavlović, A.

# DEVELOPMENT OF TECHNOLOGY OF EXISTING EQUIPMENT FOR DISCHARGING BRAKE FLUID IN THE PROCESS DETOXIFICATION OF ELV

Received: 15 September 2015 / Accepted: 30 November 2015

***Abstract:*** *Detoxication of motor vehicle brings a whole range of security processes and precaution because of a big quantity of hazardous materials in vehicles. One of the most dangerous is brake fluid which is defined as a dangerous waste material on the human being and enviroment. By that fact alone discharging of brake fluid, adequate treatment and his recycling presents constructive challenge for equipment. Aim of paper is advancement of technology of existing equipment for detoxication motor vehicle in process of ELV, concretely on a part of discharging brake fluids with maintaining current quality of appliance.*
***Key words:*** *Motor vehicles, technology, advancement of equipment, detoxification, brake fluid*

**Unapređenje tehnologije postojeće opreme za istakanje kočionog fluida u procesu detoksikacije ELV-a.** *Detoksikacija motornih vozila donosi čitav niz sigurosnih procesa i mera zbog prisutne velike količine opasnih materija u automobilima. Jedna od najopasnijih materija je kočioni fluid, koji je definisan kao opasni otpadni materijal po čoveka i životnu sredinu. Samim tim istakanje kočionog fluida, adekvatan tretman i njegova reciklaža predstavljaju konstruktivni izazov za opremu. Cilj rada jeste unapređenje tehnologije postojeće opreme za detoksikaciju motornih vozila u procesu ELV-a, konkretno dela za istakanje kočionog fluida, uz zadržavanje postojećeg kvaliteta uređaja.*
***Ključne reči:*** *motorna vozila, tehnologija, unapređenje opreme, detoksikacija, kočioni fluid*

## 1. INTRODUCTION

Motor vehicle recycling today is representing as one of the generators of development and entrepreneurship in the world, as from the side of economic and technological development of the market and as from the aspect of reducing touching toxic materials with enviroment.

To successfully recycling process of motor vehicle precede adequate detoxication and treatment of toxic waste from vehicles such as fuels, motor oils, oils from gearshifts, oils from differential, hydraulic oils, antifreeze, acids from the accumulator, liquids from air-conditioner [1] among which is fluid from the brake systems.

By discharging fluids from the vehicle, vehicle becomes to have a treatment as dangerous waste which results to higher level of safety of environmental protection.

After elimination toxic waste materials from the vehicle which leads to further elimination and recycling of metal parts of vehicles which are comprising the biggest part.

## 2. RULES AND STANDARDS FOR MANAGING WITH DANGEROUS FLUIDS

Directive of council 75/439/ESS for dumping waste oils, amended with directives 1987/101/ESS, 91/692/ESS and 2000/76/ES promotes gathering and dumping of mineral lubricants or industrious waste oil that are no longer usable for original usage. This directive: prohibits handling used oils which cause air pollution beyond the limit found in regulations, demands providing safe and efficient system of gathering, treatment, storage and dumping of waste oil; highest priority is awarded to regenerating waste oils, then burning it with use of energy, whilst lowest priority is given to its destruction or controlled storage; prohibits dumping waste oils in surface or underground waters, including land [2].

Domestic legislature features rule book about conditions, method and process of managing waste oils [3], which establishes conditions, method and process of managing waste oils which are unusable for purpose they were designed in the first place.

## 3. FLUID OF BRAKE SYSTEM

Break fluid, as parts of any hydraulic transmission braking mechanism, has the task of transmission of braking force. For that reason, and because of the importance of the braking system, which represents the most important factor of drivers security, and all for the purpose of general traffic security, important demands are placed before brake mediums, amongst which the most important are: high boiling points, good havings at low temperatures, corrosion protection, appropriate ability of lubrication so as compatibility with sealants [4].

### 4.1 The structure of brake fluid

The widest use have the brake mediums which represent the mixture of polyglycol and glycol with the addition of suitable additives. For its features, basic requirements are placed before this type of fluids, that

are defined with standards and specifications:

- ISO 4925
- SAE J 1703
- FMVSS 166 (Federad Motor Vehicle Safety Standard), for DOT 3, DOT 4 и DOT 5, and they are shown in Table 1.

| | FM VSS 116 | | | | ISO 4925 | SAE J 1703 |
|---|---|---|---|---|---|---|
| | DOT 3 | DOT 4 | DOT 5.1 | DOT 5 | | |
| Point boiling of dry liquids, °C, minimum. | >=205 | >=230 | >=270 | >=260 | >=205 | >=205 |
| Point boiling of wet liquids, °C, minimum. | >=140 | >=155 | >=185 | >=180 | >=140 | >=140 |
| Maximum viscosity at -40 °C , $mm^2/s$ | <1500 | <1800 | <820 | <1900 | <1500 | <1800 |
| Maximum viscosity at 100 °C, $mm^2/s$ | >1,5 | >1,5 | >2,1 | >1,5 | >1,5 | >1,5 |

Table 1. Basic requirements for brake fluids [4].

Their chemical and technical characteristics are given by the table 2.

| Type of brake fluid | Chemical characteristics | Technical characteristics |
|---|---|---|
| DOT 3 | On the basis of polyalkylene. | Shortly period of usage and smaller reliability in relative to DOT 4 и DOT 5 [4]. |
| DOT 4 | Complex mixture of (poly) glycol ethers and borate ester with special inhibitors of corrosion and oxidation and suitable additives [4, 5]. | Brake fluid is hydroscopic, absorb moisture (include moisture in the air) over microporosity sealing catridge connectors for braking system. It can be mixed with other synthetic liquids at same quality, except liquids on the mineral base, type LHM (vehicles Citroen) [6]. |
| DOT 5.1 | On the basis of borate ester [4]. | Synthetic fluid with Appropriately viscosity even on the low temperatures. Provides high boiling point and highly ability to absorb water. It is recommended for systems with hydraulic brakes which have ABS (Anti-lock Breaking Systems) [7]. |
| DOT 5 | On the basis of silicone oil [4]. | Not allowed mixing DOT 5 with DOT 3, DOT 4 I DOT 5.1 [4]. |

Table 2. Chemical and technical characteristics of the brake fluid

### 4.2 Importance of adequate treatment of this toxic matter

Shown chemical structures point out that the brake fluid represent hazardous waste, unless it is recycled. Mixing with brake oil doesn't allow further recycling.

Brake fluid must not be treated as used oil, as it has characteristics of toxicity. Mix with chlorinated solvents from spray, which is used for cleaning the brakes, makes the brake fluid extremely hazardous. Brake fluid shouldn't be dumped on landfills.

As we can see from the aforementioned, attention should be paid to the adequate treatment of this medium, which cannot be recycled or reused in its original use, which requires providing of safe and efficient system of gathering, treatment, storage and dumping.

### 4.3 The quantities of waste brake fluid in the territory of the Republic of Serbia

Facts based on the Table 3., that presents the number of registered motor vehicles with minimal, maximum and average number of ELV in the last 14 years in Republic of Serbia, and Table 4. that shows us the percentage of brake fluid in one (representative) vehicle, lead us to quantitative number of brake fluid on the territory of the aforementioned country.

Adding together the average number of vehicles that reach the ELV in the last 14 years in the Republic of Serbia, we come to the figure of 1160677 vehicles, which, when multiplied with by the amount of this toxic substance by vehicle, totals almost half a million kilograms or more precisely 464270,8 kg. On average, on an annual basis this figure amounts 33162,2 kg. This amount represents not so small amount of this hazardous substance, which irregular dumping can cause contamination of soil and surface waters, which represents a difficulty for the environment and endangers the wildlife and people's health.

Since this is an unrecyclable material, which cannot be returned to the reusing process, it can be used for collecting energy, by burning and/or storing in an environmentally safe way [9].

| Year | Number of registred passengers cars | Minimum number of ELV-a (4% of the number of registered vehicles) | Maximum number of ELV-a (6,7% of the number of registered vehicles) | Average number of ELV-a (5,35% of the number of registered vehicles) |
|---|---|---|---|---|
| 2001. | 1382396 | 55296 | 92621 | 73959 |
| 2002. | 1343658 | 53747 | 90025 | 71886 |
| 2003. | 1388109 | 55524 | 93003 | 74294 |
| 2004. | 1449843 | 57994 | 97139 | 77567 |
| 2005. | 1481498 | 59260 | 99260 | 79260 |
| 2006. | 1511837 | 60473 | 101293 | 80883 |
| 2007. | 1476642 | 59066 | 98935 | 79001 |
| 2008. | 1486608 | 59464 | 99603 | 79534 |
| 2009. | 1637002 | 65480 | 109679 | 87580 |
| 2010. | 1565550 | 62622 | 104892 | 83757 |
| 2011. | 1677510 | 67100 | 112393 | 89747 |
| 2012. | 1726190 | 69048 | 115655 | 92352 |
| 2013. | 1770162 | 70806 | 118601 | 94704 |
| 2014. | 1797252 | 71890 | 120416 | 96153 |

Table 3. The number of registered and waste vehicles in the Republic of Serbia in the last 14 years, period 2001-2014 [8]

| | Weight by car | | The degree of recyclability | |
|---|---|---|---|---|
| | % | kg | kg | % |
| Brake fluid | 0,04 | 0,4 | 0 | 0 |

Table 4. Quantity and degree of recyclability of brake fluid on the example of vehicle brand „Zastava“ (Fiat car) [6]

All this induces that the process of discharging this fluid from a motor vehicle must be done with reliable detoxification equipment, on a high level and with high level of safety, to prevent adverse effects. prevent adverse effects.

## 5. DESCRIPTION OF THE EXISTING EQUIPMENT FOR DISPENSING FLUIDS FROM AUTOMOBILES

Motor vehicles that reached the ELV, besides the metal waste which makes the majority of it, also contain a great amount of various fluids, including the fluid for the brake system. Only after their safe exclusion from the car, can we proceed to further recycling process of the other parts of the car, which induces that every center for car recycling should have suitable detoxification equipment for hazardous fluids. In the aim of all this, within the project TR 35033, they have developed the Facility for removing the fluid from a End of Life Vehicle [10].

Facility for removing the fluid from a end of life vehicle, which represents a technical solution, is a fixed station for combined removal of all vehicle fluids with minimum influence on the environment, including the brake fluid.

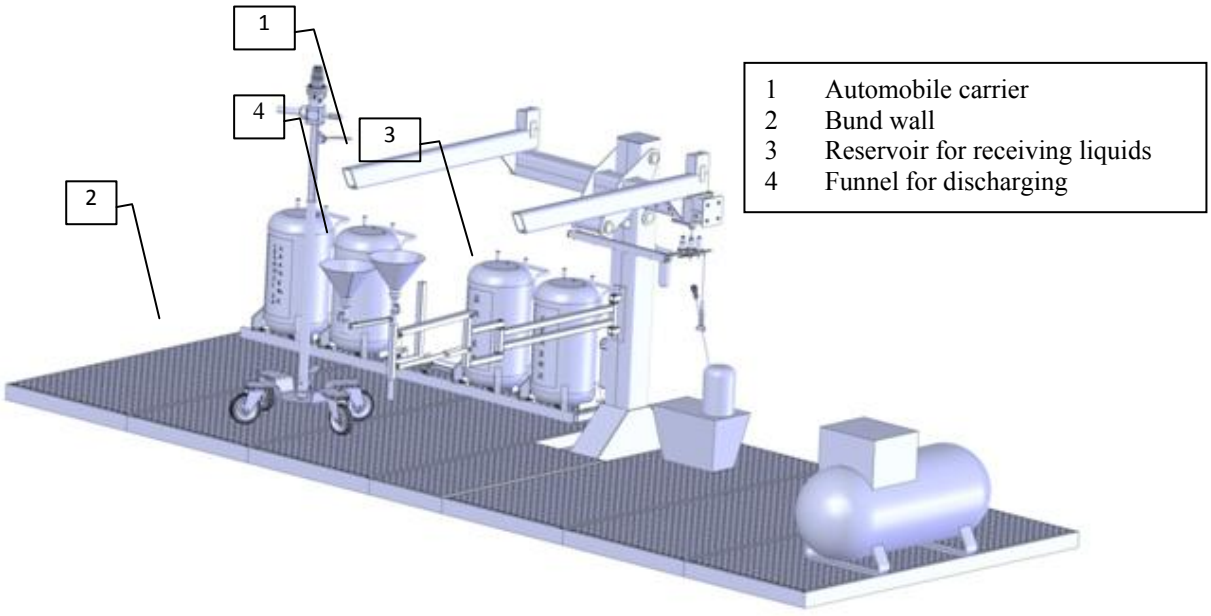


Fig. 1. Plant model for discharging liquids from vehicles in the procces of ELV [8]

After placing the car on the rack, the device turns on, which gears the hydraulic and pneumatic subsystems of the device, turns the taps in their provided position on metal tank for fluid acceptance, admits air from the compressor through the Ejector Venturi which creates a subpressure in the acceptance tanks, due to suction of air through the Ejector Venturi [10]. The device has a possibility of leaning, using the hydraulic piston, from around 6 % from the horizontal axis, which makes the fluid extraction easier.

A part of dispensing, which applies on brake fluid, is performed using a funnel that is positioned under the cylinder on the wheels of a car (4). By unscrewing the screw on brake cylinders, the brake fluid outflows in the funnel by free fall, from where, under the effect of subpressure, it is transported into the suitable tank for brake fluid acceptance. A connection is installed, on the tank for brake fluid in the motor area, which provides the transfer of air from the compressor into the mentioned tank. The created overpressure in the brake system of the car improves the dispensing of the brake fluid and prevents the fluids from reservation in the brake system of the car [10].

## 6. DEVELOPMENT TECHNOLOGY OF EQUIPMENT AND PROCCES OF DISCHARGING BRAKE FLUID WITH MAINTAINING EXISTING QUALITY

Proposal improvement of existing equipment is that not comes to unscrewing the screw on brake cylinders. Direct perforation of brake hose using the redesigned locking pliers drain away liquid into the hose system which under the influence of subpressure transports liquid into the adequate reservoir.

Proposal is that to drill a hole on the „upper jaw“ on the locking pliers (Fig. 2.) on which will be set hose system for discharging which on his top would have "sharply open port" for perforation and directly discharging fluid from brake hose into the reservoir only assigned to for that purpose.

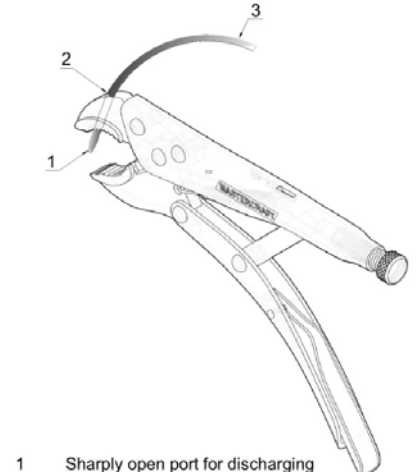


1 Sharply open port for discharging
2 Aperture on the top of the locking pliers on which is fixed the hose for discharging
3 Hose for discharging

Fig. 2. Propose of redesigned locking pliers for purpose of perforation and removing liquids

By dint of redesigned locking pliers provides that not come to free dropping of liquids at opening brake cylinders. With handgrip on the redesigned locking pliers on the brake hose leads to perforation of brake hose. Sufficient force for perforation of brake hose is about 150 N, while the maximum handgrip of an adult is 700 N. Even handgrip with 30 % perforate the brake hose because the average force handgrip of an adult is more than 200 N [11].

New generation“ brake hose are made from teflon and they are reinforced by steel braided of stainless steel which protect the teflon but since it is a detoxification of old vehicles which comes to the ELV, we will analysed “old generation” brake hose which are made mainly from copper.

„Sharply open port“ will be used for perforation of copper brake hose.

The most suitable material for making this part is highly quality alloy steel which contain from 5-10 [%] W, 0,25-0,45[%] C and additives Cr, V, Ni, [12]. From this type of steel are making tools which are most loaded mechanically and thermically which makes Č.6451 adequate for production “sharply open port”.

The proposed layout of “sharply open porn” are shown in Fig. 3.

Fig. 3. „Sharply open port“

By dint of redesigned locking pliers provides that not come to free dropping of liquids at opening brake cylinders, whereby prevent eventually dropping of fluid outside the appropriate funnel, which ensure that every drop of toxic fluid goes to safety reservoir thus provide higher level protection for operator of device.

After discharging of brake hose, hose became unuseful because absorption of moisture inside the brake fluid and his abrasive contents which leave consequences on the inside walls of brake hose and like that brake hose is unuseful for reuse and recycling.

## 7. CONCLUSION

Motor vehicles with all yours components, metal parts and toxic fluids which come to the ELV presents important contaminants of environment.

Hazardous materials with complex chemical

composition comes with development of science and technology. Some of that materials are not biodegradable on the natural way and their degradation last infinitely long. All this leads to the conclusion that inadequate treatment, begin from the detoxification to the dumping and placing waste are very risky and ruinous job on the environment.

With fulfillment legislature norms for managing with this materials and development of different technologies for their detoxification and recycling it can be achieved higher level for safety environment. Consequently, in this paper is suggested upgraded technology of existing appliance which prevents contact between toxic liquid and environment and with that protecting disposer from this carcinogenic toxic waste.

Development and upgrading stages like this of existing systems lead to aim which presents general protection of environment and participants in it.

## 8. REFERENCES


[1] Pavlovic, M., Karanovic, N., Djuric, A.: *Uputstvo za detoksikaciju motornih vozila na kraju životnog ciklusa u skaldu sa pozitivnim zakonodavstvom Republike Srbije* - deo projekta „Postavljanje održivog modela reciklaže motornih vozila u Banatu u skladu sa novim nacionalnim zakonodavstvom“, Pokrajinski sekretarijat za urbanizam, graditeljstvo i zaštitu životne sredine, Novi Sad

[2] *Strategija upravljanjaotpadom za period 2010-2019. godine*, Službeni glasnik RS, br. 55/05, 71-05 ispravka, 101/07 и 65/08

[3] *Pravilnik o uslovima, načinu i postupku upravljanja otpadnim uljima*, Službeni glasnik RS, br. 71/2010

[4] http://www.nisotec.eu

[5] http://www.trigema.rs

[6] http://www.renault.rs

[7] http://molserbia.rs

[8] *Registovana vozila od 2001-2014. godine*, Republički zavod za statistiku, Republika Srbija

[9] Dabić, S., Miljuš, M., Mijailović, R.: *Management of materials flow from ELV vehicles*, The International of Transport and Logistic, TL-19/10, p.p. 47-60

[10] Pavlović, M., Arsovski, S., Ćurčić, S., Milovančević, M., Tolmač, D., Tomović, A.: *Postrojenje za uklanjanje tečnosti iz vozila na kraju životnog ciklusa - prototp*, Tehničko rešenje, Technicial faculty „Mihajlo Pupin“, Zrenjanin, 2013

[11] Kljajić, D., Eminović, F., Trgovčević, S., Dimitrijević, R., Dopsaj, M.: *Funkcionalni odnos dominantne i dominatne ruke pri motoričkom zadatku - izdržljivosti u sili stiska šake*, Specijalna edukacija i rehabilitacija, Volume 11 number 1, p.p. 67-85, 2012

[12] *Osmo predavanje iz mašinskih materijala*, Fakultet inženjerskih nauka, Kragujevac, 2003



***Authors:*** **M.Sc. Miroslav Vulić**, University of Novi Sad, Tehnicial faculty „Mihajlo Pupin“, Đure Đakovića bb, 23000 Zrenjanin, Serbia, Phone.: +381 63 619-742
E-mail: miroslav.vulic@tfzr.rs
**M.Sc. Aleksandar Tomović**, University of Belgrade, Faculty of mechanical engineering, Kraljice Marije 16, 11120 Beograd 35, Serbia, Phone.: +381 62 296-396
E-mail: aleksandar.tomovic@hotmail.com
**M.Sc. Aleksandar Pavlović,** University Business academy in Novi Sad, Faculty of Economics and Engineering Management of Novi Sad, Cvećarska 2, 21000 Novi Sad, Serbia
E-mail: alpa226@yahoo.com



***Note:*** This paper is a result of the research activities conducted under the project TR 35033, which is financed by the Ministry of Science and Technological Development of Republic of Serbia.

Journal of Production Engineering
Vol.18 No.2
JPE (2015) Vol.18 (2) Original Scientific Paper
Petrović, M., Petronijević, J., Mitić, M., Vuković, N., Plemić, A., Miljković, Z., Babić, B.

# THE ANT LION OPTIMIZATION ALGORITHM FOR FLEXIBLE PROCESS PLANNING

Received: 27 September 2015 / Accepted: 20 November 2015

**Abstract:** *Obtaining an optimal process plan according to all alternative manufacturing resources has become very important task in flexible process planning problem research. In this paper, we use a novel nature-inspired algorithm called Ant Lion Optimizer (ALO) to solve this NP-hard combinatorial optimization problem. The network representation is adopted to describe flexibilities in process planning and mathematical model for the minimization of the total production time and cost is presented. The algorithm is implemented in Matlab environment and run on the 3.10 GHz processor with 2 GBs of RAM memory. The presented experimental results show that the proposed algorithm performs better in comparison with other bio-inspired optimization algorithms.*
***Key words:*** *flexible process planning, ant lion optimizer, particle swarm optimization, genetic algorithms, simulated annealing*

**Algoritam zasnovan na koloniji mrava za optimizaciju projektovanja fleksibilnih tehnoloških procesa.**
*Dobijanje optimalnog sadržaja tehnološkog procesa na osnovu dostupnih proizvodnih resursa postaje veoma važan zadatak u istraživanju problema koji se odnose na projektovanje fleksibilnih tehnoloških procesa. U ovom radu, koristi se novi prirodno orijentisan algoritam (Ant Lion Optimizier-ALO) kako bi se rešili NP-teški nedeterministički poloinomni kombinatorni optimizacioni problemi. Mrežno prikazivanje je usvojeno u cilju opisivanja fleksibilnosti kod projektovanja tehnoloških procesa, dok je matematički model usvojen u cilju postizanja minimalnih ukupnih troškova i vremena. Algoritam je implementiran u okviru programskog okruženja Matlab i pokreće ga procesor 3.1 GHz sa 2 GB RAM memorije. Eksperimentalni rezultati ukazuju na činjenicu da predloženi algoritam bolje rešava zadatke u odnosu na druge biološke orijentisane optimizacione algoritme.*
***Ključne reči:*** *Fleksibilno projektovanje tehnološkog procesa, optimizacija kolonije mrava, optimizacija roja čestica, genetski algoritmi, simulirano kaljenje.*

## 1. INTRODUCTION

Computer Aided Process Planning (CAPP) represents one of the most important research directions in Computer Integrated Manufacturing (CIM). It was developed at the end of the 20th century for the purpose of integrating computer aided design (CAD) and computer aided manufacturing (CAM). Its aim consists of determining detailed methods for manufacturing a part economically and concurrently starting from the initial phase (drawing of the finished part) up to the final phase (the desired shape of the finished part).

As opposed to traditional manufacturing systems, most jobs produced in today's manufacturing systems may have a large number of alternative process plans due to the variety of alternative manufacturing resources. This problem is NP hard (*non deterministic polynomial optimization problems*) which means that time exponentially increases with increase of alternatives. Conventional nonheuristic methods are not able to find optimal solution for this combinatorial problem. In recent years metaheuristic algorithms have been used as primary techniques for obtaining the optimal solutions of process planning problem. Some of the most popular algorithms in this field are: genetic algorithms (GA), genetic programming (GP), simulated annealing (SA), tabu search (TS), swarm intelligence (ant colony optimization (ACO), particle swarm optimization (PSO)) or hybrid algorithms.

Li et al. [1] proposed GP-based approach to optimize flexible process planning with minimum total processing time as criteria. Network representation was adopted to describe flexibility of process plans and efficient genetic representations and operator schemes were also considered. Using the same optimization objective and representation, Shao et al. [2] presented a modified GA-based approach for generating optimal and near optimal process plans. Lv and Qiao [3] proposed new approach called cross-entropy (CE) to optimize flexible process planning. They used AND/OR network to represented flexibility of process planning and established mathematical model for minimization of total processing time and total cost. Hybrid GA-SA algorithm used to solve flexible process planning problem with the objective of minimizing the production time was presented in [4].

Although these algorithms are able to solve optimization problems, the so-called No Free Lunch theorem [5] allows researchers to propose new algorithms. This paper proposes a new algorithm called Ant Lion Optimizer (ALO) as an alternative approach for solving flexible process planning problem.

The structure of this paper consists of the following sections. In the Section 2 we briefly introduce a flexible process planning problem and describe its representation. Mathematical model of the problem with two objective functions is formulated in Section 3.

Section 4 outlines ant lion optimization concept. Section 5 shows comparative results and Section 6 gives concluding remarks. Finally, acknowledgements and references are stated in Section 7 and Section 8, respectively.

## 2. FLEXIBILITY AND REPRESENTATION

### 2.1 The flexible process planning problem

In this paper, we consider the following types of flexibility for process planning optimization: machine flexibility, process flexibility, and sequencing flexibility. Machine flexibility relates to the possibility of performing one operation on different alternative machines, with various processing times and costs. Process flexibility refers to the possibility of producing the same part in different ways with alternative operations or sequences of operations. Sequencing flexibility implies the possibility to interchange the ordering of required manufacturing operations.

### 2.2 Representation of flexible process plans

The flexible process plans representation consists of the information about alternative machines, processing times, operation sequences, and all the operations needed to manufacture the part. Networks, Petri nets, OR network [1, 2], AND/OR network graphs [3] are some of numerous representation methods used to describe aforementioned types of flexibilities. AND/OR network methodology, described in details in literature [1, 2, 4], is employed to represent flexible process plans.

## 3. MATHEMATICAL MODELING OF OPTIMIZATION PROBLEM

In this paper, minimization of the total production time and total production cost are two objectives of the optimization problem to be considered. Production time is the one of commonly used minimization criterion in process planning optimization (see e.g. [1, 2]). In this research production time comprises processing time and transportation time.

Processing time (*TW*) is the time needed to machine a material under some operation(s) and can be computed as:

$$TW = \sum_{i=1}^{n} TWI(i, j) \tag{1}$$

where *n* is the (total) number of operations in process plan, *TWI(i,j)* the processing time of operation *i* on the alternative machine *j*.

Transportation time (*TT*) is the time spent for transport of raw materials, goods, or parts between machines and can be computed as:

$$TT = \sum_{i=1}^{n-1} TTI((i, j_1),(i+1, j_2)) \tag{2}$$

where $TTI(i,j_1),(i+1,j_2)$ is the transportation time between the alternative machine $j_1$ and $j_2$ for two consecutive operations.

The total production time (*TPT*) is defined as:

$$TPT = TW + TT \tag{3}$$

The production cost is another criterion commonly used to select flexible process plans and to quantitatively measure its quality. The total production cost contains the machine cost and the machine change cost, where each cost factor can be described and computed as follows.

Machine cost (*MC*) is the total cost of the machines selected in flexible process plan and it is computed as:

$$MC = \sum_{i=1}^{n} MCI_i \tag{4}$$

where n is the total number of operations and $MCI_i$ is the predetermined machine cost index for using machine *i,* which is a constant for a particular machine.

Machine change cost (*MCC*) is required to be considered when two consecutive operations are performed on different machines, and it can be computed as:

$$MCC = MCCI \times \sum_{i=1}^{n} \Omega(M_{i+1} - M_i) \tag{5}$$

where *MCCI* is the machine change cost index and $M_i$ is the identity of the machine used for operation *i*.

All this costs are included in the total cost (*PC*) according to the following equation:

$$PC = MC + MCC \tag{6}$$

## 4. THE ANT LION OPTIMIZER

Antlions belong to group of insects in the family Myrmelentidae. The two main phases of the antlions lifecycle are larval stage and adult stage. The antlion larva is often called "doodlebug" because of the trails it leaves in the sand while looking for a good location to build its trap, see Fig. 1. During the process of hunting, antlion makes funnel pits in soft sand and then waits patiently at the bottom of the pit, Fig. 2. Slipping to the bottom, the prey is immediately seized by the antlion. Or, if prey attempts to escape from the trap, antlion throw sands towards the edge of the pit to slide the pray into the bottom of the pit. By throwing up loose sand from the bottom of the pit, the larva also undermines the sides of the pit, causing them to collapse and bring the prey with them. Mathematical modeling of the behavior of antlions and ants is given in the following section [6].

Fig. 1. Pits made by the antlion in soft sand [7]

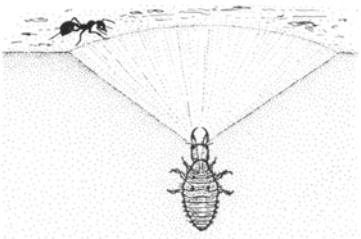

Fig. 2. Hunting behaviour of antlions [8]

### 4.1 Operators of the ALO algorithm

Random walks of ants when searching food in nature can be described as follows:

$$X(t) = [0, cumsum(2r(t_1) - 1), cumsum(2r(t_2) - 1), ..., cumsum(2r(t_n) - 1)] \quad (7)$$

where *cumsum* calculates the cumulative sum, *n* is the maximum number of iterations, *t* shows the step of random walk, and *r(t)* is stochastic function defined according to the following equation:

$$r(t) = \begin{cases} 1 \ if \ rand > 0.5 \\ 0 \ if \ rand \le 0.5 \end{cases} \quad (8)$$

where *t* shows the step of random walk and rand is a random number generated according to uniform distribution in the range [0,1].

The position of ants is presented with the matrix:

$$M_{Ant} = \begin{bmatrix} A_{1,1} & A_{1,2} & \cdots & A_{1,n} \\ A_{2,1} & A_{2,2} & \cdots & A_{2,d} \\ \vdots & \vdots & \ddots & \vdots \\ A_{n,1} & A_{n,2} & \cdots & A_{n,d} \end{bmatrix} \quad (9)$$

where $M_{Ant}$ is the matrix for each ant position, $A_{i,j}$ present the value of *j-th* variable of *i-th* ant, *n* is the number of ants, and *d* is the number of variables.

Fitness function of each ant is saved in the following matrix $M_{OA}$:

$$M_{OA} = \begin{bmatrix} f([A_{1,1}, A_{1,2}, ..., A_{1,d}]) \\ f([A_{2,1}, A_{2,2}, ..., A_{2,d}]) \\ \vdots \\ f([A_{n,1}, A_{n,2}, ..., A_{n,d}]) \end{bmatrix} \quad (10)$$

where *f* is objective function (see eq. (3) and (6)).

$$M_{Antlion} = \begin{bmatrix} AL_{1,1} & AL_{1,2} & \cdots & AL_{1,n} \\ AL_{2,1} & AL_{2,2} & \cdots & AL_{2,d} \\ \vdots & \vdots & \ddots & \vdots \\ AL_{n,1} & AL_{n,2} & \cdots & AL_{n,d} \end{bmatrix} \quad (11)$$

where $M_{Antlion}$ is the matrix for each antlion position, $AL_{i,j}$ present the value of *j-th* variable of *i-th* antlion, *n* is the number of antlions, and *d* is the number of variables.

Analogously, fitness function of each antlion is saved in the following matrix $M_{OAL}$:

$$M_{OAL} = \begin{bmatrix} f([AL_{1,1}, AL_{1,2}, ..., AL_{1,d}]) \\ f([AL_{2,1}, AL_{2,2}, ..., AL_{2,d}]) \\ \vdots \\ f([AL_{n,1}, AL_{n,2}, ..., AL_{n,d}]) \end{bmatrix} \quad (12)$$

In order to keep random walks of ants inside the search space, they are normalized using the following equation:

$$X_i^t = \frac{(X_i^t - a_i) \times (d_i - c_i^t)}{(d_i^t - a_i)} + c_i \quad (13)$$

where $a_i$ is the minimum of random walk of *i-th* variable, $b_i$ is the maximum of random walk in *i-th* variable, $c_i^t$ is the minimum of *i-th* variable at *t-th* iteration, and $d_i^t$ is the maximum of *i-th* variable at *t-th* iteration.

Mathematical modelling of ants trapping in antlion's pits is given by the following equations:

$$c_i^t = Antlion_j^t + c^t \quad (14)$$

$$d_i^t = Antlion_j^t + d^t \quad (15)$$

where $c^t$ is the minimum of all variables at *t-th* iteration, $d^t$ is the maximum of all variables at *t-th* iteration, and $Antlion_j^t$ is the position of the selected *j-th* antlion at *t-th* iteration.

Antlion's hunting capability is modelled by fitness proportional roulette wheel selection. The mathematical model that describes the way how the trapped ant slides down towards antlion is given as follows:

$$c^t = \frac{c^t}{I} \quad (16)$$

$$d^t = \frac{d^t}{I} \quad (17)$$

where *I* is a ratio calculated as:

$$I = 10^w \cdot \frac{t}{T} \quad (18)$$

where *t* is the current iteration, T is the maximum number of iterations, *w* is the constant that depends on current iteration as follows:

$$w = \begin{cases} 2 \ if \ t > 0.1T \\ 3 \ if \ t > 0.5T \\ 4 \ if \ t > 0.75T \\ 5 \ if \ t > 0.9T \\ 6 \ if \ t > 0.95T \end{cases} \quad (19)$$

Finally, elitism is applied in the following way: the best antlion in each iteration is considered to be elite. It means that every ant randomly walks around selected antlion and has position according to:

$$Ant_i^t = \frac{R_A^t + R_E^t}{2} \quad (20)$$

where $R_A^t$ is the random walk around the antlion selected by the roulette wheel at *t-th* iteration, and $R_E^t$ is the random walk around the elite antlion at *t-th* iteration.

## 5. EXPERIMENTAL RESULTS

In order to evaluate the performance and illustrate the effectiveness of the ALO approach, the algorithm procedure is coded in Matlab software and implemented on a personal computer with a 3.10 GHz processor. In this experiment, job 1 (see Fig. 3) is considered and the transportation time between the machines is given in Table 1. The parameters of algorithm are set as follows: the size of the population is 40 and the number of iterations is 30. The optimization objective is to get an optimal operation sequence that results in minimum production time (eq. (3)) and cost (eq. (6)). Fig. 4a illustrates the convergence curves for the GA, hybrid GA-SA, PSO, and ALO algorithm and Fig. 4b shows error bar plot of production time after 10 runs. The obtained optimal sequence according to minimal production time is (1,2)-(5,3)-(8,7)-(9,8), *TPT=117*, and according to minimal production cost is (1,2)-(5,3)-(8,7)-(9,8), *TPC = 545*.

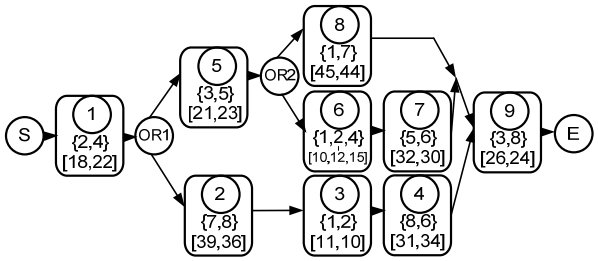


Fig. 3. Alternative process plans network [3]

| machine | 1 | 2 | 3 | 4 | 5 | 6 | 7 | 8 |
|---|---|---|---|---|---|---|---|---|
| 1 | 0 | 3 | 7 | 10 | 3 | 5 | 8 | 12 |
| 2 | 3 | 0 | 4 | 7 | 5 | 3 | 5 | 8 |
| 3 | 7 | 4 | 0 | 3 | 8 | 5 | 3 | 5 |
| 4 | 10 | 7 | 3 | 0 | 10 | 8 | 5 | 3 |
| 5 | 3 | 5 | 8 | 10 | 0 | 3 | 7 | 10 |
| 6 | 5 | 3 | 5 | 8 | 3 | 0 | 4 | 7 |
| 7 | 8 | 5 | 3 | 5 | 7 | 4 | 0 | 3 |
| 8 | 12 | 8 | 5 | 3 | 10 | 7 | 3 | 0 |

Table 1. Transportation time between machines [3]

| machine | $M_1$ | $M_2$ | $M_3$ | $M_4$ | $M_5$ | $M_6$ | $M_7$ | $M_8$ |
|---|---|---|---|---|---|---|---|---|
| cost | 30 | 10 | 30 | 40 | 100 | 60 | 10 | 15 |
| MCCI | 160 | | | | | | | |

Table 2. Machine cost and machine change cost

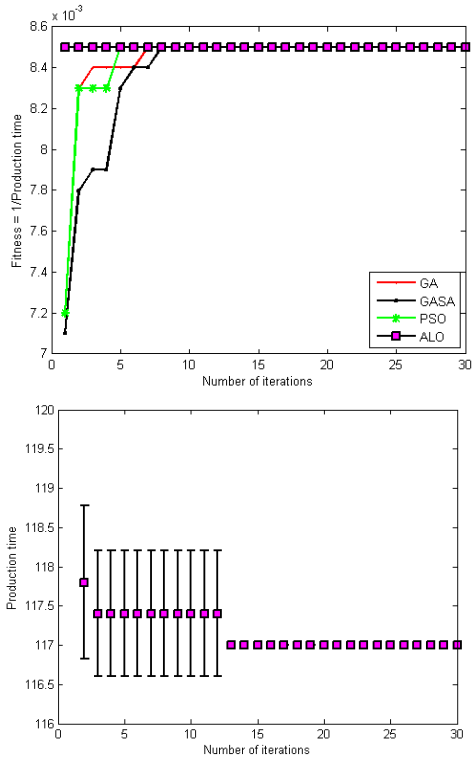


Fig. 4. (a) Comparison of the GA, hybrid GA-SA, PSO and ALO algorithm; (b) Error bar plot of production time

## 6. CONCLUSION

In this paper, new approach based on Ant Lion Optimization (ALO) algorithm is proposed to optimize combinatorial NP-hard flexible process planning problem. The network representation method is adopted to describe process flexibility, sequencing flexibility, and machine flexibility. The main steps of ALO algorithms are implemented on process planning problem. The performance of the presented ALO algorithm are verified and evaluated in comparison with the results obtained with GA, SA, and PSO standalone algorithms as well as hybrid GA-SA algorithm. Experimental results indicate that the proposed algorithm performs better in comparison with other bio-inspired optimization algorithms.

## 7. REFERENCES


[1] Li, X.Y., Shao, X.Y., Gao, L.: *Optimization of flexible process planning by genetic programming*, International Journal of Advanced Manufacturing Technology 38(1-2), pp. 143–153, 2008.

[2] Shao, X., Li, X., Gao, L., Zhang, C.: *Integration of process planning and scheduling—a modified genetic algorithm-based approach*, Computers and Operations Research 36(6), pp. 2082–2096, 2009.

[3] Lv, S., Qiao, L.: *A cross-entropy-based approach for the optimization of flexible process planning*, International Journal of Advanced Manufacturing Technology 68(9-12), pp. 2099–2110, 2013.

[4] Petrović, M., Miljković, Z., Babić, B.: *Optimization of Operation Sequencing in CAPP Using Hybrid Genetic Algorithm and Simulated Annealing Approach*, In: Proceedings of the 11th International Scientific Conference MMA 2012 – Advanced Production Technologies, Novi Sad, Serbia, pp. 285–288, 2012.

[5] Wolpert, D.H., Macready, W.G.: *No free lunch theorems for optimization*, Evolutionary Computation, IEEE Transactions, 1(1), pp. 67-82, 1997.

[6] Mirjalili, S.: *The ant lion optimizer*, Advances in Engineering Software, 83, pp. 80-98, 2015.

[7] http://www.asknature.org/media/image/3305

[8] http://oldblockwriter.blogspot.com/2012/02/ant-lions-and-angle-of-rest.html


## ACKNOWLEDGMENT


This paper is part of the project: *An innovative, ecologically based approach to the implementation of intelligent manufacturing systems for the production of sheet metal parts*, financed by the Ministry of Education, Science and Technological Development of the Serbian Government, Grant *TR-35004* (2011-2015).



***Authors:*** **M.Sc. Milica Petrović, M.Sc. Jelena Petronijević, Dr. Marko Mitić, Dr. Najdan Vuković, Aleksandar Plemić, prof. dr. Zoran Miljković, prof. dr. Bojan Babić**, University of Belgrade, Faculty of Mechanical Engineering, Production Engineering Department, Kraljice Marije 16, 11120 Belgrade 35, Serbia, Phone: +381 11 3302-264, Fax: +381 11 3302-274.

E-mail: mmpetrovic@mas.bg.ac.rs; jpetronijevic@mas.bg.ac.rs; mmitic@mas.bg.ac.rs; nvukovic@mas.bg.ac.rs; aleksandarplemic@gmail.com; zmiljkovic@mas.bg.ac.rs; bbabic@mas.bg.ac.rs;

Journal of Production Engineering
Vol.18 No.2
JPE (2015) Vol.18 (2) Original Scientific Paper

Tamás, P., Illés, B.

# SIMULATION EXAMINATION OF LOGISTICS SYSTEMS IN THE AUTOMOTIVE INDUSTRY

Received: 02 August 2015 / Accepted: 28 October 2015

***Abstract**: The automotive enterprises apply simulation methods for the examination of the complex material flow systems. This paper introduces the more important possibilities of simulation examination and the obtainable possible advantages at different automotive logistics systems. Furthermore some research projects will be introduced in a nutshell. We will describe the defined aims and achieved results of the examinations.*
***Key words:** simulation, automotive industry, logistics system*

**Ispitivanje simulacijom logističkih sistema u automobilskoj industriji.** *Preduzeća u automobilskoj industriji primenjuju metode simulacije za ispitivanje složenih tokova materijala. U ovom radu su predstavljene neke od važnijih mogućnosti ispitivanja simulacijamama i moguće prednosti koje se mogu postići u različitim logističkim sistemima automobilske industrije. Neki od istraživačkih projekata će biti predstavljeni. Takođe će se opisati definisani ciljevi i postignuti rezultati istraživanja.*
***Ključne reči:** simulacija, automobilska industrija, logistički sistem*

## 1. INTRODUCTION

The application of the simulation techniques was needed in the interest of the reduction of enterprises' wastes regarding the complex logistics systems [1]. In the last decades the simulation modeling's application was very useful at more logistics fields, such as production scheduling [2], development of the material flow processes [3], optimization of the disaster relief systems [4], planning of the logistics systems [5-6].

The Logistics Institute of the University of Miskolc has been using simulation modeling for more than ten years [7-8]. In the last few years we have taken part in the solution of numerous practical problems regarding the automotive industry. We can use simulation modeling in two cases, which are the improvement of the current logistics systems and the planning of new subsystems. In general we have to use simulation modeling if mathematical description of the logistics processes is very difficult or impossible and we would like to improve this logistics process.

Basically the aim of simulation modeling is the determination of the future working of a logistics system on the basis of defined operational processes, conditions and aims. We can increase the efficiency of the logistics processes with this device. The values stream mapping's method is an important device of the lean philosophy which was created in the interest of decreasing logistics processes' waste [9-10]. We can distinguish two versions of this method namely the static and the dynamic value stream mapping. The static value stream mapping can be used for only process improvement of a product line in order to guarantee transparent [11]. The application of this method is realized on the basis of the collected data on an A3 sheet of paper, thus we can examine simultaneously only one product line. The dynamic value stream mapping's method is based on simulation modeling, which enables simultaneously examination of more product lines' processes too [12].

In this paper we will introduce the simulation examination possibilities of the automotive logistics systems, steps of the simulation examination, some practical research projects and educational possibilities of this method.

## 2. SIMULATION INVESTIGATIONAL POSSIBILITIES

The automotive logistics processes have a very big complexity in a lot of cases, which is the consequence of the next causes:

- creation of the corresponding product variation for the customers [13],
- ensurance of the JIT/JIS principled material catering,
- application of the multilevel assembly process,
- use of the flexible manufacturing systems.

The simulation examinations' realization is in a lot of cases necessary in the interest of the improvement of the complex logistics processes. The automotive logistics processes' more important investigational possibilities are the following:

- elimination of planning failures at the complex logistics systems [2],
- optimal planning of the procurement-, manufacturing and distribution logistics systems,
- comparison of planning variations,
- determination of the highest performances and boundary status,
- support of the Kaizen workshops,
- comparison of the system control variations,

- modeling of the system failures and their eliminations.

We can see from the listed research areas that this is a very useful device. The simulation process improvement is realizable through the total value stream or in the case of an assigned subsystem (procurement-, production-, distribution-, recycling logistics).

## 3. STEPS OF REALIZATION OF THE SIMULATION EXAMINATION

We have to realize numerous tasks in the interest of the solution of the complex logistics problems with simulation method. These are the following:

- *Determination of the simulation's aim, define the examined logistics system's boundary:* We have to determine clearly the investigational aims before making the simulation program and after that we can assign the logistics area to be examined.

- *Understanding the working of the examined system:* The examination maker people have to understand the material flow properties and working principles of the assigned logistics system in order that these people could take into consideration the most important things at the creation of the simulation model.

- *Determination of the logistics indicators' set:* In this phase we have to determine the set of those logistics indicators which enable the comparison and evaluation of the investigational results (e.g.: operational workstations' utilization, lead time, …, etc.).

- *Determination of the input and output data:* After the previous steps, we have to define the input and output data of the simulation model, so we can determine the final data request to the examined enterprise. The requested data are not available in every case, so we have to decide whether we will create these data with estimations or field measurements.

- *Creation of the simulation model:* The simulation model is created on the basis of the available information. After this we can examine the working of the modeled logistics systems with the use of the given input data.

- *Control and repair of the realized simulation model:* We have to calibrate the investigational model together with enterprise professionals (for example: with comparison of the current status' logistics indicators and/or with control of the modeled material flow). Numerous cases can occur when we have to modify the created model in the interest of the correct working.

- *Evaluation of the investigational results, elaboration of the proposals:* Using the calibrated model we can determine the working characteristics of the examined logistics with the changing of the selected parameters. With the analyzation of the given data we can elaborate proposals to the examined enterprise. In a lot of cases the task is the optimal determination of more parameters, in such cases we need to use optimization algorithms.

## 4. PRACTICAL APPLICATION OF SIMULATION MODELING

In the last few years we have made a lot of simulation models for more enterprises (for example: AUDI Hungaria Motor Ltd., ClaasHungaria Ltd., …, etc.), as a result of this the materials processes' working efficiency was increased. Besides the industrial research tasks more PhD research topics were elaborated in which the simulation modeling played a relevant role [2, 7]. Henceforth, some practical examples will be presented and the achieved results in connection with them (because of the privacy causes they will not be introduced in details)

Simulation examination of the flexible manufacturing systems [2]:

Manufacturing of the small-scale body parts has a very relevant complexity from the point of view of material flow. The cause of the complexity is that a workstation is able to work products of more product lines, consequently the products' material flow routes are very different.

Inside the material flow different materials handling equipments and unit loads making devices are used. The simulation modeling enables the examination of such complex systems too. The examined enterprise have planned the enhancement of the manufacturing activities because of the customer demand's increase at the manufacturing of the small-scale body parts. The expansion of the plant was necessary in the interest of the realization of these plans.

The essential problem was the determination of the warehouses and work in processes' sizes because of the complexity of the material flow. We determined the relative frequency functions of the various storage areas' stock levels, which function shows the occurrence of the various storage areas' stock levels in percentage (for example: 4 unit loads was placed in the work in process 1 through in the 40 % of the examination time).

The examined enterprise's worker determined the final storage areas on the basis of this data. In addition, the elaborated investigation model was able to run and evaluate the different manufacturing plans too.

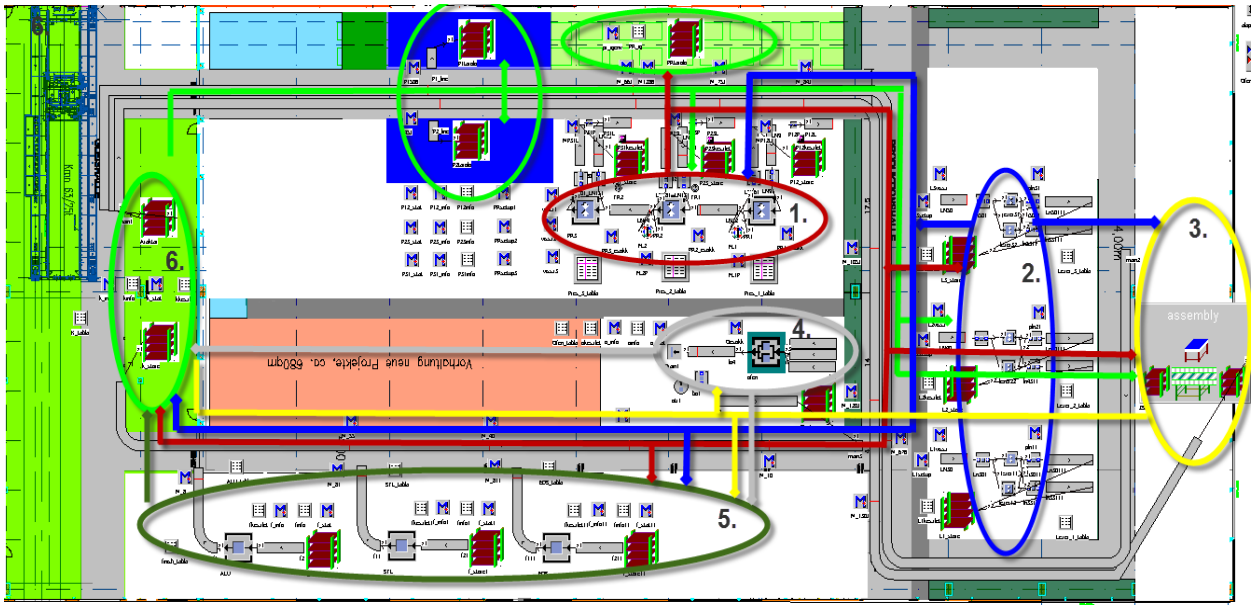


Fig. 1. Simulation model of a flexible manufacturing system

Simulation examination of the finished goods storage activities' outsourcing [14-15]:

The finished products' storage position and stockpiling mechanism play a relevant role in the competitiveness of the distribution logistics systems (they have effect on changing of the logistics costs and/or service quality).

We have created such a simulation model which enables the examination of the finished good warehousing system's working in the future state, consequently we can make a better decision regarding creation of the corresponding warehousing system.

Essentially the examinational system determine the storage places and stockpiling strategies of the examined enterprise' products in order that we can get the most efficient distribution logistics system working. The examination's goal function contains more components (cost, quality indicators). The examined enterprise's experts determine the weight of this components.

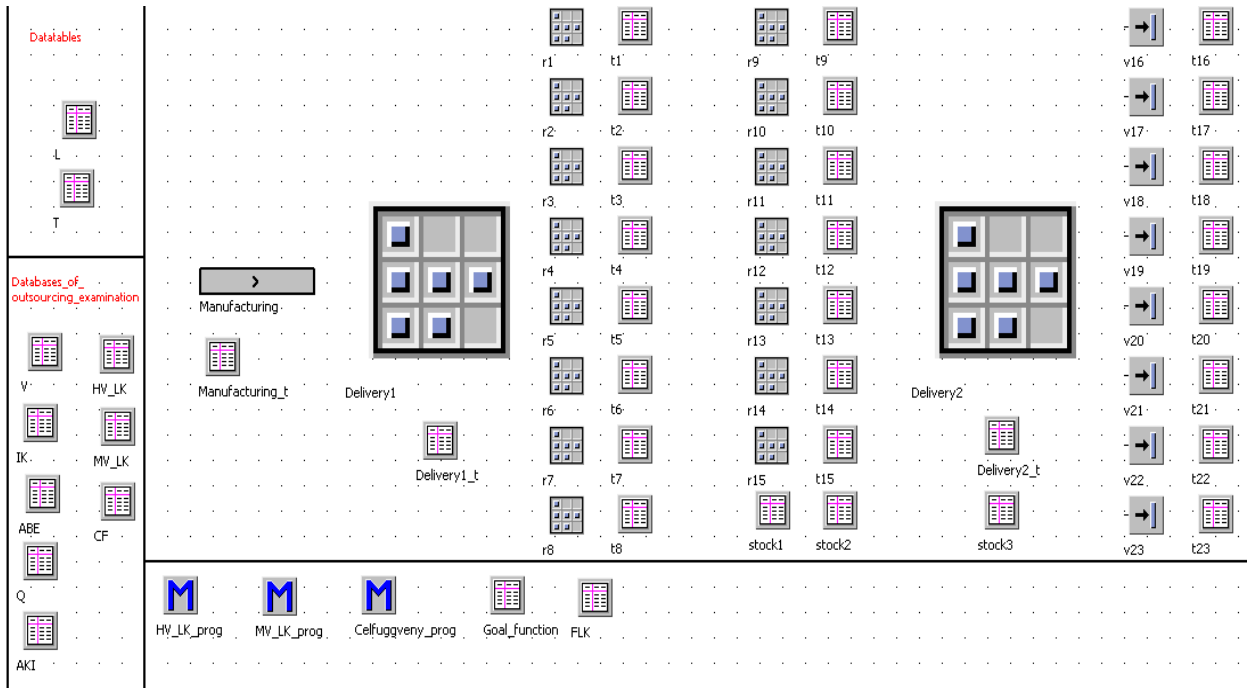


Fig. 2. Simulation model of the outsourcing examination

## 5. SIMULATION MODELING IN THE EDUCATION

More and more automotive companies need to make simulation models, first of all because of theirs complex logistics processes and application of the lean philosophy [16]. The essential demand of the enterprises in this area is the training of such professionals in the higher education, who are able to determine the aims of the improvement, assign the

examined logistics system and solve the determined tasks.

In the interest of these demands' catering the Institute of Logistics of the University of Miskolc created a simulation investigational lab. The students can learn the use of the simulation softwares and the methodology of the simulation examination through examples in this lab. The other important knowledge (for example: planning of the systems, optimization, …, etc.) can be learnt in other subjects. The Institute of Logistics have started this training in two areas, which are the Software engineering BSc and the Logistics engineering BSc.

## 6. SUMMARY

This paper introduced such a modern planning system which enables the decrease of the wastes inside the logistics processes in the interest of enhancement of the enterprises' competitiveness. The application possibilities of this device and some realized practical researches' results were presented. This paper mentioned the educational demands from the part of the enterprises, as well as the created simulation lab at the University of Miskolc.

## 7. REFERENCES


[1] M.P. Fanti, G. Iacobellis, W. Ukovich, V. Boschian, G. Georgoulas, C. Stylios: A simulation based Decision Support System for logistics management, Journal of Computational Science, Volume 10, September 2015, pp. 86-96

[2] P. Tamás, B. Illés, S. Tollár: Simulation of a flexible manufacturing system. Advanced Logistic System Theory and practice, Volume 6. (2012), HU ISSN 1789-2198, pp. 25-33.

[3] N. Bin Ali, K. Petersen, B. B. Nicolau de França: Evaluation of simulation-assisted value stream mapping for software product development: Two industrial cases: Information and Software Technology, Volume 68, December 2015, Pages 45-61.

[4] A. D'Uffizi, M. Simonetti, G. Stecca, G. Confessore: A Simulation Study of Logistics for Disaster Relief Operations, Procedia CIRP, Volume 33, 2015, pp. 157-162

[5] D. Leriche, M. Oudani, A. Cabani, G. Hoblos, J. Mouzna, J. Boukachour, A. El Hilali Alaoui: Simulating new logistics system of Le Havre Port, IFAC-PapersOnLine, Volume 48, Issue 3, 2015, pp. 418-423

[6] A. A. Tako, S. Robinson: The application of discrete event simulation and system dynamics in the logistics and supply chain context, Decision Support Systems, Volume 52, Issue 4, March 2012, pp. 802-815

[7] B. Illés, P. Tamás, S. Tollár, M. Kiss: Simulationsuntersuchung der BestandteilProduktion in kleinerSeriebeimWerkzeugbau von AHM, Universitätstreffenbei der AUDI HUNGARIA MOTOR Kft.,Győr, 25 October 2011.

[8] J. Cselényi, B. Illés: Planning and controlling of material flow systems. Textbook, Miskolci Egyetemi Kiadó, 2006.

[9] M. Rother, J. Shook: Learning to See: Value Stream Mapping to Add Value and Eliminate Muda, Lean Enterprise Institute, 2003.

[10] J. P. Womack, D. T. Jones: Lean thinking, Simon & Schuster Inc., 2008.

[11] B. Keyte, D. A. Locher: The complete lean enterprise: Value stream mapping for administrative and office processes, ISBN: 978-1-4200-8153-4, CRC Press, Taylor and Francis Group, 2004.

[12] A. Mahfouz, A. Arisha, Lean distribution assessment using an integrated framework of value stream mapping and simulation, Proceedings of the 43rd Winter Simulation Conference, IEEE Computer Society,2013, pp.3440–3449.

[13] P. Košťál, K. Velíšek: Flexible manufacturing system (Scopus) In: World Academy of Science, Engineering and Technology. - ISSN 2010-376X. - Vol. 77 (2011), pp. 825-829

[14] P. Tamás, Gy. Kovács, B. Illés: *Decision making method relating to outsourcing of finished goods storage activities*, Advanced Logistic Systems, Theory and Practice, 2009, Volume 3, pp 120-126, HU ISSN 1789-2198.

[15] K. Ali, C. ERMAN, C. TURAN: Factors to consider for outsourcing decision in supply chain management, 4th International Logistics and Supply Chain Congress, Turkey, Izmir, 2006.

[16] P. Košťál, A. Mudriková, , D. Cagáňová: The Virtual Laboratory of Program Control. (Web of Science, Scopus) In: ASME 2010 10th Biennial Conference on Engineering Systems Design and Analysis (ESDA2010): Turkey, Istanbul, July 12-14, 2010. - : ASME, 2010. - ISBN 978-0-7918-3877-8. – pp. 1-9



**Acknowledgements**

"This research was (partially) carried out in the framework of the Center of Excellence of Mechatronics and Logistics at the University of Miskolc."



***Authors:*** **Dr. Péter Tamás (assistant professor), Dr. Béla Illés (university professor)**, University of Miskolc, Faculty of Mechanical Engineering and Informatics, Institute of Logistics, H-3515, Miskolc-Egyetemváros
E-mail: alttpeti@gmail.com
altilles@uni-miskolc.hu

Journal of Production Engineering
Vol.18 No.2
JPE (2015) Vol.18 (2) Original Scientific Paper
Milojević, Z., Tabaković, S., Bojanić, M., Zeljković, M.

# MULTI AXIS NC CODE SIMULATION BASED ON THREE-DEXEL MODEL REPRESENTATION AND GPU

Received: 27 September 2015 / Accepted: 20 November 2015

**Abstract:** *This paper presents a program system for multi axis NC code simulation based on three-dexel approach. Computing of tool subtraction from a workpiece is done in the GPU (Graphics Processing Unit) as computation power of modern GPU is 10 to 100 times higher than the CPU (Central Processing Unit). Initially, blank workpiece STL model is converted to three-dexel model by depth peeling algorithm. Then, structures for dexels in all three dimensions are transferred into the GPU. Tool movement is approximated by instances between two consecutive positions. For every tool instance, depth and normal textures are generated in all three directions and subtracted from the workpiece model.*
***Key words:*** *three-dexel model, NC code simulation, GPU computation*

**Simulacija višeosnog upravljačkog programa za cnc mašine baziran na tri-dexel metodi i GPU.** *U radu je predstavljen programski sistem za višeosnu simulaciju NC upravljačkog programa baziran na tri-deksel pristupu. Proračun oduzimanja alata od radnog predmeta je izvršen primenom grafičke kartice. Brzina proračuna na modernim grafičkim karticama je 10-100 puta veća od brzine proračuna na modernim mikroprocesorima. Na početku u sistemu, STL model pripremka se konvertuje u tri-deksel model depth peeling algoritmom. Zatim se vrši transfer generisanih tri-deksel struktura u grafičku karticu. Kretanje alata je aproksimirano instancama alata između dve pozicije. Za svaku instancu alata dubinske teksture i teksture normala se generišu u sva tri ortogonalna pravca i oduzimaju od modela radnog predmeta.*
***Ključne reči****: tri-dexel model, Simulacija NC koda, GPU proračun*

## 1. INTRODUCTION

In the NC (Numerically Controlled) simulation process, workpiece is usually approximated with voxel or dexel elements. The voxel model represents an object with many small cubes, whilst dexel model represents an object with a grid of long columns compacted together. Dexel representation is widely used in NC simulation process, because it is less memory demanding than voxel representation [1].

In Fig. 1a, one circle is represented with dexels in one dexel direction (single dexel representation). The weak point of single dexel representation is that surfaces which are almost parallel with dexel direction can be missed in dexel generation. Much better surface representation for the same number of rays is shown in Fig 1b, where circle is intersected with rays in two orthogonal directions. For three dimensional case presented in Benouamer et al. [1], three dexel model is introduced, where model is approximated with dexels in three orthogonal directions.

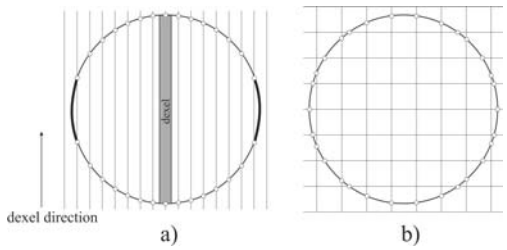

Fig. 1. a) Single dexel representation, b) Dexels generated in two dimensions

Because of simplicity and fast Boolean operations, dexel representation is widely used in program systems where a real-time performance is important, such as, NC machining simulations [2,3,4,5] or virtual sculpting systems [6,7,8,9].

## 2. MODEL OF THE DEVELOPED PROGRAM SYSTEM

Program system is primarily developed with a goal to simulate free form modelling by hand movement in a virtual environment [9]. User moves tool in space and program system should subtract a tool from workpiece as soon as possible. Also, tool can be of a freeform shape. This program system had two limitations. Model and tool were approximated by a single dexel representation and it was a view dependent. This system is therefore extended with a three-dexel model representation, with subtraction operations now done with the GPU and it is not view dependent. It can also be used in the NC multi axes code simulation, as it is shown in this paper.

Model of the developed program system is shown in Fig. 2. Blank workpiece and tools models are imported in the system as STL files as shown in Fig. 2. Next step presents a generation of three-dexel textures in GPU (Graphics Processing Unit). After that, from generated textures, structures of every dexel are formed by CPU (Central Processing Unit). Matrices of tool instances are generated from the NC code. Then, formed dexel structures are transferred into GPU and

complete simulation of tool subtraction from workpiece is performed by the GPU. For every tool instance, model of the tool is transformed by the matrix, and three-dexel textures of the tool are generated. Then, tool instance textures are subtracted from the workpiece and the workpiece is modified. This step is repeated for every tool instance. When computation is done, three-dexel model of machined workpiece can be transferred from the GPU to the main memory, where it can be processed afterwards.

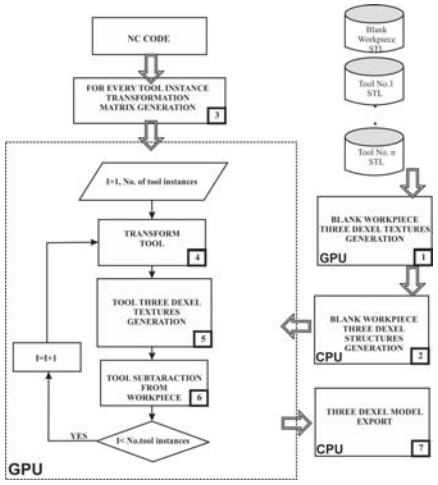

Fig. 2. Model of the developed program system

Detailed steps of the procedure explained above are presented in the following sections.

### 2.1 Blank workpiece STL to three-dexel model conversion

Blank workpiece model is imported in the program system in STL format (as triangle polygon collection where each triangle has a normal). For three-dexel model generation, ray intersection with model in three orthogonal directions should be calculated. This process can be very time consuming (blank workpiece may consist of millions of triangles). To speed up computation, depth peeling algorithm [10] is applied in the program system. Model is rendered in projection as many times as maximal complexity of point in this projection is. In Fig. 3, 2D case is presented.

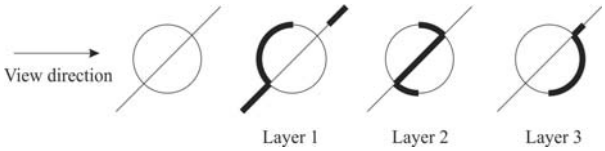

Fig. 3. Depth peeling principle

As shown in Fig. 3, all visible faces are rendered first (Layer 1). After that, these faces are discarded and next visible faces are rendered. Process is finished when there are no faces left to render. Shape shown in Fig. 3 has a complexity of three in the view direction. Surfaces are rendered in images (textures) and every texture pixel has a depth value of surface point in the view direction.

For the model presented in Fig. 4a, rays in x and y direction intersect model in four points (two dexels) when rays in z direction intersect model in two points (one dexel). This means that in depth peeling of the model shown in Fig. 4 number of passes in x and y direction is four, and in z direction is two. Before depth peeling algorithm is applied, bounding view volume should be determined in respect that it covers complete model in all three orthogonal dimensions.

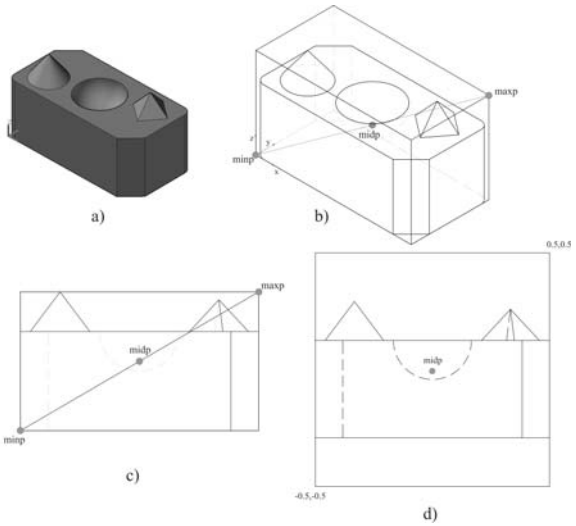

Fig. 4. a) Example model b,c) Bounding box parameters and d) Transformed model prepared for depth peeling

First step presents model bounding box determinations with *minp, maxp and midp* points (Fig. 4b). After that, maximal projection on one of orthogonal axis is determined (Fig. 4c). This projection is an edge of the cube (with center *midp*) from which view bounding box is calculated. Then, model is scaled and transformed in position in such way that *midp* is transformed in WCS origin and bounding square for texture generation is (-0.5,-0.5 ÷ 0.5,0.5). Transformed and scaled model in front view is shown in Fig. 4d. For any depth peel layer model is rendered by the GPU and two images (textures) are generated. In the first texture (depth texture) every pixel contains depth value in the range 0.0-1.0. In the second texture (normal texture) every pixel has a RGB (Red Green Blue) colour, where red, green and blue components contain x, y and z normal information.

Generated depth textures in all three orthogonal directions are shown in Fig. 5. Also, in Fig. 5a, generated normal texture for first layer in z direction is shown.

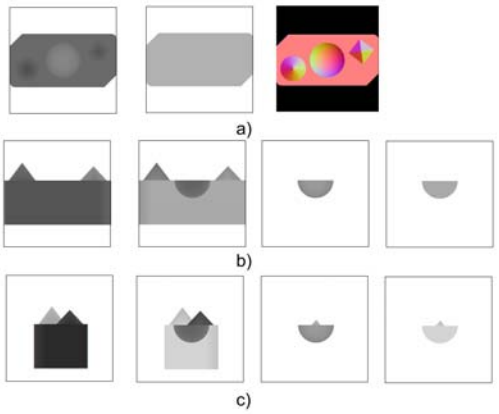

Fig. 5. Generated depth textures a) in z direction with one normal texture, b) in y and c) in x direction

### 2.2 Three-dexel structure definition

Based on the generated textures in the previous step, structures for dexels in all three dimensions should be generated and transferred into GPU. Parameters for dexel definition are presented in Fig. 6. Every texture has a resolution (*texture resolution*). For dexel presented in Fig. 6a, parameters *depth* and *length* define coordinates of first and last point of dexel in the view direction, when *positionx* and *positiony* define dexel position in a plane. Also, from normal textures every dexel point normals are calculated *normal1* and *normal2*. Two last parameters in dexel structure, *cut1* and *cut2,* give information if blank workpiece dexels are cut in the simulation process.

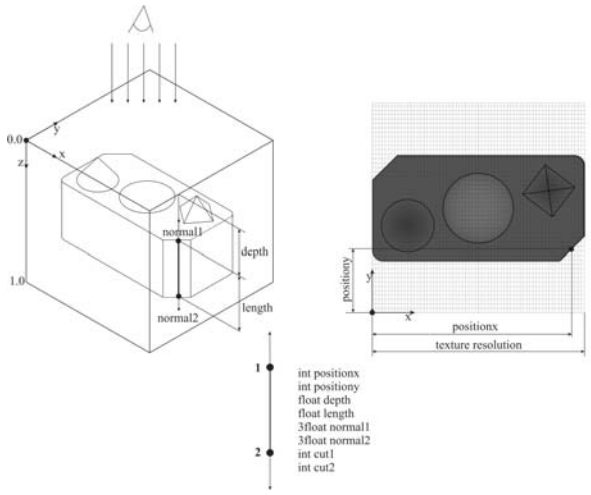


Fig. 6. Dexel structure parameters

When dexel structures for all three directions are generated, they are transferred into GPU as three buffers.

Dexels in all three dimensions generated from textures from Fig. 5 are presented in Fig. 7.

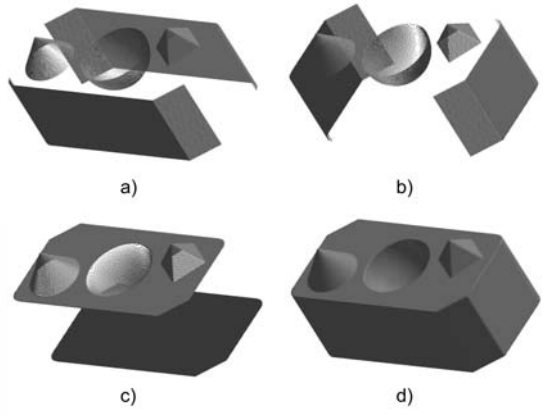


Fig. 7. Generated dexels in y(a), x(b) , z(c) directions and a complete three dexel model (d)

### 2.3 Tool definition in program system

Tool position in the developed program system is presented with instances between two consecutive tool positions. Another approach is to generate tool swept volume and subtract it from a workpiece. Drawback of the second approach is that tool swept volume generation and its subtraction is more time consuming than subtraction of tool instances. Also, for free shape tool, swept volume is very difficult and sometimes impossible to generate. An example of generated tool instances for different interpolation steps is shown in Fig. 8.

Fig. 8. Tool instances with different interpolation steps

Interpolation of tool positions is done by quaternions and after that position and orientation of every tool instance is presented by 4x4 transformation matrix.

### 2.4 Subtracting a tool from a workpiece

Tool instance is transformed and rendered in all three directions as a workpiece. As a result, depth and normal textures of tool instance are generated. Subtracting is performed in GPU geometry shader stage and six possible cases are shown in Fig 9.

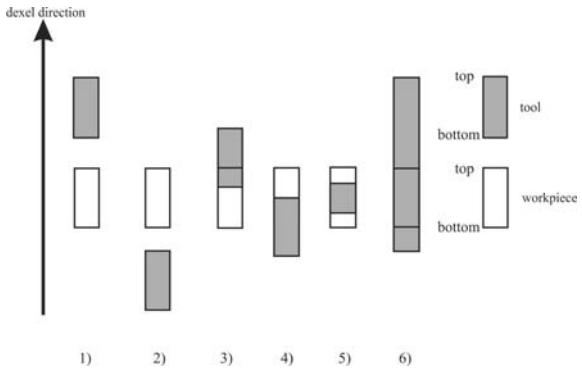


Fig. 9. Possible cases for subtracting tool from workpiece dexels

When tool dexel is above (1) or bellow (2), intersection does not exists. If tool is cutting workpiece from top (3), top workpiece dexel is set with bottom tool dexel. When tool is cutting workpiece from above (4), bottom worpiece dexel is set with top tool dexel. If a tool dexel divides workpiece dexel (5), then two workpiece dexels are generated. And the last case (6) is when tool dexel completely removes workpiece dexel, then workpiece dexel is deleted from dexel buffer.

## 3. A SIMULATION EXAMPLE

Simulation example of the developed program system is NC code for five axis milling, which consists of 20976 lines of code. Tools are flat end mill with 10mm diameter and ball end mill with diameter of 5mm. Blank workpiece is box with dimensions 140x80x70mm and it is defined with approximately $7x10^5$ dexels.

Simulation is performed on a computer with the following configuration:

- CPU Intel i5 760, 2,8 GHz
- GPU NVidia GTX 660 (960 shader units)
- Memory 4 GB

In Fig. 10 screenshots from this simulation are shown. Simulation is done with 160 fps (frames per second), which means that operation of tool instance subtraction from workpiece takes 6.25ms.

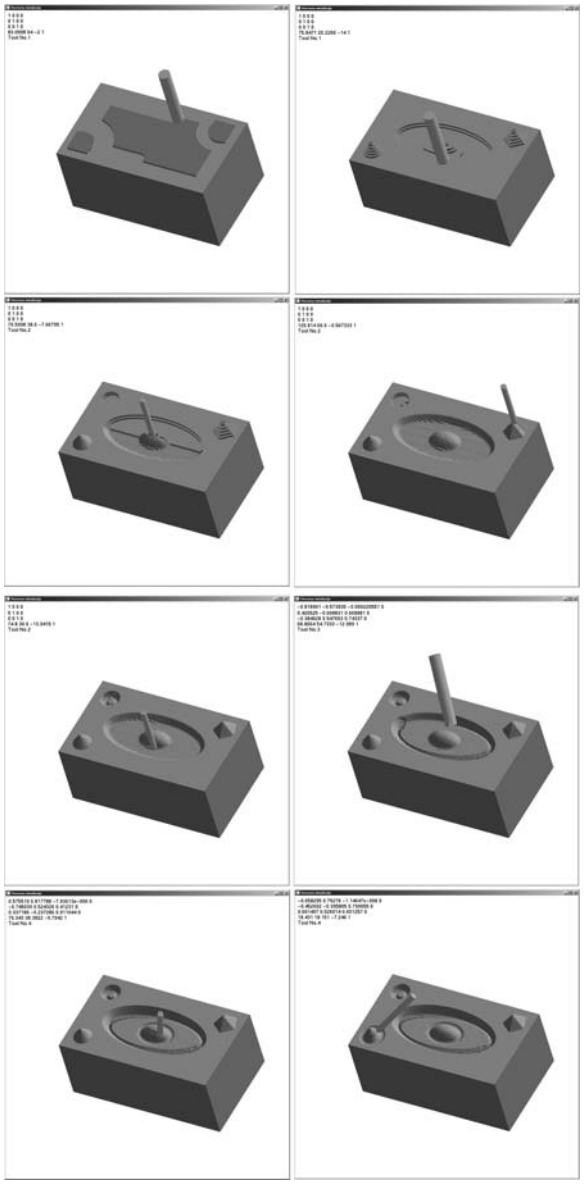

Fig. 10. Program system screenshots of simulated NC code operations

## 4. CONCLUSION

In this paper, a program system for multi axis NC code simulation based on three-dexel approach is presented. Tool can be a free form shape, which enables program system to be used for free form modelling with very few modifications. Computing of tool subtraction from a workpiece is done by the GPU, which causes very short computation time. Expectation of this system is that with the latest GPU generation subtraction time may be close to 1ms. This will be convenient for free form sculpting and force feedback generation in real time.

## 5. REFERENCES


[1] Benouamer, M. O., Michelucci, D.: *Bridging the Gap between CSG and Brep via a Triple Ray Representation*, In Proc. Fourth ACM/Siggraph Symposium on Solid Modeling and Applications, p.p. 68-79, 1997.

[2] Van Hook, T.: *Real-time shaded NC milling display*, Computer Graphics, SIGGRAPH Proceedings, Vol. 20, No 4, p.p. 15-20, 1986.

[3] Huang, Y., Oliver, J.H.: *NC milling error assessment and tool path correction*, Computer Graphics Proceedings (SIGGRAPH '94), p.p. 287-294, 1994.

[4] Muller, H., Surmann, T., Stautner, M., Albersmann, F., Weinert, K.: *Online Sculpting and Visualization of Multi-Dexel Volumes*, Proceedings of the eighth ACM symposium on Solid modeling and applications, p.p. 258-261, 2003.

[5] Tukora, B., Szalay, T.: *Multi-dexel based material removal simulation and cutting force prediction with the use of general-purpose graphics processing units*, Advances in Engineering Software 43, p.p. 65-70, 2012.

[6] Zhu, W., Lee, Y.S.: *Dexel-based force–torque rendering and volume updating for 5-DOF haptic product prototyping and virtual sculpting*, Computers in Industry 55, p.p. 125-145, 2004.

[7] Leu, M. C., Peng, X., Zhang, W.: *Surface Reconstruction for Interactive Modeling of Freeform Solids by Virtual Sculpting,* Annals of CIRP, 54/1, p.p. 131–134, 2005.

[8] Peng, X., Zhang, W.: *A Virtual Sculpting System Based on Triple Dexel Models with Haptics*, Computer-Aided Design & Applications, 6(5), p.p. 645-659, 2009.

[9] Milojevic, Z., Navalusic, S., Zeljkovic, M., Tabakovic, S., Vicevic, M., Beju, L.: *Sculpting system based on the dexel approach*, International Conference on Manufacturing Science and Education - MSE2013, p.p. 3-6, Sibiu, Romania, 2013.

[10] Everitt, C.: *Interactive order-independent transparency,* White paper, nVIDIA 2.6, 2001.



In this paper some results of the project: CONTEMPORARY APPROACHES TO THE DEVELOPMENT OF SPECIAL SOLUTIONS RELATED TO BEARING SUPPORTS IN MECHANICAL ENGINEERING AND MEDICAL PROSTHETICS – TR 35025**,** carried out by the Faculty of Technical Sciences, University of Novi Sad, Serbia, are presented. The project is supported by the Ministry of science and technological development of the Republic of Serbia.



***Authors:*** **Assoc. Prof. dr Zoran Milojević, Assoc. Prof. dr Slobodan Tabaković, Assist. MSc. Mirjana Bojanić, Full Prof. dr Milan Zeljković**, University of Novi Sad, Faculty of Technical Sciences, Institute for Production Engineering, Trg Dositeja Obradovica 6, 21000 Novi Sad, Serbia, Phone.: +381 21 450-366, Fax: +381 21 454-495.
E-mail: zormil@uns.ac.rs; tabak@uns.ac.rs; bojanicm@uns.ac.rs; milanz@uns.ac.rs

Journal of Production Engineering
Vol.18 No.2
JPE (2015) Vol.18 (2) Original Scientific Paper
Tabaković, S., Živanović, S., Zeljković, M.

# THE APPLICATION OF VIRTUAL PROTOTYPE IN DESIGN OF A HYBRID MECHANISM BASED MACHINE TOOLS

Received: 27 September 2015 / Accepted: 20 November 2015

**Abstract:** *Designing of products by using of virtual prototypes in modern conditions allows much faster and cheaper selection of elements and optimisation of construction. The paper presents the application of virtual prototype of manufacturing capabilities verification process in case of machine tools with kinematic structure which is based on O-X hybrid mechanism.*
***Key words:*** *Virtual prototype, hybrid mechanism, CNC*

**Primena virtuelnog prototipa u procesu projektovanja mašina alatki na primeru hibridnog mehanizma.** *Projektovanja proizvoda primenom virtuelnih prototipova u savremenim uslovima omogućava znatno brži i jeftiniji izbor elemenata i optimizaciju konstrukcije. U radu je prezentovana primena virtuelnog prototipa u procesu verifikacije mogućnosti obrade kod mašina alatki čija je kinematska struktura bazirana na O-X hibridnom mehanizmu*
***Ključne reči:*** *virtuelni prototip, hibridni mehanizam, CNC*

## 1. INTRODUCTION

Development of a product with a large number of moving elements, before building of physical prototype, involves various types of analysis of exploitation conditions in the goal of verification and optimisation of conceptual design.

Machine tools with a large number moving components and exploitation in different conditions is a typical representative of this group of products. A key role in the choice of components, in process of its development, has an analysis of the working of machine tools in the operating conditions.

Developing of a virtual prototype using DMU (Digital Mock Up) concept is more often replacing physical prototype and allows the combination of CAD and CAE technology to optimize product [1]. Usage of DMU technology in optimization allows analysis of kinematic parameters through collision detection and singularities in mechanism work and analysis of the workpiece machining borders before making a physical prototype.

This paper describes a part of the research of patented O-X mechanism usage possibilities [2], [3] as a base for machine tools through the analysis of machining characteristic capabilities forms on the workpiece by using DMU technology.

## 2. CHARACTERISTICS OF THE O-X MECHANISM

The base of virtual prototype is hybrid O-X glide mechanism composed of planar parallel kinematic mechanism and support structure that enables translational movement (Fig. 1). [3]

Figure presents planar parallel mechanism whose base is movable platform (1), connected with four struts (3) using spherical joints. Struts are at the other end attached to the sliders (5) over the joints with one rotary degree of freedom (4). Each of sliders can move at own guide (6). Sliders are grouped into pairs that are connected with rigid connection (7) thus providing their same speed and acceleration. In order to increase the autonomy movement of the slider, they are positioned at different distances in the direction of the vertical axis, which allows their passing in the plane, and the duality of movement of the mechanism. That are the movement in the extended (O) and the crossed (X) position. Compensation of differences in the distances between the slider and moving platforms is performed by introducing vertical compensating elements (8), at higher sliders.

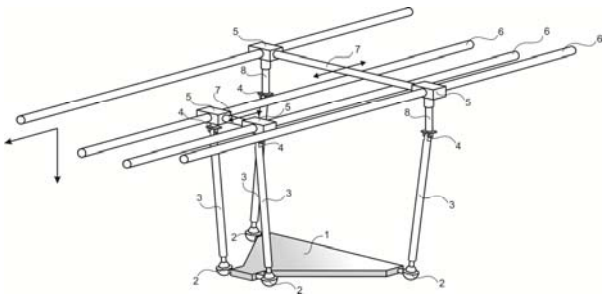

Fig. 1. Planar parallel mechanism

Primary specificity of O-X glide mechanism makes the duality of its structure in a plane element. This enables it to work in extended and crossed form. Except this, dimensions of the workspace are larger than similar mechanisms, because of hybrid structure.

The geometric model of parallel mechanism (Fig. 2), which is base of a hybrid O-X glide mechanism, can be presented in a simpler form using of a parallelogram A'B'C'D, which is connected with constant length struts. At the other end the struts are connected with

sliders AB and CD, moving on horizontal guides (D''D, A''A, B''B, C''C).

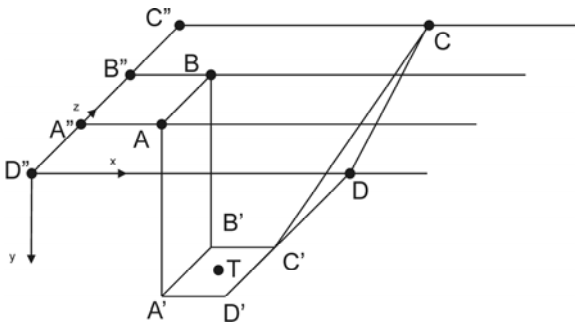


Fig. 2. Simplified geometrical model of a parallel mechanism

Based on the this, we can write vector equations of parallel mechanism

$$\overrightarrow{OD} + \overrightarrow{DD''} = \overrightarrow{TD''} + \overrightarrow{OT''}$$
$$\overrightarrow{OA''} + \overrightarrow{A''A} + \overrightarrow{AA'} = \overrightarrow{OT} + \overrightarrow{TA'}$$
$$\overrightarrow{OB''} + \overrightarrow{B''B} + \overrightarrow{BB'} = \overrightarrow{OT} + \overrightarrow{TB'}$$
$$\overrightarrow{OC''} + \overrightarrow{C''C} + \overrightarrow{CC'} = \overrightarrow{OT} + \overrightarrow{TC'}$$

Assuming that:

$$\overrightarrow{OD''} = \vec{0}; \quad \overrightarrow{OA''} = \begin{pmatrix} 0 \\ 0 \\ a \end{pmatrix}; \quad \overrightarrow{OB''} = \begin{pmatrix} 0 \\ 0 \\ 2a \end{pmatrix};$$

$$\overrightarrow{OC''} = \begin{pmatrix} 0 \\ 0 \\ 3a \end{pmatrix}.$$

Where is

a –distance between horizontal sliders

In addition, the structure of the planar mechanism imposes certain restrictions:

$$\overrightarrow{A''A} = \overrightarrow{B''B}$$
$$\overrightarrow{C''C} = \overrightarrow{D''D}$$

## 3. KINEMATIC ANALYSIS OF THE O-X GLIDE MECHANISM

### 3.1 Inverse kinematics

The general expression for inverse kinematic chain is:

$$\boldsymbol{P_{A,B,C,D} = f(x_T, y_T, z_T)}$$

Because of the O-X glide mechanism kinematic analysis is carried out in two configurations.

#### *3.1.1 Extended form*

Fig. 3 presents planar projection of extended form of the O-X glide mechanism for which is carried out the inverse kinematic analysis.

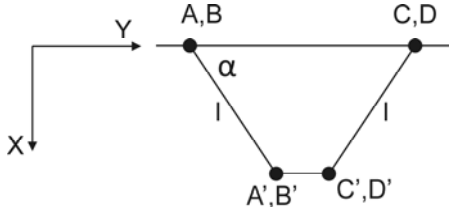


Fig. 3. Planar projection of extended form of O - X glide mechanism

The position of points A and B, can be expressed as follows:

$$x_{A,B} = x_T - \frac{s}{2} - l\cos\alpha = x_T - \frac{s}{2} - l\sqrt{1 - \left(\frac{y_T}{l}\right)^2},$$
$$x_{A,B} = x_T - \frac{s}{2} - \sqrt{l^2 - {y_T}^2}.$$

The position of the points C and D in the same manner can be expressed as:

$$x_{C,D} = l\cos\alpha + \frac{s}{2} + x_T = l\sqrt{1 - \left(\frac{y_T}{l}\right)^2} + \frac{s}{2} + x_T,$$
$$x_{C,D} = \sqrt{l^2 - {y_T}^2} + \frac{s}{2} + x_T.$$

Where are:

l- lenght of struts
*s* – width of mobile platform
*a* – distance between horizontal guides
*α* – angle between the struts and horisontal guides

#### 3.1.2 Crossed form

Fig. 4 presents planar projection of crossed form of the O-X mechanism and his inverse kinematic analysis.

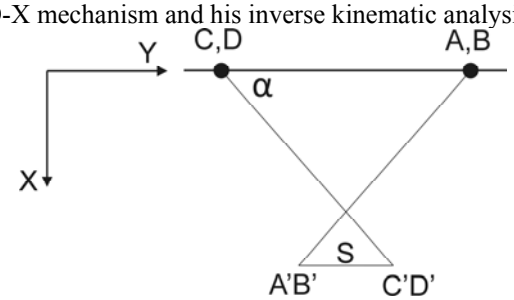


Fig. 4. Planar projection of crossed form of the O-X mechanism

Position of the points A, B, C and D can be expressed as follows:

$$x_{A,B} = x_T - \frac{s}{2} + l\cos\alpha = x_T - \frac{s}{2} + l\sqrt{1 - \left(\frac{y_T}{l}\right)^2},$$
$$x_{A,B} = x_T - \frac{s}{2} + \sqrt{l^2 - {y_T}^2};$$

$$x_{C,D} = \frac{s}{2} + x_T - l\cos\alpha = \frac{s}{2} + x_T - l\sqrt{1 - \left(\frac{y_T}{l}\right)^2},$$
$$x_{C,D} = \frac{s}{2} + x_T - \sqrt{l^2 - {y_T}^2}..$$

### 3.2 Direct kinematic

Direct kinematic chain can be expressed as follows:

$$\boldsymbol{P_T = f(x_A, x_B, x_C, x_D)}$$

Generally, the inverse kinematics of parallel mechanisms is quite simple, while direct kinematics often very complex. However, because of simple construction in the case of the O-X glide mechanism direct and inverse kinematics are very simple.

#### 3.2.1 Extended form

Direct kinematics analysis of extended form of the O-X mechanism (Figure 4), explains position of the point T depending on the position of points A, B, C and D can be represented as follows:

$$\begin{pmatrix}0\\0\\a\end{pmatrix}+\begin{pmatrix}x_A\\0\\0\end{pmatrix}+\begin{pmatrix}l\cos\alpha\\l\sin\alpha\\0\end{pmatrix}=\begin{pmatrix}TA'_x\\TA'_y\\TA'_z\end{pmatrix}+\begin{pmatrix}x_T\\y_T\\z_T\end{pmatrix}.$$

### 3.2.2 Crossed form

Similarly as in the previous case, the position of the point T on the movable platform for crossed form of the O-X glide mechanism (Figure 5) can be represented as follows:

$$\begin{pmatrix}0\\0\\a\end{pmatrix}+\begin{pmatrix}x_A\\0\\0\end{pmatrix}+\begin{pmatrix}-l\cos\alpha\\l\sin\alpha\\0\end{pmatrix}=\begin{pmatrix}TA'_x\\TA'_y\\TA'_z\end{pmatrix}+\begin{pmatrix}x_T\\y_T\\z_T\end{pmatrix}.$$

## 4. STRUCTURE OF THE VIRTUAL PROTOTYPE

The final version of the virtual prototype differs from the concept caused by the physical dimensions of the elements of the prototype. In the final version changes in elements such as the position of the slider, length of the struts and the like are introduced. Figure 5 presents adopted solution of the virtual prototype of the hybrid mechanism.

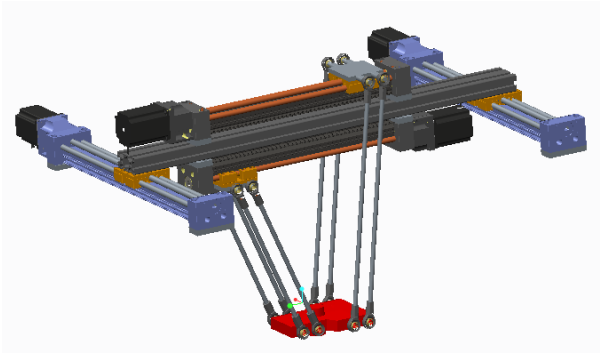

Fig. 5. Virtual prototype of the hybrid mechanism

The virtual prototype which is defined in this way has been subjected to tests that include analysis of capabilities of machining geometric shapes characteristic for the milling. For simulations workpiece with shape based on the NCG recommendations is used.

## 5. SIMULATION OF MACHINING

Machine simulation by running the program is possible due to the applied modelling of the O-X glide parallel mechanism with all kinematic connections between the components, which allows the motion of a virtual model as a system of rigid bodies.

Fig. 6 shows a detailed virtual prototype of O-X glide parallel mechanism with all kinematic relationships.

This assembly enables the motion of models in the range defined for each connection, which is of particular importance for the identification of possible collisions during the work of the parallel mechanism.

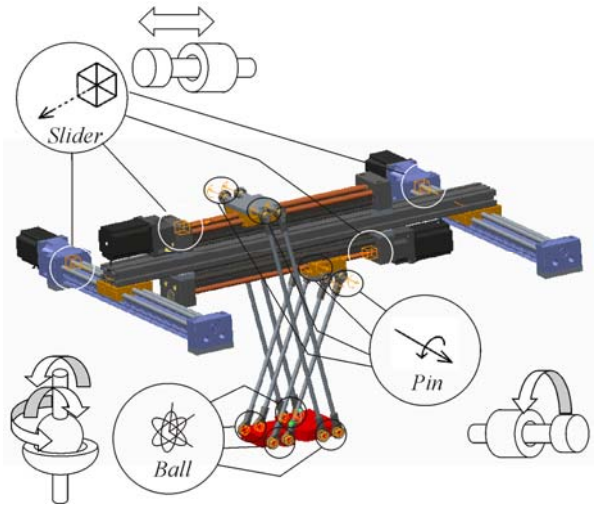


Fig. 6. CAD model for the simulation of parallel mechanism kinematics

Machining simulation of the virtual prototype allows the motion of movable segments with a tool at the end. The tool path is a result of the execution program obtained by programming using the CAD/CAM system PTC Creo 2.

For the test, a scaled ISO test workpiece whose dimensions are 150×150×40mm is used. Because of the particular shape and size of the workspace of parallel kinematics machines, attention should be paid when setting up a workpiece, which must be within the limits of the workspace of the machine. For the test workpiece shown in Fig. 7, the zero point in the middle of the underside of the workpiece has been adopted, with the coordinate axes *x*, *y*, *z* as has been used in the vertical 3-axis milling machine, marked as MACH_ZERO. The identical zero point exists on the machine (on the working table) on which the workpiece is placed, Fig. 7. Matching these two coordinate systems is accomplished by setting the workpiece on the machine during the machining simulation. Fig. 7 also presents the simulated tool path on the scaled ISO test workpiece, based on the generated CL file. The tool coordinate system is defined in the same way as the workpiece coordinate system and marked as a TOOL_POINT.

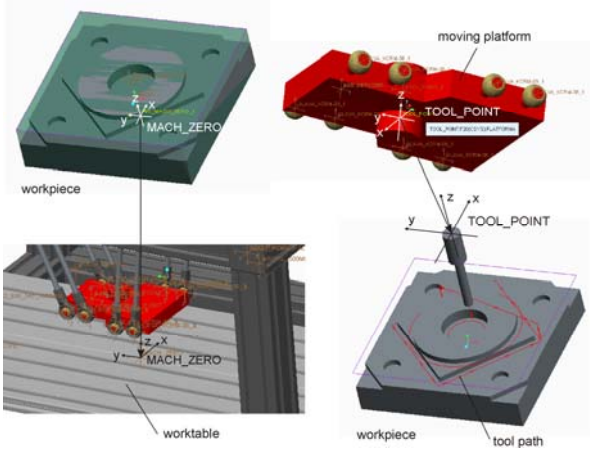


Fig. 7. Coordinate system of the workpiece and tool with tool path simulation

During the simulation of tool paths, a complete prototype of the virtual machine can be included into the simulation, with a machine play option. An example of machine simulation for O-X glide virtual prototype is shown in Fig. 8 for an ISO test workpiece.

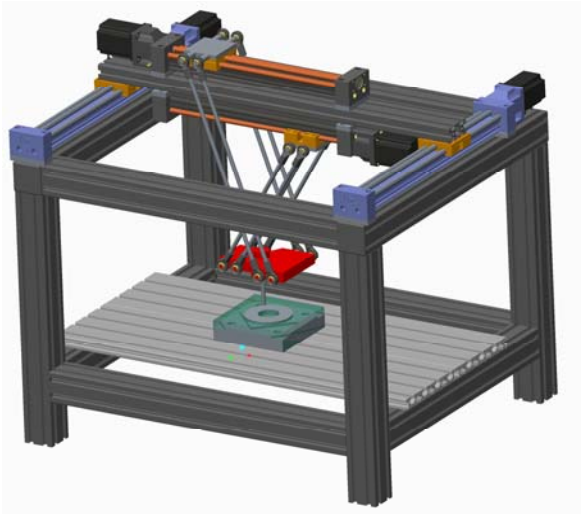

Fig. 8. Machining simulation in the CAD/CAM system

## 6. RESULTS

Tested workpiece is based on the test workpieces for analyzing of the accuracy of machine tools with numerical control with a three-axis. They could be produced by four characteristic sequence of machining in which had been combined all movements which are expected in the structure of modern machine tools (linear and circular). The dimensions of the workpiece are selected based on the maximum dimensions of the workspace of a parallel mechanism. Results are presented in table 1.

| No | Type of moving of the tools/ platform | Successfully completed |
|---|---|---|
| 1 | Face milling, linear movement | ■ |
| 2 | Profile milling, linear movement | ■ |
| 3 | Profile milling, circular movement ϕ50 | ■ |
| | Profile milling, circular movement ϕ250 | ■ |
| 4 | Combined milling, linear movement | ■ |
| 5 | Combined milling, circular movement ϕ50 | ■ |
| 6 | Combined milling, circular movement ϕ250 | ■ |
| 7 | Hole machining | ■ |

Tab. 1. Successfulness of machining on virtual machine tool

## 7. DISCUSION AND CONCLUSIONS

Conducted research indicates that the virtual prototypes methods application might decrease machine tools development time especially the time needed for the selection of machine components. In addition, analysis of kinematic and dynamic motion parameters and machining capabilities indicate problems that may occur during the machining of pre-defined shapes. This provides a wide range of possibilities during the design of special type of machines [4] [5].

Present stage of the research identified a number of disadvantages of the initial configuration of machines such as the length and position of the slider struts. All of them were corrected and formed functional virtual prototype. Currently the project is in final stages of building of the physical prototype.

**Acknowledgements:** In this paper are presented some results of the project: Contemporary approaches to the development of special solutions related to bearing supports in mechanical engineering and medical prosthetics – TR 35025. The project is supported by the Ministry of Science and Technological Development of the Republic of Serbia.

## 5. REFERENCES

[1] Altintas, Y., Brecher, C., Week, M., Witt, S. Virtual Machine Tool, CIRP Annals - Manufacturing Technology Volume 54, Issue 2, 2005, Pages 651-674

[2] Mlađenović C., Tabaković S., Zeljković M.: Kinematic analysis of machine tool based on O-X glide hybrid mechanism using a symbolic virtual model, Journal of Production Engineering, Vol. 15, No. 1, Str. 37-40, ISSN: 1821-4932 Faculty of technical sciences;

[3] Tabaković, S., Zeljković, M., Gatalo, R., Mlađenović, C.: Uređaj za manipulaciju radnim predmetima ili alatima kod mašina alatki i industrijskih manipulatora, Glasnik intelektualne svojine, Br. 2/2012, Zavod za intelektualnu svojinu Republike Srbije, Beograd, Broj: 20111243

[4] Fortunato, A., Ascari, A.: The virtual design of machining centers for HSM: Towards new integrated tools, Mechatronics, Volume 23, Issue 3, April 2013, Pages 264-278

[5] Zivanovic, S., Glavonjic, M., Milutinovic, D., Configuring A Mini-Laboratory and Desktop 3-Axis Parallel Kinematic Milling Machine, Strojniški vestnik - Journal of Mechanical Engineering, Vol.61, No1, pp. 33-42 (2015), DOI:10.5545/sv-jme.2013.1619, 2015.

***Authors:*** **Prof. dr Slobodan Tabakovic, Prof. dr Milan Zeljkovic,** University of Novi Sad, Faculty of Technical Sciences, Department for Production Engineering, Trg Dositeja Obradovica 6, 21000 Novi Sad, Serbia, Phone.: +381 21 485-23-30, Fax: +381 21 454-495. E-mail: tabak@uns.ac.rs ; milanz@uns.ac.rs ;

**Doc. dr Sasa Zivanovic,** University of Belgrade, Faculty of Mechanical Engineering, Production Engineering Department,, Kraljice Marije 16, 11120 Belgrade, Serbia, Phone.: +381 11 3302-423, Fax: +381 11 3370-364. E-mail: szivanovic@mas.bg.ac.rs

Journal of Production Engineering
Vol.18 No.2
JPE (2015) Vol.18 (2) Original Scientific Paper
Kokotovic, B., Zivanovic, S., Jakovljevic Z.

# VERIFICATION OF A PROCEDURE FOR FEEDRATE SCHEDULING FOR CONSTANT FORCE IN 2D MILLING OPERATIONS

Received: 27 September 2015 / Accepted: 20 November 2015

**Abstract:** *This paper presents a brief overview of the developed procedure for off-line optimization of CNC program. The procedure refers to milling operations in plane z=const, using flat end mills. The goal of optimization is to create modified version of part program, using feedrate scheduling, in order to keep desired milling force component on predefined value along tool path. Detailed experimental verification of this procedure is carried out using a representative example and machining test.*
***Key words:*** *CNC milling, milling forces, optimization, federate scheduling*

**Utvrdivanje procedura za raspodelu pomaka pri konstantnoj sili glodanja kod 2D operacija glodanja.** *Ovaj rad predstavlja kratak pregled razvijene procedure za off-line optimizaciju CNC programa. Postupak se odnosi na operacije glodanja kod kojih je z=const, primenom čeonih glodala. Cilj optimizacije je da se napravi modifikovana verzija dela programa, koristeći raspored pomaka, kako bi se sačuvala željena snaga glodanja, koja je unapred definisanja duž putanje alata. Detaljna eksperimentalna verifikacija ove procedure je izvedena korišćenjem reprezativnog uzorka i testa na mašini alatki.*
***Ključne reči:*** *CNC glodanje, sile pri glodanju, optimizacija, raspodela pomaka.*

## 1. INTRODUCTION

Nowadays many research activities in the field of CNC machining are clustered in a concept of Virtual machining (VM) [1]. Besides function of realistic predictions of outputs of machining process through simulation, extremely important function of VM is its ability to perform off-line optimization of designed process. Optimization criteria are different: keeping constant cutting force, maximization of material removal rate, limitation of machining errors, chatter-free machining, etc. The function of CNC program re-planning in order to keep cutting force level constant along tool path is partly implemented in modern CAM software [2,3]. Very impressive results were achieved through re-planning of tool path shape (trochoidal paths and morphing spiral paths in pocket machining) in the software. Such paths assume constant tool/workpiece immersion on the whole path. Another way to keep cutting force constant assumes re-planning of feedrates along programmed path. In CAM systems it is achieved through keeping constant material removal rate. A number of published research results use more precise and more demanding approaches which include milling force prediction based on generated simulation model.

## 2. PROCEDURE FOR FEEDRATE OPTIMIZATION

Simplified description of the procedure for off-line feedrate optimization is shown in Fig. 1. Such optimization procedure for milling operations in plane (*z*=const), with flat end mills, with helical flutes and arbitrary shape of stock material was developed [4].

Term *adaptation* refers to obtaining the feedrate value which can guarantee keeping the desired level of arbitrary milling force component in specific point of programmed tool path, with predefined workpiece material, cutter geometry, and configuration of tool engagement (engagement map) in the point. Procedure for feedrate adaptation has to be conducted in each point of uniformly discretized tool path. Next step is feedrate *optimization* along tool path. In this step, adapted values are subject to modifications, according to several additional criteria and re-discretization of tool path with constant feedrate on each path segment described by one block of optimized part program.

For arbitrary set of cutting parameters and engagement map, instant and representative values of milling force components can be identified. Instant values of one force component assume its periodic variation during one spindle revolution. Representative value of this component can be obtained by extraction of min/max/mean values from instant values. Important building block of optimization procedure is a module for reliable milling force prediction, as a part of step K2 (Fig. 1).

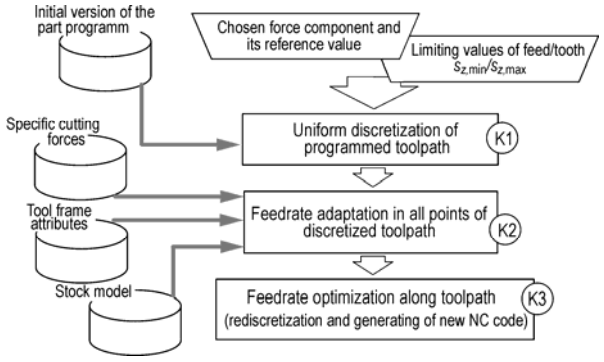


Fig. 1. Basic steps in procedure for feedrate optimization

Many authors [5,6] use procedure for feedrate adaptation which has two steps. In the first step, adaptation process for a given point on the tool path assumes calculation of feedrate based on reference force level $F_{\text{ref}}$, and predicted force value $F_{p(0)}$ for initially programmed feedrate $v_{s,0}$:

$$v_s^{Ad} = v_s^{Ad(1)} = v_{s,0}\frac{F_{\text{ref}}}{F_{p(0)}} \quad (1)$$

This feedrate and spindle speed $n_{GV}$ result in a feed/tooth value as input for new simulation of instant force values (1 turn of cutter) for predicting appropriate representative force value $F_{p(1)}$ of a chosen force component. Then, it is possible to obtain adapted value of feedrate in the second step:

$$v_s^{Ad} = v_s^{Ad(2)} = v_s^{Ad(1)} + \frac{(v_s^{Ad(1)} - v_{s,0})(F_{\text{ref}} - F_{(0)})}{F_{p(1)} - F_{(0)}} \quad (2)$$

## 3. AN EXAMPLE OF OFF-LINE FEEDRATE OPTIMIZATION IN END MILLING OF PLANAR CONTOUR

For illustration of functionality of the developed program modules for off-line feedrate optimization, an example of down milling of planar contour is presented in this section. Pre-machined stock and machined part are presented in Fig. 2.

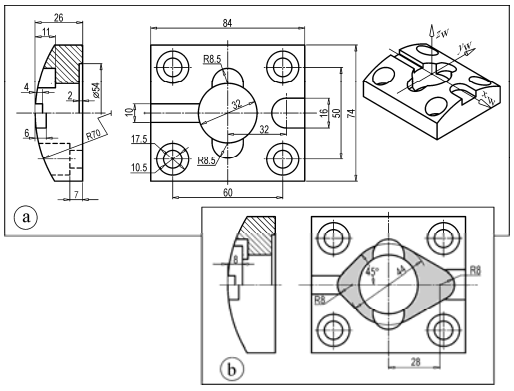


Fig. 2. Dimensions of stock (a) and machined part (b) in representative example

Workpiece coordinate system, contour shape and initial version (with constant feedrate) of the part program are shown in Fig. 3.

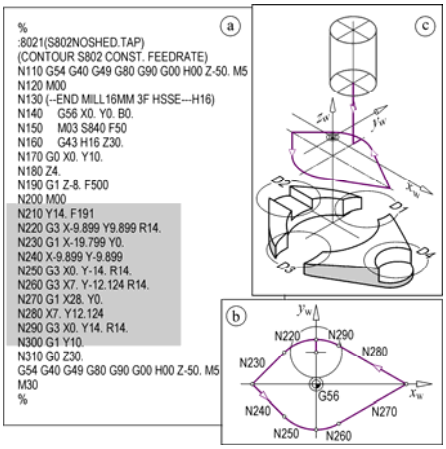


Fig. 3. Example of the feedrate optimization procedure checking: part program (a), tool path (b), and material volume which will be removed (c)

Workpiece material was AlZn4Mg2 (ENAW 7019) with $R_m$=390MPa and hardness of 125HB. Tool was DIN327 end mill, HSSE (8%Co) with 3 teeth, $D$=16mm, helix angle 30° and rake angle 11°. Clamping of tool: ISO40/OZ52∅16 collet. Measured runout parameters of the cutter: $\rho_b$=0.01mm, $\varphi_b$=81°. Experimentally identified specific cutting forces [4] for given workpiece material and cutting geometry were:

$[K_{tc}\ K_{rc}]$ = [ 1113.0 384.2] N/mm$^2$,

$[K_{te}\ K_{re}]$ = [11.1 11.6 ] N/mm.

Keeping constant value of the resulting milling force in $xy$ plane - $F_{xy}$ on the level of 800N, along the tool path, was chosen as optimization criterion.

Form of the stock and shape of the tool path were chosen to ensure rapid changes in cutting depth as well as cutting width along the tool path. Cutting parameters, used in initial version of part program (before feedrate optimization) are shown in Table 1.

| $a$ [mm] | $n_S$ [min$^{-1}$] | $v_{f(0)}$ [1)] [mm/min] | $b$ [mm] | $s_{t,0}$ [1)] [mm/t] |
|---|---|---|---|---|
| min. 0<br>max. 8 | 796 | 191 | min. 0<br>max.16 | 0.08 |

[1)] Programmed in initaial version of part programm

Table 1. Parameters of machining test

### 3.1. Feedrate adaptation

According to flow chart in Fig.1, it was necessary to prepare stock model. This preparation assumes building its Z-map model. Such map, made from STL-file (exported from CAD program) of the stock is shown in Fig.4. Values of other parameters of the procedure for feedrate adaptation are shown in Table 2.

| | |
|---|---|
| Toolpath discretization increment $\Delta L_p$ [mm] | 0.5 |
| Increment of the $Z$-map base $\Delta m$[mm] | 0.5 |
| Disc thickness of discretized tool $h_d$ [mm] | 0.5 |
| Increment for one turn simulation $\Delta\theta$ [°] | 1.0 |
| Reference force value, $F_{\text{ref}}$ [N] | 800 |
| Feed limits $s_{z,min}$, $s_{z,max}$ [mm/t] | [0.03, 0.25] |

Table 2. Parameters of the procedure for adaptation of the feedrate in points of dicretized tool path

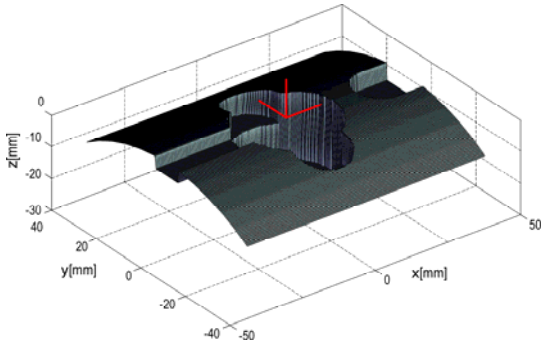


Fig. 4. Z-map of the stock for given example

Totally 250 points were obtained on tool path through its uniform discretization with given increment $\Delta L_p$. Each of these points was a subject of feerdate adaptation (1,2). This procedure assumes calculation of appropriate feedrate which will keep milling force $F_{xy}$ on $F_{\text{ref}}$ level, respecting lower $s_{z,min}$ and upper level $s_{z,max}$ of feed per tooth (Tab.2) and specific cutting conditions in this point.

Some details of this procedure for one point are shown in Fig.5: obtaining tool engagement map (using updated workpiece Z-map, tool attributes, instant direction of feedrate vector and position of point), obtaining enter/exit angles for each tool disc in engagement map, and prediction of instant values of milling forces through simulation in single turn of the tool. This simulation has to be carried out two times: for initial feedrate and for feedrate per tooth $s_z^{(Ad1)}$ obtained from (1). It is enough to find required value for $s_z^{(Ad2)}$ (2). Lower diagram in Fig.5 shows predicted instant values of milling force components for $s_{z,0}$, $s_z^{(Ad1)}$ and finally for $s_z^{(Ad2)}$. Fig 6. shows adapted values of feedrate in all points of discretized tool path, as well as predicted values of representative force, before and after adaptation.

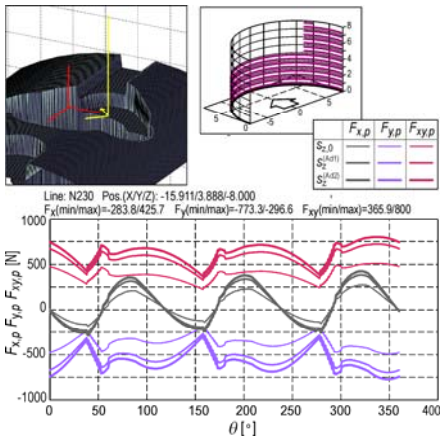


Fig.5. An example of feedrate adaptation in specific point of the tool path

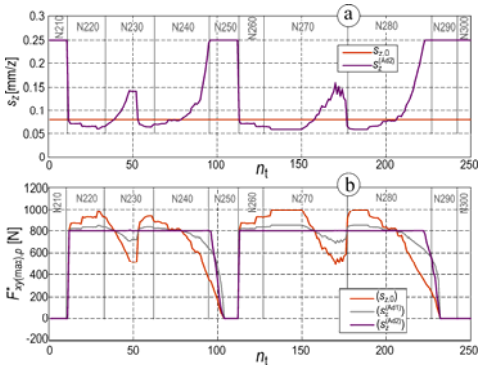


Fig.6. Programmed feedrate and feedrate after adaptation (a) and predicted representative force values (b) for programmed (constant) feedrate and with adapted feedrates

### 3.2. Feedrate optimization along tool path

Optimization of feedrate along tool path starts from calculated values obtained through adaptation process in points of uniformly discretized path. Keeping such discretization can lead to forming enormously long code of part program and undesirably frequent variation of feeedrate on short path segments (high acceleration/decceleration and unstable operation). In this sense, optimization should have the following steps:

S1. Filtration of feedrate values obtained in process of its adaptation
S2. Rounding of adapted values of feedrate on discrete values of scale with previously chosen increment and aggregating subsequent path segments (uniform discretization) of the same block of initial program into longer segments with one value of the feedrate (the first step of re-discretization)
S3. Second step of re-discretization with modified values obtained in S2 in order to guarantee limited accel/decelerations of machine servo axis.

Through the procedure of feedrate adaptation, regarding initial description of tool path (program of Fig.3a) and according to given parameters (Tab.2) the re-discretization of tool path is carried out. According to steps S1-S3 this re-discretization reduced number of tool path segments from 250 (uniform discretization) to 55. These segments with assigned feedrates are shown in optimized version of the part program (Fig.7) in blocks from N200 to N740.

```
%
:8022(S802RESSHED.TAP)
(SHEDULING FXY 800N )
(RESHED. VSINCR=30MM/MIN)
G54 G40 G49 G90 G0 H00 Z0. M5
M00
N130 (-- 16MM 3F HSSE---H16)
N140 G56 X0. Y0. B0.
N150 M03 S796 F191
N160 G43 H16 Z30.
N170 G0 X0. Y10.
N180 G1 Z-8. F200
N190 M00
N200 G1 X0. Y14.000 F570
N210 G3 X-0.500 Y13.991 R14. F360
N220 G3 X-0.999 Y13.9643 R14. F180
N230 G3 X-7.987 Y11.4979 R14. F150
N240 G3 X-9.543 Y10.2436 R14. F120
N250 G3 X-9.899 Y9.8990 R14. F150
N260 G1 X-11.313 Y8.485 F150
N270 G1 X-12.374 Y7.424 F180
N280 G1 X-13.435 Y6.364 F210
N290 G1 X-13.788 Y6.010 F240
N300 G1 X-14.495 Y5.303 F270
N310 G1 X-15.203 Y4.596 F300
N320 G1 X-16.617 Y3.182 F330
N330 G1 X-16.970 Y2.828 F180
N340 G1 X -19.799 Y0. F150
N350 G1 X-16.970 Y-2.828 F150
N360 G1 X-13.081 Y-6.717 F180
N370 G1 X-12.020 Y-7.778 F210
N380 G1 X-10.960 Y-8.838 F240
N390 G1 X-9.899 Y-9.899 F270
N400 G3 X-9.540 Y-10.247 R14. F330
N410 G3 X-9.168 Y-10.581 R14. F390
N420 G3 X-8.784 Y-10.901 R14. F420
N430 G3 X-8.389 Y-11.208 R14. F480
N440 G3 X0. Y-14.000 R14. F570
N450 G3 X 0.500 Y-13.991 R14. F180
N460 G3 X7.000 Y-12.124 R14. F150
N470 G1 X8.7321 Y-11.124 F150
N480 G1 X17.392 Y-6.124 F120
N490 G1 X19.558 Y-4.874 F150
N500 G1 X20.424 Y-4.374 F180
N510 G1 X21.723 Y-3.624 F210
N520 G1 X23.022 Y-2.874 F240
N530 G1 X24.321 Y-2.124 F270
N540 G1 X24.754 Y-1.874 F300
N550 G1 X25.620 Y-1.374 F330
N560 G1 X27.676 Y-0.187 F300
N570 G1 X28.000 Y0. F270
N580 G1 X22.804 Y3.000 F120
N590 G1 X19.340 Y5.000 F150
N600 G1 X14.143 Y8.000 F180
N610 G1 X13.277 Y8.500 F210
N620 G1 X12.844 Y8.750 F240
N630 G1 X11.978 Y9.250 F270
N640 G1 X11.545 Y9.500 F300
N650 G1 X11.112 Y9.750 F330
N660 G1 X10.679 Y10.000 F360
N670 G1 X10.246 Y10.250 F390
N680 G1 X 9.813 Y10.500 F420
N690 G1 X 9.380 Y10.750 F450
N700 G1 X8.947 Y11.000 F510
N710 G1 X8.514 Y11.250 F540
N720 G1 X7.000 Y12.124 F570
N730 G3 X0. Y14.000 R14. F570
N740 G1 X0. Y10.000 F570
N750 G0 Z30.
G54 G40 G49 G90 G0 H00 Z0. M5
M30
%
```

Fig.7. Part program after optimization of feedrates along tool path

## 4. MACHINING TEST

Quality of the described procedure for off-line feedrate optimization was proven through machining test that was carried on the horizontal machining center (HMC500/40, Lola Corp.). Components of experimental setup were: four component dynamometer with strain gauges (DYN3F1M-M83, KaProM), two displacement sensors (W50, HBM), 4 amplifiers (KWS3082A, HBM), DAQ system (cDAQ9174 + 9215 Voltage module, NI) and computer with software for DAQ (LabView, NI). Workpiece was clamped on the platform of the dynamometer (Fig. 8)

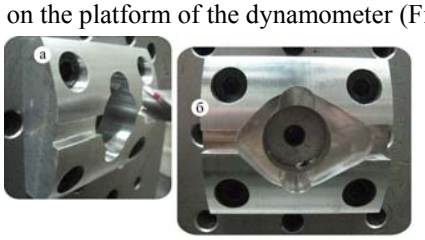


Fig.8. Stock (a), and machined contour (b), in machining test

Experimental setup allows acquisition of two signals from dynamometer (force components along $x_w$ and $y_w$ axes), as well as two signals of actual positions $x_w$ and $y_w$ of machine servo axis. These four signals are enough for reconstruction of changes of resulting milling force $F_{xy}$, along tool path. Fig.9 shows measured instant values of one force component ($F_{x.w}$) during machining of the contour, according to part program from Fig.7. During experiment a chatter vibrations occurred on some segments of the tool path. It is shown in details (W1 and W2) in Fig.9.

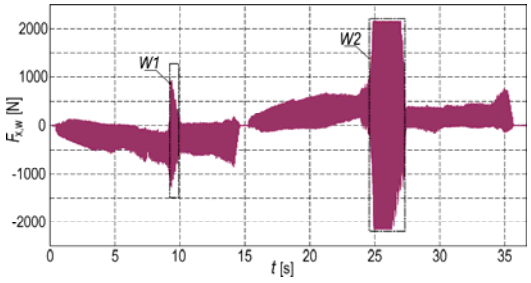


Fig. 9. Instant values of $F_{x.w}$ milling force component (signal from dynamometer) during machining of the contour

Measured positions of machine servo axis ($x_w$, $y_w$) during machining test in given example are shown in Fig.10.

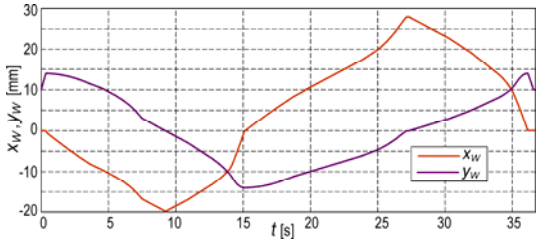


Fig. 10. Measured positions of machine servo axis ($x_w$, $y_w$) during machining of the contour

All four signals were collected simultaneously during experiment and allow generation of diagram with distribution of representative cutting force along the tool path. Such diagram is shown in Fig.11. Instant values of milling force, in sample $k$, were obtained as:

$$F_{xy}(k) = F_{xy,\mathrm{w}}(k) = \sqrt{F_{x,\mathrm{w}}^2(k) + F_{y,\mathrm{w}}^2(k)} \qquad (3)$$

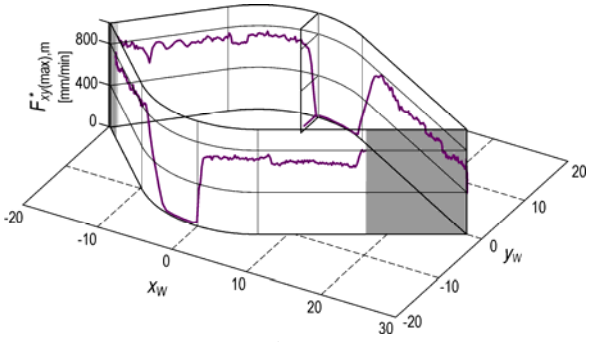


Fig. 11 . Distribution of $F^*_{\mathrm{xy(max),m}}$ milling force along tool path, obtained from experiment

Representative values of milling force, extracted for every spindle revolution were obtained as:

$$F^*_{xy(\max),m}(q) = \max\{F_{xy,\mathrm{w}}(k)\}$$
$$k = (q-1)\cdot n_s \div q \cdot n_s, \quad q = 1,2,... \qquad (4)$$

Integer $n_s$ denotes the number of samples that refer to one spindle revolution. These values are assigned to points on tool path with coordinates:

$$x_w(q) = x_w(k), \; y_w(q) = y_w(k), \; k = q \cdot n_s \qquad (5)$$

Diagram in Fig.11 is broken into two too lpath segments. These segments are shaded and they refer to chattering which is not included in developed model for milling force prediction.

## 5. CONCLUSION

This paper presents an example of experimental verification of developed procedure for off line optimization of NC program for a class of milling operations. This optimization is based on feedrate scheduling for keeping the constant milling force level. Good quality of the procedure was shown through machining test. In the trade-off between efficacy and performances of the proposed procedure, arguments are on the latter. Lower efficacy comes from the need of simulation of forces on whole turn of discretized cutter geometry in each point of uniformly discretized tool path. Improvements, in this sense, are the subject of our present research activities.

**Acknowledgements**. The authors would like to thank the Ministry of Education and Science of the Republic of Serbia for providing financial support that made this work possible.

## 6. REFERENCES

[1] Altintas Y., Brecher C., Weck M., Witt S.: *Virtual* Machine Tool, Keynote Paper of STC M, Annals of CIRP, Vol. 54, No2, p.p.651-674, 2005.

[2] Solid CAM i-machining, from *www.solidcam.com*, accessed on Sept 2015.

[3] Open Mind Technologies AG, from *www.openmind-tech.com*, accessed on Sept 2015.

[4] Kokotović B.: *Obrada glodanjem u virtuelnom obradnom sistemu*, doktorska disertacija, Univerzitet u Beogradu, Mašinski fakultet, 2014.

[5] Boz Y., Demir O., Lazoglu I.: *Model Based Feedrate Sheduling for Free-Form Surface Machining*, Int. J. of Automation Technology, Vol.4, No.3, p.p. 273-283, 2010.

[6] Kokotović, B., Glavonjić, M.: *Predicting of milling forces in a virtual manufacturing system*, Tehnički vjesnik, Vol. 20, No.6, p.p. 1027-1035, 2013.

***Authors:*** **Assistant Professor Branko Kokotovic, Assistant Professor Sasa Zivanovic, Assistant Professor Zivana Jakovljevic**, University of Belgrade, Faculty of Mechanical Engineering, Production Engineering Department,, Kraljice Marije 16, 11120 Belgrade, Serbia, Phone.: +381 11 3302-375, Fax: +381 11 3370-364.
E-mail: bkokotovic@mas.bg.ac.rs
szivanovic@mas.bg.ac.rs
zjakovljevic@mas.bg.ac.rs

Journal of Production Engineering
Vol.18 No.2
JPE (2015) Vol.18 (2) Original Scientific Paper
Bojanić, M., Hadžistević, M., Mladjenović, C.

# STRAIGHTNESS EXAMINATION OF CMM AXES

Received: 27 September 2015 / Accepted: 20 November 2015

**Abstract:** *It is generally known that the parts with tight tolerances can only be measured on precise, or accurate measuring machines. Accuracy is one of the indicators of quality of measuring equipment. By controlling the parameters of accuracy from the very beginning of machine life cycle, it is possible to maintain the permissible limits of its quality characteristics. The straightness deviation represents line flow in two perpendicular planes. The straightness is one of the essential characteristics of exploitation that must be strictly controlled. Measurement of straightness is applied in many areas such as manufacturing and testing of precision instruments, measuring dimensions of large objects, assembly and adjustment of large equipment.*
*In this paper, the emphasis is placed on the straightness of the numerically controlled measuring machines (CMM) elements movement along the X and Y axes. The measurement is carried out by laser measuring system (LMS).*
***Key words:*** *CMM, Straightness, Laser measuring system*

**Ispitivanje pravosti pomeranja elemenata NUMM.** *Opšte je poznato da delove sa uskim tolerancijama mogu meriti samo precizne, odnosno tačne merne mašine. Tačnost predstavlja jedan od pokazatelja kvaliteta merne mašine. Kontrolom parametara tačnosti od samog početka eksploatacionog veka mašine, moguće je održavati u dozvoljenim granicama njene karakteristike kvaliteta. Pravost predstavlja odstupanje toka linije u dve upravne ravni. Pravost predstavlja jednu od bitnih eksploatacionih karakteristika koja mora biti strogo kontrolisana. Merenje pravosti se primenjuje u mnogim oblastima kao što su proizvodnja i ispitivanje preciznih instrumenata, merenje dimenzija velikih predmeta, montaža i podešavanje velike opreme.*
*U ovom radu akcenat je stavljen na pravost pomeranja elementa numerički upravljane merne mašine NUMM) pri kretanju duž X i Y ose. Merenje je izvršeno laserskim mernim sistemom (LMS).*
***Ključne reči:*** *NU merna mašina, Pravost, Laserski merni sistem*

## 1. INTRODUCTION

The paper describes numerically controlled measuring machines, and presents some of experimental results obtained during the straightness examination of coordinate measuring machine elements along the X and Y axes, on the example of Carl Zeiss Contura G2. All results are presented graphically.

Methods for determining the work table moving straightness can be realized by measuring the angle deviation or lateral displacement of the table during the movement. An auto-collimator, precision level, or laser interferometer can be adopted to determine the angle deviations, whereas a straightedge, taut-wire and microscope, alignment telescope, four-quadrant photo-detector, or laser interferometer can be used to determine the lateral displacements.

Although some other methods have been proposed, the laser interferometer for lateral displacement measurements is widely used due to the advantages of high signal to noise ratio, high linearity, high resolution, non-contact, and direct measurement. Laser interferometer was used in the experiment, which was carried out in this paper.

Numerically controlled measuring machines are complex metrology systems. Key elements for the development of CMM are computers, sensors and micro electrical engineering. Numerically controlled measuring machines have two primary applications. The first application of CMM is for measuring and control of all types of tolerance, and second is for adaptive conformity quality management.
The basic characteristics of CMM are [1]:

- Metrological universality
- High resolution, accuracy and reliability compared to conventional measurement technique
- High productivity
- Complete automation of almost all the work cycles
- High flexibility
- Low total cost of metrology process
- Relatively simple and quick preparation process, calibration, adjustable measuring objects, programming and handling CMM system

The parameters that determine the quality of a CMM are shown in Figure 1 [1].

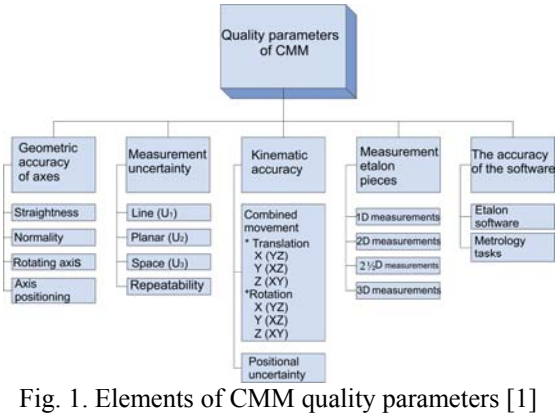

Fig. 1. Elements of CMM quality parameters [1]

## 2. AXES STRAIGHTNESS

The straightness represents deviation of line flow in the two perpendicular planes (Figure 2). Figure 2a) and 2b) shows parameters of deviation from straightness and Figure 2c) shows the straightness measurement results.

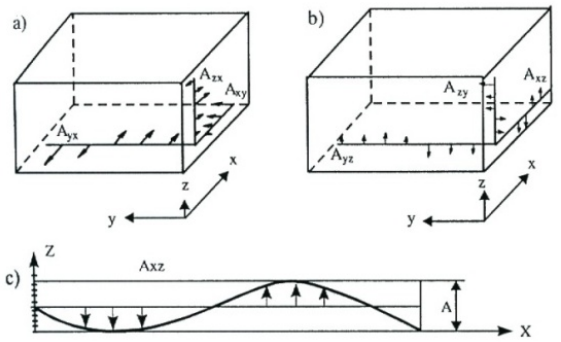


Fig. 2. The parameters and the presentation of axes straightness measurement results [2]

In this way is obtained 6 straightness parameters:

- $A_{xy}$- straightness of X axis measured in the Y direction
- $A_{zx}$- straightness of Z axis measured in the X direction
- $A_{yx}$- straightness of Y axis measured in the X direction
- $A_{xz}$- straightness of X axis measured in the Z direction
- $A_{zy}$- straightness of Z axis measured in the Y direction
- $A_{yz}$- straightness of Y axis measured in the Z direction

By SRPS standard straightness testing includes:

- The line straightness in two planes
- The straightness of the machine parts (components)
- The straightness of movement (movement paths of machine elements)

Path straightness testing is crucial for examination the straightness of machines slide and base. The path straightness of the machine can be defined as parallelism of machine element movement trajectory and the reference line, which is parallel to a measured axis.

Testing can be done in several ways, such as trial by using a measuring ruler and measuring comparator, using stretched wire and a microscope, and using a laser alignment, or a laser interferometer.

As already mentioned, in this paper straightness is measured by the LMS. During the measurement the laser beam passes through the interferometer (Wollaston prism) and being separates in two beams at an angle θ. These beams are normally deducted from the reflector and return to the laser head, passing through the interferometer, where they are again combined into a single beam. It should be noted that the reflector consists of two rigidly connected mirrors under precise angle. The lateral movement of the interferometer relative to the axis of the reflector is detected inside laser head, and sent to data recording device (Figure 3).

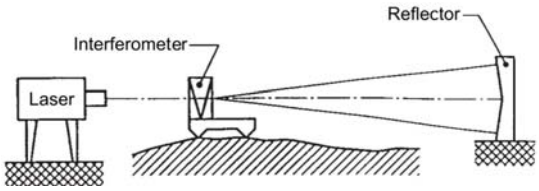


Fig. 3. Testing straightness by using laser interferometer [3]

## 3. MEASURING INSTRUMENTS

Testing the straightness of above mentioned CMM (Carl Zeiss Contura G2) elements along the X and Y axes was carried out using a laser measuring system (LMS) 5526 A, produced by "Hewlett-Packard", with the accuracy of 0.5 μm/m ± 0.2 μm/m (Figure 4). This system consists of:

- Laser head (He- Ne gas laser)- 5500 C
- Automatic compensator- 5510A
- Laser display HP- 5505A
- Straightness adapter
- Optical components

Laser head 5500C is one of the first HP laser for metrology which has an integrated optical receiver for the return laser beam [4-6].

Automatic compensator 5510 A is used to correct the influence of environmental factors such as temperature, humidity and air pressure. These factors are measured by using the appropriate sensors connected to the compensator.

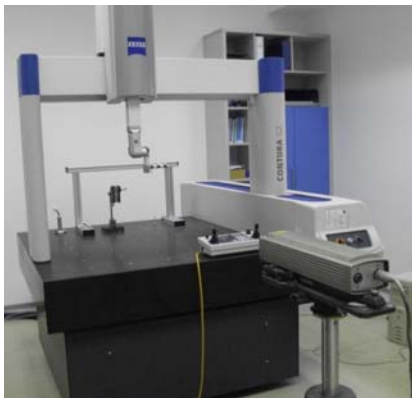

Fig. 4. Numerically controlled measuring machine with mounted LMS

Straightness adapter (Figure 5) consists of partially transmissive mirror that turns the reflected laser beam to the lower opening on the laser head. The laser beam passes through the de-modular polarizer to photo decoder where further signal processing is performed in the usual way.


Fig. 5. Straightness adapter [4]

Optical components for measuring straightness are used:

- *Straightness interferometer* (Figure 6), depending on the length of the measuring way can be used short range and long range interferometer. In this case is used short range interferometer that allows examination of straightness from 100 mm up to 30 m.
- *Straightness reflector* (Figure 6), as well as an interferometer, can be for a short and for a long range examination. It consists of a pair of flat mirrors rigidly connected under the precise angle. The difference between the short and long range straightness reflector is in the angle between mirrors. In this case, is used short range reflector.


Fig. 6. Straightness interferometer and straightness reflector [4]

## 4. STRAIGHTNESS TEST RESULTS OF THE MEASUREMENT SENSOR CARRIER MOVEMENT

To test the straightness of above mentioned CMM elements along the X and Y axes is used already described laser measuring system, while collecting and processing data are carried out with computer system.

Measuring the straightness of CMM elements moving along X direction is done in relation to the two planes XY and XZ plane. The only difference in these two measurements is in adjustment of the LMS, i.e. straightness reflector.

Total measuring way in the X direction is 700 mm, and the distance between the measuring position is Li = 70 mm. The movement of the measuring sensor carrier was performed using a PC, the measurement was performed in linear cycle (Figure 7), and the first passage is used to test the program. After this passage, measurements were carried out five times in both horizontal and vertical planes. Measured straightness values for measuring sensor movement along the X axis, measured relative to the Z axis, are shown in Table 1. The calculated values of deviations from straightness are shown in Table 2 and graphically in Figure 8.

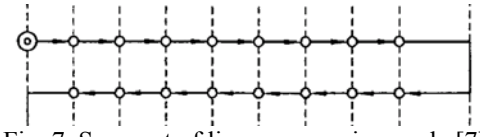

Fig. 7. Segment of linear measuring cycle [7]

Due to lack of space below will not be displayed measurement results and calculated values of deviations from straightness, but only graphical presentation. Figure 8 shows the deviation from straightness of the X axis in relation to Y.

| Redni broj | I merenje | | II merenje | | III merenje | | IV merenje | | V merenje | |
|---|---|---|---|---|---|---|---|---|---|---|
| | → | ← | → | ← | → | ← | → | ← | → | ← |
| 0 | 0 | -0,0108 | -0,0144 | -0,018 | -0,018 | -0,018 | -0,018 | -0,018 | -0,018 | -0,0144 |
| 1 | -0,036 | -0,0432 | -0,0432 | -0,0468 | -0,0468 | -0,0468 | -0,0468 | -0,0468 | -0,0432 | -0,0432 |
| 2 | -0,0648 | -0,072 | -0,0756 | -0,0756 | -0,0756 | -0,0756 | -0,0756 | -0,072 | -0,072 | -0,072 |
| 3 | -0,0972 | -0,1008 | -0,1044 | -0,1044 | -0,1044 | -0,1044 | -0,1044 | -0,1044 | -0,1008 | -0,1008 |
| 4 | -0,1296 | -0,1332 | -0,1332 | -0,1368 | -0,1332 | -0,1332 | -0,1332 | -0,1332 | -0,1296 | -0,1296 |
| 5 | -0,1584 | -0,162 | -0,162 | -0,1656 | -0,1656 | -0,162 | -0,162 | -0,162 | -0,1584 | -0,1584 |
| 6 | -0,1908 | -0,1908 | -0,1944 | -0,1944 | -0,1944 | -0,1908 | -0,1908 | -0,1908 | -0,1872 | -0,1872 |
| 7 | -0,2232 | -0,2232 | -0,2232 | -0,2232 | -0,2232 | -0,2232 | -0,2232 | -0,2196 | -0,2196 | -0,216 |
| 8 | -0,252 | -0,252 | -0,252 | -0,2556 | -0,252 | -0,252 | -0,252 | -0,252 | -0,2484 | -0,2448 |
| 9 | -0,2808 | -0,2844 | -0,2808 | -0,2844 | -0,2844 | -0,2844 | -0,2808 | -0,2808 | -0,2772 | -0,2772 |
| 10 | -0,3132 | -0,3132 | -0,3132 | -0,3132 | -0,3132 | -0,3132 | -0,3096 | -0,3132 | -0,306 | -0,306 |

Table 1. The measured straightness for movement along the X axis

| Merne tačke | | Odstupanje od pravosti | |
|---|---|---|---|
| Redni broj $n_i$ | Položaj $x_i$ | Srednje izmerene vrednosti [mm] | $\Delta Px_i$[$\mu$m] |
| 0 | 100 | -0,01476 | 0 |
| 1 | 170 | -0,04428 | -0,144 |
| 2 | 240 | -0,07308 | -1,008 |
| 3 | 310 | -0,1026 | -1,152 |
| 4 | 380 | -0,13248 | -0,936 |
| 5 | 450 | -0,16164 | -1,44 |
| 6 | 520 | -0,19116 | -1,584 |
| 7 | 590 | -0,22176 | -0,648 |
| 8 | 660 | -0,25128 | -0,792 |
| 9 | 730 | -0,28152 | -0,216 |
| 10 | 800 | -0,3114 | 0 |

Table 2. Calculated values of deviations from straightness

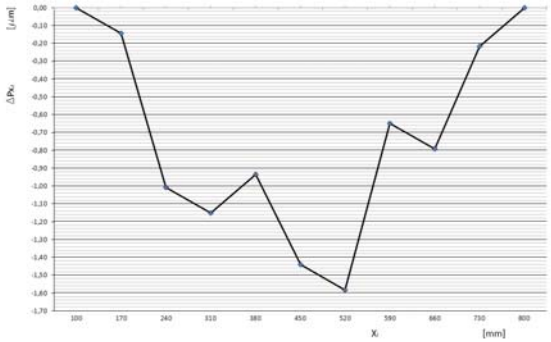


Fig. 7. Graphical representation of deviation from straightness of the X axis in relation to the Z axis

Measuring the motion straightness of CMM elements in the Y direction is also carried out in relation to the two planes. Total measurement length is 800 mm, and the distance between the measuring positions are Li = 80 mm. The movement of the portal was performed using a PC, the measurement was also performed by linear cycles and the first pass is used to test the program. After this passage, measurements were carried out five times in the YX and YZ planes.

In Figures 9 and 10, are graphs showing deviation of the Y axis in relation to the X and Z axes.

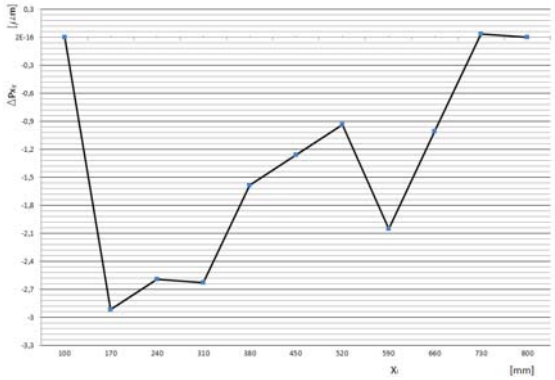


Fig. 8. Graphical representation of deviation from straightness of the X axis in relation to the Y axis

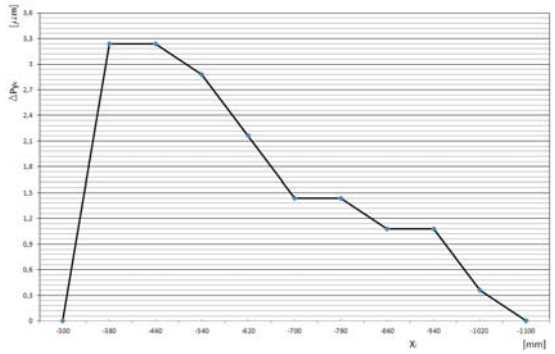

Fig. 9. Graphical representation of deviation from straightness of the Y axis in relation to the X axis

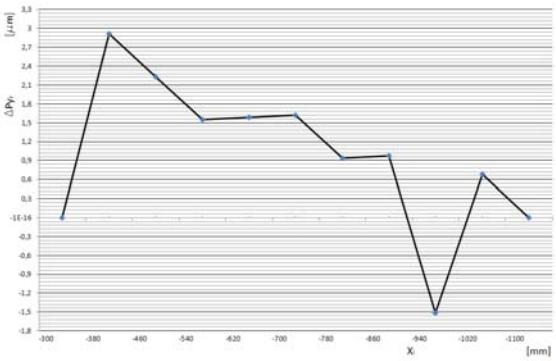

Fig. 10. Graphical representation of deviation from straightness of the Y axis in relation to the Z axis

Data on deviation from straightness by individual axes are obtained based on the movement of coordinate measuring machine movable elements along the X and Y axes. Total deviation from straightness measured for the X axis is displayed spatially, and on the same chart are showed value variation in the two axes, Y and Z (Figure 11). Deviation from straightness along Y axis, relative to the axes X and Z, is displayed in the same way (Figure 12).

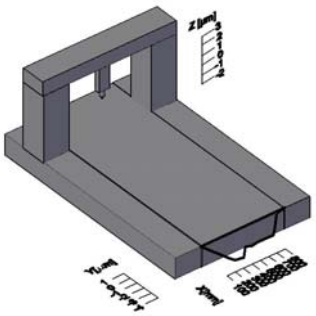

Fig. 11. Spatial graphical representation of the total deviation from straightness of the X axis

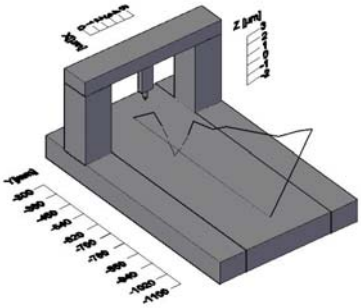

Fig.12. Spatial graphical representation of the total deviation from straightness of the Y axis

## 5. CONCLUSION

The application of numerically controlled measuring machines is becoming more common in modern industrial systems. To ensure the implementation of various CMM metrology tasks and high accuracy, the machine itself must possess a high level of quality.

The issues presented in this paper deals with examination of straightness of CMM elements motion. Since the value of the deviations from straightness on numerically controlled machines are very small, they can be carried out only by a laser measurement system.

Testing was performed by moving the measurement sensor along the X and Y axes, and the deviation from straightness is measured in the direction of Y, and Z axes, i.e. in the direction of X and Z axes.

Along the X axis with respect to the Y axis is obtained maximum deviation of -2.916 μm, and with respect to the Z axis is obtained deviation -1.584 μm.

The maximum values of deviations from straightness for movement along the Y axis, with respect to the X axis are 3.24 μm, and with respect to the Z axis 2.916 μm.

The obtained results show that the straightness of the machine is at a satisfactory level.

## 6. REFERENCES


[1] Majstorović, V., Hodolič, J.: *Numerički upravljane merne mašine*, Fakultet tehničkih nauka, Institut za proizvodno mašinstvo, Novi Sad, 1998.

[2] CMMA, *Accuracy Specification for Coordinate Measuring machines*, Entwurf, 1989.

[3] ISO 230-1: *Prüfregeln für Werkzeugmaschinen, Teil 1: Geometrische Genauigkeit von Maschinen, die ohne Last oder unter Schlichtbedingungen arbeiten*, 1996

[4] Laser Measurment System 5526A, *Operator's handbook supplement for straightness interferometrs*, Hewllet Packard, Santa Clara, 1982.

[5] Bojanić, M.: *Ispitivanje pravosti pomeranja elemenata numerički upravljanih mernih mašina*, Ispitni rad, Fakultet tehničkih nauka, Novi Sad, 2012.

[6] Chen, Q., Lin, D., Wu, J., Yan, J., Yin, C.: *Straightness/coaxiality measurement system with transverse Zeman dual-frequency laser,* Measurement Science and Technology, Volume 16, p.p. 2030-2037, 2005.

[7] You, F., Zhang,B., Feng Q.: *A novel laser straightness measurement method with beam bend compensation*, Optik, Volume 122, Issue 17, p.p. 1530–1534, 2011.



**ACKNOWLEDGEMENTS**

*The work is part of research project on "Modern approaches in the development of special bearings in mechanical engineering and medical prosthetics," TR 35025, supported by the Ministry of Education, Science and Technological Development, Republic of Serbia.*



***Authors:*** **M.Sc. Mirjana Bojanić, Prof. dr Miodrag Hadžistević, M.Sc. Cvijetin Mlađenovic**, University of Novi Sad, Faculty of Technical Sciences, Trg Dositeja Obradovica 6, 21000 Novi Sad, Serbia, Phone.: +381 21 450-366, Fax: +381 21 454-495.

E-mail: bojanicm@uns.ac.rs;miodrags@uns.ac.rs; mladja@uns.ac.rs

Journal of Production Engineering
Vol.18 No.2
JPE (2015) Vol.18 (2) Original Scientific Paper

Šebo, J.

# APPROPRIATENESS OF GENETIC ALGORITHM USE FOR DISASSEMBLY SEQUENCE OPTIMIZATION

Received: 17 July 2015 / Accepted: 25 Septembre 2015

***Abstract:*** *One of the objectives of product disassembly planning is to find economically optimal disassembly sequence, so to decide, which nodes of the product structure to disassemble, and which not, to achieve maximum economic benefits of product disassembly. The aim of article is to find out appropriateness and pros and cons of genetic algorithm (GA) use in disassembly area in comparison to traditional approaches, in our case linear programing optimization model. The models comparison is based on their application on the same product (mobile phone Nokia 7250i). Application of GA methodology is fully described in the article [1], while linear programing model application [2] is fully described in the other article of the author [3]. From multiple application of GA, it seems, that GA is not appropriate method for the case of mobile phone disassembly sequence optimization and has more disadvantages as advantages in comparison to linear programing model.*
***Key words:*** *Disassembly sequence, optimization, genetic algorithm, linear programing, mobile phone.*

**Adekvatnost korišćenja genetskog algoritma za optimizaciju sekvenci demontaže.** *Jedan od ciljeva planiranja demontaže proizvoda je da se pronađe ekonomski optimalna sekvenca demontaže, tako da se odluči, koji sklopovi strukture proizvoda se demontiraju, a koji ne, zarad ostvarivanja maksimalne ekonomske koristi od demontaže proizvoda. Cilj rada je da se sazna adekvatnost, kao i razloza za i protiv korišćenja genetskog algoritma (GA) u oblasti demontaže, u poređenju sa tradicionalnim pristupima, u našem slučaju optimizacije preko modela linearnog programiranja. Poređenje modela se zasniva na njihovoj primeni na isti proizvod (mobilni telefon Nokia 7250i). Primena metodologije GA je u potpunosti opisana u radu [1], dok je primena modela linearnog programiranja [2] u potpunosti opisana u drugom radu autora [3]. Od svestrane primene GA, čini se, da GA nije adekvatan metod u slučaju optimizacije sekvenci demontaže mobilnog telefona i da ima više nedostataka od prednosti u odnosu na model linearnog programiranja.*
***Ključne reči:*** *Sekvenca demontaže, optimizacija, genetski algoritam, linearno programiranje, mobilni telefon.*

## 1. INTRODUCTION

In the the disassembly sequence optimization is often included in the wider topic of disassembly planning. There are described different algorithms for optimization of disassembly sequence. A number of articles are related to linear programing use in disassembly optimization [2,4]. Some articles are focused on other non-standard optimization techniques as genetic algorithms [1], petri nets [5,6] and neural networks [7]. There are also other approaches to disassembly planning such as case-based reasoning [8], etc..

In past we have done a few applications of optimization methods (e.g. linear programing, heuristic method) on disassembly sequence optimization [3]. There are some optimization methods that are relatively easy to use [2,9] and gives reasonable results for one specific mobile phone. In the following we focus on practical application of genetic algorithm (GA) with the maintaining precedence relationships on mobile phone disassembly sequence optimization. Applied GA methodology is based on the article of Kongar and Gupta [1]. The goal of our paper is to find out appropriateness and pros and cons of GA use in disassembly area in comparison to traditional approaches mentioned above.

## 2. APPLICATION OF GA BASED DISASSEMBLY SEQUENCE OPTIMIZATION ON MOBILE PHONE NOKIA 7250I

In the practical application of GA we have followed the Kongar and Gupta [1] methodology with some minor adjustments, so the GA was applied in these steps:

1. To determine the number and type of particular components we have experimentally disassembled the mobile phone. After disassembly of the components we created a product structure diagram (Figure 1), from which we identified disassembly precedence relationships and conditions.

Based on product structure diagram we set the precedence conditions for Nokia 7250i, which are following:

- Component 1 must be removed before all other components,
- Before component 2 must be removed component 1
- Before component 3 must be removed component 1
- Before component 4 must be removed component 2
- Before components 5 - 10 must be removed component 4

- Before components 11 and 12 must be removed component 5
- Before component 13 must be removed components 6 and 7
- Before component 14 must be removed components 8, 9 and 10
- Before component 15 must be removed components 11 and 12

During and after experimental disassembly we wrote down disassembly directions (+/- x, y, z) and methods of removal of the components (D-destructive, N-non-destructive). On the base of material composition of each particular component we also identify whether or not is component demanded (D-demand, N- no-demand) (Table 1). These information are needed for calculation of fitness values.

| Component num. | 1. | 2. | 3. | 4. | 5. | 6. | 7. | 8. | 9. | 10. | 11. | 12. | 13. | 14. | 15. |
|---|---|---|---|---|---|---|---|---|---|---|---|---|---|---|---|
| Demand for the component | A | A | A | A | A | N | N | N | N | N | N | N | A | A | A |
| Disassembly direction of the component | -y | +y | -y | +y | +y | -y | -y | -y | +y | +y | -y | +y | +y | -y | +y |
| Methods of removal of the component | N | N | N | N | N | N | N | D | N | N | N | N | N | N | N |

Table 1. Identified demand, disassembly directions and disassembly methods of Nokia 7250i components

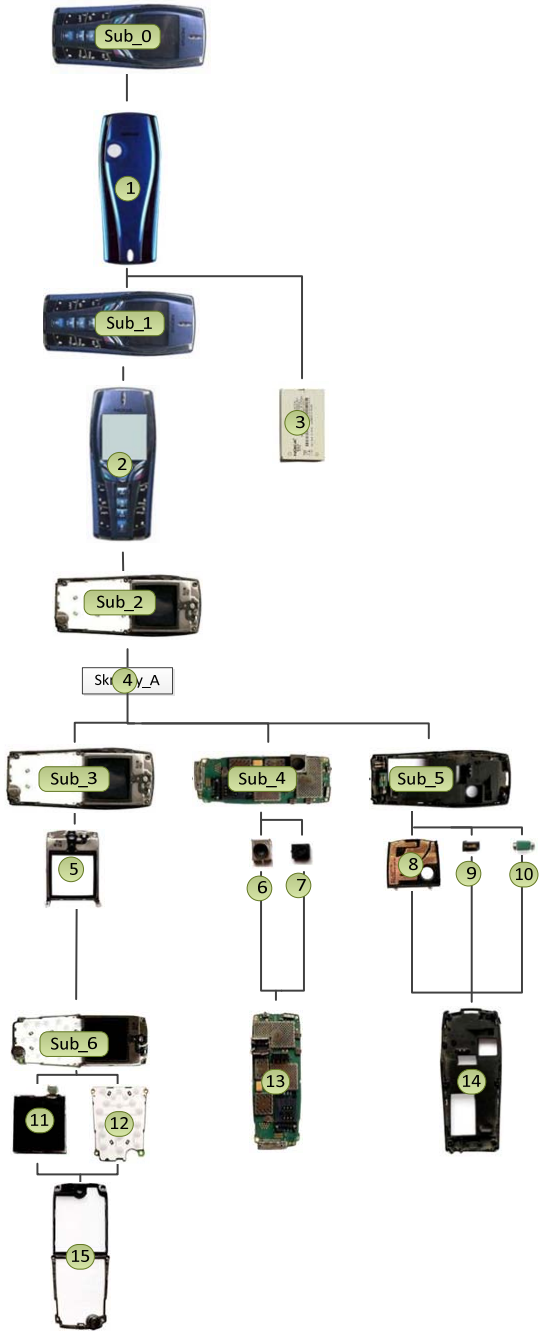


Figure 1. Product structure diagram of Nokia 7250i

2. Further we have created an original population of 10 "individuals"("individual" is in our sense equal to chromosome composed from 15 genes) so that each "individual" had a different order of "genes"(„gene" in our sense is part of chromosome, which could take the values 1, 2, 3, … ,15, that represent specific components of mobile phone), i.e., that no two "individuals" in the original population were the same, and order of "genes" in individuals respect order preference conditions (Table 2).

3. In the next step we have calculated the fitness of the current generation of "individuals" (Table 2). Fitness function in our case is depending on demand for component, directional changes in disassembly and disassembly method changes. Higher fitness of "individual" means better disassembly sequence it represents. (Remark: In the first generation the current population = original population.)

4. After calculation of fitness we have chosen from the current population five "individuals" with the highest fitness, we have cloned them, and thus have received 10 "individuals" (10 parents).

5. On this current population (10 "individuals"/parents) we have applied genetic operators (crossover and mutation) and thus we have created a new generation (10 children).

First we have applied crossover. We chose 5 pairs of parents randomly, and through two randomly generated "masks" (Remark. These "masks" ensure maintaining of precedence relationships.) *we* have created two children for each pair of parents. This way we have created a new generation (10 children).

Next we have applied mutation on this new generation (10 children). Application of mutation was a bit complicated part of GA application. One reason was, that we cannot mutate in a way that we just change "gene" (component) to another "gene" (component). We have to use only mutation, which is switching two "genes" (components) position, because each our "individual" represents sequence of components and every component have to be just once in the sequence. It implies, that before we can run a mutation we have to know if „genes" (components) could be mutated and if yes, which „genes" (components) they could be interchanged with. We did found that some of

components could not be mutated, because if we mutate them we will not maintain precedence conditions. Considering this idea, we can switch "genes" without breaking the precedence conditions if the "genes" (components) are at the same level of product structure and are under the same „node" of product structure (the „node" is equal to component in product structure diagram). On the base of these assumptions we have created 2 groups of switchable genes (1st group (5,6,7,8,9 and 10), 2nd group (11,12)). After this we applied mutation operator in a following way. First we randomly set a number of mutated „genes"(resp. pairs of "genes") for each generation from the interval 1 to 4 (Remark. This interval is based on the fact that we have 8 switchable genes, what means 4 possible pairs of "genes"). Then we applied mutation operator on first 4 „individuals"(children) (Remark. We take this number („4") from mentioned methodology of Kongar and Gupta. This number of mutated „individuals" is fixed for all generations.) and thus we have created new generation after mutation (Table 3).

| "Gene" position „Individuals" | 1 | 2 | 3 | 4 | 5 | 6 | 7 | 8 | 9 | 10 | 11 | 12 | 13 | 14 | 15 | Fitness |
|---|---|---|---|---|---|---|---|---|---|---|---|---|---|---|---|---|
| Individual 1 | 1 | 2 | 4 | 10 | 9 | 8 | 3 | 14 | 6 | 7 | 13 | 5 | 11 | 12 | 15 | 985 |
| Individual 2 | 1 | 2 | 4 | 6 | 7 | 13 | 5 | 11 | 12 | 15 | 10 | 9 | 8 | 3 | 14 | 945 |
| Individual 3 | 1 | 2 | 4 | 6 | 7 | 13 | 5 | 11 | 12 | 15 | 3 | 10 | 9 | 8 | 14 | 925 |
| Individual 4 | 1 | 2 | 4 | 5 | 11 | 12 | 15 | 6 | 7 | 13 | 10 | 9 | 8 | 3 | 14 | 1065 |
| Individual 5 | 1 | 2 | 4 | 6 | 7 | 13 | 3 | 10 | 9 | 8 | 14 | 5 | 11 | 12 | 15 | 705 |
| Individual 6 | 1 | 2 | 3 | 4 | 10 | 9 | 8 | 14 | 6 | 7 | 13 | 5 | 11 | 12 | 15 | 965 |
| Individual 7 | 1 | 2 | 3 | 4 | 6 | 7 | 13 | 5 | 11 | 12 | 15 | 10 | 9 | 8 | 14 | 1165 |
| Individual 8 | 1 | 2 | 3 | 4 | 6 | 7 | 13 | 5 | 11 | 12 | 15 | 10 | 9 | 8 | 14 | 1165 |
| Individual 9 | 1 | 3 | 2 | 4 | 5 | 11 | 12 | 15 | 6 | 7 | 13 | 10 | 9 | 8 | 14 | 1485 |
| Individual 10 | 1 | 3 | 2 | 4 | 6 | 7 | 13 | 10 | 9 | 8 | 14 | 5 | 11 | 12 | 15 | 1025 |

Table 2. Original population and its fitness values

| "Gene" position „Individuals" | 1 | 2 | 3 | 4 | 5 | 6 | 7 | 8 | 9 | 10 | 11 | 12 | 13 | 14 | 15 |
|---|---|---|---|---|---|---|---|---|---|---|---|---|---|---|---|
| Child 1 | 1 | 2 | 4 | 5 | 3 | 12 | 11 | 8 | 15 | 7 | 13 | 10 | 9 | 6 | 14 |
| Child 2 | 1 | 2 | 4 | 3 | 8 | 5 | 12 | 11 | 15 | 7 | 13 | 10 | 9 | 6 | 14 |
| Child 3 | 1 | 2 | 3 | 4 | 10 | 5 | 12 | 7 | 11 | 15 | 13 | 6 | 9 | 8 | 14 |
| Child 4 | 1 | 2 | 4 | 9 | 3 | 12 | 11 | 6 | 15 | 7 | 13 | 10 | 5 | 8 | 14 |
| Child 5 | 1 | 3 | 2 | 4 | 5 | 6 | 7 | 13 | 11 | 12 | 15 | 10 | 9 | 8 | 14 |
| Child 6 | 1 | 2 | 3 | 4 | 6 | 7 | 5 | 11 | 12 | 15 | 13 | 10 | 9 | 8 | 14 |
| Child 7 | 1 | 2 | 4 | 5 | 11 | 3 | 6 | 12 | 7 | 13 | 15 | 10 | 9 | 8 | 14 |
| Child 8 | 1 | 2 | 3 | 4 | 5 | 11 | 12 | 15 | 6 | 7 | 13 | 10 | 9 | 8 | 14 |
| Child 9 | 1 | 2 | 3 | 4 | 5 | 6 | 7 | 13 | 11 | 12 | 15 | 10 | 9 | 8 | 14 |
| Child 10 | 1 | 2 | 3 | 4 | 5 | 11 | 12 | 6 | 7 | 15 | 13 | 10 | 9 | 8 | 14 |

Table 3. New generation received after crossover and mutation

6. In this step we test the "stop" conditions (Remark. "Stop" conditions are: serial number of generation and the "ratio" indicator). To enable monitoring of GA behavior we have made a change to the original methodology in a way, that we do not respect the "ratio" indicator as „stop" condition and leave algorithm to run longer (in our research until the 40th generation is met).

7. The "individual" (representing specific order of disassembled components) with the highest achieved value of fitness across all generations represents the optimal disassembly sequence.

The maximum value of the acquired fitness in this application of GA (resp. in 1st attempt) was (1565). This fitness value comes with "individual" shown in the Table 4. Optimal disassembly sequence corresponding to "individual" with highest fitness (1565) is shown in Table 5.

| "Gene" position „Individuals" | 1 | 2 | 3 | 4 | 5 | 6 | 7 | 8 | 9 | 10 | 11 | 12 | 13 | 14 | 15 |
|---|---|---|---|---|---|---|---|---|---|---|---|---|---|---|---|
| Individual with the highest fitness | 1 | 2 | 4 | 5 | 3 | 11 | 7 | 6 | 12 | 15 | 13 | 10 | 9 | 8 | 14 |

Table 4. "Individual" with the highest fitness (achieved in the 1st attempt of GA application)

| | | |
|---|---|---|
| 1. | component - | 1 (back cover) |
| 2. | component - | 2 (front cover) |
| 3. | component - | 4 (screws) |
| 4. | component - | 5 (display frame) |
| 5. | component - | 3 (battery) |
| 6. | component - | 11 (LCD display) |
| 7. | component - | 7 (camera module) |
| 8. | component - | 6 (camera cover) |
| 9. | component - | 12 (el. circuit of keyboard) |
| 10. | component - | 15 (plastic frame) |
| 11. | component - | 13 (motherboard) |
| 12. | component - | 10 (vibration engine) |
| 13. | component - | 9 (power connector) |
| 14. | component - | 8 (GSM signal module) |
| 15. | component - | 14 (internal plastic cover) |

Table 5. Optimal disassembly sequence (order of disassembled components) (achieved in the 1st attempt of GA application)

## 3. MULTIPLE APPLICATION OF GA BASED DISASSEMBLY SEQUENCE OPTIMIZATION ON MOBILE PHONE NOKIA 7250I WITH THE SAME ORIGINAL POPULATION

To analyze GA behavior we have made six GA applications (attempts) with the same original population and by the same methodology (steps) as described above for 1st attempt.

As we can see from the Table 6 in six experiments of GA application with the same original generation we have gained improvement of the maximum fitness of original generation (best solution in original generation) in 5 attempts. In two attempts have improved maximum fitness by 5.39% (from 1485 to 1565) and in two attempts have improved maximum fitness by 9.43% (from 1485 to 1625). In one attempt the maximum fitness have not improved. On average, in six attempts we have improved the maximum fitness by 6.51% (from 1485 to 1582). The maximum fitness in all six experiments has been reached between first and fifth generation (on average between 2nd and 3rd generation).

| Attempt number | Maximum fitness value | Number of generation in which was reached maximum fitness |
|---|---|---|
| 1. | 1565 | 4. |
| 2. | 1625 | 2. |
| 3. | 1625 | 2. |
| 4. | 1565 | 5. |
| 5. | 1625 | 2. |
| 6. | 1485 | 1. |
| Average | 1582 | 2,67 |

Table 6. Maximum fitness values obtained in individual attempts

In the graphs below, describing development of the maximum fitness in six attempts (experiments), we can see, that in half of the attempts (attempts no. 1,3 and 6) the maximum fitness values tend to decline during the first 10 (resp. 20) generations with their further stabilization at lower levels than the total maximum value within a single attempt. Further we can see, that in two attempts (attempt no. 2 and 5) the maximum fitness slightly has increased and then has stabilized at the moderately increased levels. In one attempt (attempt no. 4) maximum fitness has had alternating development (a few times has decreased and increased) followed by stabilization at the level close to the maximum fitness of the original generation.

From this we come to the conclusion that the GA in the form applied in our attempts does not achieve standard outputs, it does not achieve on average a significant improvement in maximum fitness in comparison to original population, and in the majority of attempts the maximum fitness value does not tend to increase with the growth of the number of generations, rather, on the contrary in most of the attempts it tend to decrease.

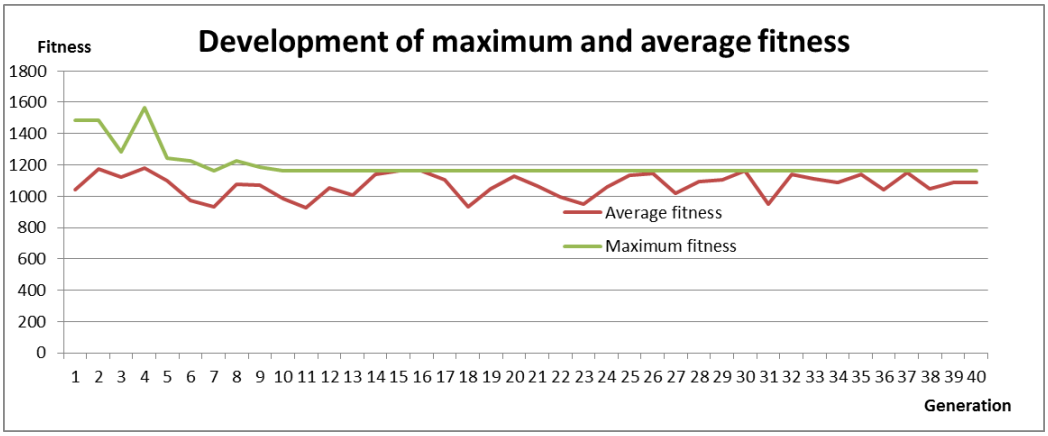


Figure 2. Development of maximum and average fitness – attempt no. 1

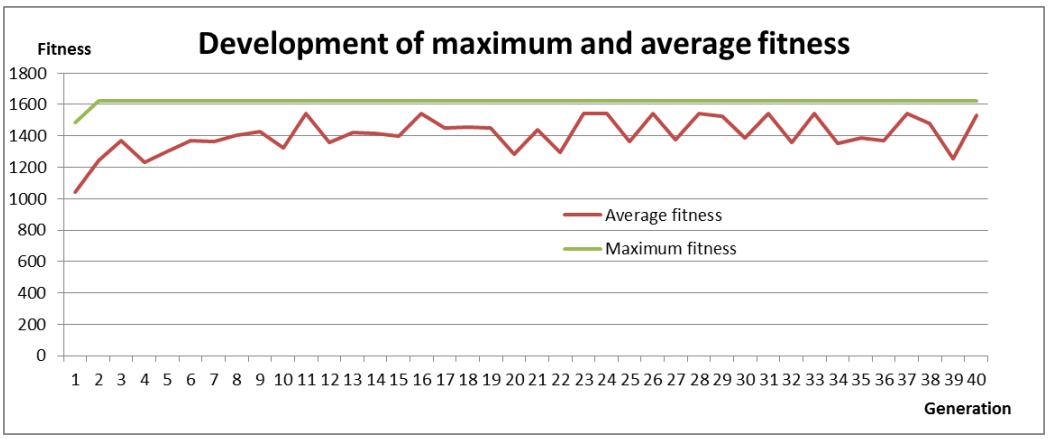


Figure 3. Development of maximum and average fitness – attempt no. 2

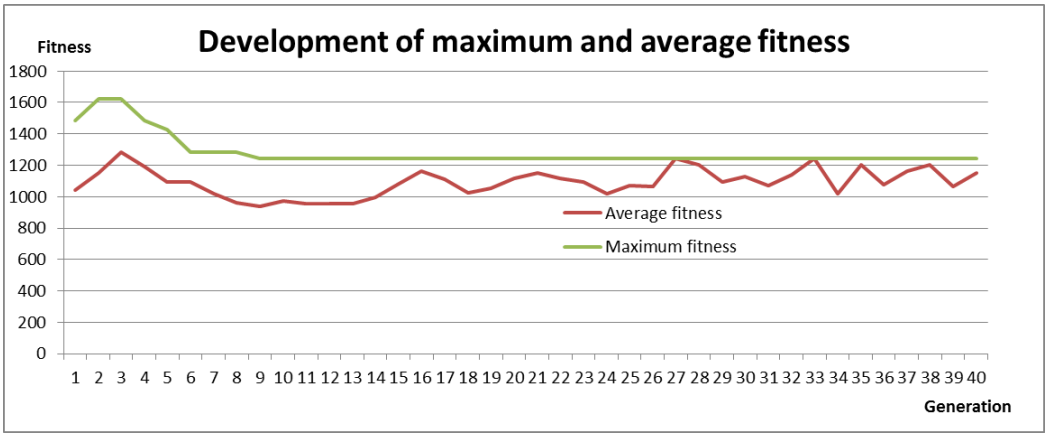


Figure 4. Development of maximum and average fitness – attempt no. 3

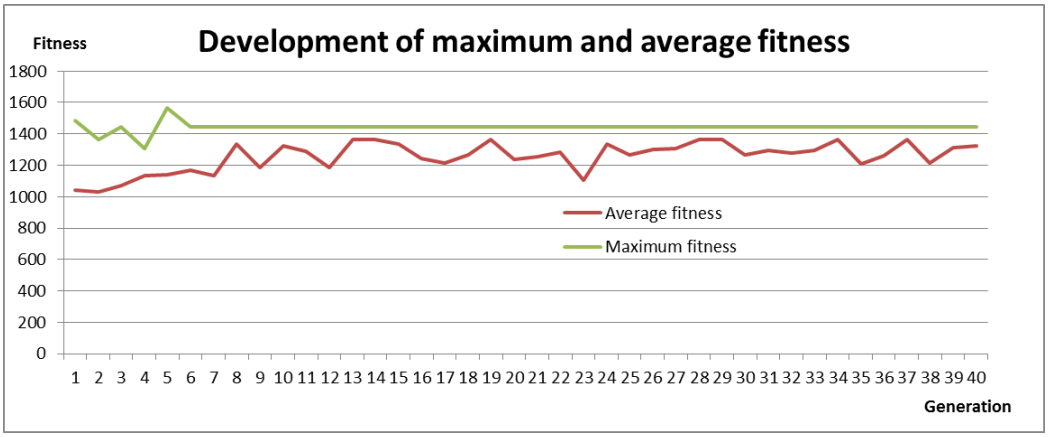


Figure 5 Development of maximum and average fitness – attempt no. 4

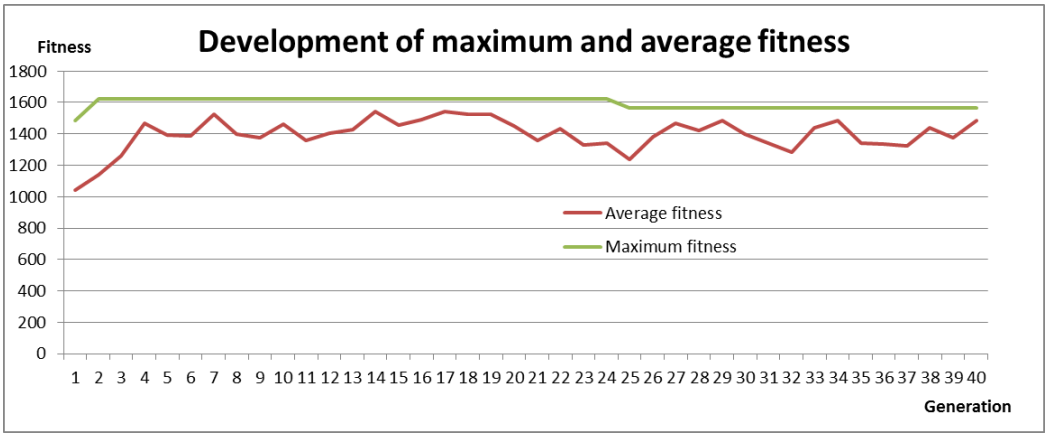


Figure 6. Development of maximum and average fitness – attempt no. 5

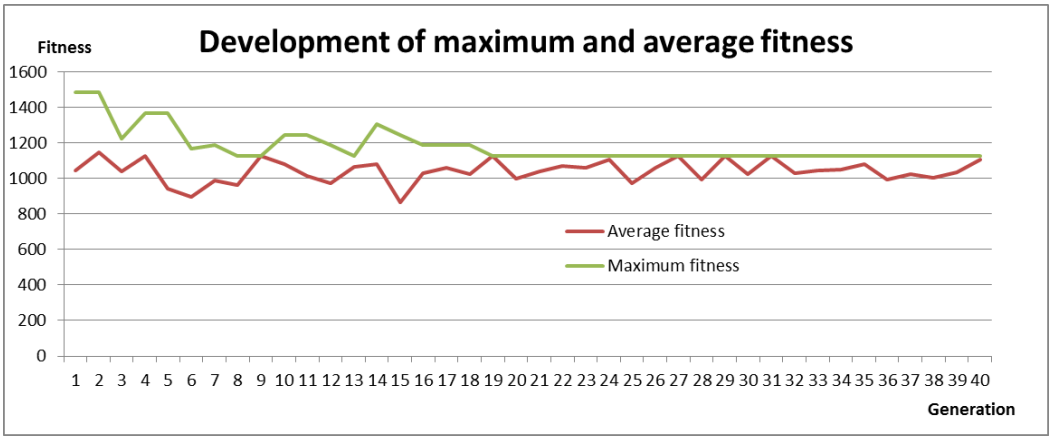

Figure 7. Development of maximum and average fitness – attempt no. 6

| "Gene" position „Individuals" | 1 | 2 | 3 | 4 | 5 | 6 | 7 | 8 | 9 | 10 | 11 | 12 | 13 | 14 | 15 |
|---|---|---|---|---|---|---|---|---|---|---|---|---|---|---|---|
| Individual with the highest fitness | 1 | 3 | 2 | 4 | 5 | 6 | 7 | 11 | 13 | 12 | 15 | 10 | 9 | 8 | 14 |

Table 7. "Individual" with the highest fitness (achieved in all six attempts of GA application)

| | | |
|---|---|---|
| 1. | component - | 1 (back cover) |
| 2. | component - | 3 (battery) |
| 3. | component - | 2 (front cover) |
| 4. | component - | 4 (screws) |
| 5. | component - | 5 (display frame) |
| 6. | component - | 6 (camera cover) |
| 7. | component - | 7 (camera module) |
| 8. | component - | 11 (LCD display) |
| 9. | component - | 13 (motherboard) |
| 10. | component - | 12 (el. circuit of keyboard) |
| 11. | component - | 15 (plastic frame) |
| 12. | component - | 10 (vibration engine) |
| 13. | component - | 9 (power connector) |
| 14. | component - | 8 (GSM signal module) |
| 15. | component - | 14 (internal plastic cover) |

Table 8. Optimal disassembly sequence (order of disassembled components) (achieved in all six attempt of GA application)

The maximum fitness value acquired in all six application of GA (resp. in all six attempts) is equal to 1625. In comparison with maximum fitness value of 1st attempt (1565) it is of 3,83 % higher. This new highest maximum fitness value comes with "individual" shown in the Table 7. Optimal disassembly sequence corresponding to "individual" with new highest fitness (1625) is shown in Table 8.

## 4. ADVANTAGES AND DISADVANTAGES OF GA IN COMPARISON WITH LINEAR PROGRAMING MODEL USED FOR DISASSEMBLY OPTIMIZATION

One of the major disadvantage of GA disassembly optimization is its failure to consider selective (resp. incomplete) disassembly, which in real life currently prevails over complete disassembly. All alternatives envisaged represent disassembly of all components (i.e. complete disassembly).

The weakness of this GA methodology is also product structure diagram that cannot clearly show some real structures (relations) of components. Product structure diagram appears to us insufficient. For example, in our mobile phone case, the disassembly of "subassembly" (front cover with keyboard) cannot be clearly described in the product structure diagram. According to our understanding of the product structure diagram (according to Kongar and Gupta methodology) transition from one "level" to the lower "level" is possible only through disassembly of the component and not through disassembly of "subassembly". For this reason, in our application we have had to simplify the mobile phone structure, so that the "subassembly" (front cover with keyboard) have been considered as one component, although in reality is rubber keyboard detachable from the plastic front cover, so they represent a two separate components.

The disadvantage of the GA model in comparison to linear programing could be also in the probability that it reach global (and not local) optimum [2]. In conditions where a number of components in each subassembly of a product is not high (not more than 4 or 5), what is often case in real life (e.g. in the mobile phone structure), the linear programing model could calculate all product structure combinations, so there is 100 % probability of reaching global optimum and not fall to local one, what based on our experiments could be a problem in the case of GA.

The GA output is less complex as linear programing model [2], because it gives no information about how to treat disassembled components and also gives no information in economic (profit/loss) terms.

As advantage of GA could be considered the form of the output, which is in the structure of order of components, so it is easy to use in real life (e.g. disassembly facility). In comparison the output of disassembly (economic) optimization model based on linear programing involves table of connections which

should be disconnected and which leaved intact, table of optimal treatment (recover or dispose) of components and subassemblies, and overall profit/loss from the disassembly of the product [2].

In the case of more complicated products and when we want to calculate all combinations in linear programing model, the potential advantage of GA could be the calculation times, but if we apply Branch and Bound method in linear programing model, the advantage probably could not be relevant.

## 5. CONCLUSIONS

From the outputs of the multiple application of GA based disassembly sequence optimization on mobile phone we come to the conclusion that the GA in the form applied in our experiments (attempts) does not achieve standard outputs, it does not achieve on average a significant improvement in maximum fitness in comparison to original population, and in the majority of attempts the maximum fitness value does not tend to increase with the growth of the number of generations, rather, on the contrary in most of the attempts it tend to decrease.

When comparing GA with linear programing disassembly optimization model we found out some advantages and disadvantages. One of the major disadvantage of GA disassembly optimization is its failure to consider selective (resp. incomplete) disassembly, which in real life currently prevails over complete disassembly. The weakness of this particular GA methodology is also product structure diagram that cannot clearly show some real structures (relations) of components. The disadvantage of the GA model in comparison to linear programing (see (Lee, Cho and Hong, 2010)) could be also the lower probability that it reach global (and not local) optimum. The GA output is also less complex as linear programing model (gives no information about how to treat disassembled components and also no information in economic (profit/loss) terms). As advantage of GA could be considered the form of output, which is in the structure of order of components, so it is easy to use in real life (e.g. disassembly facility). The potential advantage of GA could be also the calculation times.

**Acknowledgement**

The paper is the result of the project implementation: University Science Park TECHNICOM for Innovation Applications Supported by Knowledge Technology, ITMS: 26220220182, supported by the Research & Development Operational Programme funded by the ERDF.

## 6. REFERENCES

[1] Kongar, E. and Gupta, S.M. (2001) 'Genetic Algorithm for Disassembly Process Planning', Proceedings of the SPIE International Conference on Environmentally Conscious Manufacturing II, Newton (Massachusetts), 54-62.

[2] Lee, H.B., Cho, N.W. and Hong, Y.S. (2010) 'A hierarchical end-of-life decision model for determining the economic levels of remanufacturing and disassembly under environmental regulations', *Journal of Cleaner production*, no. 18, pp. 1276-1283.

[3] Šebo, J. and Fedorčáková, M. (2013) ' Economic optimization of recycling oriented disassembly of consumer electronics: the case study of mobile phone', *Journal of Production Engineering*, vol. 16, no. 2, pp. 81-85.

[4] Lambert, A.J.D. (1999) 'Linear programming in disassembly/clustering sequence generation', *Computer and Industrial Engineering* , no. 36, pp. 723-738.

[5] Moore, K.E., Gungor, A. and Gupta, S.M. (1998) 'Disassembly process planning using Petri nets.', Proceedings of ISEE International Symposium on Electronics and the Environment , 88-93.

[6] Zussman, E., C, Z.M. and Caudil, l.R. (1998) 'Disassembly Petri Net Approach to Modeling and Planning Disassembly Processes of Electronic Products', Proceedings of the 1998 IEEE International Symposium on Electronics and the Environment, ISEE – 1998, , New York.

[7] Huang, H.-H., Wang, M.H. and Johnson, M.R. (2000) 'Disassembly Sequence Generation Using aNeural Network Approach', *Journal of Manufacturing Systems*, vol. 19, no. 2.

[8] Veerakamolma, l.P. and Gupta, S.M. (2002) 'A case-based reasoning approach for automating disassembly process planning', *Journal of Intelligent Manufacturing,* vol. 13, no. 1, pp. 47-60.

[9] Meacham, A., Uzsoy, R. and Venkatadri, U. (1999 ) 'Optimal Disassembly Configurations for Single and Multiple Products, ', *Journal of Manufacturing Systems*, vol. 18, no. 5, pp. 311-322.

***Author:*** **Ing. Juraj Šebo, PhD.,** Technical University of Košice, Faculty of Mechanical Engineering, Department of Industrial Engineering and Management, Nemcovej 32, 04200 Košice, Slovak Republic, Phone.: +421 55 6023241
E-mail: juraj.sebo@tuke.sk

Journal of Production Engineering
Vol.18 No.2
JPE (2015) Vol.18 (2) Preliminary Note

Olorunmaiye, J. A., Ohijeagbon, I. O.

# RETROFITING COMPOSITE CEILING BOARDS WITH JATROPHA CURCAS SEEDCAKE MATERIAL

Received: 5 November 2015 / Accepted: 30 November 2015

**Abstract:** *Estimations of properties of composite ceiling boards which employ wood waste particles and jatropha seed cake was studied. Predictive models for the simulation of physical and mechanical properties of the composite products was conducted; and were used to study the characteristics of bulk density (BD), thickness swelling index (TS), modulus of rupture (MOR), modulus of elasticity (MOE) and internal bonding strength (IB) of the composite ceiling boards analysed. Equal amounts of jatropha and sawmill dust in the theoretical composite particle/ceiling board resulted in values of properties, bulk density 0.8975 g/cm$^3$, thickness swelling index 9.83%, modulus of rupture 25.05 MPa, modulus of elasticity 2.42 GPa and internal bonding strength 13.86 MPa respectively. Improved mechanical properties and denser composite particle/ceiling board can generally be produced with addition of jatropha to sawmill dust under specified control conditions of fiber-matrix mixture aggregates.*
***Key words:*** *Ceiling boards, jatropha, sawmill dust, fiber-matrix*

**Dopuna kompozitnih ploča plafona sa barbadoskim oraščićem (Jatropha Curcas).** *U ovom radu je izvršena procena osobina kompozitnih plafonskih ploča napravljenih od otpadnog drveta i semena barbadoskog oraščića. Konstruisan je prediktivni modela za simulaciju fizičkih i mehaničkih osobina kompozitnih proizvoda, koji je posle korišćen za proučavanje karakteristike gustine (BD), indexa otoka debljine (TS), modula kidanja (MOR), modula elastičnosti (ME) i unutrašnje snage vezivanja (IB) kompozitnih plafonskih ploča. Jednaki količinski udeli barbadoskog oraščića i piljevine u kompozitnom materijalu plafonskih ploča rezultiralo je sledećim vrednostima osobina: gustina 0,8975 g/cm$^3$, index otoka debljine 9,83%, modul kidanja 25,05 MPa, modul elastičnosti 2.42 GPa i unutrašnje snage vezivanja 13.86 MPa. Poboljšane mehaničke osobine i gušće kompozitne ploče plafona mogu generalno biti proizvedeni sa dodatkom barbadoskog oraščića u piljevinu, pod određenim kontrolisanim uslovima.*
***Key words:*** *Plafonske ploče, barbadoski oraščić (Jatropha), piljevina, matrica vlakana*

## 1.0. INTRODUCTION

### 1.1. Threats to naturally existing biomass sources

The conservation of the environment is a growing concern amongst stake holders in the agricultural, manufacturing and industrial sectors especially as regards sustainable use of renewable biomass materials such as wood for production of vast household and office furniture, and structural constructional materials, such as particleboards used for facing, partitioning and ceiling boards' applications. Constant growth in the world population coupled with urbanisation and industrialisation continues to threaten naturally existing biomass sources for furniture and construction wood materials, and for energy consumption. Presently, there is a high dependence of biomass sources for energy sources and consumption in Nigeria. Osaghae, (2009) as cited in Ojolo and Orisaleye [1], suggests that traditional biomass (wood fuels) accounts for the largest share of the total energy consumption in Nigeria; this is put at 51%, followed by petroleum products 41%, natural gas 5.2%, and electricity 3.1%. In an attempt to address this rising non-sustainable practice which can lead to several environmental degradation, such as deforestation, erosion and flooding, extinction of endangered species of some animals, land sliding, amongst others. There is the need to begin to pay more attention to ways of recycling less important by-products such as jatropha curcas seedcake as suitable resources for manufacturing purposes.

### 1.2. Jatropha curcas seedcake as a suitable composite material

This study examines the prospect of using jatropha curcas seedcake as a suitable ceiling board composite material. Although, composite materials primarily offers several benefits such as lightweight, heat resistance, mechanical and control characteristics [2], with the objective of making a component which is strong and stiff and of a low density [3]. However, composite engineering can also serve as a means of addressing issues of waste in industrial production processes, thereby enhancing conservation of the environment and sustainability [4]. When adequately explored, jatropha curcas seedcake could be turned into more useful commercial product as wood which is a good renewable resource material due to its valuable industrial applications [5].

### 1.3. Characteristics of jatropha curcas seed cakes

The jatropha curcas seed cakes are produced by expelling oil from high oil-bearing seeds. Expelled oilseed cake contains 8-12% oil depending on the efficiency of expeller. The seed cake left as a by-product after oil extraction by screw press can contain as much as 500–600 g/ kg indigestible shells [6]. This accounts for about 50-60% by weight of the seed. The residue matter or cake can be as much as 75% of the

weight of seeds as press-cake [7]. Jatropha seed cake has been found to be a good substituted for chemical fertilizers. The cake's high organic matter content makes it suitable for biogas generation which is found to produce 60% more biogas than cattle dung. Detoxified seed cake may also be used for animal feed shells [6]. The specific energy density by mass in MJ/kg of jatropha seed cake is given as 21 MJ/kg for low expelling efficiency (25%) with seed weight to oil ratio of 4:1, and 17 MJ/kg for High expelling efficiency (34%) with seed weight to oil ratio of 3:1 [8].

### 1.4 . Recycling-means to environmental conservation and sustainability

Growing interest had been made of recent to find means of recycling agricultural waste into profitable uses. Alade *et al.* [9] suggested that sawdust and related wood by-products from sawmills be converted into value-added products for particle board production rather than disposing off through the traditional method of incineration which has adverse consequences of polluting the environmental with harmful substances such as poly aromatic hydrocarbons (PAHs), nitogen oxide (NOx) and sulphur oxide (SOx). Idowu *et al.* [10] had used the fibre from corn cobs, a post-harvest material estimated at over 200 million tons from maize in Nigeria to produce stable particleboards with cement to fibre ratio of 3:1 and 3% additive concentration of calcium chloride ($CaCl_2$), resulting in particleboard of density of 1200 kg/m$^3$, modulus of rupture 0.49 MPa and modulus of elasticity 4391 MPa respectively. The enormous amount of wasted corn cobs from post-harvest activities could be utilised as alternative substitute to wood-based biomass so as to achieve environmental conservation and sustainability.

Similarly, Scatolino *et al.* [11] had adduced that agricultural residues such as, maize cob generated in large quantities in Brazil accumulates to such extent as to cause environmental problems. To ameliorate on the prevailing circumstances Scatolino *et al.* [11] suggests that an alternative use for maize cob to produce particleboard panels in association with wood particles should be encouraged, which was the spur of their study. They investigated the feasibility of using maize cob for production of particleboard panels in which maize cob percentages of: 0%, 25%, 50%, 75% and 100%, in association with particles of Pinus oocarpa wood. They made panels with 8% of urea formaldehyde and 1% of paraffin (based on dry weight of particles), and compressed the panels with a pressure of 3.92 MPa at a temperature of 160° C, for 8 minutes. Scatolino *et al.* [11] discovered that increased replacement of pinewood by maize cob residue resulted in increased water absorption and thickness swelling, while the mechanical properties were decreased.

### 1.5. Potential of allied agricultural products for particle/ceiling boards production

#### 1.5.1. Bamboo

Bamboo mat board (BMB) was the first bamboo-based panel to be produced commercially. It is produced on a commercial scale in China (under the name bamboo mat plywood), India, Thailand and Vietnam. The earliest boards produced were casein-bonded and their principal use was for interiors of aircrafts; only species with long internodes, such as Bambusa textilis, were used. In the 1970s, synthetic resin-bonded BMB was developed in China. Although urea formaldehyde (UF), phenol formaldehyde (PF) and phenol-tannin formaldehyde (PTF) were employed as the bonding resin, UF-bonded BMB is the most common. The physical and mechanical properties of typical UF-bonded common BMB produced in China are given as density 850 kg/m$^3$, internal bond strength 1.57 MPa, modulus of rupture 93.0 MPa, tensile strength 72.6 MPa, and impact tenacity 3.1 J/cm$^2$ respectively [12].

Laemlaksakul [13] investigated the feasibility of making single-layer particleboard panels from bamboo waste (Dendrocalamus asper Backer). Bamboo was converted into strips, which were used to make laminated bamboo furniture. The experimental variables were density (600-800 kg/m$^3$) and conditioning temperature (25-55 °C). The experimental panels were tested for their physical and mechanical properties including modulus of elasticity (MOE), modulus of rupture (MOR), internal bonding strength (IB), screw holding strength (SH) and thickness swelling values according to the procedures defined by Japanese Industrial Standard (JIS). Laemlaksakul [13] concluded that a valuable renewable biomass, bamboo waste could be used to manufacture boards.

#### 1.5.2. Cambara, canelinha and cedrinho fibres

Mello da Silva *et al.* [14], investigated, with the aid of the Brazilian NBR 14810:2002 standard, the physical properties, namely, bulk density and moisture and mechanical properties, namely, flexural strength modulus and internal compliance of particleboards manufactured with bicomponent polyurethane resins derived from castor oil and cambara, canelinha and cedrinho fibres. The factors investigated were: nominal density (0.80 g/cm$^3$), nominal thickness (10mm), moisture content of the particles (5%), percentage of resin (15%), time used in the pressing cycle (10min), hot pressing (100°), pressing pressure (5MPa) and length of the particles (3 to 5mm), leading to a full factorial design of $2^2$ type, providing four different experimental conditions. Mello da Silva *et al.* [14] discovered that the mechanical properties of both materials prepared showed higher values than those stipulated by the standard. And for the physical properties, only the density was found to have exceeded the limits set by the NBR 14810:2002, rating the particleboards produced as high density.

#### 1.5.3. Water melon peels

Idris *et al.* [15] studied the suitability of using water melon peels as alternatives to wood-based particleboard composites. They produced water melon peels composite boards by compressive moulding using recycled low density polyethylene (RLDPE) as a binder. The RLDPE was varied from 30 to 70% by weight at intervals of 10%. They determined the microstructure, water absorption (WA), thickness

swelling index (TS), modulus of rupture (MOR), modulus of elasticity (MOE), internal bonding strength (IB), impact strength and wear properties of the boards. Their results showed that high modulus of rupture of 11.45 MPa, MOE of 1678 MPa, IB of 0.58 MPa, wear rate of 0.31 g was obtained from particleboard produced at 60% RLDPE. Idris *et al.* [15] concluded that water melon particles can be used as a substitute to wood-based particleboards for general purpose applications. Aside from being environmental friendly, using watermelon and RLDPE in production of particleboard was also found to be very cost-effective.

**1.5.4. Rice husk**

Johnson and Yunus [16] suggested that rice husk particleboard is one of the materials which are being considered for development as a potential substitute for wood and wood-based board products in order to mitigating the growing shortage of wood especially in urban cities, due to the rapid growth of the construction industry as a consequence of increasing population and standard of living. They further alludes the reasons behind the use of rice husk in the construction industry was as a result of its high availability, low bulk density (90-150 kg/m$^3$), toughness, abrasiveness, resistance to weathering and unique composition. Also, the use of rice husk enables the production of much cheaper ceiling boards. The main components of rice husk are silica, cellulose and lignin. The composition of rice husk as a percentage of weight was given as $SiO_2$ 18.80-22.30%, lignin 9-20%, cellulose 28-38%, protein 1.90-3.0%, fat 0.30-0.80% and other nutrients 9.30-9.50% respectively. Ceiling boards produced from rice husk is done by combining rice husk and sawdust; slurry is produced by heating rice husk with caustic soda. This slurry is then washed with water and beaten into pulp, to which sawdust (filler) and glue is added. The slurry is formed into sheets in the press and sun dried [16].

In their study, Johnson and Yunus [16] observed that boards with the admixture of rice husk and sawdust have a higher tensile strength (32 N/m$^2$) compared to only rice husk boards (22 N/m$^2$) and are comparable to commercial ceiling boards (23.5 N/m$^2$). Phenol-formaldehyde (PF) resin creates strong and water resistant bonds, but requires the longest pressing time and higher temperatures. The modulus of elasticity (MOE) and modulus of rupture (MOR) of rice husk particleboards with PF as binder are 2.6 GPa and 13 MPa, while in the case of ground rice husk, the modulus drops to 1.6 GPa and 7 MPa [16].

**1.5.5. Groundnut shell**

Raju *et al.* [17] investigated the properties of groundnut shell particles reinforced polymer composite (GSPC). They prepared composite samples with different weight percentages of particles in polymer matrix and the physical and mechanical properties were tested. They observed that the sample with 20 wt% of reinforcement had maximum MOR of 40.57 MPa and sample with 60 wt% of reinforcement had maximum MOE of 8.204 GPa. The tensile test shows that sample with 40 wt % had maximum tensile strength and young's modulus of 28.09 MPa and 8204 MPa respectively. The impact test results show a steady increase in impact strength up to 50 wt % of filler addition. Moisture content of GSPC varied from 1.92 to 4.96% and water absorption was only 1.51-8.82% for 15 days.

**1.5.6. Bagasse**

A three layer experimental particleboards using a mixture of bagasse and industrial wood particles was investigated by Ghalehno *et al.* [18]. They produced the boards with ratio of the mixture of bagasse and wood particles, in the surface and middle layers given as 20:80, 30:70 and 40:60, respectively. They selected the press times at two levels of 5 and 7 minutes. Two levels of urea formaldehyde resin were selected for the surface layers, namely: 9 and 11 percent. The Modulus of elasticity (MOE), modulus of rupture (MOR), internal bonding (IB) and thickness swelling (TS) of the panels were determined according to the procedure of DIN 68763 Standard. Their results indicated that all mechanical and physical properties of particleboards improved with an upper percentage of bagasse particles added. They also observed that the treatment with 40% bagasse, 11% resin in the surface layers and with a 7 min press time resulted in an optimum particleboard product.

**1. 6. Aim and objective of study**

Even though many uses had been discovered for Jatropha seed cake (biomass), it has however not been popularly used as composite material for construction products as some other biomass products, especially in the area of particle ceiling boards.

The aim of this study is the theoretical estimations of properties of composite ceiling boards which employs wood waste particles and jatropha seed cake as recycled resource materials to produce potentially economically viable ceiling boards. The objective was the determination and investigation of the physical and mechanical properties of the composite ceiling boards made from wood waste particles and jatropha seed cake, such as bulk density (BD), thickness swelling index (TS), modulus of rupture (MOR), modulus of elasticity (MOE) and internal bonding strength (IB) of the composite ceiling boards analysed; and also, the determination of predictive models for the simulation of physical and mechanical properties of the composite products.

**2.0. MATERIALS AND METHODS**

**2.1. Analysis of composites**

Usually, composites have strong, stiff fibres in a matrix which is weaker and less stiff. The primary aim of producing composite products is to enhance strength and stiffness while lowering density of the product [3]. The stronger or weaker member of a composite is determined by their characteristic properties. The theoretical techniques in composite materials design and analysis employed in this study was as described by Gay *et al.*, (2003) as cited in Jweeg *et al*. [19] as follows,

The fibre and matrix mass fraction are defined as,

$$M'_f = \frac{\text{Mass of fibres}}{\text{Total mass}} \quad (1)$$

$$M'_m = \frac{\text{Mass of matrix}}{\text{Total mass}} \quad (2)$$

Where, $M'_m = 1 - M'_f$ (3)

Similarly, for the fibre and matrix volume fraction, we have

$$V'_f = \frac{\text{Volume of fibres}}{\text{Total volume}} \quad (4)$$

$$V'_m = \frac{\text{Volume of matrix}}{\text{Total volume}} \quad (5)$$

Where, $V'_m = 1 - V'_f$ (6)

Conversion from mass fraction to volume fraction and vice versa is possible if the specific densities of fibre and matrix are given as $\rho_f$ and $\rho_m$. Thus,

$$V'_f = \frac{M'_f / \rho_f}{M'_f / \rho_f + M'_m / \rho_m} \quad (7)$$

$$M'_f = \frac{V'_f . \rho_f}{V'_f . \rho_f + V'_m . \rho_m} \quad (8)$$

### 2.2. Bulk density of matrix and fibre of composite ceiling board and properties of particle boards from different composites

Pan *et al.* [20] had produced particleboards from 20-40 mesh, with a target bulk density of 0.72 g/cm$^3$, which corresponded to 0.55 cm thickness square samples of 15.4 cm x 15.4 cm of the finished particleboard, and the press time, temperature and pressure were 8 min, 140 $^0$C and 3 MPa. Pan *et al.* [20] used polymeric methane diphenyl diisocyanate (PMDI) resin as adhesive for experimental particleboards. Typical average value of density of jatropha briquettes presented by Ghosh *et al.* [21] as 1.075 g/cm$^3$ was used for the bulk density of jatropha. Hence, the bulk densities of fibre (jatropha seed cake) and matrix (sawmill dust) adapted for this study are1.075 g/cm$^3$ and 0.72 g/cm$^3$ respectively. The volume of the ceiling board analysed in this study was maintained at same values of those of Pan *et al.* [20], that is, 0.55 cm x 15.4 cm x 15.4 cm (130.438 cm$^3$)

The physical and mechanical properties of composite particle boards produced from various constituents were determined in different studies by Ganapathy [12], Idris *et al.* [15] and Ghalehno *et al.* [18], and presented in Table 1. The properties of the boards given in Table 1 were used to develop general predictive models as a function of the bulk density of the composite products. The determined values of bulk density of the expected composite produced from sawmill dust and jatropha seed cake residue was in turn used together with the general predictive models developed to determine the physical and mechanical properties of ceiling board analysed at different mass and volume ratios respectively.

Table 1. Properties of Particle Boards from Different Composites

| Composite Product | Type of Adhesive | Physical Properties | | Mechanical Properties | | | Reference |
|---|---|---|---|---|---|---|---|
| | | BD (g/cm$^3$) | TS (%) | MOR (MPa) | MOE (GPa) | IB (MPa) | |
| Bamboo board (Canada) | Phenol formaldehyde (PF) resin | 0.75 | 14.00 | 17.20 | 3.100 | 0.345 | [12] |
| Water melon peals particleboard | Recycled low density polyethylene | 0.75 | 10.05 | 12.00 | 1.650 | 0.65 | [15] |
| Bagasse and wood particleboard | Urea formaldehyde (UH) resin | 0.70 | 11.84 | 16.59 | 2.384 | 0.76 | [18] |

### 2.3. Determination of internal bonding strength of particleboards

The internal bonding strength of particleboards was estimated by expressions for modulus of rupture (MOR) and internal bonding strength (IB) as described by Laemlaksakul [13] as follows,

$$MOR = \frac{3P_b L}{2bh^2} \quad (9)$$

Where, $P_b$ is the maximum load (N), $b$ is the width of the specimen (mm), $h$ is the thickness of the specimen (mm), and L is the span (mm). In conducting the static bending test, a concentrated bending load was applied at the center by Laemlaksakul [13] with a span of 15 times the thickness of the specimen.

$$IB = \frac{P_s}{bl} \quad (10)$$

Where, $P_s$ is the rupture load, and $l$ is the length of the specimen. Hence $IB$ was estimated by assuming $P_b = P_s$ in equations 9 and 10. Therefore, since $b = l$ in this study, we have,

$$IB = \frac{2 \times MOR \times h}{45 \times b} \quad (11)$$

### 2.4. Modelling of properties of composite ceiling boards

The physical properties, namely, thickness swelling index (TS) and bulk density (BD), and mechanical properties, namely, modulus of rupture (MOR), modulus of elasticity (MOE), and internal bonding strength (IB), of the composite ceiling boards analysed were modelled so as to simulate the physical and mechanical properties of the composite products as a function of the mass and volume ratios.

Multivariate functions, that is, functions having two or more independent variables are usually given by tabular data. Multivariate approximation is necessary for interpolation, differentiation, and integration. Caution must be exercised to ensure that the number of data points must be equal to the number of coefficients [22]. Since six data points have been used in this study, hence six coefficients suffice. The generic model equation for modelling of the composite product as a function of the mass and volume ratios can be expressed as,

$$Y = \beta_0 + \beta_1 Z_1 + \beta_2 Z_2 + \beta_3 Z_3 + \beta_4 Z_4 + \beta_5 Z_5 \quad (12)$$

Equation 12 may be re-written specifically in terms of the mass and volume ratio as follows,

$$Y = \beta_0 + \beta_1 M'_f + \beta_2 M'_m + \beta_3 V'_f + \beta_4 V'_m + \beta_5 M'_f M'_m \quad (13)$$

Furthermore, statistical analysis using advanced regression techniques was used to develop functional models of the physical and mechanical properties of the theoretical composite particle/ceiling board with respect to the mass and volume ratios of the fibre (jatropha) and matrix (sawmill dust) members of the board. In other words, board properties represented by the function given in by equation 14 were solved from generated data and relation given in equation 13.

$$Y = f(M'_f, M'_m, V'_f, V'_m) \quad (14)$$

### 3.0. RESULTS AND DISCUSSIONS

General models developed from data of previous studies as presented in Table 1 which relates properties of particleboards to bulk density $\rho$ are given for thickness swelling index (TS), modulus of rupture (MOR) and modulus of elasticity (MOE) as stated in equations 15-17 respectively. The internal bonding strength was estimated using the expression derived in equation 11 as previously explained.

$$TS = 3.7\rho + 9.25, \quad se = \pm 2.793\% \quad (15)$$

$$MOR = -39.8\rho + 44.45, \quad se = \pm 3.677\ MPa \quad (16)$$

$$MOE = -0.18\rho + 2.51, \quad se = \pm 1.025\ GPa \quad (17)$$

The thickness swelling index (TS), bulk density (BD), modulus of rupture (MOR), modulus of elasticity (MOE), and internal bonding strength (IB), of the composite ceiling boards composed of jatropha and sawmill dust, modelled as a function of the mass and volume ratios of the fibre (jatropha), that is, $Y = f(M'_f, V'_f)$ are stated in equations 18-22 accordingly.

$$TS = 0.437V'_f + 9.613 \quad (18)$$

$$\rho = 0.355V'_f + 9.613 \quad (19)$$

$$MOR = 0.202M'^2_f + 0.251M'_f - 0.685V'_f + 25.221 \quad (20)$$

$$MOE = 9.1\times10^{-4}M'^2_f + 1.14\times10^{-3}M'_f - 3.09\times10^{-3}V'_f + 2.42 \quad (21)$$

$$IB = -22.43M'_f + 25.073 \quad (22)$$

The model equations 18-22 was used to simulate the properties of the theoretical composite particle/ceiling boards and their characteristics are shown in Figures 1-4 respectively. The thickness swelling index (TS), bulk density (BD) internal bonding strength (IB) (Figures 1-3) all increased with increasing values of fibre (jatropha) in the composite product; while the modulus of rupture (MOR) and modulus of elasticity (MOE) (Figures 3 and 4) both experiences deceases with increases in quantity of jatropha. However, the modulus of rupture (MOR) was almost constant.

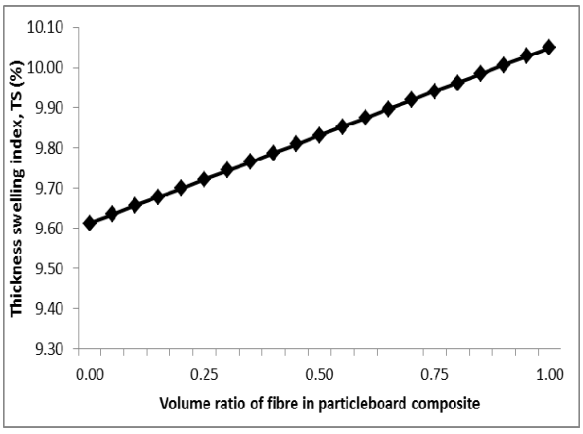


Figure 1. Thickness swelling index with respect to volume ratio of fibre (jatropha)

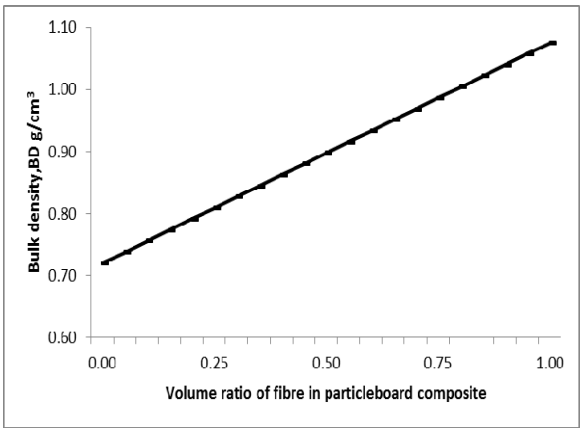


Figure 2. Bulk density variation with respect to volume ratio of fibre (jatropha)

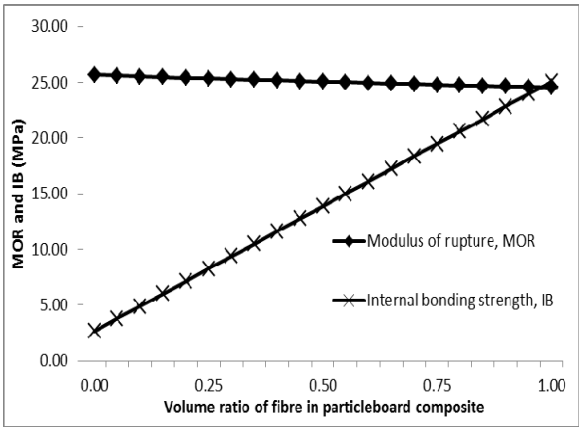


Figure 3. Modulus of rupture and internal bonding strength with respect to volume ratio of fibre

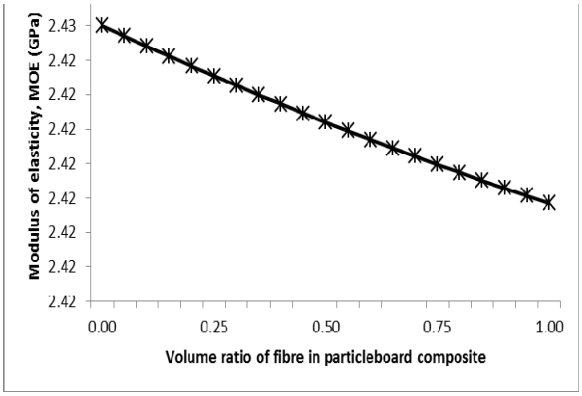


Figure 4. Modulus of elasticity with respect to volume ratio of fibre (jatropha)

For equal amounts of jatropha and sawmill dust in the theoretical composite particle/ceiling board, the properties are obtained as bulk density (BD) 0.8975 g/cm$^3$, thickness swelling index (TS) 9.83%, modulus of rupture (MOR) 25.05 MPa, modulus of elasticity (MOE) 2.42 GPa and internal bonding strength (IB) 13.86 MPa respectively. When compared with previous studies indicated in Table 1, that is bulk density (BD) 0.70-0.75 g/cm$^3$, thickness swelling index (TS) 10.05-14%, modulus of rupture (MOR) 12.00-17.20 MPa, modulus of elasticity (MOE) 1.650-3.100 GPa and internal bonding strength (IB) 0.345-0.760, results shows that addition of jatropha in composite particle board resulted in a denser product due to higher value of bulk density of jatropha seed cake. The modulus of rupture was improved while comparable modulus of elasticity was obtained. The internal bonding strength was significantly higher than that obtained from previous studies, although, this may not be the case in reality.

## 4.0. CONCLUSION

A denser composite particle/ceiling board can generally be produced with improved mechanical properties with the addition of jatropha to sawmill dust under specified control conditions of fiber-matrix mixture aggregates. Other undisclosed benefits may be discovered when composite particle/ceiling board are experimentally produced and investigated. The possibility of replacing wood biomass for particleboard and related products would go a long way in achieving a greener and sustainable environment, and value addition on naturally occurring agricultural resources and in areas yet to be explored.

## 5.0. REFERENCES

[1] Ojolo, S. J. and Orisaleye, J. I.: *Estimation of Biomass Potential for Solving Energy Problem in Nigeria*, In Building a Non-Oil Export Based Economy for Nigeria: The Potential of Value-Added Products from Agricultural Residues, Jekayinfa, S. O. (ed.) 69-75. Bonn-Germany; Published by Alexander von Humboldt Foundation, 2012.

[2] Lee, S., Jeong, S., Park, J., Kim, S. and Cho, G.: *A Study on Mechanical Properties of Carbon Fiber Reinforced Plastics by Three-Point Bending Testing andTransverse Static Response*, Journal of Materials Processing Technology, 201: 761–764, 2008.

[3] Clyne, B. and Tanovic, B.: *Mechanics of Composite Materials*, Accessed on July 17, 2009, Available from World Wide Web: http://www.matter.org.uk/matscicdrom/manual/co.html, 2009.

[4] Ohijeagbon, I.O. *Retrofiting Composite Ceiling Tiles with Sawdust*, In Building a Non-Oil Export Based Economy for Nigeria: The Potential of Value-Added Products from Agricultural Residues, Jekayinfa, S. O. (ed.) 291-295. Bonn-Germany; Published by Alexander von Humboldt Foundation, 2012.

[5] Kunaver, M., Jasiukaityte, E., Cuk, N., Medved, S., Opresnik, S. R. and Katrasnik, T.: *Biomass waste – a source of raw materials and new energy source*, World Renewable Energy Congress 2011-Sweden, 8-13 May 2011, 239-246, Bioenergy Technology (BE), Linkoping, Sweden, 2011.

[6] Winrock International India: *Byproducts of Biodiesel Manufacture (As part of Status Reports on Themes Related to Technical and Scientific Utilization of Biofuel Utilization)*, Department of Science and Technology, Government of India, India, 2012.

[7] Jingura, R. M., Musademba, D., and Matengaifa, R.: *An Evaluation of Utility of Jatropha Curcas L. as a Source of Multiple Energy Carriers*, International Journal of Engineering, Science and Technology, Vol. 2 (7), 2010, 115-122, 2010.

[8] *Energetic Value of Jatropha*, www.jatrofuels.com, Accessed July10, 2014.

[9] Alade, A. O., Okelana, O. A., Araromi, D. O., Jimoda, L. A. and Aremu, M. O.: *The Potential of Value-Added Products from Agricultural Residues*, In Building a Non-Oil Export Based Economy for Nigeria, Jekayinfa, S. O. (ed.) 129-135. Bonn-Germany; Published by Alexander von Humboldt Foundation, 2012.

[10] Idowu, D. O., Abegunrin, T. P. and Adejumobi, M. A.: *Effect of Some Processing Methods on the Physio-Mechanical Properties of Particle Board Made from Maize Cob Fibres*, In Building a Non-Oil Export Based Economy for Nigeria: The Potential of Value-Added Products from Agricultural Residues, Jekayinfa, S. O. (ed.)

129-135. Bonn-Germany; Published by Alexander von Humboldt Foundation, 2012.
[11] Scatolino, M. V., Silva, D. W., Mendes, R. F. and Mendes, L. M.: *Use of Maize Cob for Production of Particleboard*, Cienc. Agrotec., Lavras, 37(4): 330 – 337, 2013.
[12] Ganapathy, P. M., Huan-Ming, Z., Zoolagud, S. S., Turcke, D. and Espiloy, Z. B.: *Bamboo Panel Boards a State-of-the-Art Review* (Technical Report No. 12), International Network for Bamboo and Rattan, Beijing, New Delhi and Eindhoven, 1999.
[13] Laemlaksakul, V.: *Physical and Mechanical Properties of Particleboard from Bamboo Waste*, World Academy of Science, Engineering and Technology, 4: 507-511, 2010.
[14] Mello da Silva, S. A., Christoforo, A. L., Filho, S. L. M. R., Varanda, L. D. and Lahr, F. A. R.: *Particleboard Manufactured with Bicomponent Polyurethane Resin Base on Castor Oil*, International Journal of Composite Materials, 2(6): 115-118, DOI: 10.5923/j.cmaterials.20120206.01, 2012.
[15] Idris, U. D., Aigbodion, V. S., Atuanya, C. U. and Abdullahi. J.: *Eco-Friendly (Water Melon Peels): Alternatives to Wood-based Particleboard Composites*, Tribology in Industry, 33(4): 173-181, 2011.
[16] Johnson, A. C. and Yunus, N.: *Particleboards from Rice Husk: A Brief Introduction to Renewable Materials of Construction*, JURUTERA, 12-15, 2009.
[17] Raju. G. U., Kumarappa, S. and Gaitonde, V. N.: *Mechanical and Physical Characterization of Agricultural Waste Reinforced Polymer Composites*, J. Mater. Environ. Sci. 3 (5): 907-916, 2012.
[18] Ghalehno, M. D., Nazerian, M. and Bayatkashkoli, A.: *Experimental Particleboard from Bagasse and Industrial Wood Particles*, International Journal of Agriculture and Crop Sciences, 5 (15): 1626-1631, 2013.
[19] Jweeg, M. J. , Hammood, A. S. and Al-Waily, M.: *Experimental and Theoretical Studies of Mechanical Properties for Reinforcement Fiber Types of Composite Materials*, International Journal of Mechanical & Mechatronics Engineering IJMME-IJENS, 12 (4): 62-75, 2012.
[20] Pan, Z., Zheng, Y., Zhang, R. and Jenkins, B. M.: *Physical Properties of Thin Particleboard made from Saline Eucalyptus*, Industrial Crops and Products 26: 185–194, 2007.
[21] Ghosh, P. K., Mishra, S. C. P. and 16 More: *Integrated Process for the Production of Jatropha Methyl Ester and by Products*, IFI CLAIMS Patent Services, www.google.com/patents/EP2475754A1?cl=en, Accessed on May 10, 2014, 2012.
[22] Hoffmann, J. D.: *Numerical Methods for Engineers and Scientists*, Marcel Dekker Inc., New York, 2nd edition, 2001.

***Authors*:**
**Professor. Dr. John A. Olorunmaiye, Senior Lecturer. Dr. Idehai O. Ohijeagbon,** University of Ilorin, Department of Mechanical Engineering, P.M.B. 1515, Ilorin, Nigeria, Phone: 234-7030092411,
E- mail: adeolorunmaiye@gmail.com
idehaiohi@yahoo.com

Journal of Production Engineering
Vol.18 No.2
JPE (2015) Vol.18 (2) Preliminary Note
Ćuković, S., Devedžić, G., Luković, V., Anwer, N., Zečević Luković, T., Subburaj, K.

# 3D MODELING OF SPINAL DEFORMITIES SHAPES USING 5TH DEGREE B-SPLINES

Received: 27 September 2015 / Accepted: 20 November 2015

**Abstract:** *In this article, we present a new methodology to model spinal deformities in patients with idiopathic scoliosis. This approach uses a5th degree B-spline to characterize the deformities by taking central spinal line as a reference for positioning and orienting vertebrae.Generic 3D model of the spine and 3D optical scans of dorsal surfaces were used to generate the control vertices required to generate the central spinal line. B-spline based mathematical representation of central spinal line provides a set of quantitative measures to assess spinal deformities. This methodology was applied on a representative dataset consists 372 adolescent idiopathic scoliosis patients and tested for its effectiveness.*
***Key words:*** *Scoliosis, B-spline Curves, Adolescents, CAD, 3D Spinal Model*

**3D modeliranje oblika spinalnih deformiteta primenom b-spline krivih petog stepena.** *U radu je predstavljena nova metodologiju u modelovanju deformiteta kičmenog stuba kod pacijenata sa idiopatskom skoliozom. Ovaj pristup koristi B-spline krive petog stepena da se karakterišu deformiteti kičmenog uzimajući centralnu liniju kao referencu za pozicioniranje i orijentaciju vertebrae. Generički 3D model kičme i 3D optičko skeniranje leđne površine su korišćeni za generisanje kontrolnih tačaka potrebnih za generisanje centralne spinalne linije. B-spline na bazi matematičkog predstavljanje centralnog kičmene linije obezbeđuje skup kvantitativnih mera u cilju utvrđivanja kičme deformiteta. Ova metodologija je primenjena na reprezentativnom uzorku koji se sastoji od 372 adolescenata sa idiopatskom skoliozom pacijenta i testiran je za njenu efikasnost.*
***Ključne reči:*** *Scoliosis, B-Spline krive, Adolescenti, CAD, 3D model kičme*

## 1. INTRODUCTION

Adolescent Idiopathic Scoliosis (AIS) is a spinal deformity that can be characterized by lateral deformities of the dorsal surface and trunk. This deformity causes various health problems for these patients with continuous progression in addition to being unaesthetic, so the secondary lifestyle diseases, like clinical depression and difficulties of doing activities in the workplace also increases. The current clinical standard for diagnosis and monitoring of these patients is based on Cobb's angles, measured using sagittal and frontal radiographic images. Significant technical and procedural advances in non-invasive imaging modalities offer new avenues to diagnose and monitor scoliosis [1]. One of these modalities is 3D optical scan that digitize dorsal surfaces using traditional raster-stereography principle with modern equipment.

In this study, we have used generic 3D model of spine and 3D optical scan to generate central spinal line. To represent an intricate 3D shapes and curves in computer aided design (CAD) environment, we tested various freeform curves including μ-splines, β-splines, nonlinear splines, exponential splines, splines in tension, and B-splines. Although B-spline curves are the most widely used, due to easy handling and computational efficiency [2], we have adopted them for modeling spinal deformities.

### 1.1 Characteristics of B-splineCurves

This section describes the main characteristics of B-spline curves that are needed to model spinal deformities in patients with AIS. If there are positive integer parameters $k$ and $n$, where in $k < n+2$, and known knot vector $(t_0 < t_1 < ... < t_n < t_{n+1} < ... < t_{n+k})$, as well as the $n+1$ points of the control polygon: $a_0, a_1, ..., a_n$, then the parametric curve $c$ represented by the function $p(t)$ in formula (1) is B-spline curve, defined on the control knot polygon $a_0, a_1, ..., a_n$ and by the node vector $(t_0, ..., t_{n+k})$. Points denoted as $a_i$ are control points of the control knot polygon, or de Boor's points, $N_{i,j}(t)$ is basic spline function [3]. If the node interval is $[t_i, t_{i+1}]$ and if lengths between corresponding nodes are equal, the node vector is then uniform. B-spline curve created by this property is called uniform B-spline curve (Figure 1). The node vector with non-uniform distribution of nodes defines the non-uniform B-spline (non-uniform B-spline curve). Parameter *n* in (1) represents degree of B-spline curve.

$$p(t) = \sum_{i=0}^{n} N_{i,j}(t) \cdot a_i \text{ for } t \in [t_{k-1}, t_{n+1}], \qquad (1)$$

In accordance with mentioned, main characteristics of the B-spline curves are:

- For $t \in [t_l, t_{l+1}]$ applies that segment of B-spline defined on the interval $[t_l, t_{l+1}]$ depends only on the $k$ control points: $a_{l-k+1}, ..., a_l$, and then it can be

described as follows:

$$p(t)=\sum_{i=0}^{n} N_{i,j}(t)\cdot a_i=\sum_{i=l-k+1}^{l} N_{i,k}(t)\cdot a_i \qquad (2)$$

-Curve is invariantly associated with the control polygon $a_0,...,a_n$ by affine transformations;

-If B-spline curve is smooth at each subinterval of interval $[t_i,t_{i+1}]$, then B-spline curves are $C^{k-2}$ continuous in points $p(t_i)$.

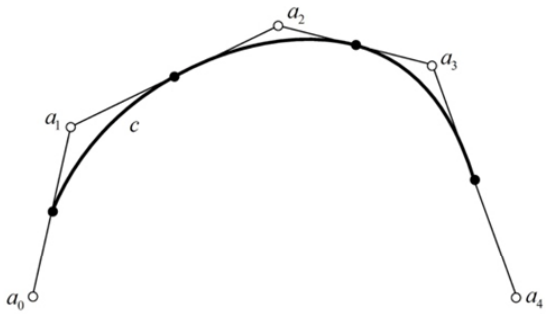


Fig. 1. Uniform B-splinecurve for $n=4$ and $k=3$

In order to represent and analyze the central spinal line and shape for diagnosis as well as characterization of the spinal deformity in adolescent patients with idiopathic scoliosis, after testing on 372 patients, we propose theuse of 5th degree B-splines [4].

## 2. MATERIALS AND METHODS

### 2.1 Central Spinal Line Representation

To achieve an optimum smoothness ofthe central spinal line and symmetry line of the dorsal surface, we have performed interpolation of vertices obtained by scanner using simple spline curves [5]. Then we obtained best-fit curves for the interpolated set of points. This interpolation enables us to have sufficient number of vertices to perform deformity analysis on the spinal line.

A set of focal points on the transverse profiles that was derived from the 3D scans of dorsal surface was used to measure "symmetry" as shown in figure 2.The line connecting these focal points may be single, double or triple curved depending on the angle of deformity and in ideal case it coincides with the line of spinal processus [1].

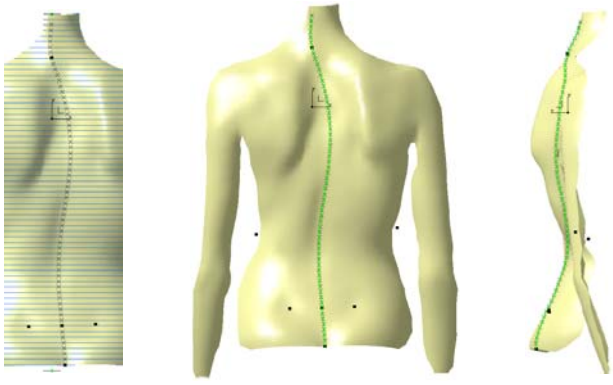

a) b)

Fig. 2. Interpolation of points of the symmetry line on dorsal surface a) posterior and b) sagittal view

We have defined the "angle of deformity (degrees)" as an angle at an instance (vertices) in the frontal plane, measured similar to Cobb's angle measurement method [4].

Central spinal line was derived by connecting centroids of all vertebral bodies in both frontal and sagittal plane [6,7]. Its mathematical representation allows us to localize inflection vertices for downstream curvature analysis of the spine and also to measure Cobb's angles to characterize idiopathic scoliosis (Figure 3). By projecting the spinal line on two planes (sagittal and frontal) analysis of its projections inflection points can be determined in places where the 2nd derivative is equal to Zero. Then the radius of the osculating circle be comes in finite. Analysis of the central spinal curve of deformity or its projections enables generation of a set of quantitative measures for physicians to determine positions and orientations of dislocated vertebrae, structure of deformity, and other postural parameters [6]. Having in mind that most of deformities occur between the spinal levels from L5 to C7, obtained 3D curve is segmented from projected *fix_C7*to*fix_DM* points (Figure 3) [8].

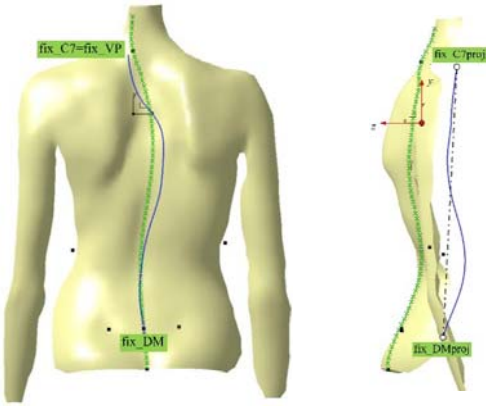


a) b)

Fig. 3. Segmentation of the spina lcurve from *fix_C7*to*fix_DM* a) posterior and b) sagittal view

Interpolation of the large number of near points consequently causes many changes of its curvatures. Approximation of the spinal curve in order to improve its smoothness is performed in PLM system CATIA using 5th degree of B-spline curve (Figure 4).

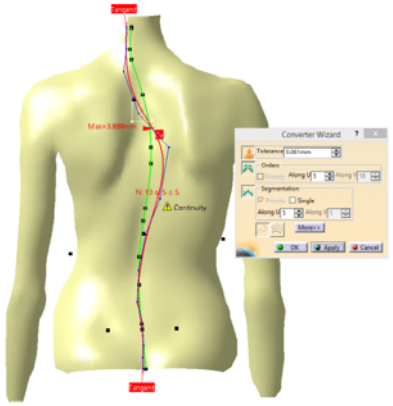

Fig. 4. Approximation of spinal line by B-spline

This stepis essential because the parameter of the segmented length determines the parameter of vertebral

scaling factor. Unit scaling factor is normalized according to the Panjabi's anthropometric measures and recommendations [8]. In addition, the resulting curve segment *Split_L*is base for generating the skeletal CAD model (3D geometrical set) or reference 3D model to regenerate master model of the spine, inflection points, Cobb's and SOSORT-these angles in the sagittal and frontal plane, and also axial rotation of each vertebrae inthe transverse plane.

### 2.2 Influence of Order of Degrees of B-spline on Spinal Curve Approximation

The process of generating the spinal shape from 2D radiographic (x-rays) images is a complex one. Many authors have used a set of known anatomical landmarks which are easily recognizable in radiographic images to determine the inflection points ($I_1$, $I_2$, $I_3$, $I_4$ in Figure 5a) and the position of apex vertebrae of each segment ($F_{12}$, $F_{23}$, $F_{34}$ in Figure 5d), required to represent the curve, curve's control vertices (lines of control polygon). For a detailed representation of the spinal profile on the frontal plane projection, the central spinal line should passes through the centroids of the vertebral bodies in x-rays, from 6 to 9 (8 to 10) representative points and should have $C^2$ continuity [9, 10] (Figure 5).

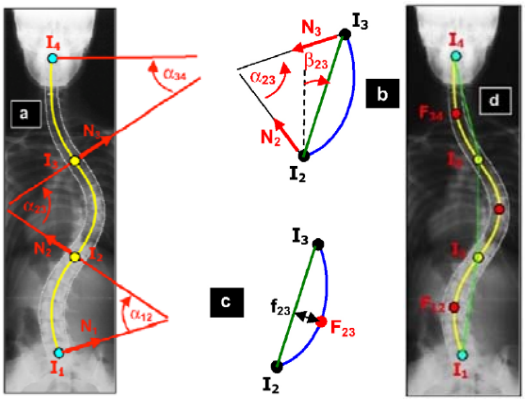


Fig. 5. Segmentation of frontal projection of spinal line by planar B-spline, adopted from [9]

The approximation of central spinal line was realized automatically to eliminate physicians' bias. The control vertices are generated directly from the 3D optical scan data of the dorsal surface. Reference lines, required to quantify Cobb's angle or angle of deformity, were automatically generated. Quality of the central spinal line - depends on the quality of interpolation and approximations of spinal line by B-spline and inflection points. Central spinal line in frontal plane is described by the ($n=5$) 5th degree of polynomial line and a method of analysis and generation of analytical Cobb's angles,as described in [10]. In this study we have used nth degree spatial curve and quality control was performed with different degrees in approximation phase it self.

## 3. RESULTS AND DISCUSSION

### 3.1 Effect of Degrees of Approximation on Cobb's Angle Measurement

Table 1 provides a sensitivity of the central spinal curve of a patient, with different degrees of approximation ($n=6$ to $n=4$). A similar sensitivity analysis was performed on sagittal projection of spinal line as well, but not given here. After testing we concluded that for 3D representation of central spinal line in the space, 5th degree B-spline is the most suitable [4]. By decreasing degree of B-spline, the formof the initial interpolation line will be significantly distorted, and by increasing, system will generate greater number of inflection points and unrepresentative Cobb's angles.

| B-spline | Frontal plane | Spinal line |
|---|---|---|
| | Maximal Cobb angle: **40.36°, T11-T6**<br>**9 referent lines** | |
| **Degree 6**<br>$n=6$ | 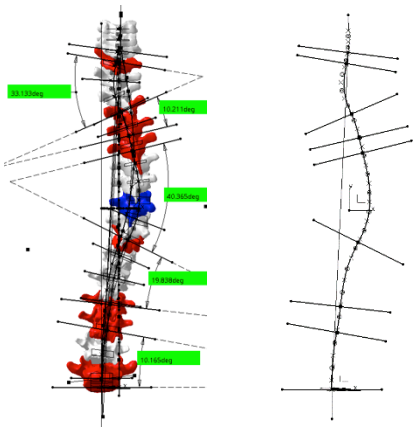 | |
| | Maximal Cobb angle: **53.21°, T11-T4**<br>**8 referent lines** | |
| **Degree 5**<br>$n=5$ | 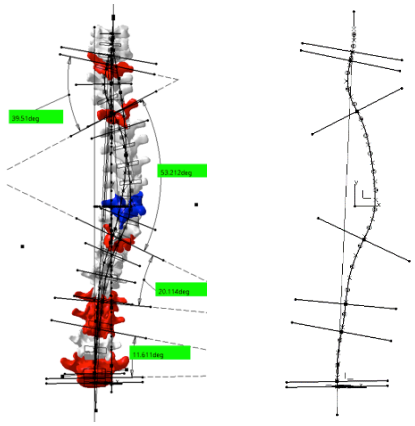 | |
| | Maximal Cobb angle: **42.42°, T11-T4**<br>**6 referent lines** | |
| **Degree 4**<br>$n=4$ | 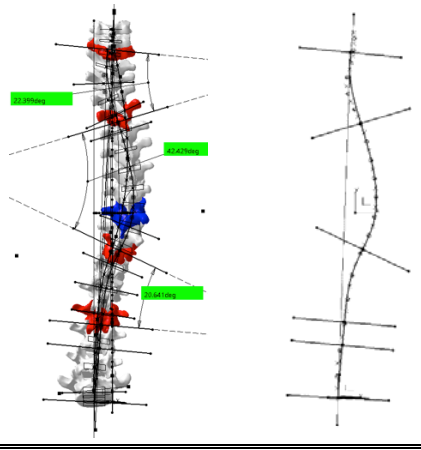 | |

Table 1. The influence of the degree of B-spline approximation on the smoothness and number of Cobb's angles

### 3.2 Deformity Curve Measures

Segment of the 3D spinal line denoted as a *Split_L* between dorsal anatomical markers *fix_C7*to*fix_DM* allows calculation of *ScalingFactor* parameter.

Those internal parameters of the spinal line are presented for 231 female and 141 male adolescents in table 2.

**Descriptive statistics of spinal line lengths and scale factor for female and male adolescents**

| | N | Range | Min. | Max. | Mean | Std. Dev. |
|---|---|---|---|---|---|---|
| ScalingFactor Female | 231 | .39 | .67 | 1.07 | .89 | .06 |
| ScalingFactor Male | 141 | .44 | .66 | 1.11 | .93 | .08 |
| Split_L Female | 231 | 197.73 | 336.73 | 534.46 | 442.2 | 32.17 |
| Split_L Male | 141 | 220.37 | 331.06 | 551.44 | 466.14 | 44.65 |

Table 2. Descriptive statistics of spinal curve parameters for 372 adolescents

### 3.3 Cobb's Angles in Frontal Plane

In table 1 comparative review of frontal spinal line projection for the same patient is presented. Cobb's angles in frontal plane were measured based on the generated segment *Split_L* of the spinal line. In the case of 6$^{th}$ degree of B-spline, software generated 5 different Cobb's angles (max=40.36º, T11-T6). In the case of 5$^{th}$ degree of B-spline, software generated 4 different Cobb's angles (max=53.21º, T11-T4). In the case of 4$^{th}$ degree of B-spline software generated 3 different Cobb's angles (max=42.42º, T11-T4). After testing, we concluded that 5$^{th}$ degree B-spline best fits given points, make smooth curve and doesn't distort projection as in a case of higher and lower degrees. Similar analysis can be performed in sagittal plane in order to quantify kyphosis and lordosis.

## 4. CONCLUSIONS

The diagnosis and treatment of adolescent idiopathic scoliosis rely on characterization of the spinal deformity. We have proposed a new method to quantitative measure the spinal deformity based on central spinal line that was computed from (i) generic 3D spine model, (ii) radiographic images, and (iii) 3D optical scan of dorsal surface. The central spinal line was generated in both frontal and sagittal planes to measure angular deformity of each segment of spinal curve (Cobb's angle). We have approximated and represented the central spinal line using 5$^{th}$ degree B-splines. Sensitivity analysis of degree and parameterson the deformity line was studied and found to be reproducible and satisfactory. Proposed methodology leads to more precise diagnosis and automated Cobb angles extracting in two planes, based on optical scans, compared to traditional methods where angles are measured manually on dimmed x-rays with low interobserver and intraobserver reliability. The representation needs to be evaluated on a larger data set with additional quantitative measures to be able to translate to clinical settingsacceptable in daily praxis.


## ACKNOWLEDGMENTS

This research work is supported by the Serbian Ministry of Science and Technology under the grant III-41007: "Application of Biomedical Engineering in Preclinical and Clinical Practice".


## 5. REFERENCES


[1] Devedžić, G., Ćuković, S., Luković, V., Milošević, D., Subburaj, K., Luković, T.: *ScolioMedIS: Web-oriented information system for idiopathic scoliosis visualization and monitoring,* Computer Methods and Programs in Biomedicine, vol. 108, no. 2, p.p. 736-749, 2012.

[2] Piegl, L., Wayne, T.: *The NURBS Book*, 2nd ed., University of South Florida: Springer-Verlag Berlin, Heidelberg, 1997.

[3] Munira, M., Nur, N., Fazilah, A., Nooraizedfiza, Z.: *Review on Non Uniform Rational B-spline (NURBS): Concept and Optimization,* in International Manufacturing Engineering Conference (IMEC 2013), Bukit Gambang Resort City, Kuantan, Pahang, 2013.

[4] Ćuković, S., "Non-rigid registration of sculptured surfaces in Internet Environment", Doctoral thesis, University of Kragujevac, Faculty of Engineering, 2015.

[5] Hana, K., Hak, S., Eun, S., Choon-Sik, Y., Tae-Sub, C., Ho-Taek, S., Jin-Suck, S., Young, H., Sungjun, K.: *Scoliosis Imaging: What Radiologists Should Know,* RadioGraphics, vol. 30, p.p. 1823-1842, 2010.

[6] Berthonnaud, E., Dimnet, J., Hilmia, R.: *Classification of pelvic and spinal postural patterns in upright position. Specific cases of scoliotic patients,* Journal of Computerized Medical Imag ing and Graphics, vol. 33, p.p. 634-643, 2009.

[7] Stokes, I.: *Theree-Dimensional Terminology of Spinal Deformity. A Report Pesented to the Scoliosis Research Society by The Scoliosis Research Society Working Group on 3D Terminology of Spinal Deformity,* Spine, vol. 19, no. 2, p.p. 236-248, 1994.

[8] Cukovic, S., Devedzic, G.: *3D Modeling and Simulation of Scoliosis – an Integrated Knowledgeware Approach,* in 4th IEEE Mediterranean Conference on Embedded Computing - MECO, Budva, Montenegro, 2015.

[9] Berthonnaud, E., Dimnet, J.: *Analysis of structural features of deformed spines in frontal and sagittal projections,* Computerized Medical Imaging and Graphics, vol. 31, p.p. 9-16, 2007.

[10] Kanayama, M., Tadano, S., Kaneda, K., Ukai, T., Abumi, K.: *A Mathematical Expression of Three-Dimensional Configuration of the Scoliotic Spine,* Journal of Biomechanical Engineering, vol. 118, p.p. 247-252, 1996.



***Authors:*** **Dr Ćuković Saša, Prof. dr Devedžić Goran** University of Kragujevac, Faculty of Engineering, Sestre Janjić 6, 34000 Kragujevac, Serbia. **Mr Luković Vanja,** University of Kragujevac, Faculty of Technical Sciences, Svetog Save 65, 32000 Čačak, Serbia. **Prof. dr Nabil Anwer,** Paris Nord University, IUT Saint Denis, Place du 8 mai 1945, 93206 Saint-Denis Cedex, France. **Doc. dr Luković-Zečević Tanja,** Faculty of Medical Sciences, S. Markovića 69, 34000 Kragujevac, Serbia. **Dr. Subburaj Karupppasamy**, Singapore University of Technology and Design (SUTD), (EPD) Pillar, 8 Somapah Road, Singapore – 487372, Singapore.

E-mail: cukovic@kg.ac.rs; devedzic@kg.ac.rs vanja.lukovic@ftn.kg.ac.rs, nabil.anwer@ens-cachan.fr,, tanjalukovic_kg@yahoo.com, subburaj@sutd.edu.sg

Journal of Production Engineering
Vol.18 No.2
JPE (2015) Vol.18 (2) Preliminary Note

Tamás, P., Illés, B.

# THE CONCEPT OF A VIRTUAL LOGISTICS CENTER FOR A HUNGARIAN REGION

Received: 02 August 2015 / Accepted: 28 October 2015

***Abstract:*** *This paper is presenting a virtual logistics enterprise's operational concept. This concept was elaborated for the Northern-Hungarian Region by the researchers of the Institute of Logistics (University of Miskolc). The essay presents the center's logistics services and its working principles. Furthermore, the possible advantages of the virtual logistics enterprise's realization are presented. In our opinion the conception which will be introduced can be easily applied at the other regions too in the interest of increasing the competitiveness of the companies.*
***Key words:*** *virtual logistics enterprise, Hungarian region, logistics*

**Koncept virtuelnog logističkog centara za region Mađarske.** *U ovom radu je predstavljen koncept virtuelnog logističkog operacionog centra. Pomenuti koncept je formiran za sevrno-mađarski region od strane istraživača Instituta za logistiku (Univerzitet Miškolc). Rad prikazuje logističke mogućnosti centra i njegov princip funkcionisanja. Takođe su navedene i moguće prednosti realizacije virtuelnog logističkog centra. Po mišljenju autora, opisani koncept može biti iskorišćen i u drugim regionima u cilju povećanja konkurentnosti preduzeća.*
***Ključne reči:*** *virtuelno logističko preduzeće, mađarski region, logistika*

## 1. INTRODUCTION

The term of the virtual enterprises was created from the beginning 1990s. According to one of the more important opinions the term means network of the independent companies, which are managed on the basis of IKT technology [1]. Numerous authors underline that the main goals of the virtual enterprises are sharing skills, costs, resources and gaining new markets [2-4]. We can define the virtual logistic enterprises as a system of the objects (SMEs, multinational companies, logistics services providers, …, etc.) which are connected with computer network, where a virtual logistics center enhances the working efficiency of the objects' logistics tasks [5]. There are numerous possibilities for economic development of a region, from these the virtual logistics enterprises represent a significant untapped potential [6-7]. The enterprises which are connected to the virtual logistics center can gain competitive edge thereby that they can reach the logistics services to be realized at lower costs and/or higher service quality than their competitors [8-9]. The virtual logistics enterprise's concept was elaborated regarding the Northern-Hungarian Region (Borsod-Abaúj-Zemplén county, Heves county, Nógrád county) in this paper. The main aim to be achieved of this concept is a competitiveness enhancement of an assigned region's enterprises by a virtual logistics center.

This paper introduces the virtual logistics enterprise's:

- structure,
- planned services and their essential working principles,
- a fundamental function's detailed working concept,
- possible advantages and risks of the realization.

## 2. STRUCTURE OF THE VIRTUAL LOGISTICS ENTERPRISE

We can determine the Northern-Hungarian Virtual Logistics Enterprise's three kinds of components on the basis of Figure 1. These are the following:

- R&D organizations: Two institutes of the University of Miskolc (Institute of Logistics, Institute of Informatics) will take part in the development of the virtual logistics center's services. The researchers of the Institute of Logistics will elaborate the detailed conception of the new services, the researchers of the Institute of Informatics will play a relevant role in the realization of these services.
- Virtual logistics center: Our concept is that the ATI DEPO LTD. will operate this virtual logistics whose more important tasks will be the following:
  - registration of new partners in the system (on the basis of the connection contracts's data),
  - request of new developmental needs form the R&D organizations,
  - catering of the marketing, financial and management activities.
- Enterprises which join in virtual logistics center: The Northern-Hungarian Region's enterprises requiring logistics services and all logistics services providers can join in the virtual logistics center after contracting with the ATI DEPO LTD. (the most important aim is the enhancement of the competitiveness of the enterprises requiring logistics services). The virtual logistics center's services are available after login to the web application.

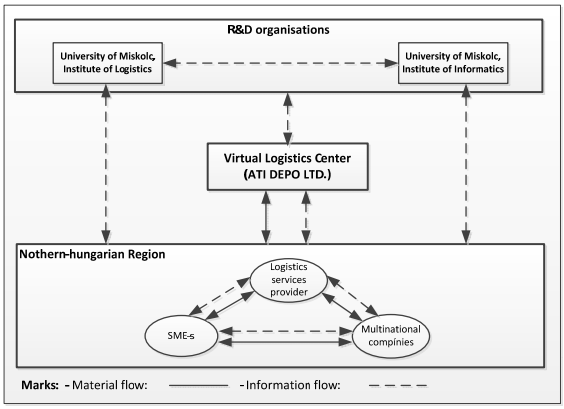


Fig. 1. Structure of virtual logistics enterprise

## 3. PLANNED SERVICES OF VIRTUAL LOGISTICS CENTER

We selected the types of the logistics services to be realized on the basis of the examined region's more important enterprises' asking and more literature's overview [10-12].

We have been planning the creation of the next logistics services regarding the virtual logistics enterprise (we can also create new logistics services on the basis of the needs):

- Electronic marketplace function (transport): The task of this module is to support the business transactions between enterprises requiring logistics services and the logistics services providers in case of delivery tasks. The logistics services needs and the bids will be given via the web application. The speciality of this module is that the enterprises requiring logistics services can view the logistics services providers' quality indicators, which are determined on the basis of the realized logistics services. Consequently, the selection of the logistics services providers can be realized on the basis of the bid and quality indicators as well.
- Electronic marketplace function (warehousing): The task of this module is to support the business transactions between enterprises requiring logistics services and the logistics services providers in case of warehousing tasks. Working principles of this module are the same as at the previous module.
- Tendering: The tendering process will be realized more easily with the use of this module. The module's user interface will be created in such a way that the enterprises can use it in case of all logistics services
- Consultative activity: The enterprises which will be connected to the virtual logistics center can request various qualified professionals via the web system in the fields of logistics, informatics, system planning, marketing, financial, interpretation and legal. These qualified professionals will be ensured by the University of Miskolc.
- Joint raw material and/or parts procurement: This module supports the joint procurement of the raw material and/or parts thus the enterprises can reach discounts at the suppliers. The companies can give the amount of the required raw materials and/or parts, as well as the deadlines of the performance on the user interface. On the basis of these data the system will determine the optimal order decision (product-amount-supplier).
- Optimization the transport tasks' realization: with the use of this module we can determine the optimal coupling of the transportation requests and the free transport capacities on the basis of the determined conditions and the defined goal function (for example: costs, services quality, …, etc.) We have to use optimization algorithms in order to realize this module.
- Optimization the warehousing tasks' realization: with the use of this module we can determine the optimal coupling of the warehousing requests and the free warehousing capacities on the basis of the defined conditions and goal function (for example: costs, services quality, …, etc.). We have to use optimization algorithms in order to realize this module.

Various knowledge is needed in the interest of elaboration of the software modules, which are the following: logistics systems' working, optimization, modeling, process planning, database management, concept creation. The Institute of Logistics and the ÁTI DEPO LTD. have these kinds of knowledge. The realization of the elaborated concept needs high level of programming knowledge which is available at the Institute of Informatics.

## 4. WORKING CONCEPT OF THE ELECTRONIC MARKETPLACE

The virtual logistics center's services will be available on the basis of the client-server conception. We will introduce from these services the electronic marketplace service's main steps in this chapter, which are the following:

1. Contracting: The logistics service provider and/or the enterprises requiring logistics services have to make a contract with the ATI DEPO LTD. before the first system use.
2. Data recording, maintenance of data: The VLC's operator has to write the data of contract in a center database and has to maintain them in the future (necessary modifications, deletions, …, etc.).
3. Login: The VLC's operator gives a username and a password to the contracted partner. These login information will define the mode of the system use (availability, useable modules).
4. Selection of the logistics services to be realized: The user selects a logistics service in the client program.
5. Defining of the task to be realized: The logistics service requiring can give the logistics tasks to be realized with filling in an electronic data form.
6. Selection of the logistics services providers: The logistics service requiring can select from those logistics services providers which are contracted partners of the virtual logistics center.
7. Sending of proposal request: The proposal request is sent to the selected logistics services providers

via the VLC's client program.

8. View of the realizable tasks: The logistics services provider views the tasks to be realized with the use of the client program.
9. Making of proposal: The logistics services provider fills in an electronic form of proposal via the client program.
10. Sending of the proposal to the customer: The realized proposal is sent to the customer.
11. Evaluation of the proposal(s): The logistics service requiring can evaluate the proposals with the use of the evaluation module. This module contains more important quality data from the earlier realized logistics tasks (logistics service requiring will write this data to the database).
12. Selection of the logistics provider: The customer can choose the adequate logistics services provider after the evaluation of proposals.
13. Agreement with the logistics services provider: The customer agrees with the logistics services provider about the details of logistics tasks to be realized.
14. Selection of the next logistics provider: If the logistics provider is not adequate for the customer then it will select the following best logistics services provider.
15. Realization of the logistics task: The logistics services provider will work out the logistics task undertaken after the agreement.
16. Invoicing: The logistics services provider sends an invoice to the customer after realization of the logistics task.
17. Payment of the service: The customer pays the value of the realized service.
18. Evaluation of the realized logistics service: The customer evaluates the realized logistics service with the use of the evaluation module. These data will help the customers with selecting the next logistics services provider.

## 5. POSSIBLE ADVANTAGES AND RISKS OF THE REALIZATION

Creation of the virtual logistics center can result relevant advantageous for the participants, however there can be also risks of the realization. In this chapter the possible advantageous and risks regarding the assigned region will be introduced.

Possible advantages:

- The competitiveness of the VLE's members can be improved with the use of the VLC's application since these enterprises can get the logistics services at lower costs and/or higher service quality than earlier. The lower cost follows from the economics of scale, the higher services level comes from more efficient selection of the logistics service providers.
- The realized logistics services's data will be collected in a database which is useable in the interest of the logistics services providers and/or manufacturing companies' attraction to the region (if the realized logistics services' cost is high and the logistics services' quality is low then this is advantageous for the new logistics services providers; in the inverse case advantageous for new manufacturing companies).
- The ATI DEPO LTD. can reach higher warehousing utilization and more profit with the creation of the virtual logistics center (ATI DEPO LTD. will operate the virtual logistics center, thus it can gain more income with introduction of the registration fees).
- The University of Miskolc can get continuous orders to the improvement of the virtual logistics center's applications. This can enhance significantly the incomes of the university, respectively it can contribute to professional development of the researchers.

Possible risk:

- If the number of the contracted enterprises will be few, then working of the virtual logistics center will be not cost efficient. In order to reduce this risk a very significant marketing activity will be necessary.

## 6. SUMMARY

This paper introduced an elaborated virtual logistics center's planned structure and working concept regarding the Northern-Hungarian Region. Numerous economic developmental advantages can be reached with realization of this concept which are introduced in this essay. We plan submission of a tender in the interest of the realization. The main cost components will be the detailed elaboration and programming of the conception.

## 7. REFERENCES


[1] J. A. Byrne, R. Brandt, O. Port: The virtual corporation, Business Week 8, 1993, pp. 36-40.

[2] H. S. Jagdev, J. Browne: The extended enterprise - a context for manufacturing, Production Planning & Control 9 (1998), 216-219.

[3] M. T. Martinez, P. Fouletier, K. H. Park, J. Favrel: Virtual enterprise organization, evolution and control. International Journal of Production Economics 74 (2001), pp. 225-238.

[4] L. Mikhailov: Fuzzy analytical approach to partnership selection in formation of virtual enterprises, Omega – International Journal of Management Science 30 (2002), 393-401.

[5] R. Skapinyecz, B. Illés: Introducing a risk-management concept for holonic manufacturing supply chains KEY ENGINEERING MATERIALS 581: pp. 547-553. (2013).

[6] T. Hartványi, P. Földesi, J. Kovács, L. Lajos: Multi-centre logistics systems for improving competitive status of logistics service suppliers in Hungary = Hungarian Electronic Journal Of Sciences 2001. Interneten http://hej.szif.hu ISSN 1418-7108

[7] Gy. Kovács, B. Illés, P. Tamás, R. Bálint: Conception for establishment of a regional virtual logistics network In: La Universidad Central "Marta Abreu" (szerk.) COMEC 2010 VI. Conferencia

Cientifica Internacional de Ingeniera Mecánica. Konferencia helye, ideje: Villa Clara, Kuba, 2010.11.02-2010.11.04. Santa Clara: Universidad Central Marta Abreu de Las Villas, 2010. pp. 1-6. (ISBN: 978-959-250-602-2)
[8] O. Khalil, S. Wang: Information technology enabled meta-management for virtual organizations, International Journal of Production Economics, Volume 75, Issues 1–2, 10 January 2002, Pages 127–134.
[9] J. Choi, D. Kang, H. Chae, K. Kim: An enterprise architecture framework for collaboration of virtual enterprise chains, The International Journal of Advanced Manufacturing Technology, February 2008, Volume 35, Issue 11, pp 1065-1078
[10] C. Scholz: Die virtuelle Organisation als Strukturkonzept der Zukunft? Arbeitspapier No. 30, Universität des Saarlandes Saarbrücken, Lehrstuhl für Betriebswirtschaftslehre, 1994. szept.
[11] C. Martin: Logistics and Supply Chain Management, Creating Value-Adding 111 Networks, ISBN 0 273-68176-1.
[12] B. L. Kacsukné, J. Cselényi: On the Optimization Problems of Emmil Marketplaces, microCAD International Conference, Miskolc 2005.

**Acknowledgements**
"This research was (partially) carried out in the framework of the Center of Excellence of Mechatronics and Logistics at the University of Miskolc."

***Authors:*** **Dr. Péter Tamás (assistant professor), Dr. Béla Illés (university professor)**, University of Miskolc, Faculty of Mechanical Engineering and Informatics, Institute of Logistics, H-3515, Miskolc-Egyetemváros
E-mail: alttpeti@gmail.com
altilles@uni-miskolc.hu

# INSTRUCTIONS FOR CONTRIBUTORS

| | |
|---|---|
| No. of pages: | 4 DIN A4 pages |
| Margins: | left: 2,5 cm |
| | right: 2 cm |
| | top: 2 cm |
| | bottom: 2 cm |
| Font: | Times New Roman |
| Title: | Bold 12, capitals |
| Abstract: | Italic 10 |
| Headings: | Bold 10, capitals |
| Subheadings: | Bold 10, small letters |
| Text: | Regular 10 |
| Columns: | Equal column width with 0,7 cm spacing |
| Spacing: | Single line spacing |
| Formulae: | Centered and numerated from 1 in ascending order.<br>Equations must be typed in Equation Editor, with following settings:<br>Style>Math – Times New Roman<br>Size>Full 12pt, Subscript/Superscript 7pt, Symbol 18 pt |
| Figures: | High quality, numerated from 1 in ascending order (e.g.: Fig.1, Fig. 2 etc.); Figures and tables can spread over both two columns, please avoid photographs and color prints |
| Tables: | Numerated from 1 in ascending order<br>(e.g..: Tab. 1, Tab. 2, etc.) |
| References: | Numerated from [1] in ascending order; cited papers should be marked by the number from the reference list<br>(e.g. [1], [2, 3] ...) |
| Submission: | **Papers prepared in MS Word format should be e-mailed to: pkovac@uns.ac.rs, savkovic@uns.ac.rs** |
| Notice: | **Papers are to be printed in Journal of Production Engineering**<br>Sample paper with detailed instructions can be found at: **http://www.jpe.ftn.uns.ac.rs/** |

## FOR MORE INFORMATION, PLEASE CONTACT:

**Prof. Pavel Kovač, PhD, MEng.**
**Borislav Savković, *MSc. Assistant***
**FACULTY OF TECHNICAL SCIENCES**
**Department for Production Engineering**
**Trg Dositeja Obradovica 6**
**21000 Novi Sad**
**Serbia**
**Tel.: (+381 21) 485 23 24; 485 23 20 ; 450 366;**
**Fax: (+381 21) 454 495**
**E-mail: pkovac@uns.ac.rs, savkovic@uns.ac.rs**
**http://www.jpe.ftn.uns.ac.rs/**